Synthesis of Organic Carbonates by Direct Condensation of Alcohols with Carbon Dioxide

O'Neill, Matthew

Award date:
2021

Awarding institution:
University of Bath

Synthesis of Organic Carbonates by Direct Condensation of Alcohols with Carbon Dioxide

Matthew F. O'Neill

A Thesis submitted for the degree of Doctor of Philosophy

University of Bath

Department of Chemistry

December 2020

The Material presented here for examination for the award of higher degree of research has not been incorporated into a submission for another degree.

I am the author of this thesis and the work described herein was carried out by myself. With the exception of quantum chemical calculations in Chapter 4 where the contribution from Dr Keane is detailed.

Signature: ……

“All creation necessarily ends in this: Creators, powerless, fleeing from the things they have wrought” — David Eagleman

Acknowledgements

I would like to acknowledge Dr Ulrich Hintermair and Dr M Sankar for providing me with the opportunity to work on such an interesting, albeit demanding, project, as well as the EPSRC and Catalysis CDT for the funding. Thank you, Dr Theo Keane, for your support and for performing quantum chemical calculations. Thanks also to the technical teams in the CCI and in Bath across the schools of chemical engineering, mechanical engineering, pharmacy and chemistry for their training and expertise. With a special mention to Dr John Lowe and Dr Tim Woodman for having faith in our high-pressure NMR tube and letting us put 110 bar in the spectrometer.

I would like to thank my parents and siblings for their support and pretending to understand a word of what I'm saying. Stuart, Matt, David, and Dan for helping to keep me (mostly) sane with boardgames, coffee and conversation. Kasia for reading every word of this thesis and helping me to stay on track. Maya for her support and regular supply of cat videos. Rachel Johnston for running the last few NMR to help solve my last conundrums. I would also like the thank the rest of the Hintermair group, Sankar's group, as well as members of the CCI and Suschem labs for providing a fantastic environment in which to work. Thank you to COVID-19 for the extension, and to my mental health for just about managing to keep itself together.

Finally, I would like to thank Helen for her unwavering support and belief in me, she has dragged me over the finish line and for that I am eternally grateful. Your strength is an inspiration to me every single day.

Abstract

Dialkyl carbonates (DAC) are an important class of compounds for a variety of industries, with demand currently outstripping production for their use as solvents, electrolytes, and fuel additives. Current industrial processes rely on atom inefficient methods of production, such as transesterification or utilise hazardous starting materials such as carbon monoxide or phosgene that come with a large energy and carbon footprint.

The direct synthesis of carbonates from CO_2 and alcohols promises to be a more atom economic route, though the unfavourable thermodynamics of these reactions make the development of efficient processes challenging.

In this work, a number of high surface area pure cerium oxide materials have been produced using polymer templates achieving surface areas exceeding 400 $m^2.g^{-1}$, compared to 50 $m^2.g^{-1}$ for commercial samples. Mixed metal oxides, containing cerium, zirconium, and aluminium, have also been produced by precipitation. These have been evaluated for their activity and stability in the direct synthesis of dimethyl carbonate (DMC) with chemical dehydrating agents and were shown to be stable across five batchwise reuse cycles.

The direct synthesis of DMC using different dehydrating agents has been investigated. The use of diisopropyl carbodiimide (DIC) allows for 20–40% conversion to be achieved in 2–4 h. The use of 2-cyanopyridine allows for similar conversions over 6 h, while also exceeding 80% methanol conversions in 20 h. We observe that the reaction with DIC has an onset temperature of 100 °C, below which the reaction progresses much more slowly. We also observe that the reaction progresses more rapidly at pressures below the critical point of the methanol/CO_2 mixture. Above the mixture critical point, reaction rates are decreased by up to 90% in batch, due to liquid phase expansion by CO_2.

The thermodynamics have been calculated for both the formation of DMC and diethyl carbonate (DEC) from published enthalpies of formation and standard entropies. These show the reaction to be endergonic at 298 K by over 25 $kJ.mol^{-1}$, and the negative entropy of these reactions also shows that the reactions become more endergonic as temperature increases. An iterative multivariate model has been

written to allow for the calculation of equilibrium concentrations of each reaction component. This has been used to determine the best-case equilibrium conversions, as well as in scenarios where wet starting material is utilised. Our model has also been applied in several scenarios where products are continually removed from the reactor, in which we demonstrate that a strategy where both the DAC and the water by-product is removed from the reactor, in a non-reactive manner, allows for greater cumulative conversion than water sequestration alone.

The thermodynamic model has been validated by performing reactions without dehydrating agents with a <5% discrepancy between the experimental and calculated values. A productive flow system for synthesis of DMC and DEC has been demonstrated, with our optimised system showing equal productivity for both DMC and DEC. Evaluation of catalyst stability has also been performed in flow, where a less active ceria-zirconia mixed metal oxide catalyst produced in this work showed superior stability and productivity compared to the commercial cerium oxide catalyst which showed higher activity in batch mode. Further development of the system could allow for continuous removal of products, and recycling of reactants, allowing for a more sustainable production of DACs.

Abbreviations

Å	–	Angstrom
ATR-IR	–	Attenuated Total Reflectance Infrared spectroscopy
BET	–	Brunauer-Emmett-Teller
BPA	–	Bisphenol A
BPR	–	Back Pressure Regulator
°C	–	Degrees Centigrade
Cat.	–	Catalyst
C_p	–	Heat capacity at constant pressure
CSV	–	Comma–Separated Values
ΔG^0	–	Gibbs free energy change at standard conditions
ΔH^0	–	Enthalpy change at standard conditions
ΔH_f	–	Enthalpy change of formation
ΔS^0	–	Entropy change at standard conditions
d	–	Density
D_1	–	Relaxation delay
DA	–	Dehydrating agent
DAC	–	Dialkyl carbonate
DCM	–	Dichloromethane
DIPPR	–	Design Institute for Physical Properties
DEC	–	Diethyl Carbonate
DFT	–	Density Functional Theory
DIC	–	Diisopropyl Carbodiimide
DIU	–	Diisopropyl Urea
DMC	–	Dimethyl Carbonate
$[R]_{eq}$	–	Equilibrium concentration of compound R
DME	–	Dimethyl Ether
DMF	–	Dimethylformamide
DMSO	–	Dimethyl Sulfoxide
DRIFTS		Diffuse Reflectance Infrared Fourier Transform Spectroscopy
EDX	–	Energy Dispersive X-ray spectroscopy
EPA	–	Environmental Protection Agency
EtmimOH	–	1-ethoxyl-3-methylimidazolium hydroxide
EtOH	–	Ethanol
FID	–	Flame Ionisation Detector
FWHM	–	Full Width at Half Maximum
g	–	Gram

Abbreviations

GC	–	Gas Chromatography
h	–	Hour
HPLC	–	High-Performance Liquid Chromatography
IL	–	Ionic Liquid
Im	–	Imidazolium
K	–	Kelvin
$k_{d(obs)}$	–	Observed deactivation constant
k_{eq}	–	Equilibrium constant
kJ	–	Kilojoule
k_{obs}	–	Observed rate constant
L	–	Litre
Li-ion	–	Lithium ion
ln	–	Natural logarithm
µm	–	Micrometre
m	–	Metre
M	–	Molar
mM	–	Millimolar
mA	–	Milliampere
MeOH	–	Methanol
MFI-57	–	Zeolite Membrane
mg	–	Milligram
Min	–	Minute
mL	–	Millilitre
mol	–	Mole
mmol	–	Millimole
MS	–	Mass spectrometry
n	–	Number of moles
NIST	–	National Institute of Standards and Technology
NMR	–	Nuclear Magnetic Resonance Spectroscopy
NS	–	Number of scans
OATS	–	Organic Aqueous Tuneable Solvents
p	–	Productivity
P	–	Pressure
pH	–	Potential of hydrogen ($-\log_{10}([H^+])$
PID	–	Proportional Integral Derivative control
PKa	–	Acid dissociation constant ($-\log_{10}(k_a)$)
ppm	–	Parts per million
PVA	–	Polyvinyl Alcohol

Abbreviations

pXRD	–	Powder X-ray Diffraction
QCC	–	Quantum Chemical Calculation
R	–	Ideal gas constant (8.314 $J.K^{-1}.mol^{-1}$)
R^2	–	linear correlation coefficient
$Rate_0$	–	Rate at 0 concentration
Ref	–	Reference
RPM	–	Revolutions Per Minute
S	–	Entropy
SBA-15	–	Santa Barbara Amorphous type material (mesoporous silica)
$scCO_2$	–	Supercritical carbon dioxide
SEM	–	Scanning Electron Microscopy
SRK	–	Soave-Redlich-Kwong
t	–	Time
$t_{1/2}$	–	Half life
T	–	Temperature
T_0	–	Starting temperature
TCD	–	Thermal Conductivity Detector
TDE	–	ThermoData Engine
TGA	–	Thermal Gravimetric Analysis
THF	–	Tetrahydrofuran
TMM	–	Trimethoxy Methane (methyl orthoformate)
TOF	–	Turnover Frequency
TON	–	Turnover Number
TPD	–	Temperature Programmed Desorption
TPR	–	Temperature Programmed Reduction
v	–	Volume
VOC	–	Volatile organic compound
XRD	–	X-Ray Diffraction

Table of Contents

Table of Figures

Table of Schemes

Table of Tables

Chapter 1 - Literature review

This literature review aims to provide some background on the synthesis and applications of dialkyl carbonates (DACs). The first part of this review will focus on the applications of DACs, which have been used as green solvents for organic reactions,[1] as reagents for alkylation and alkoxycarbonylation,[2] and as fuel additives due to their high oxygen content and octane number.[3] Two dialkyl carbonates in particular are of interest as bulk chemicals, due to their versatility: dimethyl carbonate (DMC) and diethyl carbonate (DEC). The market for DACs is projected to increase in value, the DMC market is currently valued at around $895 million and is projected to grow to $1.2 billion by 2024.[4] The second part of this review focuses on the synthesis and the challenges involved in terms of safety, productivity and substrate scope.

1.1 Applications of dialkyl carbonates

1.1.1 Solvents

Solvents are widely used in catalysis and organic synthesis, and typically account for 80–90% of total reaction volume.[5] Due to this, using solvents that are safe, both for the user and for the environment, is preferred. Dialkyl carbonates, and specifically DMC and DEC, have similar safety profiles to acetone, and in some instances, they can replace chlorinated solvents which are widely used.

For solvents to be successful as replacements however, it is not enough to be greener, they need to be able to facilitate reactions to the same or greater extent than the solvents they replace.[6] Organic carbonates belong the same category as DMSO and DMF, polar aprotic solvents. Unlike these however, DMC and DEC show lower miscibility with water and have lower boiling points (90 and 125 °C respectively), making them easier to separate, recover and reuse.

DMC has a similar polarity to solvents such as dichloromethane (DCM) whilst also being safer both within the laboratory and in the environment.[7] Safety and polarity are just two factors that determine the use of a solvent however, and DMC has been shown to be effective in a wide variety of reactions.[7–9] Moreover, in the paint and coatings industry, DMC has also been used in formulations in

the US due to its fast evaporation and status as an EPA volatile organic compound (VOC) exempt solvent.[10]

The lithium ion battery industry also relies on carbonates. Ethylene carbonate is used as an electrolyte solvent due to good solvent properties for lithium ions and stability in charge and discharge cycles.[11,12] Linear carbonates such as DMC and DEC are also added as they provide properties which are synergistic with ethylene carbonate. The addition of linear carbonates supresses the melting point of ethylene carbonate, allowing batteries to be used at lower temperatures. Their addition also reduces solvent viscosity, which improves ion transport. Proprietary blends of ethylene carbonate with a variety of dialkyl carbonates are now standard within the lithium ion battery industry.[13]

1.1.2 Organic transformations

Traditionally organic transformations rely on the use of high energy reactive reagents. Reagents such as methyl iodide (MeI), for methylation reactions, and phosgene, for methoxy carbonylation reactions. The toxicity of the halogenated by-products is not commonly considered when developing new synthetic routes, however these can have a major impact on the economic and ecological footprint of the process when scaled up. Dialkyl carbonates have been shown to be able to replace these reagents in some reactions.[14]

An example for this is in the synthesis of anisole,[15] reagents such as dimethyl sulphate and MeI can be replaced with DMC (Scheme 1.1). This produces less hazardous waste and has a higher atom economy (59% for DMC vs 40% for MeI and dimethyl sulphate).

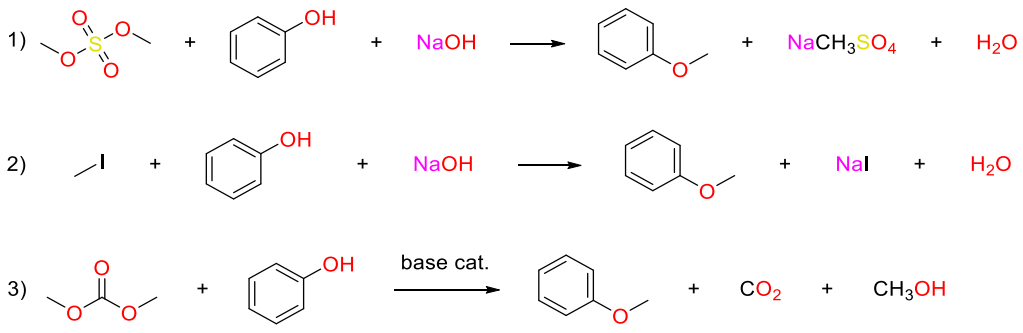

Scheme 1.1: Anisole synthesis from phenol with Dimethyl sulphate (1), MeI (2), and DMC (3).[15]

In terms of the mass of waste produced, a simple e-factor calculation for the above reactions was performed.[16] At its most simple, e-factor is a measure of the ratio of waste to product mass (Equation 1.1).

Equation 1.1 $$e - factor = \frac{kg\ waste}{kg\ product}$$

Based on reaction stoichiometry the DMC reaction has an e-factor of 0.7, and the dimethyl sulphate and MeI reactions have e-factors of 1.4 and 1.5 respectively. Indicating that the DMC reaction produces 30% more product than waste by mass. This can be extended by multiplication by an arbitrarily assigned "unfriendliness" quotient, to take into account the difference between 1 kg of waste H_2O and 1 kg of waste NaI.[17]

Other transformations that utilise DACs include the alkylation of aromatic amines,[2] mono-methylation of drug intermediates,[18,19] methylation of alkyl aryl sulphones,[20] the upgrading of succinate to dimethyl succinate,[8] and many others[21] have been reported.

Whilst DMC and DEC are classified as green solvents,[1,22] they are synthesised in a variety of ways. Each method has its drawbacks, either in terms of waste generated, toxicity of starting materials, or high energy costs. In order for these compounds to be truly "green", we must take into consideration not only the synthesis of the carbonates themselves, but also the upstream and downstream processes.

1.2 Synthesis methods

1.2.1 Phosgenation of alcohols

Historically carbonates have been synthesised using phosgene. Whilst its use in chemical transformations is not unheard of, for safety and product quality, there have been efforts to replace it.[23–25] Phosgene is a known nerve agent and was used as a chemical weapon in the first world war.[26] Its synthesis uses carbon monoxide and chlorine gas, themselves hazardous reagents. The synthesis of DACs from phosgene (Scheme 1.2) produces stoichiometric amounts of hydrochloric acid, which needs to be neutralised and disposed of safely.

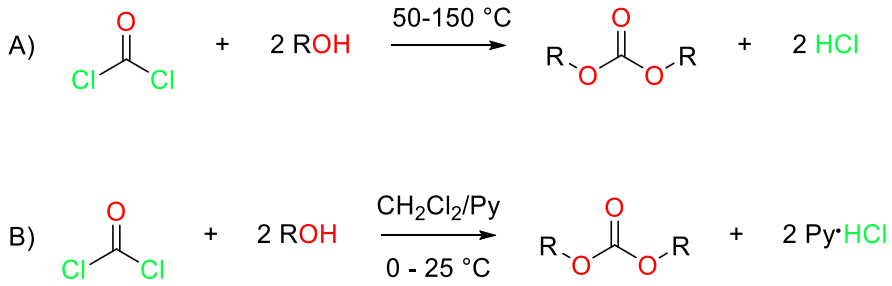

Scheme 1.2: Synthesis of dialkyl carbonates from phosgene and alcohols without a base (A) and in the presence of a base (B).

Phosgenation does, however, have a wide substrate scope. As a result, it is capable of producing carbonates from small alcohols such as methanol and ethanol, sterically hindered alcohols such as tert-butanol,[27] large drug molecules[28] and cyclic carbonates from diols.[29] Substituting phosgene with safer variants such as di-phosgene and tri-phosgene has been used to synthesise a variety of cyclic carbonates with good yields.[30] In practice, the use of phosgene without a base leads to lower performance and selectivity. Bases such as pyridine or tri-ethyl amine are typically used to increase reaction efficiency (Scheme 1.2B).[31] This also lowers the required temperature for the reaction to progress to between 0–25 °C (down from 50–150 °C).[32] Reactivity towards alcohols favours aliphatic alcohols over aromatic and is slower for more acidic alcohols such as phenol.

The use of phosgene in the production of carbonates can lead to chloride contamination in downstream processes. For dialkyl carbonates used in polycarbonate synthesis, chloride compounds such as NaCl, chloroformates and chlorinated hydrocarbons, in concentrations up to several hundred ppm have been observed, decreasing performance in downstream moulding.[33] For bulk chemicals this cost and decrease in performance may not be economical. For fine chemicals and pharmaceuticals however, the increased substrate scope may be worth the extra costs for purification.

Therefore, due to safety and product quality, other methods for dialkyl carbonate synthesis are preferred.

1.2.2 Alcoholysis of urea

Alcoholysis of urea (Scheme 1.3) is a more attractive route to dialkyl carbonates than phosgenation due to lack of chlorinated waste.

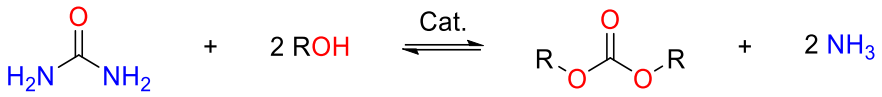

Scheme 1.3: Alcoholysis of urea to form a dialkyl carbonate and ammonia.

The waste ammonia from the alcoholysis can be reacted with carbon dioxide to regenerate the urea (Scheme 1.4A).[34] Depending on the conditions used, the ammonia will boil out of the reaction vessel, providing the driving force for the reaction by shifting the equilibrium position.[35]

The alcoholysis reaction could be considered a pre-dehydrated form of the direct synthesis from CO_2 and alcohol, as the formation of urea from CO_2 and ammonia releases water as a by-product. This essentially makes the alcoholysis of urea, from start to finish, equivalent to the direct synthesis from CO_2 and alcohols (Scheme 1.4). With the water producing step physically separated from the carbonate producing step.

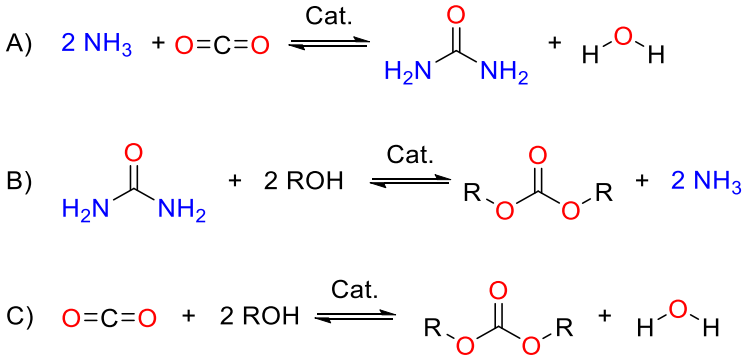

Scheme 1.4: A) Formation of urea from NH_3 and CO_2 with H_2O as a by-product. B) formation of dialkly carbonate by the alcoholysis of urea with NH_3 as a by-product. Combining A and B gives an overall reaction scheme of C) Synthesis of dialkyl carbonates from CO_2 and alcohol.

The utility of this method relies on process economics. The generation of urea from NH_3 and CO_2 requires high temperatures and pressures and is reversible. Upstream from this is ammonia synthesis from N_2 and H_2, which also requires high temperature and pressure and is again reversible. Whilst the alcoholysis step is attractive at first glance, considering the overall footprint of the process makes this method of dialkyl carbonate synthesis less enticing from a carbon footprint perspective, especially as H_2 for ammonia synthesis is usually produced by the steam reforming of methane.

Table 1.1 shows some of the substrates investigated in alcoholysis reactions. Several different alcohols and catalysts have been investigated and good yields

have been demonstrated for a range of alcohols, with glycols and glycerol achieving greater than 90% yields.[36–38]

Table 1.1: Substrates and reaction conditions investigated for urea alcoholysis reactions.

Alcohol	Reaction Temperature (°C)	Catalyst	Carbonate yield (%)	Ref
Methanol	140	Polyphosphoric acid	67	39
Ethanol	190	Mn-Mg-Al	57	40
Glycerol	150	AuPd/MgO	93	36
1,2-Propylene glycol	180	Zn-Cr mixed metal oxide	98	37
Ethylene glycol	150	ZnO	93	38

Like the phosgenation reactions, the alcoholysis of urea has good substrate scope. However, this method may still not be considered "green" due to the upstream energy cost of ammonia and urea production. Special considerations also need to be taken when dealing with ammonia waste, which in the presence of water is corrosive.

1.2.3 Oxidative carbonylation of alcohols

Oxidative carbonylation (Scheme 1.5) utilises carbon monoxide as a C_1 source which bypasses the need for the use of ammonia to make a more reactive starting material.

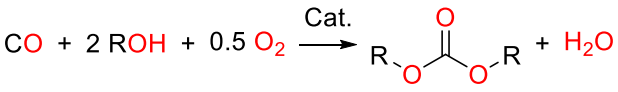

Scheme 1.5: Synthesis of dialkyl carbonates by oxidative carbonylation.

This method is more atom economic than phosgenation and urea alcoholysis, as the only by-product is water. The "green" credentials of oxidative carbonylation come from the source of the carbon monoxide and alcohol. Scheme 1.6 shows several methods of carbon monoxide and methanol production. Carbon monoxide production from steam reforming (Scheme 1.6A) or CO_2 reforming (Scheme 1.6B) produce hydrogen as a by-product. This syngas (mixture of carbon monoxide and hydrogen) can then be utilised for methanol synthesis

(Scheme 1.6D) or the hydrogen used for the reverse water gas shift reaction (Scheme 1.6C). "Greener" syngas can be produced from agro-industrial biomass[41] and utilises carbon recently captured from the atmosphere whereas steam or CO_2 reforming of methane[42] by comparison utilises fossil carbon.

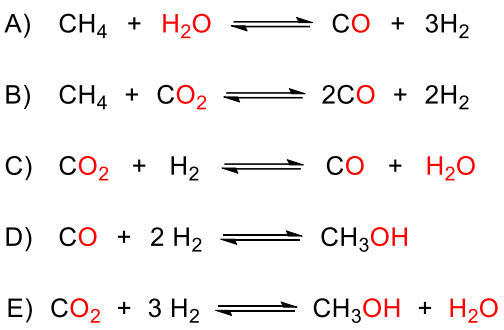

Scheme 1.6: Synthesis of CO by steam reforming (A) and CO_2 reforming of methane (B) or by reverse water gas shift (C), and the synthesis of methanol from syngas (D) and CO_2 (E).

If a reverse water-gas shift reaction[43–45] is used, the overall oxidative carbonylation reaction is indirectly from CO_2 and alcohol. The waste produced by oxidative carbonylation is much safer when compared to HCl, from phosgenation, or ammonia, from alcoholysis of urea.

The first example of oxidative carbonylation of methanol was developed in 1983 by the Enichem Company and was a liquid phase process utilising a CuCl catalyst.[14] In 1986 a vapour phase process was then developed by the Dow Company which did not suffer from the same corrosion issues as the liquid phase process.[46] The catalyst and reaction conditions can be tuned to give carbonates, using a CuCl catalyst, (Scheme 1.5) or oxalates (Scheme 1.7), with a mixture of $Pd(acac)_2$ and CuCl.[47]

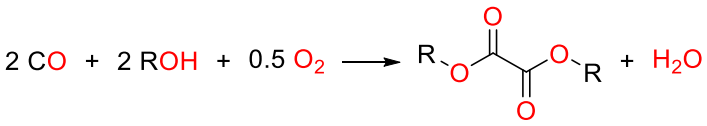

Scheme 1.7: Synthesis of dicarbonate by oxidative carbonylation of alcohols.[47]

Another variation of the oxidative carbonylation reaction utilises methyl nitrite as an intermediate with a two-step reactor system[48] (Scheme 1.8) which was originally developed by UBE as a method of dimethyl oxalate production.[49]

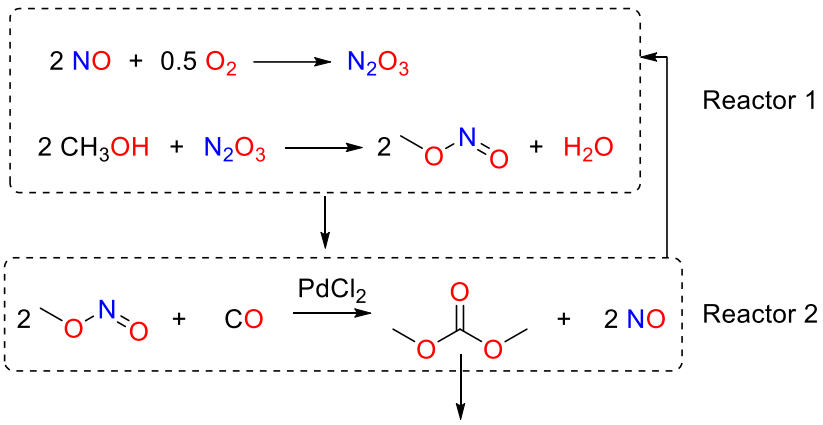

Scheme 1.8: Two-step reactor system for indirect oxidative carbonylation of a methanol via methyl nitrite.[48]

Oxidative carbonylation yields alcohol conversions ranging from 20-30% with selectivity up to 95% at 100 °C.[50] Substrate scope for this method has been shown to be broad (Table 1.2). Linear carbonates from ethanol[51] and methanol[50,52] have been synthesised. Aromatic carbonates have also been synthesised with phenol for the synthesis of diphenyl carbonate.[53,54] Cyclic carbonates, such as glycerol carbonate, have also been synthesised using this method.[54]

Table 1.2: A selection of substrates and reaction conditions investigated for oxidative carbonylation reactions.

Alcohol	Reaction temperature (°C)	Catalyst	Carbonate yield (%)	Ref
Ethanol	120	$CuCl_2$/[BMIm]BF_4	38.8	51
Methanol	100	$LiSeO_2(OCH_3)$	30.7	50
Methanol - Methyl nitrite	120	(Pd–$CuCl_2$)/γ-Al_2O_3	70.9	52
Glycerol	140	$PdCl_2$(Phen)/KI	92	54
Phenol	120	COSalen	37.0	53
Phenol	100	Pd/10% PbO-$MnFe_2O_4$	33.1	54

1.2.4 Transesterification of carbonates

Transesterification enables the synthesis of bulky carbonates, such as polycarbonates, by transesterifying easily produced carbonates with the desired alcohol (Scheme 1.9).

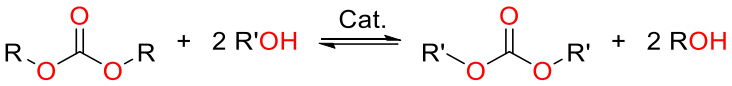

Scheme 1.9: General reaction scheme for transesterification of carbonates.

Carbonates such as ethylene- or propylene carbonates can be synthesised by reaction of CO_2 with a reactive species as a starting material, followed by transesterification with an alcohol. This method is utilised by the Japanese company, Asahi Kasei, in their bisphenol-A polycarbonate synthesis.[25,33] This process starts with the epoxidation of ethylene to ethylene oxide, which is then reacted with CO_2 to give ethylene carbonate (Scheme 1.10A). The ethylene carbonate is then trans-esterified with methanol to give DMC and monoethylene glycol (Scheme 1.10B), which is made selectively and in high yield. This method produces less CO_2 per tonne of carbonate than the equivalent phosgenation.[55] However, the ethylene or propylene oxide, which is used for 90% of DMC produced in China,[46] is usually fossil fuel derived.

From the DMC, other carbonates can be produced such as diphenyl carbonate from transesterification of DMC with phenol (Scheme 1.10C). Asahi Kasei then polymerise bisphenol-A by transesterification of the diphenyl carbonate to give a polycarbonate and phenol (Scheme 1.11A).

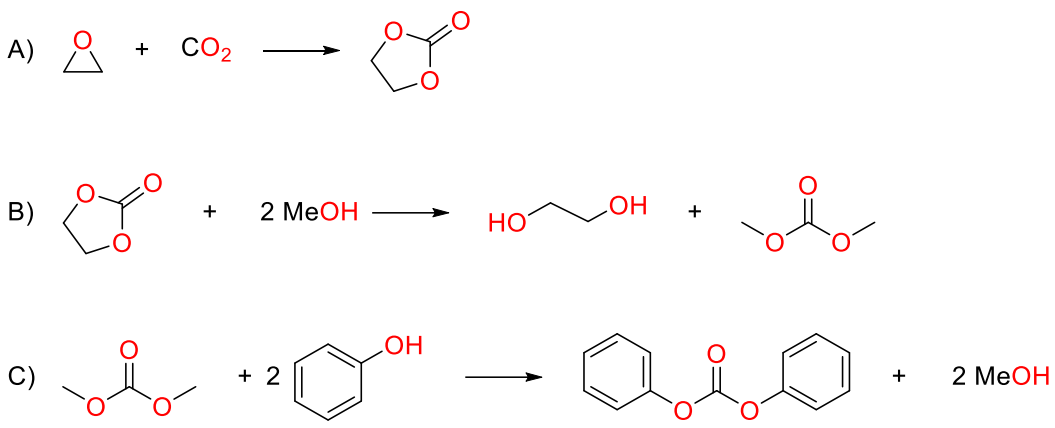

Scheme 1.10. A) Synthesis of ethylene carbonate from CO_2 and ethylene oxide. B) Transesterification of ethylene carbonate with methanol to give mono ethylene glycol and DMC. C) Transesterification of DMC with phenol to give diphenyl carbonate and methanol.

Scheme 1.11 shows three routes to polycarbonates from transesterification of linear carbonates. In the Asahi Kasei process this leads to lower molecular weight polycarbonates (n ≈ 10–20) which then undergo solid-state polymerisation to produce higher molecular weight engineering plastics (n ≈ 30–60).[23,25,56] Transesterification has also been used in polyisosorbide carbonate synthesis, both from DPC (Scheme 1.11B) and DMC (Scheme 1.11C).[56]

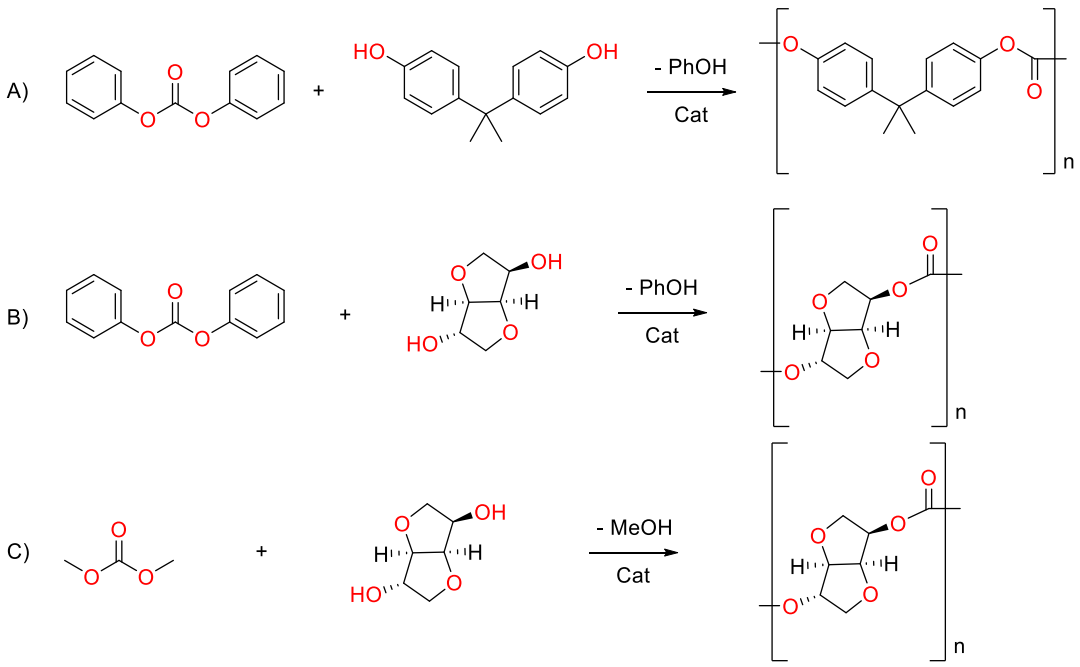

Scheme 1.11: Transesterification to poly-BPA carbonate (A) and poly-isosorbide carbonate (B, C).

Transesterification enables a multitude of carbonates to be synthesised but produces more by-products than other methods. Some of these by-products,

such as monoethylene glycol are valuable, and the Asahi Kasei process recycles their waste methanol and phenol. Transesterification is a viable method for producing polycarbonates, as the atom economy of transesterifying a small carbonate, such as DMC, with a large alcohol, such as isosorbide, is greater than the inverse. For bulk dialkyl carbonate synthesis however, this method is too wasteful unless the by-products also have a suitable market.

1.2.5 Direct synthesis of dialkyl carbonates

Each of the above methods have their advantages, particularly the use of reactive starting materials which makes the reaction progress rapidly. However, each of the methods presented above can utilise CO_2 in their reaction or reagent synthesis. Utilising CO_2 directly therefore, improves the atom economy as the only waste product produced is water (Scheme 1.12).

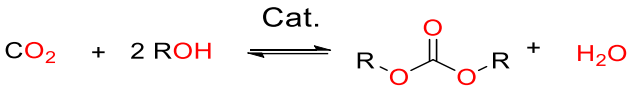

Scheme 1.12: Direct synthesis of dialkyl carbonate from CO_2 and alcohols.

Due to the low toxicity of its starting reagents and by-products, the direct synthesis of DACs is considered "green". The direct synthesis of dimethyl carbonate has been widely investigated in a number of conditions with heterogeneous catalysts,[57–79] basic catalysts[80–82] and ionic liquids[83,84].

For the two dialkyl carbonates of interest: DMC and DEC, renewable feedstocks exist. Methanol can be produced by pyrolysis[85] and gasification[86] of waste biomass. Ethanol can be produced from fermentation of agricultural waste,[87,88] the fermentation itself producing CO_2 which could be captured and used for synthesis.

The direct synthesis is less hazardous than most of those discussed above, there is no phosgene, carbon monoxide, HCl waste or ammonia. Unlike oxidative carbonylation, there are also no pressurised oxygen and flammable gas mixtures involved. Thermodynamics are the major downside for the direct synthesis, due to the high stability of CO_2.[55] Reported numbers vary, but agree that the direct synthesis of DMC and DEC are exothermic but endergonic due to unfavourable entropic contributions.[76,89,90]

The direct synthesis does, however, have the advantage of using benign starting materials and producing benign by-products. This reaction also adheres to most of the principles of green chemistry listed below:[91]

1. Prevents waste – The synthesis produces only the desired product and water. Utilises CO_2, a waste product from other industries.
2. Atom economic – DMC synthesis directly from CO_2 and methanol uses 83% of the starting atoms in the product, DEC uses 86%.
3. Less hazardous synthesis – When compared to phosgene and oxidative carbonylation, the direct synthesis uses much safer starting materials and produces safer by-products.
4. Safe chemicals – As above, the most toxic reagent in the direct synthesis is likely to be the alcohol or catalyst.
5. Benign solvents – At higher pressures, the synthesis can be conducted in a supercritical CO_2 solvent, allowing for facile separation of the solvent from the reactants.
6. ~~Design for energy efficiency~~ – Current state of the art utilises high pressures and temperatures.
7. Renewable feedstocks – The production of methanol and ethanol from agro-industrial waste is possible. A by-product from this, as well as many other industries, is the CO_2 also required for the reaction.
8. Reduces derivatives – No need for epoxide or methyl nitrite intermediates.
9. Catalysis – Allows for CO_2 activation and removes the need for stoichiometric quantities of high energy reagents.
10. Design for degradation – Both DMC and DEC are biodegradable and pose low eco-toxicity.
11. ~~Real-time analysis for pollution prevention~~ – This could be implemented but direct synthesis is currently not undertaken industrially.
12. Inherently benign chemistry for accident prevention – Does not require the use of oxygen in the presence of combustible materials. Or the use of a nerve agent or its derivatives.

1.2.6 Comparison of DAC synthesis methods

Table 1.3 shows a comparison of the different synthesis methods. Phosgenation and oxidative carbonylation both use toxic starting materials, the other methods are low in comparison, though this depends on the alcohol being used, as methanol is more toxic than ethanol. Most of the methods presented above present a wide substrate scope, phosgenation and urea alcoholysis for example, allows for the synthesis of linear, cyclic, aliphatic, and aromatic carbonates. The direct synthesis by comparison has a lower substrate scope, though this may be due to the focus on dimethyl and diethyl carbonate.

Each method produces waste products, the toxicity of these products is an important consideration for process safety and environmental impact. The least toxic waste is produced by oxidative carbonylation and the direct synthesis, followed by transesterification which gives an alcohol product. More hazardous waste products are produced by phosgenation and urea alcoholysis which produces chloride waste and ammonia respectively, both of these can potentially cause corrosion which increases capital costs for safety measures.

Energy usage is usually correlated to the reaction conditions, however it is important to recognise the upstream energy usage too. The phosgenation reaction occurs between 0–25 °C which is classified here as low reaction energy, but the CO and Cl_2 synthesis to produce phosgene are somewhat energy intensive, relying on partial oxidation or reforming for CO and brine electrolysis for Cl_2. Urea alcoholysis can occur from 100–200 °C which is classified has moderate to high, however the upstream energy use in both ammonia, from the Haber-Bosch process, and urea production are very high.[92] Oxidative carbonylation, transesterification and the direct synthesis each have moderately energy intensive reactions, with reaction temperatures between 80–140 °C, however the upstream energy usage for transesterification and direct synthesis is much lower than the other methods due to their much simpler and easier to produce reagents.

Good selectivity has been demonstrated with each of the synthesis methods, urea alcoholysis however forms carbamates and transesterification can produce a mixture of carbonates. The direct synthesis is highly selective without a dehydrating agent, and has been demonstrated exceeding 95% even in the

presence of nitrogen containing dehydrating agents.[72,93,94] Most of the methods are performed neat, or with the alcohol as the solvent. Phosgenation however requires halogenated solvents, further decreasing the "green" profile of the waste produced. Finally, the yields for the direct synthesis depend on the catalyst system, heterogeneous metal oxides rarely exceed 1% conversion without a dehydrating agent present.[69,78] However base + MeI systems can achieve >10% conversions, though produce stoichiometric halogenated waste.[80,82] Similarly, with dehydrating agents, >80% conversions have been achieved,[72,93,94] though this decreases the atom economy and increases waste products. The other methods investigated have been shown to achieve >90% yields, depending on the alcohol and conditions used.

Table 1.3: Comparison of synthesis methods across several metrics. [a]without a dehydrating agent. [b]with a dehydrating agent (DA). [c]without a base. [d]with a base.

	Phosgenation	Alcoholysis of urea	Oxidative carbonylation	Trans-esterification	Direct synthesis	
Substrate Toxicity	High	Low	High	Low	Low	
Substrate scope	High	High	Moderate	High	Low	
Waste products	Chloride waste	Ammonia	Water	Alcohols	Water[a]	Hydrated DA[b]
Reaction energy usage	Low	Moderate /High	Moderate	Moderate	Moderate/high	
Upstream energy usage	Moderate	High	Moderate	Low	Low	
Yields	High	Moderate	Moderate	High	Low[a]/High[b]	
Selectivity	Moderate[c]/High[d]	Moderate	High	Moderate	High	
Solvent	CH_2Cl_2	Neat	Neat	Alcohol	Neat	

Based on the advantages and disadvantages presented in Table 1.3 the direct synthesis has low toxicity and requires few upstream steps, making the route attractive for sustainable synthesis of DMC and DEC as bulk chemicals. The direct synthesis allows us to utilise CO_2 directly for the synthesis of valuable products, the greatest challenge to overcome are the low yields associated with this method. For the formation of regioselective carbonates in fine chemicals or

pharmaceuticals, urea alcoholysis or phosgenation give the higher substrate scopes necessary. The larger profit margins for these classes of chemicals offset the cost of waste remediation and the smaller throughput makes for safe handling of the resultant hazardous materials.

1.3 CO_2 Utilisation

CO_2 is produced on the gigatons scale, with emissions coming from virtually every sector, from energy generation, to transport, and agriculture. In 2010 an estimated 32 gigatons of CO_2 were emitted globally due to fossil fuel use.[95] CO_2 is still regarded as a benign waste product and is allowed to be released into the atmosphere where it is one of the leading causes of anthropogenic climate change.

Of the many ways this issue is being addressed, one is to make use of waste CO_2 in other processes and use it as a raw material and carbon source. Poliakoff, Leitner and Streng[96] laid out twelve principles to evaluate carbon dioxide utilisation. In their paper they highlight the need for integrating carbon capture and storage with its subsequent use. This would require industry that utilises CO_2, either as a solvent or as a starting material, to be adjacent to sources of CO_2 production to minimise the need for transportation. A relevant consideration for this thesis is that thermodynamics cannot be beaten, however, "it may be possible to side-step thermodynamic barriers by deliberately avoiding equilibrium situations".[96] Therefore, making use of CO_2 as a starting material in endergonic processes may involve not allowing the system to reach equilibrium, but to operate in a kinetically controlled regime.

The use of CO_2 as a C_1 source is extensive, and it has been used in functionalisation of heterocycles,[97] synthesis of formic acid,[98] synthesis of carboxylates[99] and the synthesis of cyclic carbonates from epoxides[23,25,100,101] amongst others. Due to its abundance CO_2 is available cheaply and as such makes an ideal starting material, with the main concern being purity.

1.3.1 Supercritical CO_2 as a solvent

CO_2 has not only found use as a renewable feedstock but also as a solvent. Its low critical pressure and temperature makes it accessible as a supercritical solvent. Whilst this form of utilisation does not consume CO_2, it can allow for

the replacement of petroleum-based solvents in some instances (such as the replacement of benzene and DCM in caffeine extraction). As an extraction solvent, $scCO_2$ is favoured by the food industry due to its negligible residual toxicity, tuneable solvent power, high diffusivity and ease of removal, and is thus used in a number of processes.[102–107]

The supercritical phase is achieved by taking the compound beyond its critical temperature and pressure but below the pressure required to condense it into a solid. Figure 1.1 shows the phase diagram for CO_2, the supercritical point of CO_2 being at 31.0 °C and 73.8 bar.

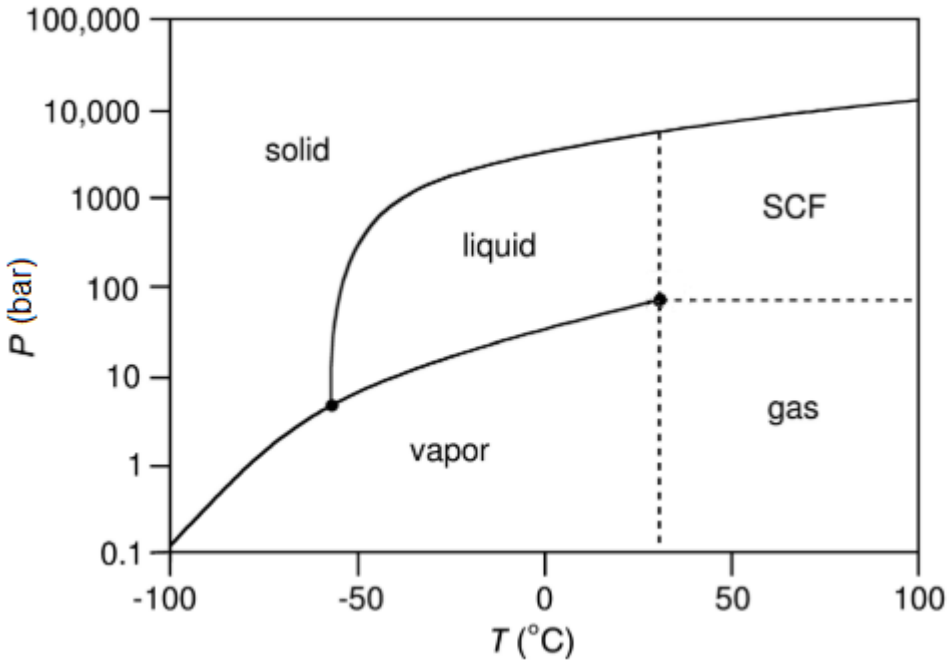

Figure 1.1: Phase diagram of CO_2. Filled circles highlight the triple and critical points. [Modified from The Handbook of Green Chemistry].[108]

In the region close to the supercritical point, known as the compressible region, density can be tuned, with changes to temperature and pressure, to vary its physico-chemical properties. Supercritical fluids exhibit the diffusivity of a gas, but with solvation power similar to that of a liquid.[109] With increasing density the solvation power typically increases. Figure 1.2 shows that at 40 °C and 500 bar, $scCO_2$ has a similar Hildebrand solubility parameter to cyclohexane, and at 230 bar is similar to n-hexane. The steep slope at 40 °C is within the compressible region, whereas 100 °C is outside of this region, giving rise to a shallower gradient. The range of Hildebrand parameters across the temperatures

and pressures shown gives an impression of the tuneability of $scCO_2$ when used as a solvent.

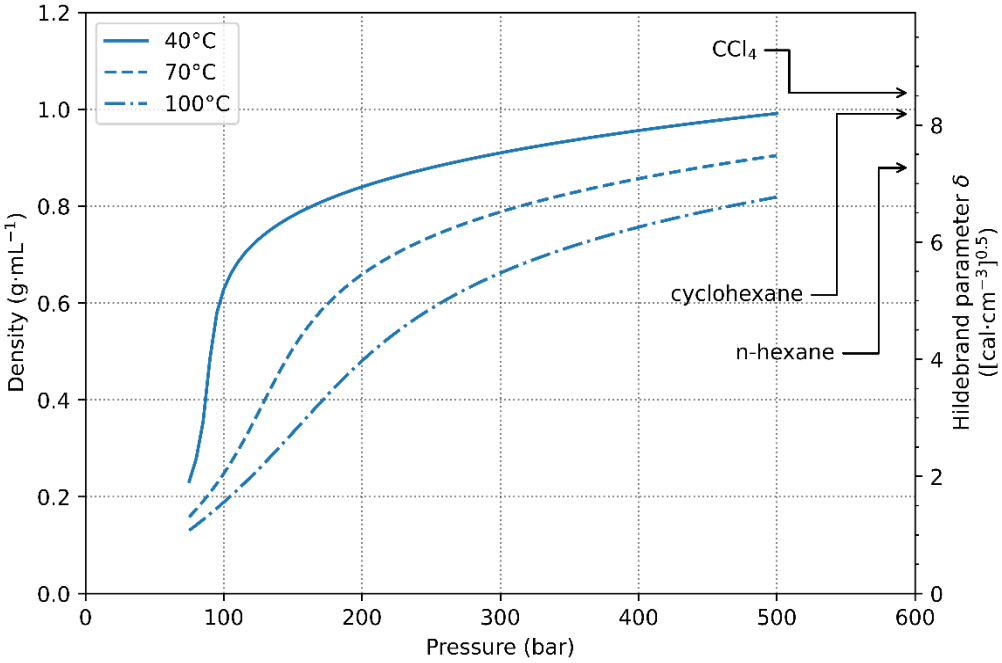

Figure 1.2: Density and solvent power of $scCO_2$ as a function of temperature and pressure. Density/pressure data obtained from NIST isothermal properties[110]*, Hildebrande parameters obtained from Belmares* et al.[111] *adapted from Handbook of Green Chemistry.*[108]

Due the solvation power of $scCO_2$, this would allow for alcohols and CO_2 to exist as a single phase, improving the mixing of the two main components in the direct synthesis.

1.3.2 Subcritical CO_2 for product separation

Near- but sub-critical conditions are also of interest for product separation and green engineering, especially in multi-component systems. Under supercritical conditions a single phase exists, under subcritical conditions however, two or more phases can exist together.

The composition of each phase is therefore theoretically tuneable across a range of conditions, this is especially useful when multiple components with differing solubilities in CO_2 are used. This is the case with organic aqueous tuneable solvents (OATS), reported by Pollet *et al.*[110] In OATS, a homogeneous reaction can be undertaken in a mixed organic and aqueous solvent such as water-THF. The mixture is then subjected to CO_2 pressures which lead to a separation of the two phases (Figure 1.3). This is due to CO_2 dissolving into the THF and

lowering the temperature required for a liquid-liquid phase boundary to form, and decreasing the mutual solubility that exists between pure THF and water. Upon the formation of the liquid-liquid bisphasic system, the organic phase containing hydrophobic components can then be removed from the reactor and purified. This use of CO_2 as a solubility switch has also been used elsewhere for catalyst use and recovery.[112]

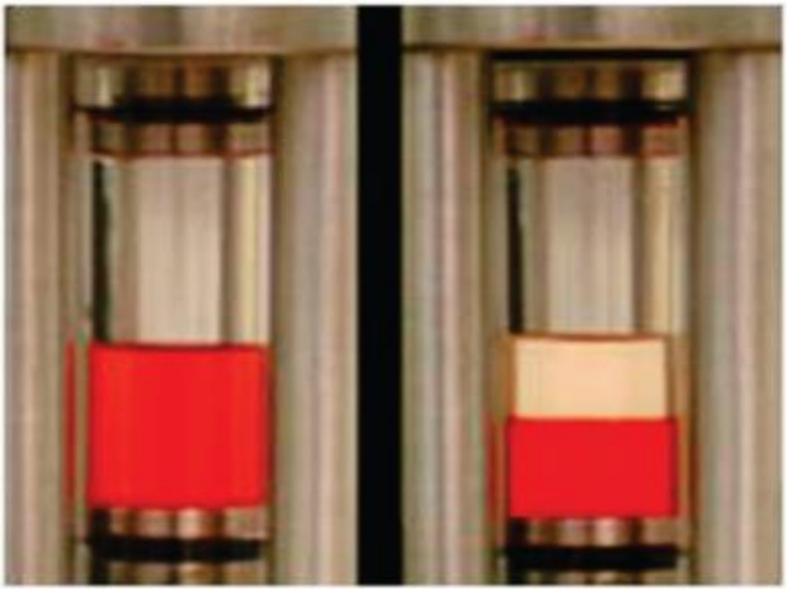

Figure 1.3: Water-THF mixture with water soluble red dye. Left: Ambient pressure. Right: 30 bar CO_2 [Reproduced with permission from Pollet et al.*][110]*

The solubility of different components in subcritical CO_2 (and other gases) systems broadly fall into three classes:

Class I:

The liquid and vapour phases are poorly soluble with each other. An expansion of the liquid phase occurs but usually increases by less than 10% of the initial volume. This is due to the poor solubility of the gas within the liquid, which is the case for CO_2 and water. Though physical properties remain similar, other properties, such as pH, may change.

Class II:

In a class II system, the solubility of the gas in the liquid phase is much greater. Likewise, the miscibility of the liquid with the gas phase, driven by vapour pressure, is also greater. For CO_2, class II compounds include many organic solvents and fluorocarbons. The expansion of the liquid phase with these

compounds is much greater than is observed with class I, up to several times their initial volume. These compounds typically expand in a non-linear fashion with increasing pressure.

Class III:

Class III systems are categorised by the lack of mutual solubility between the two phases (sometimes called asymmetric mixtures). In these systems, the gas can dissolve into the liquid phase up to its saturation point, causing some change in physico-chemical properties and volumetric expansion, however the liquid does not enter the vapour phase. This expansion is typically linear with increasing pressure. Examples of class III compounds include ionic liquids, which have negligible vapour pressures, and polymers. These systems have been used for liquid biphasic catalysis where the catalyst is immobilised in the liquid phase.[98]

Phase separation of mixtures of two class II systems has also been observed. Due to the differences in gas-liquid mixing enthalpies different components within the mixture can become separated under certain conditions.[113] This has been demonstrated with cyclohexane-ethanol and cyclohexane-DMSO among others.[113] This occurs when mixing with the vapour phase becomes more enthalpically favourable than mixing with the other liquid phase, though this is dependent upon the composition of the mixtures.

The use of CO_2 as a starting material is enticing due to the current global climate emergency. However, the possibility of selectively solvating individual reaction components within a sub- or supercritical CO_2 solvent gives the possibility of removing components from the reaction. This is exciting from a process engineering perspective as it may allow for the avoidance of equilibrium conditions discussed above.

1.4 Summary

The use of halogenated solvents and high-energy starting materials can have significant implications for the safety and sustainability of chemical processes. Dialkyl carbonates can act as more benign replacements for these both as solvents and reagents in several reactions.

Dialkyl carbonates can be considered "green" if oxidative carbonylation, transesterification or the direct synthesis from CO_2 are used in their production. These methods each have renewable feedstocks available for each component. Each of the synthesis methods discussed in this chapter have pros and cons and a compromise needs to be found. Generally, a trend is observed that substrate scope and high yields are achieved at the expense of atom economy, whilst safety and atom economy are achieved at the expense of yields and substrate scope. This thesis aims to demonstrate that high yields may be obtained without sacrificing safety and atom economy by utilising CO_2.

This thesis investigates how high DAC yields may be obtained from the direct condensation of CO_2 with alcohols by utilising the tuneable solvent properties of CO_2 to enable product separation.

1.5 References

(1) Alder, C. M.; Hayler, J. D.; Henderson, R. K.; Redman, A. M.; Shukla, L.; Shuster, L. E.; Sneddon, H. F. Updating and Further Expanding GSK's Solvent Sustainability Guide. *Green Chem.* **2016**, *18* (13), 3879–3890. https://doi.org/10.1039/c6gc00611f.

(2) Trotta, F.; Tundo, P.; Moraglio, G. Selective Mono-N-Alkylation of Aromatic Amines by Dialkyl Carbonate under Gas-Liquid Phase-Transfer Catalysis (GL—PTC) Conditions. *J. Org. Chem.* **1987**, *52* (7), 1300–1304. https://doi.org/10.1021/jo00383a024.

(3) Pacheco, M. A.; Marshall, C. L. Review of Dimethyl Carbonate (DMC) Manufacture and Its Characteristics as a Fuel Additive. *Energy and Fuels* **1997**, *11* (1), 2–29. https://doi.org/10.1021/ef9600974.

(4) Dimethyl Carbonate Market by Application (Polycarbonate Synthesis, Battery Electrolyte, Solvents, Reagents), End-Use Industry (Plastics, Paints & Coatings, Pharmaceuticals), Grade (Industry, Pharmaceutical, Battery), Region - Global Forecast to 2024 https://www.researchandmarkets.com/reports/4900562/dimethyl-carbonate-market-by-application?utm_source=dynamic&utm_medium=CI&utm_code=ptl6jq&utm_campaign=1341583+-+Global+Dimethyl+Carbonate+Market+Set+to+Exceed+%241.2+Billion+by+2024+-+Dimethyl+Carbonate+as+an+Oxygenated+Fuel+Additive+Presents+Lucrative+Opportunities&utm_exec=joca220cid (accessed Aug 3, 2020).

(5) Sansom, C. Solvents and Sustainability. *Chem. World* **2018**, *15* (4), 50–53.

(6) Welton, T. Solvents and Sustainable Chemistry. *Proceedings of the*

Royal Society A: Mathematical, Physical and Engineering Sciences. Royal Society of London November 8, 2015. https://doi.org/10.1098/rspa.2015.0502.

(7) Schäffner, B.; Schäffner, F.; Verevkin, S. P.; Börner, A. Organic Carbonates as Solvents in Synthesis and Catalysis. *Chem. Rev.* **2010**, *110* (8), 4554–4581. https://doi.org/10.1021/cr900393d.

(8) López-Garzón, C. S.; van der Wielen, L. A. M.; Straathof, A. J. J. Green Upgrading of Succinate Using Dimethyl Carbonate for a Better Integration with Fermentative Production. *Chem. Eng. J.* **2014**, *235*, 52–60. https://doi.org/10.1016/j.cej.2013.09.017.

(9) Aricò, F.; Tundo, P. Isosorbide and Dimethyl Carbonate: A Green Match. *Beilstein J. Org. Chem.* **2016**, *12*, 2256–2266. https://doi.org/10.3762/bjoc.12.218.

(10) EPA. Revision to definition of volatile organic compounds – exclusion of propylene carbonate and dimethyl carbonate http://www.epa.gov/ttn/oarpg/t1/fact_sheets/voc_exemp01011309.pdf (accessed Jan 7, 2015).

(11) Björklund, E.; Göttlinger, M.; Edström, K.; Brandell, D.; Younesi, R. Investigation of Dimethyl Carbonate and Propylene Carbonate Mixtures for LiNi0.6Mn0.2Co0.2O2-Li4Ti5O12 Cells. *ChemElectroChem* **2019**, *6* (13), 3429–3436. https://doi.org/10.1002/celc.201900672.

(12) GUYOMARD, D.; TARASCON, J. M. Rechargeable Li1+xMn2O4/Carbon Cells with a New Electrolyte Composition. Potentiostatic Studies and Application to Practical Cells. *J. Electrochem. Soc.* **2010**, *140* (11), 3071–3081. https://doi.org/10.1002/chin.199407006.

(13) Xu, K. Nonaqueous Liquid Electrolytes for Lithium-Based Rechargeable Batteries. *Chem. Rev.* **2004**, *104* (10), 4303–4417. https://doi.org/10.1021/cr030203g.

(14) Rivetti, F. The Role of Dimethylcarbonate in the Replacement of Hazardous Chemicals. *Comptes Rendus l'Academie des Sci. - Ser. IIc Chem.* **2000**, *3* (6), 497–503. https://doi.org/10.1016/S1387-1609(00)00150-X.

(15) Tundo, P.; Selva, M. The Chemistry of Dimethyl Carbonate. *Acc. Chem. Res.* **2002**, *35* (9), 706–716. https://doi.org/10.1021/ar010076f.

(16) Sheldon, R. A. The E Factor: Fifteen Years On. *Green Chem.* **2007**, *9* (12), 1273–1283. https://doi.org/10.1039/b713736m.

(17) Sheldon, R. A. Catalysis: The Key to Waste Minimization. *J. Chem. Technol. Biotechnol.* **1997**, *68* (4), 381–388. https://doi.org/10.1002/(SICI)1097-4660(199704)68:4<381::AID-JCTB620>3.0.CO;2-3.

(18) TUNDO, P.; SELVA, M. Simplify Gas-Liquid Phase Transfer Catalysis. *Chemtech*. 1995, pp 31–35.

(19) Tundo, P.; Trotta, F.; Moraglio, G. Selective and Continuous-Flow Mono-Methylation of Arylacetonitriles with Dimethyl Carbonate under Gas-Liquid Phase-Transfer Catalysis Conditions. *J. Chem. Soc. Perkin Trans. 1* **1989**, No. 5, 1070–1071. https://doi.org/10.1039/p19890001070.

(20) Bomben, A.; Selva, M.; Tundo, P. Dimethyl Carbonate as a Methylating Agent. The Selective Mono-C-Methylation of Alkyl Aryl Sulfones. *J. Chem. Res. - Part S* **1997**, No. 12, 448–449. https://doi.org/10.1039/a703510a.

(21) Ono, Y. Catalysis in the Production and Reactions of Dimethyl Carbonate, an Environmentally Benign Building Block. *Appl. Catal. A Gen.* **1997**, *155* (2), 133–166. https://doi.org/10.1016/S0926-860X(96)00402-4.

(22) GSK Solvent Selection Guide 2009. **2010**, 2009–2011.

(23) Fukuoka, S.; Fukawa, I.; Tojo, M.; Oonishi, K.; Hachiya, H.; Aminaka, M.; Hasegawa, K.; Komiya, K. A Novel Non-Phosgene Process for Polycarbonate Production from CO2: Green and Sustainable Chemistry in Practice. *Catal. Surv. from Asia* **2010**, *14* (3), 146–163. https://doi.org/10.1007/s10563-010-9093-5.

(24) Kim, W. B.; Joshi, U. A.; Lee, J. S. Making Polycarbonates without Employing Phosgene: An Overview on Catalytic Chemistry of Intermediate and Precursor Syntheses for Polycarbonate. *Ind. Eng. Chem. Res.* **2004**, *43* (9), 1897–1914. https://doi.org/10.1021/ie034004z.

(25) Fukuoka, S.; Kawamura, M.; Komiya, K.; Tojo, M.; Hachiya, H.; Hasegawa, K.; Aminaka, M.; Okamoto, H.; Fukawa, I.; Konno, S. A Novel Non-Phosgene Polycarbonate Production Process Using by-Product CO 2 as Starting Material. *Green Chem.* **2003**, *5* (5), 497–507. https://doi.org/10.1039/b304963a.

(26) Fitzgerald, G. J. Chemical Warfare and Medical Response During World War I. *Am. J. Public Health* **2008**, *98* (4), 611–625. https://doi.org/10.2105/ajph.2007.11930.

(27) Choppin, A. R.; Rogers, J. W. The Preparation of Di-t-Butyl Carbonate and t-Butyl Chlorocarbonate. *J. Am. Chem. Soc.* **1948**, *70* (9), 2967. https://doi.org/10.1021/ja01189a040.

(28) Zhang, X.; Venkatraman, M. S.; Becker, C. K. Treprostinil Derivatives And Compositions And Uses Thereof, 2016.

(29) Babad, H.; Zeiler, A. G. The Chemistry of Phosgene. *Chem. Rev.* **1973**, *73* (1), 75–91. https://doi.org/10.1021/cr60281a005.

(30) Burk, R. M.; Roof, M. B. A Safe and Efficient Method for Conversion of 1,2- and 1,3-Diols to Cyclic Carbonates Utilizing Triphosgene. *Tetrahedron Lett.* **1993**, *34* (3), 395–398. https://doi.org/10.1016/0040-4039(93)85085-B.

(31) Shaikh, A.-A. G.; Sivaram, S. Organic Carbonates †. *Chem. Rev.* **1996**,

96 (3), 951–976. https://doi.org/10.1021/cr950067i.

(32) Tan, H. Z.; Wang, Z. Q.; Xu, Z. N.; Sun, J.; Xu, Y. P.; Chen, Q. S.; Chen, Y.; Guo, G. C. Review on the Synthesis of Dimethyl Carbonate. *Catal. Today* **2018**, *316*, 2–12. https://doi.org/10.1016/j.cattod.2018.02.021.

(33) Fukuoka, S.; Tojo, M.; Hachiya, H.; Aminaka, M.; Hasegawa, K. Green and Sustainable Chemistry in Practice: Development and Industrialization of a Novel Process for Polycarbonate Production from CO2 without Using Phosgene. *Polym. J.* **2007**, *39* (2), 91–114. https://doi.org/10.1295/polymj.PJ2006140.

(34) Meessen, J. Urea Synthesis. *Chemie-Ingenieur-Technik* **2014**, *86* (12), 2180–2189. https://doi.org/10.1002/cite.201400064.

(35) Zeng, G.; Wang, Y.; Gong, D.; Zhang, Y.; Wu, P.; Sun, Y. Dual-Role Membrane as NH3 Permselective Reactor and Azeotrope Separator in Urea Alcoholysis. *ACS Cent. Sci.* **2019**, *5* (11), 1834–1843. https://doi.org/10.1021/acscentsci.9b00812.

(36) Hasbi Ab Rahim, M.; He, Q.; Lopez-Sanchez, J. A.; Hammond, C.; Dimitratos, N.; Sankar, M.; Carley, A. F.; Kiely, C. J.; Knight, D. W.; Hutchings, G. J. Gold, Palladium and Gold-Palladium Supported Nanoparticles for the Synthesis of Glycerol Carbonate from Glycerol and Urea. *Catal. Sci. Technol.* **2012**, *2* (9), 1914–1924. https://doi.org/10.1039/c2cy20288c.

(37) Wu, D.; Guo, Y.; Geng, S.; Xia, Y. Synthesis of Propylene Carbonate from Urea and 1,2-Propylene Glycol in a Monolithic Stirrer Reactor. *Ind. Eng. Chem. Res.* **2013**, *52* (3), 1216–1223. https://doi.org/10.1021/ie302108r.

(38) Li, Q.; Zhang, W.; Zhao, N.; Wei, W.; Sun, Y. Synthesis of Cyclic Carbonates from Urea and Diols over Metal Oxides. *Catal. Today* **2006**, *115* (1–4), 111–116. https://doi.org/10.1016/j.cattod.2006.02.033.

(39) Sun, J.; Yang, B.; Wang, X.; Wang, D.; Lin, H. Synthesis of Dimethyl Carbonate from Urea and Methanol Using Polyphosphoric Acid as Catalyst. *J. Mol. Catal. A Chem.* **2005**, *239* (1–2), 82–86. https://doi.org/10.1016/j.molcata.2005.06.001.

(40) Wang, D.; Zhang, X.; Liu, C.; Cheng, T. T.; Wei, W.; Sun, Y. Transition Metal-Modified Mesoporous Mg-Al Mixed Oxides: Stable Base Catalysts for the Synthesis of Diethyl Carbonate from Ethyl Carbamate and Ethanol. *Appl. Catal. A Gen.* **2015**, *505*, 478–486. https://doi.org/10.1016/j.apcata.2015.04.034.

(41) Pacioni, T. R.; Soares, D.; Domenico, M. Di; Rosa, M. F.; Moreira, R. de F. P. M.; José, H. J. Bio-Syngas Production from Agro-Industrial Biomass Residues by Steam Gasification. *Waste Manag.* **2016**, *58*, 221–229. https://doi.org/10.1016/j.wasman.2016.08.021.

(42) Liu, C. J.; Ye, J.; Jiang, J.; Pan, Y. Progresses in the Preparation of Coke Resistant Ni-Based Catalyst for Steam and CO 2 Reforming of Methane. *ChemCatChem* **2011**, *3* (3), 529–541.

https://doi.org/10.1002/cctc.201000358.

(43) Fujita, S. I.; Usui, M.; Takezawa, N. Mechanism of the Reverse Water Gas Shift Reaction over Cu/ZnO Catalyst. *J. Catal.* **1992**, *134* (1), 220–225. https://doi.org/10.1016/0021-9517(92)90223-5.

(44) Kaiser, P.; Unde, R. B.; Kern, C.; Jess, A. Production of Liquid Hydrocarbons with CO2 as Carbon Source Based on Reverse Water-Gas Shift and Fischer-Tropsch Synthesis. *Chemie-Ingenieur-Technik* **2013**, *85* (4), 489–499. https://doi.org/10.1002/cite.201200179.

(45) Yoshihara, J.; Campbell, C. T. Methanol Synthesis and Reverse Water-Gas Shift Kinetics over Cu(110) Model Catalysts: Structural Sensitivity. *J. Catal.* **1996**, *161* (2), 776–782. https://doi.org/10.1006/jcat.1996.0240.

(46) Huang, S.; Yan, B.; Wang, S.; Ma, X. Recent Advances in Dialkyl Carbonates Synthesis and Applications. *Chem. Soc. Rev.* **2015**, *44* (10), 3079–3116. https://doi.org/10.1039/c4cs00374h.

(47) Amadio, E.; Freixa, Z.; Van Leeuwen, P. W. N. M.; Toniolo, L. Palladium Catalyzed Oxidative Carbonylation of Alcohols: Effects of Diphosphine Ligands. *Catal. Sci. Technol.* **2015**, *5* (5), 2856–2864. https://doi.org/10.1039/c4cy01588f.

(48) Keller, N.; Rebmann, G.; Keller, V. Catalysts, Mechanisms and Industrial Processes for the Dimethylcarbonate Synthesis. *J. Mol. Catal. A Chem.* **2010**, *317* (1–2), 1–18. https://doi.org/10.1016/j.molcata.2009.10.027.

(49) Yamamoto, Y. Vapor Phase Carbonylation Reactions Using Methyl Nitrite Over Pd Catalysts. *Catal. Surv. from Asia* **2010**, *14* (3), 103–110. https://doi.org/10.1007/s10563-010-9102-8.

(50) Khan, Y.; Chung, C. Il; Oh, J. J.; Nguyen, T. T.; Lee, H. J.; Cheong, M.; Walker, B.; Sik, H.; Jin, Y.; Kim, H. S.; et al. Selenite-Catalyzed Oxidative Carbonylation of Alcohols to Dialkyl Carbonates. *Appl. Catal. B Environ.* **2019**, *242* (October 2018), 460–468. https://doi.org/10.1016/j.apcatb.2018.10.026.

(51) Wang, H.; Zhang, H.; Hu, J.; Wang, G.; Deng, Z. Metal-Halide/Ionic-Liquid Oxidative Carbonylation of Ethanol to Synthesize Diethyl Carbonate with High Activity and Low Corrosion. *ChemistrySelect* **2019**, *4* (45), 13265–13270. https://doi.org/10.1002/slct.201903419.

(52) Lv, D. M.; Xu, Z. N.; Peng, S. Y.; Wang, Z. Q.; Chen, Q. S.; Chen, Y.; Guo, G. C. (Pd-CuCl2)/γ-Al2O3: A High-Performance Catalyst for Carbonylation of Methyl Nitrite to Dimethyl Carbonate. *Catal. Sci. Technol.* **2015**, *5* (6), 3333–3339. https://doi.org/10.1039/c5cy00251f.

(53) Lapidus, A. L.; Pirozhkov, S. D.; Sukhov, V. V. Oxidative Carbonylation of Phenol. *Russ. Chem. Bull.* **1999**, *48* (6), 1113–1117. https://doi.org/10.1007/BF02496011.

(54) Zhang, L.; He, Y.; Yang, X.; Yuan, H.; Du, Z.; Wu, Y. Oxidative Carbonylation of Phenol to Diphenyl Carbonate by Pd/MO-MnFe2O4

Magnetic Catalyst. *Chem. Eng. J.* **2015**, *278*, 129–133. https://doi.org/10.1016/j.cej.2014.11.096.

(55) Aresta, M.; Dibenedetto, A.; Quaranta, E. State of the Art and Perspectives in Catalytic Processes for CO2 Conversion into Chemicals and Fuels: The Distinctive Contribution of Chemical Catalysis and Biotechnology. *J. Catal.* **2016**, *343*, 2–45. https://doi.org/10.1016/j.jcat.2016.04.003.

(56) Qian, W.; Ma, X.; Liu, L.; Deng, L.; Su, Q.; Ba, R.; Zhang, Z.; Gou, H.; Dong, L.; Cheng, W.; et al. Efficient Synthesis of Bio-Derived Polycarbonates from Dimethyl Carbonate and Isosorbide: Regulating Exo-OH and Endo-OH Reactivity by Ionic Liquids. *Green Chem.* **2020**. https://doi.org/10.1039/D0GC01804J.

(57) Yoshida, Y.; Arai, Y.; Kado, S.; Kunimori, K.; Tomishige, K. Direct Synthesis of Organic Carbonates from the Reaction of CO2 with Methanol and Ethanol over CeO2 Catalysts. *Catal. Today* **2006**, *115* (1–4), 95–101. https://doi.org/10.1016/j.cattod.2006.02.027.

(58) Wu, X. L.; Xiao, M.; Meng, Y. Z.; Lu, Y. X. Direct Synthesis of Dimethyl Carbonate on H3PO4 Modified V2O5. *J. Mol. Catal. A Chem.* **2005**, *238* (1–2), 158–162. https://doi.org/10.1016/j.molcata.2005.05.018.

(59) Choi, J.-C. C.; He, L.-N. N.; Yasuda, H.; Sakakura, T.; Yasudaa, H.; Sakakura, T. Selective and High Yield Synthesis of Dimethyl Carbonate Directly from Carbon Dioxide and Methanol. *Green Chem.* **2002**, *4* (3), 230–234. https://doi.org/10.1039/b200623p.

(60) Lee, H. J.; Park, S.; Song, I. K.; Jung, J. C. Direct Synthesis of Dimethyl Carbonate from Methanol and Carbon Dioxide over Ga2O3/Ce0.6Zr0.4O2 Catalysts: Effect of Acidity and Basicity of the Catalysts. *Catal. Letters* **2011**, *141* (4), 531–537. https://doi.org/10.1007/s10562-010-0544-4.

(61) Chen, L.; Wang, S.; Zhou, J.; Shen, Y.; Zhao, Y.; Ma, X. Dimethyl Carbonate Synthesis from Carbon Dioxide and Methanol over CeO_2 versus over ZrO_2 : Comparison of Mechanisms. *RSC Adv.* **2014**, *4* (59), 30968. https://doi.org/10.1039/C4RA03081H.

(62) Santos, B. A. V.; Pereira, C. S. M.; Silva, V. M. T. M.; Loureiro, J. M.; Rodrigues, A. E. Kinetic Study for the Direct Synthesis of Dimethyl Carbonate from Methanol and CO2 over CeO2 at High Pressure Conditions. *Appl. Catal. A Gen.* **2013**, *455*, 219–226. https://doi.org/10.1016/j.apcata.2013.02.003.

(63) Lee, H. J.; Park, S.; Jung, J. C.; Song, I. K. Direct Synthesis of Dimethyl Carbonate from Methanol and Carbon Dioxide over H3PW12O40/CeXZr1-XO2 Catalysts: Effect of Acidity of the Catalysts. *Korean J. Chem. Eng.* **2011**, *28* (7), 1518–1522. https://doi.org/10.1007/s11814-011-0020-x.

(64) Chen, Y.; Wang, H.; Qin, Z.; Tian, S.; Ye, Z.; Ye, L.; Abroshan, H.; Li,

G. TiXCe1-XO2 Nanocomposites: A Monolithic Catalyst for the Direct Conversion of Carbon Dioxide and Methanol to Dimethyl Carbonate. *Green Chem.* **2019**, *21* (17), 4642–4649. https://doi.org/10.1039/c9gc00811j.

(65) Li, A.; Pu, Y.; Li, F.; Luo, J.; Zhao, N.; Xiao, F. Synthesis of Dimethyl Carbonate from Methanol and CO2 over Fe-Zr Mixed Oxides. *J. CO2 Util.* **2017**, *19*, 33–39. https://doi.org/10.1016/j.jcou.2017.02.016.

(66) Liu, B.; Li, C.; Zhang, G.; Yan, L.; Li, Z. Direct Synthesis of Dimethyl Carbonate from CO2 and Methanol over CaO-CeO2 Catalysts: The Role of Acid-Base Properties and Surface Oxygen Vacancies. *New J. Chem.* **2017**, *41* (20), 12231–12240. https://doi.org/10.1039/c7nj02606d.

(67) Liu, B.; Li, C.; Zhang, G.; Yao, X.; Chuang, S. S. C.; Li, Z. Oxygen Vacancy Promoting Dimethyl Carbonate Synthesis from CO 2 and Methanol over Zr-Doped CeO 2 Nanorods. *ACS Catal.* **2018**, *8*, 10446–10456. https://doi.org/10.1021/acscatal.8b00415.

(68) Xu, W.; Ji, S.; Quan, W.; Yu, J. One-Pot Synthesis of Dimethyl Carbonate over Basic Zeolite Catalysts. *Mod. Res. Catal.* **2013**, *02* (02), 22–27. https://doi.org/10.4236/mrc.2013.22a004.

(69) Ikeda, Y.; Sakaihori, T.; Tomishige, K.; Fujimoto, K. Promoting Effect of Phosphoric Acid on Zirconia Catalysts in Selective Synthesis of Dimethyl Carbonate from Methanol and Carbon Dioxide. *Catal. Letters* **2000**, *66* (1–2), 59–62. https://doi.org/10.1023/A:1019043422050.

(70) Nakagawa, Y.; Honda, M.; Tomishige, K. Direct Synthesis of Organic Carbonates from CO2 and Alcohols Using Heterogeneous Oxide Catalysts. In *Green Carbon Dioxide: Advances in CO*; 2014; Vol. 9781118590, pp 119–148. https://doi.org/10.1002/9781118831922.ch5.

(71) Saada, R.; Kellici, S.; Heil, T.; Morgan, D.; Saha, B. Greener Synthesis of Dimethyl Carbonate Using a Novel Ceria-Zirconia Oxide/Graphene Nanocomposite Catalyst. *Appl. Catal. B Environ.* **2015**, *168–169*, 352–362. https://doi.org/10.1016/j.apcatb.2014.12.013.

(72) Bansode, A.; Urakawa, A. Continuous DMC Synthesis from CO 2 and Methanol over a CeO 2 Catalyst in a Fixed Bed Reactor in the Presence of a Dehydrating Agent. *ACS Catal.* **2014**, *4*, 3877–3880. https://doi.org/dx.doi.org/10.1021/cs501221q.

(73) Choi, J. C.; Kohno, K.; Ohshima, Y.; Yasuda, H.; Sakakura, T. Tin- or Titanium-Catalyzed Dimethyl Carbonate Synthesis from Carbon Dioxide and Methanol: Large Promotion by a Small Amount of Triflate Salts. *Catal. Commun.* **2008**, *9* (7), 1630–1633. https://doi.org/10.1016/j.catcom.2008.01.013.

(74) Fu, Z.; Zhong, Y.; Yu, Y.; Long, L.; Xiao, M.; Han, D.; Wang, S.; Meng, Y. TiO2-Doped CeO2 Nanorod Catalyst for Direct Conversion of CO2 and CH3OH to Dimethyl Carbonate: Catalytic Performance and Kinetic Study. *ACS Omega* **2018**, *3* (1), 198–207. https://doi.org/10.1021/acsomega.7b01475.

(75) Lee, H. J.; Joe, W.; Song, I. K. Direct Synthesis of Dimethyl Carbonate from Methanol and Carbon Dioxide over Transition Metal Oxide/Ce0.6Zr0.4O2 Catalysts: Effect of Acidity and Basicity of the Catalysts. *Korean J. Chem. Eng.* **2012**, *29* (3), 317–322. https://doi.org/10.1007/s11814-011-0185-3.

(76) Zhang, M.; Alferov, K. A.; Xiao, M.; Han, D.; Wang, S.; Meng, Y. Continuous Dimethyl Carbonate Synthesis from CO2 and Methanol Using Cu-Ni@VSiO as Catalyst Synthesized by a Novel Sulfuration Method. *Catalysts* **2018**, *8* (4). https://doi.org/10.3390/catal8040142.

(77) Crocellà, V.; Tabanelli, T.; Vitillo, J. G.; Costenaro, D.; Bisio, C.; Cavani, F.; Bordiga, S. A Multi-Technique Approach to Disclose the Reaction Mechanism of Dimethyl Carbonate Synthesis over Amino-Modified SBA-15 Catalysts. *Appl. Catal. B Environ.* **2017**, *211*, 323–336. https://doi.org/10.1016/j.apcatb.2017.04.013.

(78) Tomishige, K.; Kunimori, K. Catalytic and Direct Synthesis of Dimethyl Carbonate Starting from Carbon Dioxide Using CeO2-ZrO2 Solid Solution Heterogeneous Catalyst: Effect of H2O Removal from the Reaction System. *Appl. Catal. A Gen.* **2002**, *237* (1–2), 103–109. https://doi.org/10.1016/S0926-860X(02)00322-8.

(79) Al-Darwish, J.; Senter, M.; Lawson, S.; Rezaei, F.; Rownaghi, A. A. Ceria Nanostructured Catalysts for Conversion of Methanol and Carbon Dioxide to Dimethyl Carbonate. *Catal. Today* **2020**, *350*, 120–126. https://doi.org/10.1016/j.cattod.2019.06.013.

(80) Fang, S.; Fujimoto, K. Direct Synthesis of Dimethyl Carbonate from Carbon Dioxide and Methanol Catalyzed by Base. *Appl. Catal. A Gen.* **1996**, *142* (1), 8–10. https://doi.org/10.1016/0926-860X(96)00081-6.

(81) Fujita, S. I. I.; Bhanage, B. M. M.; Ikushima, Y.; Arai, M. Synthesis of Dimethyl Carbonate from Carbon Dioxide and Methanol in the Presence of Methyl Iodide and Base Catalysts under Mild Conditions: Effect of Reaction Conditions and Reaction Mechanism. *Green Chem.* **2001**, *3* (2), 87–91. https://doi.org/10.1039/b100363l.

(82) Cai, Q.; Jin, C.; Lu, B.; Tangbo, H.; Shan, Y. Synthesis of Dimethyl Carbonate from Methanol and Carbon Dioxide Using Potassium Methoxide as Catalyst under Mild Conditions. *Catal. Letters* **2005**, *103* (3–4), 225–228. https://doi.org/10.1007/s10562-005-7158-2.

(83) Sun, J.; Lu, B.; Wang, X.; Li, X.; Zhao, J.; Cai, Q. A Functionalized Basic Ionic Liquid for Synthesis of Dimethyl Carbonate from Methanol and CO2. *Fuel Process. Technol.* **2013**, *115*, 233–237. https://doi.org/10.1016/j.fuproc.2013.06.009.

(84) Zhao, T.; Hu, X.; Wu, D.; Li, R.; Yang, G.; Wu, Y. Direct Synthesis of Dimethyl Carbonate from Carbon Dioxide and Methanol at Room Temperature Using Imidazolium Hydrogen Carbonate Ionic Liquid as a Recyclable Catalyst and Dehydrant. *ChemSusChem* **2017**, *10* (9), 2046–2052. https://doi.org/10.1002/cssc.201700128.

(85) Kamarudin, S. K.; Shamsul, N. S.; Ghani, J. A.; Chia, S. K.; Liew, H. S.; Samsudin, A. S. Production of Methanol from Biomass Waste via Pyrolysis. *Bioresour. Technol.* **2013**, *129*, 463–468. https://doi.org/10.1016/j.biortech.2012.11.016.

(86) Demirbas, A. Biomethanol Production from Organic Waste Materials. *Energy Sources, Part A Recover. Util. Environ. Eff.* **2008**, *30* (6), 565–572. https://doi.org/10.1080/15567030600817167.

(87) Irfan, M.; Nadeem, M.; Syed, Q. Ethanol Production from Agricultural Wastes Using Sacchromyces Cervisae. *Brazilian J. Microbiol.* **2014**, *45* (2), 457–465. https://doi.org/10.1590/S1517-83822014000200012.

(88) Cutzu, R.; Bardi, L. Production of Bioethanol from Agricultural Wastes Using Residual Thermal Energy of a Cogeneration Plant in the Distillation Phase. *Fermentation* **2017**, *3* (2). https://doi.org/10.3390/fermentation3020024.

(89) Stoian, D.; Medina, F.; Urakawa, A. Improving the Stability of CeO2 Catalyst by Rare Earth Metal Promotion and Molecular Insights in the Dimethyl Carbonate Synthesis from CO2 and Methanol with 2-Cyanopyridine. *ACS Catal.* **2018**, *8* (4), 3181–3193. https://doi.org/10.1021/acscatal.7b04198.

(90) Kabra, S. K.; Turpeinen, E.; Keiski, R. L.; Yadav, G. D. Direct Synthesis of Dimethyl Carbonate from Methanol and Carbon Dioxide: A Thermodynamic and Experimental Study. *J. Supercrit. Fluids* **2016**, *117*, 98–107. https://doi.org/10.1016/j.supflu.2016.05.039.

(91) Anastas, P.; Eghbali, N. Green Chemistry: Principles and Practice. *Chem. Soc. Rev.* **2010**, *39* (1), 301–312. https://doi.org/10.1039/b918763b.

(92) Leigh Krietsch Boerner. Industrial Ammonia Production Emits More CO2 than Any Other Chemical-Making Reaction. *Chem. Eng. News* **2019**, *97* (24).

(93) Wang, S. P.; Zhou, J. J.; Zhao, S. Y.; Zhao, Y. J.; Ma, X. Bin. Enhancements of Dimethyl Carbonate Synthesis from Methanol and Carbon Dioxide: The in Situ Hydrolysis of 2-Cyanopyridine and Crystal Face Effect of Ceria. *Chinese Chem. Lett.* **2015**, *26* (9), 1096–1100. https://doi.org/10.1016/j.cclet.2015.05.005.

(94) Honda, M.; Tamura, M.; Nakagawa, Y.; Nakao, K.; Suzuki, K.; Tomishige, K. Organic Carbonate Synthesis from CO2 and Alcohol over CeO2 with 2-Cyanopyridine: Scope and Mechanistic Studies. *J. Catal.* **2014**, *318*, 95–107. https://doi.org/10.1016/j.jcat.2014.07.022.

(95) Intergovernmental Panel on Climate Change. *Climate Change 2014 Mitigation of Climate Change*; 2014. https://doi.org/10.1017/cbo9781107415416.

(96) Poliakoff, M.; Leitner, W.; Streng, E. S. The Twelve Principles of CO2 CHEMISTRY. *Faraday Discuss.* **2015**, *183*, 9–17. https://doi.org/10.1039/c5fd90078f.

(97) Vechorkin, O.; Hirt, N.; Hu, X. Carbon Dioxide as the C1 Source for Direct C-H Functionalization of Aromatic Heterocycles. *Org. Lett.* **2010**, *12* (15), 3567–3569. https://doi.org/10.1021/ol101450u.

(98) Wesselbaum, S.; Hintermair, U.; Leitner, W. Continuous-Flow Hydrogenation of Carbon Dioxide to Pure Formic Acid Using an Integrated ScCO2 Process with Immobilized Catalyst and Base. *Angew. Chem. Int. Ed. Engl.* **2012**, *51* (34), 8585–8588. https://doi.org/10.1002/anie.201203185.

(99) Rummelt, S. M.; Zhong, H.; Korobkov, I.; Chirik, P. J. Iron-Mediated Coupling of Carbon Dioxide and Ethylene: Macrocyclic Metallalactones Enable Access to Various Carboxylates. *J. Am. Chem. Soc.* **2018**, *140* (37), 11589–11593. https://doi.org/10.1021/jacs.8b07558.

(100) Navarro, M.; Sánchez-Barba, L. F.; Garcés, A.; Fernández-Baeza, J.; Fernández, I.; Lara-Sánchez, A.; Rodríguez, A. M. Bimetallic Scorpionate-Based Helical Organoaluminum Complexes for Efficient Carbon Dioxide Fixation into a Variety of Cyclic Carbonates. *Catal. Sci. Technol.* **2020**, *10* (10), 3265–3278. https://doi.org/10.1039/d0cy00593b.

(101) Maltby, K. A.; Hutchby, M.; Plucinski, P.; Davidson, M. G.; Hintermair, U. Selective Catalytic Synthesis of 1,2- and 8,9-Cyclic Limonene Carbonates as Versatile Building Blocks for Novel Hydroxyurethanes. *Chem. - A Eur. J.* **2020**, *26* (33), 7405–7415. https://doi.org/10.1002/chem.201905561.

(102) Yonei, Y.; Ohinata, H.; Yoshida, R.; Shimizu, Y.; Yokoyama, C. Extraction of Ginger Flavor with Liquid or Supercritical Carbon Dioxide. *J. Supercrit. Fluids* **1995**, *8* (2), 156–161. https://doi.org/10.1016/0896-8446(95)90028-4.

(103) Gopalan, B.; Goto, M.; Kodama, A.; Hirose, T. Supercritical Carbon Dioxide Extraction of Turmeric (Curcuma Longa). *J. Agric. Food Chem.* **2000**, *48* (6), 2189–2192. https://doi.org/10.1021/jf9908594.

(104) Hubert, P.; Vitzthum, O. G. Fluid Extraction of Hops, Spices, and Tobacco with Supercritical Gases. *Angewandte Chemie International Edition in English*. 1978, pp 710–715. https://doi.org/10.1002/anie.197807101.

(105) Zosel, K. Separation with Supercritical Gases: Practical Applications. *Angew. Chemie Int. Ed. English* **1978**, *17* (10), 702–709. https://doi.org/10.1002/anie.197807021.

(106) Tanaka, Y.; Sakaki, I.; Ohkubo, T. Extraction of Phospholipids from Salmon Roe with Supercritical Carbon Dioxide and an Entrainer. *J. Oleo Sci.* **2004**, *53* (9), 417–424. https://doi.org/10.5650/jos.53.417.

(107) Aizpurua-Olaizola, O.; Ormazabal, M.; Vallejo, A.; Olivares, M.; Navarro, P.; Etxebarria, N.; Usobiaga, A. Optimization of Supercritical Fluid Consecutive Extractions of Fatty Acids and Polyphenols from Vitis Vinifera Grape Wastes. *J. Food Sci.* **2015**, *80* (1), E101–E107.

https://doi.org/10.1111/1750-3841.12715.

(108) Theyssen, N.; Scovell, K.; Poliakoff, M.; Foster, N. R.; Lucien, F. P.; Mammucari, R.; Rayner, C. M.; Rose, P. M.; Barnes, D. C. *Green Solvents: Supercritical Solvents, Volume 4*; 2013.

(109) Foster, N.; Luden, F.; Mammucari, R. Basic Physical Properties, Phase Behavior and Solubility. In *Handbook of Green Chemistry - Green Solvents: Volume 4 - Supercritical Solvents*; 2010; pp 77–99. https://doi.org/10.1002/9783527628698.

(110) Span, R.; Wagner, W. A New Equation of State for Carbon Dioxide Covering the Fluid Region from the Triple-Point Temperature to 1100 K at Pressures up to 800 MPa. *J. Phys. Chem. Ref. Data* **1996**, *25* (6), 1509–1596. https://doi.org/10.1063/1.555991.

(111) Belmares, M.; Blanco, M.; Goddard, W. A.; Ross, R. B.; Caldwell, G.; Chou, S. H.; Pham, J.; Olofson, P. M.; Thomas, C. Hildebrand and Hansen Solubility Parameters from Molecular Dynamics with Applications to Electronic Nose Polymer Sensors. *J. Comput. Chem.* **2004**, *25* (15), 1814–1826. https://doi.org/10.1002/jcc.20098.

(112) Ablan, C. D.; Hallett, J. P.; West, K. N.; Jones, R. S.; Eckert, C. A.; Liotta, C. L.; Jessop, P. G. Use and Recovery of a Homogeneous Catalyst with Carbon Dioxide as a Solubility Switch. *Chem. Commun.* **2003**, *3* (24), 2972–2973. https://doi.org/10.1039/b311146f.

(113) Abbott, A. P.; Hope, E. G.; Mistry, R.; Stuart, A. M. Controlling Phase Behaviour on Gas Expansion of Fluid Mixtures. *Green Chem.* **2009**, *11* (10), 1536–1540. https://doi.org/10.1039/b915571f.

Aims and objectives

The aim of this project was to develop an efficient continuous flow synthesis of dialkyl carbonates from CO_2 and alcohols and investigate the effects and possibilities of continuous product removal and phase separations using the tuneable solvent properties of near- and supercritical CO_2.

Methanol was selected for the synthesis of dimethyl carbonate to first identify active catalysts for the reaction and to establish boundary conditions in batch and in flow. Ethanol for diethyl carbonate synthesis was subsequently included in the optimised process.

Specific objectives include:

1. Synthesis and characterisation of high surface area mixed metal oxide catalysts from literature.
2. Evaluation of catalysts under a range of conditions to identify optimal conditions with and without the use of a dehydrating agent.
3. Evaluation of catalyst stability under repeated batch use.
4. Calculation of the expected equilibrium conversions under reaction conditions from first principles.
5. Validation of calculated values with equilibrium limited batch reactions.
6. Construction of a flow reactor and evaluate the synthesis of DMC and DEC in flow under a range of conditions.
7. Evaluation of catalyst activity and stability of catalysts under sustained flow conditions.
8. Attempt to identify the phase behaviour necessary for the separation of DMC and water from methanol and CO_2.

Chapter 2 – Catalyst synthesis and Characterization

2.1 Introduction

The direct synthesis of dialkyl carbonates has been reported using both heterogeneous and homogeneous catalysts.[1] Homogeneous catalysts explored include base catalysts,[2–4] ionic liquids[5,6] and organo-tin and titanium complexes.[7–12] Heterogeneous catalysts explored include commercial metal oxides and novel materials consisting of mixed metal oxides produced by methods such as templating, precipitation, and pyrolysis.[13–21]

In this section an overview of the catalytic systems investigated for the synthesis of dialkyl carbonates is given before describing the catalysts synthesised for use in the following chapters.

2.1.1 Base Catalysts

One of the classes of catalysts that has been widely investigated in the literature is inorganic base catalysts, which have shown success at moderate temperatures and relatively low pressures. Base catalysts enable the activation of both alcohols and CO_2 and, with the addition of an alkylating agent such as methyl iodide, can be used to form dialkyl carbonates.

Scheme 2.1 shows a general reaction scheme for the synthesis of dimethyl carbonate from base catalyst with methyl iodide. This involves methanol activation by the base catalyst to form a methoxy anion, which then reacts with CO_2 to form methyl carbonate. CH_3I can then react with the methyl carbonate to form dimethyl carbonate. The resulting HI can then go on to react with methanol to form methyl iodide and water, or to react with the base causing deactivation.

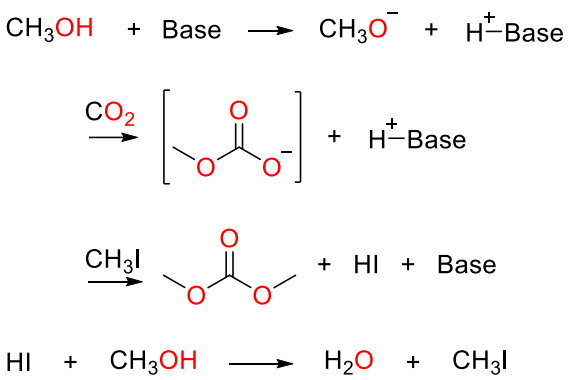

Scheme 2.1: Proposed mechanism for the base catalysed direct synthesis of dimethyl carbonate.[3,22]

Basic metal carbonates such as K_2CO_3 have been investigated for both the direct synthesis as well as transesterification routes of DMC.[23–26] It is common to use base catalysts in conjunction with KI or CH_3I, though the role of the iodide is disputed as there is evidence to suggest that it acts as more of a reactant than a promotor for these reactions.[3] Fang *et al.*[2] have also shown that for the direct synthesis of dimethyl carbonate CH_3I was essential for the reaction to progress, and even without CO_2 a small amount of DMC was still formed. The by-product of the reaction, dimethyl ether, was produced in a larger quantity, likely due to a side reaction between the CH_3I and the activated methanol (Scheme 2.2).

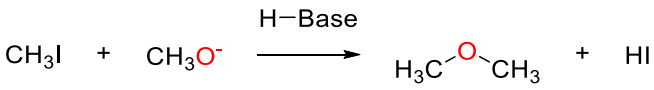

Scheme 2.2: Side reaction producing dimethyl ether from methyl iodide and carboxy ion.

Table 2.1 shows several base catalysts investigated for the direct synthesis of dimethyl carbonate. Conversion appears to increase with increasing basicity with the metal carbonates and peak conversion observed with K_2CO_3. Further increases in basicity lead to a lower conversion.

Table 2.1 Base catalysts used in the formation of DMC using CH_3I as a co-catalyst.

Entry	Base	Base loading (mol%)	MeI loading (mol%)	T (°C)	P (MPa)	Conversion (%)	t (h)	Ref
1	Li_2CO_3	1.6	12.5	100	5	1.35	2	[2]
2	Na_2CO_3	1.6	12.5	100	5	9.79	2	[2]
3	K_2CO_3	1.6	12.5	100	5	12.4	2	[2]
4	K_2CO_3	1.5	12.0	70	8	4.08	4	[3]
5	Cs_2CO_3	1.6	12.5	100	5	8.96	2	[2]
6	K_3PO_4	1.6	12.5	100	5	8.02	2	[2]
7	Me_4NOH	1.6	12.5	100	5	7.60	2	[2]
8	$KHCO_3$	1.5	12.0	70	8	2.02	4	[3]
9	Li_2CO_3	1.5	12.0	70	8	0.54	4	[3]
10	CH_3OK	6.0	9.4	80	7.3	16.2	10	[4]
11	CH_3ONa	6.0	5.6	80	7.3	2.59	10	[4]

2.1.2 Ionic liquids

Ionic liquids (ILs) have been investigated for the direct synthesis of carbonates due to their ability to sequester water from the reaction system along with their ability to solvate CO_2.[5] When used in catalytic loadings ILs tend to afford lower yields than other catalysts and are used in conjunction with bases mentioned above. Table 2.2 shows a number of reported ILs with base cocatalysts. The most recent example by Zhao *et al.* reported higher yields,[5] though the IL is used in stoichiometric quantities, and is therefore only catalytic following regeneration and reuse. It is worth noting however that the reaction proceeded under much milder conditions than are usually seen for this reaction, with a 61% methanol conversion at room temperature and up to 82% at 50 °C with increased base.

Table 2.2: Reported ionic liquids for dimethyl carbonate synthesis. CH = Choline Hydroxide, EtmimOH = 1-ethoxyl-3-methylimidazolium hydroxide.

Entry	IL (mmol/mmol substrate)	T (°C)	P (MPa)	Base (mmol)	Conversion (%)	Ref
1	$[C_1C_4Im][HCO_3]$ (1)	25	1	Cs_2CO_3 (5)	45	5
2	$[C_1C_4Im][HCO_3]$ (1)	25	1	K_2CO_3 (5)	61	5
3	$[C_1C_4Im][HCO_3]$ (1)	50	1	Cs_2CO_3 (20)	82	5
4	CH/CH_3I (0.132)	140	3	-	2.7	6
5	EtmimOH (0.132)	140	3	-	0.2	6

2.1.3 Homogeneous metal complexes

Several metal complexes have been investigated for the synthesis of DMC including $Ti(O\text{-}i\text{-}Pr)_4$,[8] alkyl tin oxides,[8,10] and alkyl tin methoxides.[10,11] These have typically been investigated in the presence of a dehydrating agent system such as orthoesters (see Chapter 3) or molecular sieves allowing these catalysts to reach DMC yields exceeding 80%.

2.1.4 Metal oxides

A wide variety of metal oxides has been investigated for the formation of dialkyl carbonates many of which are ceria[13,14,27–37] or zirconia[13,15,34,38,39] based. What makes these metal oxides active are their Lewis acid and basic sites which allow activation of both the alcohol and carbon dioxide.[40] Metal oxide catalysts allow

for a cleaner synthesis by removing the need for a methylating agent as seen above with the base catalysts.

The mechanism for zirconia and ceria catalysts has been previously reported (Scheme 2.3).[41,42] The proposed mechanism shows surface activation of the methanol by removal of a proton forming a methoxy species on the catalyst surface. This can then react with an activated CO_2 molecule to give methyl carbonate. Finally, a second methanol is activated, which can react with the bound methyl carbonate to release DMC, regenerating the hydroxyl species on the surface.

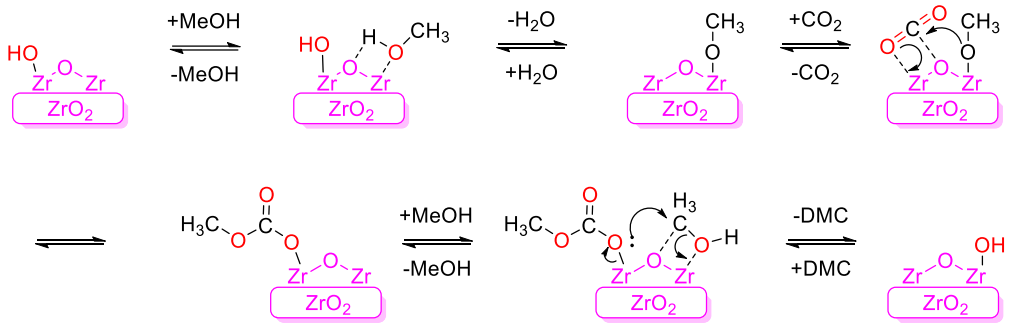

Scheme 2.3: Proposed mechanism for the formation of DMC from CO_2 and methanol over a heterogeneous zirconium oxide catalyst[19] (shown in pink).

The acid-base properties have been shown to be highly correlated with activity for direct dimethyl carbonate synthesis.[15,19,20,43] Figure 2.1 shows aggregated data from several publications. These data show that both the acidity and basicity are important in the activity of the catalysts, with the best performing catalyst in each series having the greatest acidity and the best performing catalyst overall having the highest acidity and basicity. Due to the different conditions used in catalyst testing, data from Li *et al.* (▲) was excluded from the best fit in 2.2A.

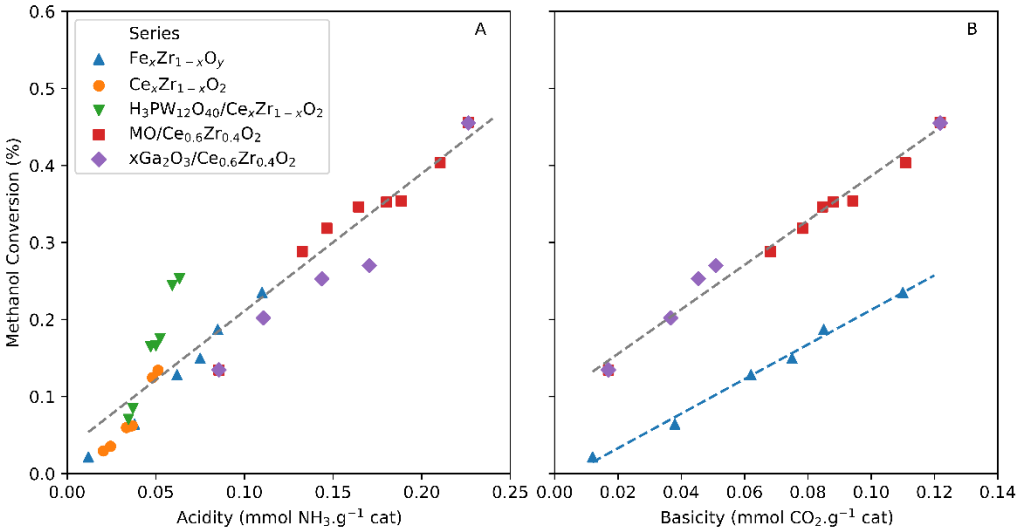

Figure 2.1: Aggregated acid (A) and base (B) data from Li et al.[15] and Lee et al.[19,20,43] showing the correlation between acid sites and Methanol conversion. conditions: Li et al. 110 °C, 50 bar, 4 h, 1 g catalyst, 374 mmol MeOH. Lee et al. 170 °C 60 bar, 3 h, 0.7 g catalyst, 740 mmol MeOH. Best fit in A excludes data from Li et al. MO = Metal oxides.

Table 2.3 below shows a number of catalysts that have been used for the formation of dimethyl carbonate. It is worth noting that the examples shown are equilibrium limited, with no dehydrating agent present (see Chapter 4). Entries 14 and 15 from Table 2.3 both appear to be greater than the expected equilibrium conversions for the temperatures and pressures investigated.

Table 2.3:A selection of literature metal oxides investigated for the direct synthesis of dimethyl carbonate along with the method of preparation and calcination temperatures.

Entry	Oxide	T (°C)	P (bar)	t (h)	Conversion (%)	Preparation method	Calcination temp (°C)	Ref
1	ZrO_2	110	60	2	0.00	Calcination of hydroxides	1000	[13]
2	$Ce_{0.2}Zr_{0.8}O_2$	110	60	2	0.74	Calcination of hydroxides	1000	[13]
3	$Ce_{0.33}Zr_{0.67}O_2$	110	60	2	0.76	Calcination of hydroxides	1000	[13]
4	$Ce_{0.5}Zr_{0.5}O_2$	110	60	2	0.13	Calcination of hydroxides	1000	[13]
5	CeO_2	110	60	2	0.05	Calcination of hydroxides	1000	[13]
6	CeO_2	135	50	3	0.35	Precipitation by NH_4OH	650	[14]
7	Al-CeO_2 (10%Al)	135	50	3	0.42	Precipitation by NH_4OH	650	[14]
8	Al-CeO_2 (3%Al)	135	50	3	0.40	Precipitation by NH_4OH	650	[14]
9	Fe-CeO_2 (7% Fe)	135	50	3	0.45	Precipitation by NH_4OH	650	[14]
10	ZrO_2	110	50	4	0.06	Precipitation by citric acid	500	[15]
11	Fe-Zr	110	50	4	0.23	Precipitation by citric acid	500	[15]
12	Fe_2O_3	110	50	4	0.02	Precipitation by citric acid	500	[15]
13	H_3PO_4/ZrO_2	130	50	2	0.32	Wet impregnation	400	[16]
14	$H_3PW_{12}O_{40}/ZrO_2$	100	40	2.5	4.04	Precipitation by NH_4OH	300	[17]
15	H_3PO_4/V_2O_5	140	6		1.80	Wet impregnation	459 / 400	[18]
16	$H_3PW_{12}O_{40}/Ce_{0.6}Zr_{0.4}O_2$	170	60	3	0.26	Precipitation by citric acid sol gel/ incipient wetness	500	[19]
17	$Ga_2O_3/Ce_{0.6}Zr_{0.4}O_2$	170	60	3	0.45	Precipitation by citric acid sol gel/ incipient wetness	500	[20]
18	Nb_2O_5/ZrO_2	135	50	3	0.30 (ethanol)	Precipitation by NH_4OH	550	[21]

The work in this chapter focuses on producing mixed ceria/zirconia and ceria/alumina which each show good activity at lower temperatures. Heterogeneous catalysts were selected for investigation due to the lack of requirements for promoters and co-catalysts which are required for base and IL catalysts as well as for the ease of separation and reuse, which is an important consideration for performing the reactions in a flow system.

2.2 Experimental

2.2.1 Cerium oxide preparation by decomposition

$Ce(NO_3)_3 \cdot 6H_2O$ (Sigma) and ethanol (Sigma) and the template, a block co-polymer Pluronic® P104 (BASF), were added to a round-bottomed flask and stirred for 3 h at high speed (1600 rpm) at room temperature until a homogeneous solution was achieved. The resultant solution was then poured into a high surface area evaporation dish and placed into a preheated convection oven at 65 °C overnight. The oven was then purged of ethanol vapour for 2-3 h before being heated to 150 °C in air for 12 h. This step had an associated fire risk and, in order to mitigate this risk, synthesis was carried out in small batches in a large surface area vessel. Samples were then calcined at 450 °C in air for 4 h with a ramp rate of 1 °C/minute.

2.2.2 Pure and mixed metal oxide preparation by precipitation

$Ce(NO_3)_3 \cdot 6H_2O$ (Sigma), $ZrO(NO_3)_2 \cdot XH_2O$ (Sigma) or a mixture of the two were loaded into a 50 mL round bottom flask along with 2.990 g Pluronic® P104 (BASF) with 40 mL ethanol or deionised water and stirred for 3 h at room temperature. After 3 h 14 mL of 35% ammonia was added dropwise over 30 minutes under constant stirring until pH 11 was achieved. This was then aged under constant stirring for 18 h before being filtered on a Buchner funnel and washed with deionised water. The sample was then dried under vacuum for 3 h, the resultant powder was weighed and calcined at 450 °C for 4 h at 1 °C/min ramp rate.

2.2.3 Brauner-Emmet-Teller analysis (BET)

0.05 g of sample was loaded into a BET tube and degassed under vacuum at 300 °C for 1 h on Quantachrome NOVA 2200e degassing station before being

weighed again. It was then placed into the BET station and run for a 5-point BET from 0.05-0.3 P/P_0 N_2 in order to determine surface area.

2.2.4 Scanning electron microscopy and energy dispersive X-ray spectroscopy (SEM-EDX)

Samples were prepared by loading a small amount of catalyst onto a self-adhesive carbon tab on a stainless-steel stub and were then analysed using a Hitachi TM3030Plus tabletop microscope equipped with a Bruker EDX detector. Samples were analysed using back scatter electrons at 15 kV and using EDX to determine composition of ceria/zirconia samples.

2.2.5 Powder X-ray diffraction (pXRD)

Samples produced by decomposition were loaded onto a silicon wafer and loaded into an X'Pert Pro PANalytical XRD with a Cu K-α source and scanned from 10–80 2θ. Samples made by precipitation were loaded into a sample holder and analysed using STOI STADI P with a Cu K-α source and scanned from 10–80 2θ.

Crystallite size was calculated using the Scherrer equation:

Eq. 2.1 $$\tau = \frac{K\lambda}{\beta \cos\theta}$$

Full width at half maximum (FWHM) β was determined in python using the SciPy package[44–46]

d-spacing was calculated using Braggs law:

Eq. 2.2 $$\lambda = 2d_{hkl} sin\theta_{hkl}$$

For a cubic crystallite the d values can be calculated by:

Eq. 2.3 $$\frac{1}{d^2} = \frac{h^2+k^2+l^2}{a^2}$$

Which can be combined to give lattice parameter a:

Eq 2.4 $$a^2 = \frac{\lambda^2}{4sin^2\theta}(h^2 + k^2 + l^2)$$

Where:

τ = crystallite size (nm)

K = dimensionless shape factor

β = Full width at half maximum (radians)

θ = Bragg angle (radians)

λ = x-ray wavelength (Å)

h, k, l = miller indices of the Bragg plane

a = lattice parameter (Å)

d = interplanar spacing (Å)

Due to the poor signal to noise, signal data for the decomposition sample 1:0.75 was smoothed using a 4-point moving average (2 points either side) to assist in peak finding and fitting.

2.2.6 Thermal gravimetric analysis (TGA)

For TGA a Perkin Elmer TGA4000 linked to a PolyScience cooler was used. Analysis was carried out under nitrogen with a 20 $mL.min^{-1}$ flow rate. The balance was zeroed using the ceramic crucible before being loaded to 50% of the crucible's maximum volume with sample. The TGA programme began at 40 °C and was held for 10 minutes. The temperature was then ramped to between 500-900 °C at 20 $°C.min^{-1}$.

2.2.7 Temperature programmed desorption (TPD)

TPD experiments were performed on a Quantachrome ChemBET TPR 3000. 0.1 g of each sample was heated under a flow of helium at 120 °C for 30 minutes, ammonia or CO_2 was then adsorbed to the catalyst at 25 °C. The adsorbate gas was then purged and the sample was held in a flow of helium at 40 $mL.min^{-1}$ for 2 h to remove physisorbed gas. The sample was then heated at a ramp rate of 10 $°C.min^{-1}$ under a 15 $ml.min^{-1}$ flow of helium. A thermal conductivity detector (TCD) was used to measure desorption, with a detector current of 180 mA.

2.3 Results and discussion

2.3.1 Catalyst synthesis by decomposition

Cerium oxide is one of the most commonly used heterogeneous materials for the direct synthesis of DMC. In this work, initial efforts focused on producing a high surface area cerium oxide, with the rationale being that with a larger surface area there will be a greater number of active sites per unit mass of

catalyst. The initial synthesis method was based on Nelson *et al.*[47] A template of block copolymer Pluronic® P104 was used to create a high surface area metal oxide. This was achieved by dispersing the cerium nitrate in ethanol with the block co-polymer dissolved, the ethanol was then evaporated off in a high surface area evaporating dish leaving behind a thin film. Once the temperature was raised above 150 °C this went from a transparent gel-like layer to a dirty orange layer. This step can lead to small flames which self-extinguish after several seconds. The remaining material was then calcined in air giving the final pale-yellow metal oxide (Figure 2.2).

Figure 2.2: Left: Cerium nitrate precursor after the pre-treatment step at 150 °C. Right: Final calcined cerium oxide.

By adjusting the ratio of precursor to the template, different surface areas could be obtained. Figure 2.3 shows the effect of different template to precursor ratios on the BET surface area of the cerium oxide. A volcano like plot was obtained with a peak at 0.75:1 and 1.15:1 to give a surface area of 425 $m^2.g^{-1}$ and 403 $m^2.g^{-1}$, respectively. Deviating from these template ratios lead to a decrease in surface area.

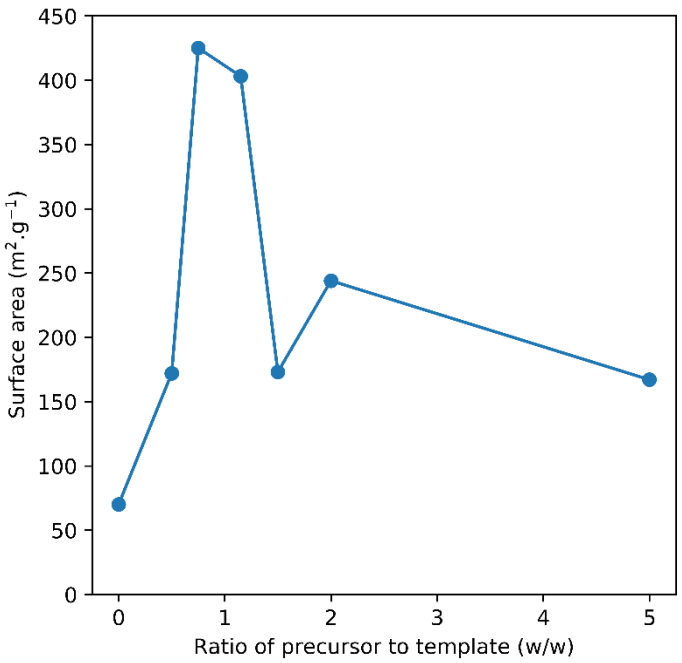

Figure 2.3: Effect of the precursor to template ratio on BET surface area of cerium oxide. Calcination in air at 450 °C 4.5 h, 1 °C.min^{-1} ramp rate. Line added as a guide to the eye.

pXRD analysis of these samples showed that all samples were indeed cerium oxide, with the only observable difference being the intensity and broadness of the peaks. This implies that at different template to precursor ratios, a change in crystallite size occurs. The commercial ceria had more intense, sharp peaks implying a higher degree of crystallinity and larger crystallite sizes (Figure 2.4). Broad, low intensity peaks have been previously shown to be caused by lower calcination temperatures.[48,49] This may indicated that the commercial ceria may have received higher calcination temperatures resulting in more intense, narrower peaks, and a higher degree of crystallinity and larger crystallite sizes.

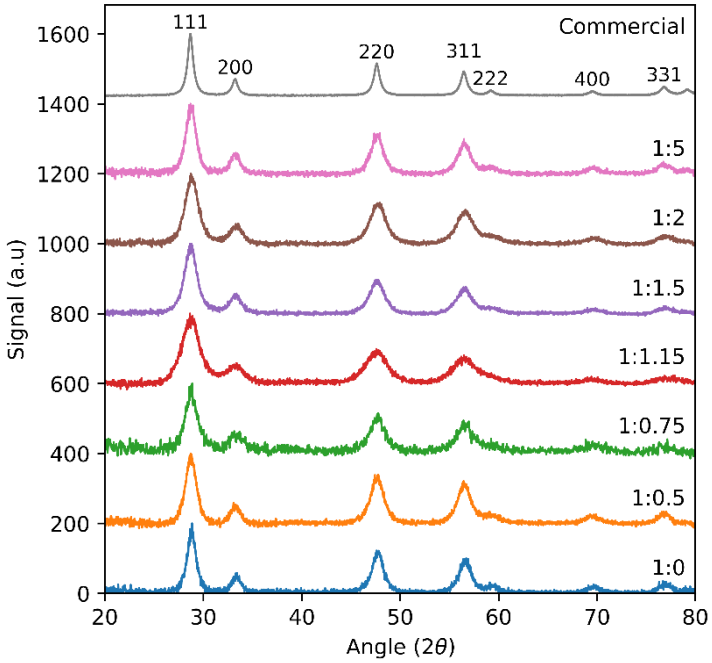

Figure 2.4: Normalised powder XRD patterns for cerium oxide samples synthesised by decomposition with varying ratios of precursor to template.

Table 2.4 shows the crystallite size, surface area and lattice parameter for each catalyst synthesised by decomposition. Interplanar spacings for each catalyst can be found in Appendix 1.

Table 2.4 Gives the ratio of precursor to template in the synthesis of cerium oxide, along with the recorded BET surface area.

Precursor: template ratio	XRD crystallite size (nm)	BET Surface area ($m^2.g^{-1}$)	Lattice parameter (Å)
1:0	8.6	70	5.3833
1:0.5	6.1	172	5.3995
1:0.75	5.3	425	5.3898
1:1.15	4.5	403	5.3898
1:1.5	5.6	173	5.3844
1:2	5.5	244	5.3697
1:5	6.6	167	5.3871
Commercial	12.3	50	5.3978

SEM was used to gain information on the topology of the cerium oxide samples. Figure 2.5 shows electron micrographs of cerium oxide samples synthesised

using the decomposition method. The micrographs show a number of pits and pores on the surface which may be linked to an increase in surface area.

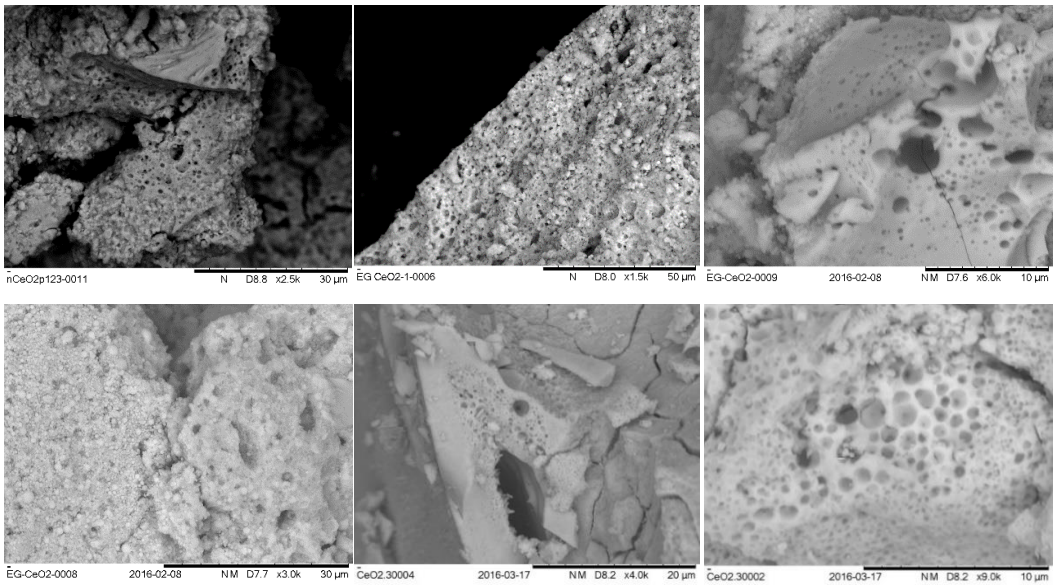

Figure 2.5: SEM micrographs of cerium oxide catalysts synthesised utilising a decomposition method. Top row: 1:1.15 ratio. Bottom row: Increasing ratios of polymer from left to right showing 1:0.5, 1:0.75 and 1:2. Samples are heat-treated at 150 °C followed by calcination at 450 °C.

As shown above, many reported catalysts have calcination temperatures in excess of 500 °C. It has been previously shown that higher calcination temperatures result in lower surface areas, due to effects such as sintering. TGA was used to confirm that calcination at 450 °C would decompose all of the precursor.

Figure 2.6 shows the TGA of cerium nitrate. Between 40 and 160 °C 9% of the mass is lost, assigned to water along with residual ethanol trapped in the surfactant.

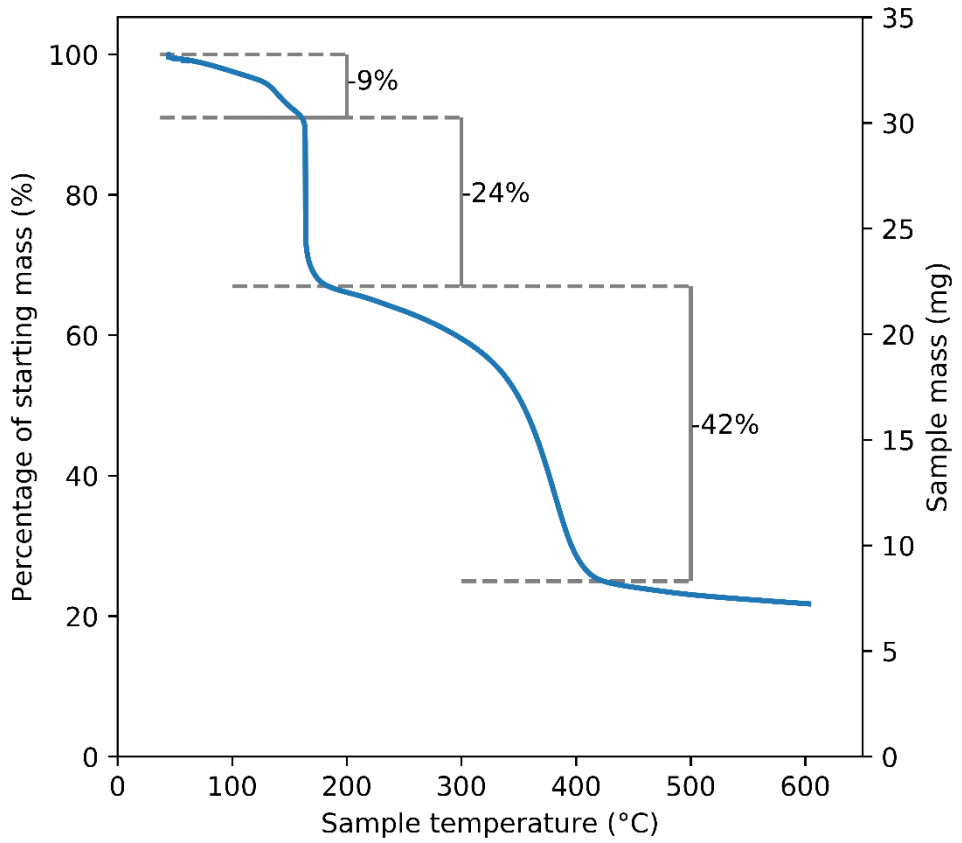

Figure 2.6: TGA trace of 1:1.15 cerium nitrate hexahydrate to precursor.

At 160 °C a 24% drop in mass was observed. This was not large enough to be the entirety of the template, as the template accounts for 54% of the total mass. Therefore, this likely corresponds to some of the polymer template and loss of water of crystallisation from the cerium nitrate. At 180 to 420 °C 42% of the mass was lost. This is attributed to the decomposition of the nitrate along with more of the template leading to stable metal oxide formation.[50] The mass loss was notable as the TGA was performed in N_2 so it was not oxidising like the calcination in air. Table 2.5 shows the expected masses of components expected to be present in the TGA sample, along with the final mass of the sample. Between 40 and 600 °C 78.2% of the initial mass was lost from the sample. Whilst these conditions are different from the final calcination conditions, the final mass was within 5% of the expected mass of CeO_2.

Table 2.5: Masses of each component in the TGA sample where a 1:1.15 ratio of w/w of precursor to template was used.

Component	Percent (%)	Mass (mg)
Pluronic® P104	53.5	17.78
$Ce(NO_3)_3.6H_2O$	46.5	15.46
Expected mass of CeO_2	18.4	6.13
Final mass	21.8	7.23

From this we can see that 450 °C is a reasonable temperature for calcination, and higher temperatures, which have previously been shown to be detrimental to the surface area of the synthesised metal oxide, can be avoided.[51]

2.3.2 Synthesis of Zirconium oxide by decomposition

Using the decomposition method of synthesis, an attempt was made to produce high surface area zirconium oxide. Zirconium oxynitrate however, is more thermally stable than cerium nitrate. Figure 2.7 shows the TGA trace of the zirconium precursor, $ZrO(NO_3)_3$, after an initial heat treatment step (removing the template). This trace showed that no appreciable loss in mass was observed until the sample was above 900 °C. This means that utilising templating along with decomposition is incompatible with producing a high surface area mixed ceria-zirconia catalyst, as calcination above 900 °C leads to a loss in surface area for both the ceria samples and zirconia samples. The zirconia produced at this temperature had a BET surface area measuring 7 m^2,g^{-1}. This is consistent with a similar method reported by Amadine *et al.*[51].

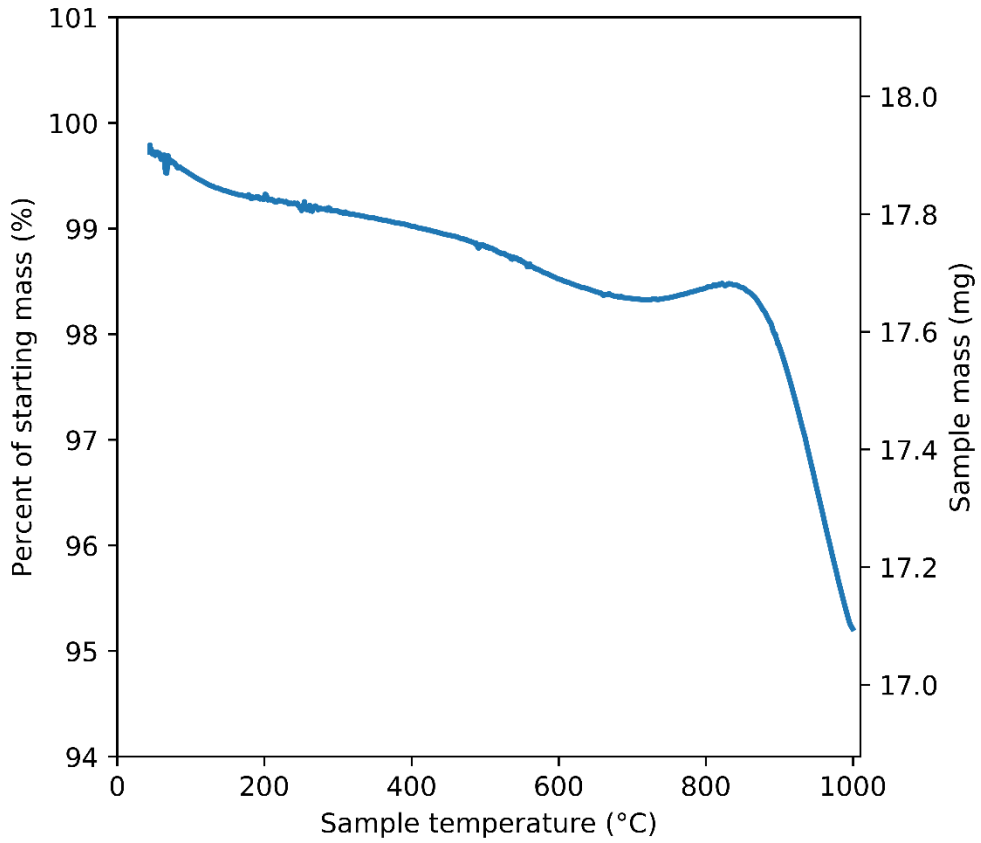

Figure 2.7: TGA trace of Zirconium oxynitrate after the 150 °C heat treatment step.

Therefore, in order to produce a mixed metal oxide, precipitation was determined to be a more promising synthesis route than thermal decomposition.

2.3.3 Catalyst synthesis by precipitation

Due to the challenges in producing a mixed metal oxide via decomposition, precipitation with ammonia was used. Precipitation either results from the chemical change of a precursor or the change in solvation of the precursor.[52] Chemical precipitation is most commonly achieved by changing the pH of the precursor resulting in a product that is insoluble or by antisolvent precipitation.[53] As has been discussed above, mixed metal oxides are popular catalysts for the synthesis of dialkyl carbonates and many are produced using precipitation such as the sol-gel method using citric acid, or with ammonia.

The precipitation was carried out by dissolving precursors ($Ce(NO_3)_3{\cdot}6H_2O$, $ZrO(NO_3)_2{\cdot}XH_2O$ or $Al(NO_3)_3$) into water along with Pluronic® P104. A solution of 35% ammonia was then added dropwise under vigorous stirring until pH 11 was reached. This was then left for 16 h to age, before being filtered and

calcined producing samples of ceria, zirconia, and several mixed metal oxides. This method was found to be more scalable than the decomposition method presented above, with precipitation yielding 3 g of catalyst in the same timescale as 0.3 g of catalyst via thermal decomposition.

Figure 2.8 shows the BET surface areas of the materials synthesised by precipitation. Surface area is dependent on the amount of zirconium present in the material. The mixed metal oxides with 50% or less zirconia gave surface areas exceeding 100 $m^2.g^{-1}$. However, unexpectedly, when increasing zirconia content above 50% a decrease in surface area was observed. This is unusual as zirconia is used in conjunction with ceria applications such as catalytic converters in order to improve stability to sintering.[54]

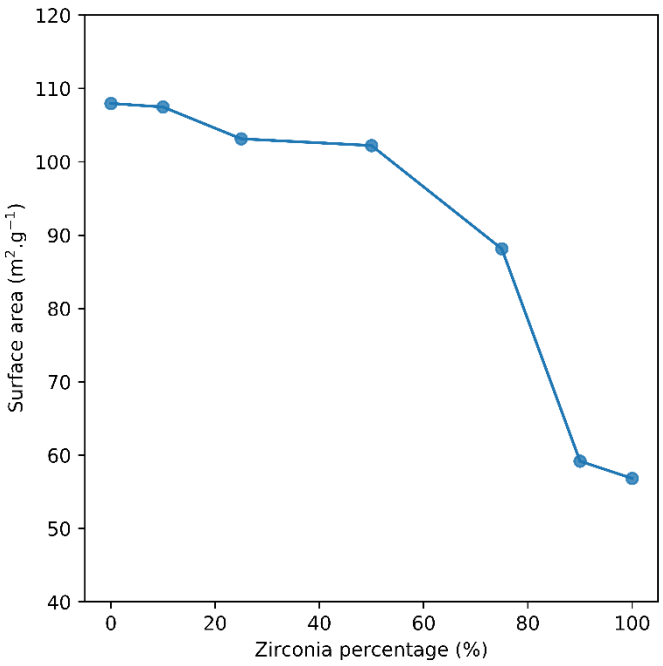

Figure 2.8: Shows the surface area measured by BET for ceria-zirconia mixtures ranging from 0–100% zirconia, line added as a guide to the eye.

A ceria alumina material, containing 10% alumina was also produced using the same method, achieving the highest surface area observed by precipitation giving 166 m^2 g^{-1}.

Figure 2.9 shows the DFT mean pore volume. This shows the general trend that materials higher in zirconia have a lower pore volume once zirconia content exceeds 50%.

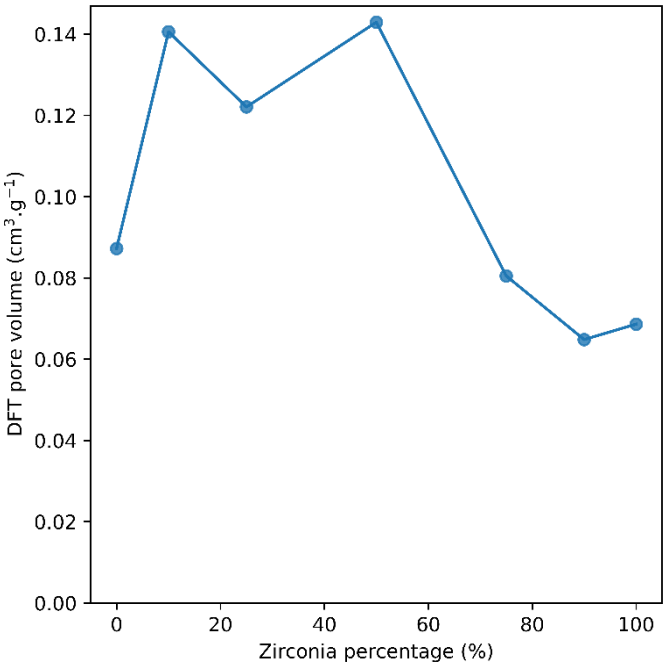

Figure 2.9: DFT pore volume of precipitated mixed metal oxides with different ceria-zirconia mixtures, line added as a guide to the eye.

SEM was used to determine the topology of the precipitation samples. Figure 2.10. shows electron micrographs of the materials produced by co-precipitation. When compared to the micrographs of the materials prepared by thermal decomposition (Figure 2.5), the materials produced by precipitation have much less pitting and roughness, which likely accounts for the decrease in surface area. The benefit is that mixed ceria-zirconia materials can be produced using coprecipitation.

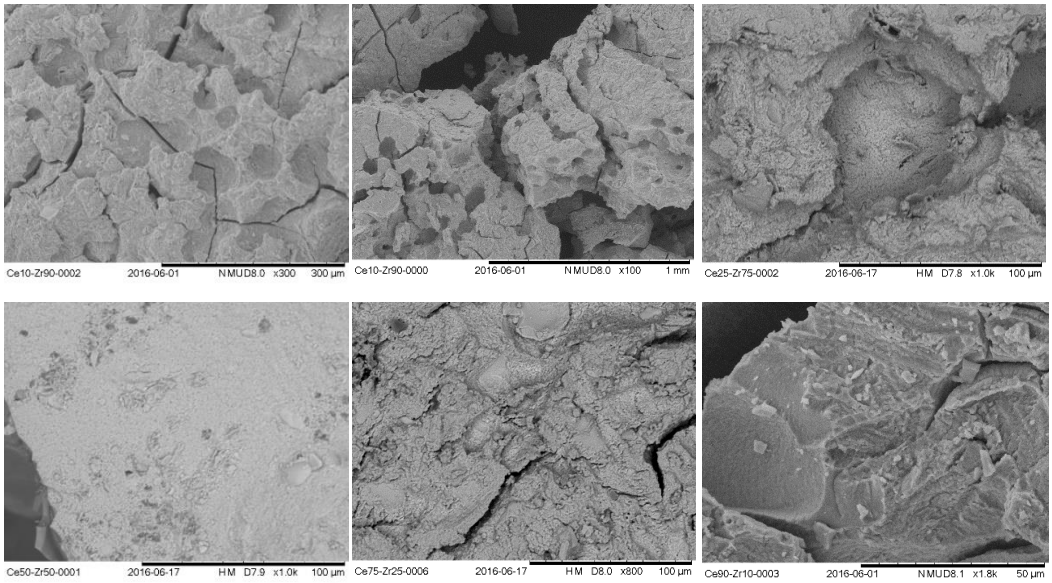

Figure 2.10: SEM Micrographs of mixed metal oxides synthesised by precipitation. Top row: $Ce_{0.1}Zr_{0.9}O_2$, $Ce_{0.25}Zr_{0.75}O_2$. Bottom row: $Ce_{0.5}Zr_{0.5}O_2$, $Ce_{0.75}Zr_{0.25}O_2$, $Ce_{0.9}Zr_{0.1}O_2$

The chemical composition of the mixed metal oxides synthesised was determined by SEM-EDX. Figure 2.11 shows EDX data with the corresponding micrograph.

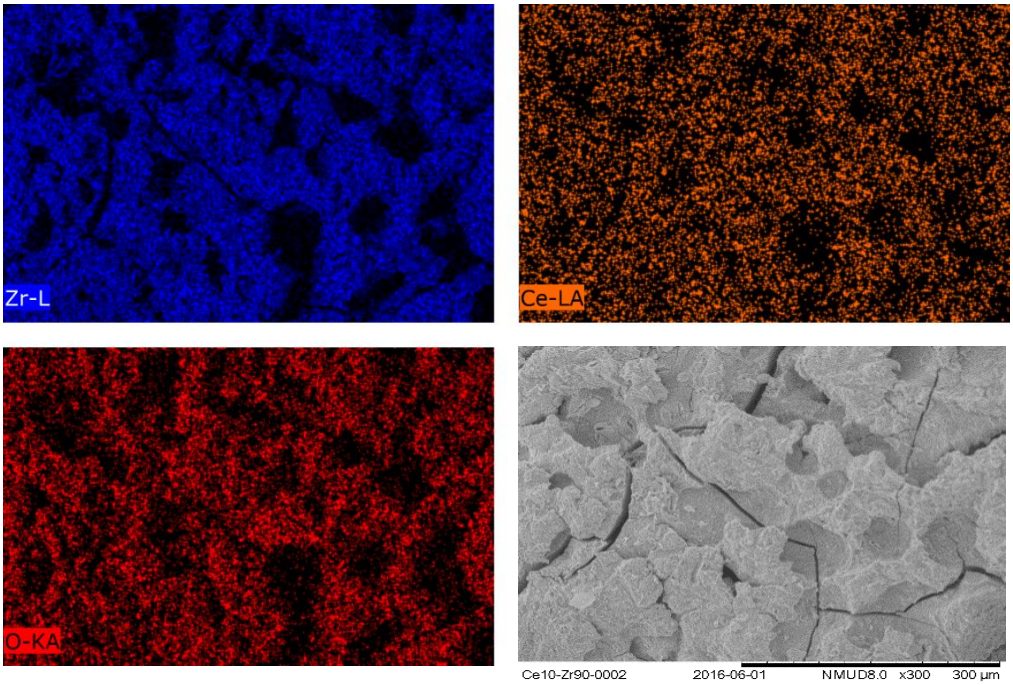

Figure 2.11: EDX and micrograph of the $Ce_{0.1}Zr_{0.9}O_2$ mixed metal oxide.

EDX is mostly a surface sensitive technique, this is due to the relatively low penetration of the electrons. Indeed in Figure 2.11 above, shadows can be seen due to the topology of the catalyst surface. The analysis of the material by EDX showed a good agreement to the ratio of ceria-zirconia expected based on the

proportion of starting material (Table 2.6). Though as the proportion of ceria increases, the more disagreement between the expected and observed ratio was seen. This means that the ratio of the metals observed by EDX was only what is on the surface and the bulk of the material may differ. However, as catalysis takes place on the material's surface, the surface composition is of more interest than the bulk composition. This intimate mixing observed by EDX showed that this coprecipitation can be used to produce a well-mixed ceria-zirconia mixed metal oxide.

Table 2.6: Showing the molar ratio of metals used in the reacting vessel compared to that measured by EDX.

Ratio of Precursors (Ce:Zr mol %)	Ratio by EDX measurement (Ce:Zr mol %)
10 : 90	10.78 : 89.22
25 : 75	32.32 : 67.68
50 : 50	58:39 : 41.61
75 : 25	81.05 : 18.95

pXRD showed that with increasing cerium percentage, the structure of the crystallite becomes more similar to pure cerium oxide (Figure 2.12). A change in 2θ for the same crystal faces was seen as the zirconium content increased, with the angle of the (111) face decreasing from 29 2θ with pure cerium oxide down to 28 2θ at 50% zirconia. This then increased with increasing zirconia content up to 30 2θ with pure ZrO_2. This corresponds to a change in the lattice parameter as due to incorporation of Zr^{4+} ions into the ceria fluorite lattice.[55,56]

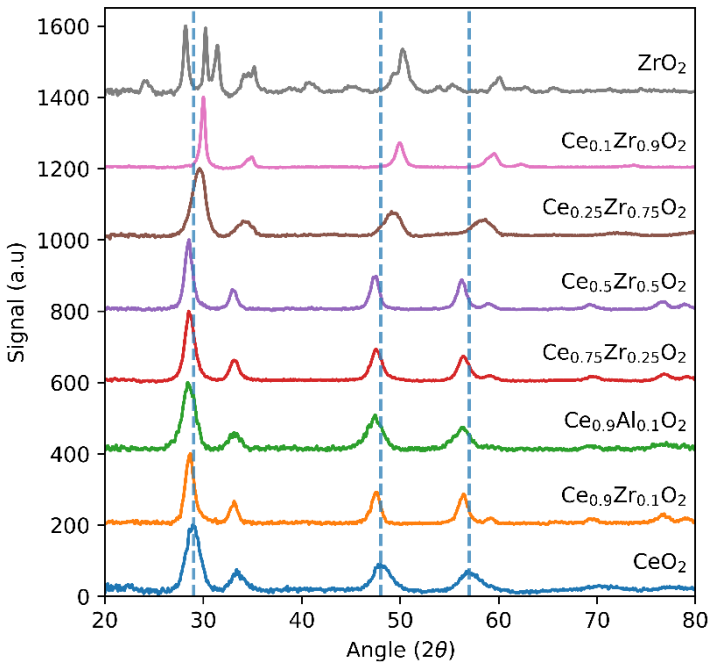

Figure 2.12: Normalised powder XRD of catalysts synthesised by precipitation. Dashed lines show the shift of 2θ as the proportion of cerium decreases in the catalyst.

The pXRD of ZrO_2 appears to be a mixture of crystal phases showing multiple peaks where the 111 peak is expected (around 30 2θ) which is consistent with a mixture of monoclinic and tetragonal zirconia.[57] Figure 2.13 shows the synthesised zirconia compared with monoclinic, orthorhombic and tetragonal ZrO_2 obtained from the American mineralogist crystal structure database.[58] Though the intensity of the monoclinic peaks was reduced from ZrO_2 to $Ce_{0.1}Zr_{0.9}O_2$ the peak shape of the 200 peak suggests that there was still a mixture of phases.

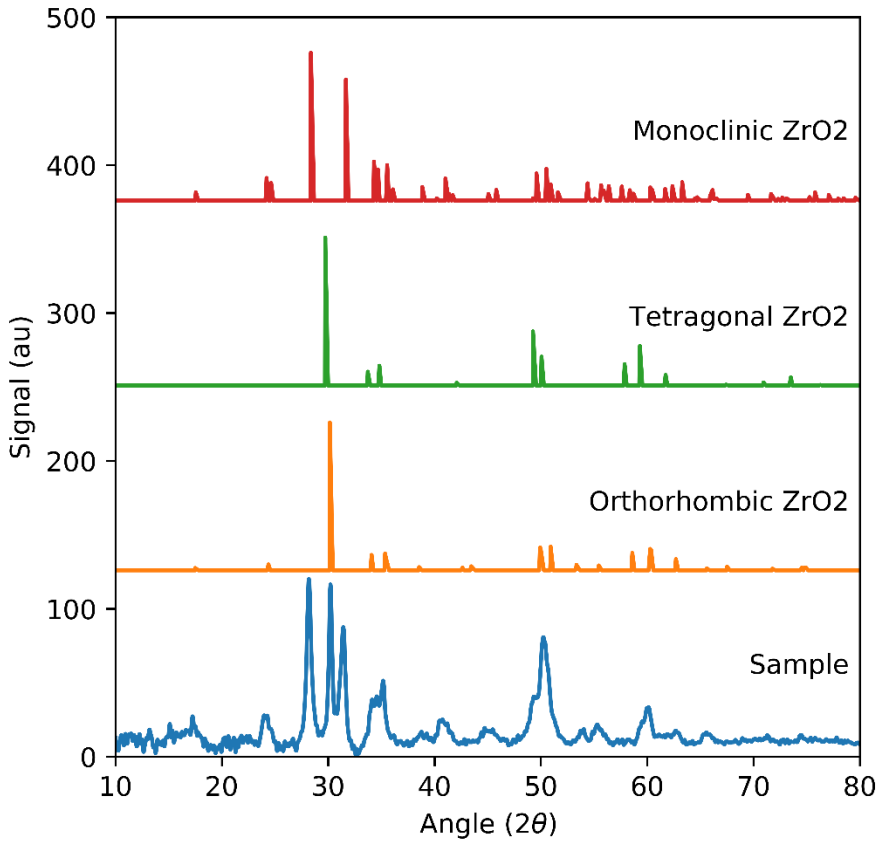

Figure 2.13: XRD of ZrO_2 sample compared with orthorhombic[59], tetragonal[60] and monoclinic ZrO_2.[61]

Crystallite size for these metal oxides were calculated using the Scherrer equation. Table 2.7 shows a trend that with increasing cerium crystallite size decreases. While peak broadening can be due to decreasing crystallite size, inhomogeneous mixtures can also cause broadening of XRD peaks which may be the cause of the broad peaks with $Ce_{0.25}Zr_{0.75}O_2$.

Table 2.7: Crystallite size, surface area and lattice parameter for pure and mixed metal oxides synthesised by precipitation.

Catalyst	XRD crystallite size (nm)	Surface area ($m^2.g^{-1}$)	Lattice Parameter (Å)
ZrO_2	13.76	57	—
$Ce_{0.1}Zr_{0.9}O_2$	9.07	59	5.1485
$Ce_{0.25}Zr_{0.75}O_2$	5.20	88	5.2348
$Ce_{0.5}Zr_{0.5}O_2$	8.83	102	5.416
$Ce_{0.75}Zr_{0.25}O_2$	7.01	103	5.4082
$Ce_{0.9}Zr_{0.1}O_2$	7.87	108	5.3986
CeO_2	4.77	108	5.3625
$Ce_{0.9}Al_{0.1}O_y$	5.48	166	5.4136

2.3.4 Temperature programmed desorption

Acid-base properties have been shown to be important for the synthesis of dialkyl carbonates from CO_2 and alcohols. TPD was used to determine acid and base properties. Due to difficulties with equipment however, only qualitative analysis of basic sites was possible. CO_2 was used as the adsorbate to determine relative concentration of basic sites.

TPD is split into three regions. Weakly basic/acidic sites should allow desorption of CO_2 at temperatures up to 50-150 °C. Moderately basic/acidic sites between 150 and 300 °C, and strongly basic/acidic sites above 300 °C.[15]

Figure 2.14 shows that the $Ce_{0.9}Al_{0.1}O_y$ contains mostly weak and moderate basic sites, with some strongly basic sites observed over 300°C. Commercial ceria had a strong signal in the weak-moderately basic region. Other catalysts synthesised had much lower signals implying lower adsorption of CO_2. However, without a calibration, a quantitative measurement of the basicity of the catalysts was not possible. And as Figure 2.1 shows, basicity alone does not determine catalyst efficacy.

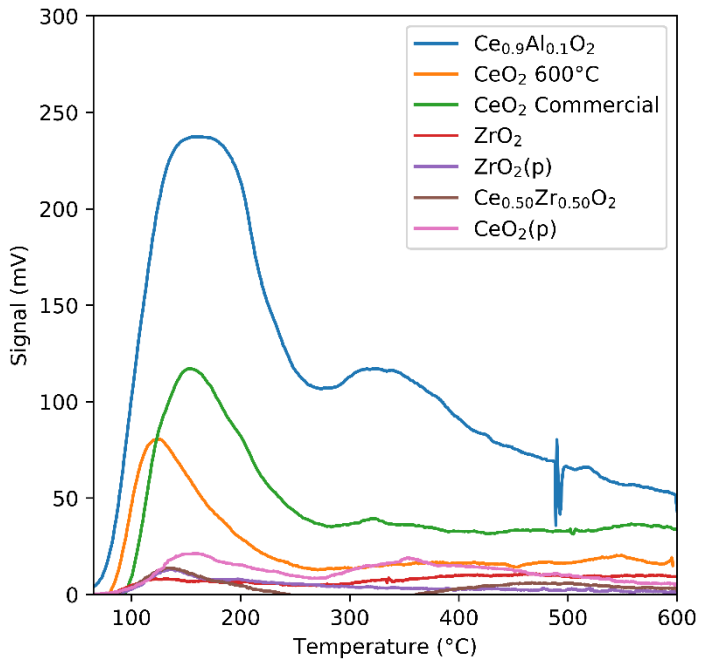

Figure 2.14: CO_2 TPD of a number of catalysts produced by precipitation along with the commercial CeO_2 used in future chapters.

Determination of acid sites was attempted using Ammonia TPD. However, due to detector drift and other technical difficulties, this has not been included.

2.4 Conclusions

In this chapter a number of materials, which have literature precedent for their use as heterogeneous catalysts for DAC synthesis, has been synthesised. Pure CeO_2 materials produced by thermal decomposition show the greatest surface areas, exceeding 400 $m^2.g^{-1}$. Due to the high decomposition temperature of zirconium oxynitrate, ammonia precipitation was used to produce pure ZrO_2 and Ce/Zr mixed metal oxides. These materials showed good mixing between the two metal oxides and exhibit lower surface areas around 100 $m^2.g^{-1}$.

The metal oxides prepared here will be tested in future chapters for their activity towards dialkyl carbonate synthesis and their stability within that reaction. From its higher surface area and weak-base peak in the TPD one might expect the $Ce_{0.9}Al_{0.1}O_2$ to perform best catalytically.

2.5 References

(1) Santos, B. A. V.; Silva, V. M. T. M.; Loureiro, J. M.; Rodrigues, A. E. Review for the Direct Synthesis of Dimethyl Carbonate. *ChemBioEng Rev.* **2014**, *1* (5), 214–229. https://doi.org/10.1002/cben.201400020.

(2) Fang, S.; Fujimoto, K. Direct Synthesis of Dimethyl Carbonate from Carbon Dioxide and Methanol Catalyzed by Base. *Appl. Catal. A Gen.* **1996**, *142* (1), 8–10. https://doi.org/10.1016/0926-860X(96)00081-6.

(3) Fujita, S. I. I.; Bhanage, B. M. M.; Ikushima, Y.; Arai, M. Synthesis of Dimethyl Carbonate from Carbon Dioxide and Methanol in the Presence of Methyl Iodide and Base Catalysts under Mild Conditions: Effect of Reaction Conditions and Reaction Mechanism. *Green Chem.* **2001**, *3* (2), 87–91. https://doi.org/10.1039/b100363l.

(4) Cai, Q.; Jin, C.; Lu, B.; Tangbo, H.; Shan, Y. Synthesis of Dimethyl Carbonate from Methanol and Carbon Dioxide Using Potassium Methoxide as Catalyst under Mild Conditions. *Catal. Letters* **2005**, *103* (3–4), 225–228. https://doi.org/10.1007/s10562-005-7158-2.

(5) Zhao, T.; Hu, X.; Wu, D.; Li, R.; Yang, G.; Wu, Y. Direct Synthesis of Dimethyl Carbonate from Carbon Dioxide and Methanol at Room Temperature Using Imidazolium Hydrogen Carbonate Ionic Liquid as a Recyclable Catalyst and Dehydrant. *ChemSusChem* **2017**, *10* (9), 2046–2052. https://doi.org/10.1002/cssc.201700128.

(6) Sun, J.; Lu, B.; Wang, X.; Li, X.; Zhao, J.; Cai, Q. A Functionalized Basic Ionic Liquid for Synthesis of Dimethyl Carbonate from Methanol and CO2. *Fuel Process. Technol.* **2013**, *115*, 233–237. https://doi.org/10.1016/j.fuproc.2013.06.009.

(7) Ballivet-Tkatchenko, D.; Ligabue, R. A.; Plasseraud, L. Synthesis of Dimethyl Carbonate in Supercritical Carbon Dioxide. *Brazilian J. Chem. Eng.* **2006**, *23* (1), 111–116. https://doi.org/10.1590/S0104-66322006000100012.

(8) Choi, J. C.; Kohno, K.; Ohshima, Y.; Yasuda, H.; Sakakura, T. Tin- or Titanium-Catalyzed Dimethyl Carbonate Synthesis from Carbon Dioxide and Methanol: Large Promotion by a Small Amount of Triflate Salts. *Catal. Commun.* **2008**, *9* (7), 1630–1633. https://doi.org/10.1016/j.catcom.2008.01.013.

(9) Choi, J. C.; Sakakura, T.; Sako, T. Reaction of Dialkyltin Methoxide with Carbon Dioxide Relevant to the Mechanisms of Catalytic Carbonate Synthesis. *J. Am. Chem. Soc.* **1999**, *121* (15), 3793–3794. https://doi.org/10.1021/ja9900499.

(10) Choi, J.-C. C.; He, L.-N. N.; Yasuda, H.; Sakakura, T.; Yasudaa, H.; Sakakura, T. Selective and High Yield Synthesis of Dimethyl Carbonate Directly from Carbon Dioxide and Methanol. *Green Chem.* **2002**, *4* (3), 230–234. https://doi.org/10.1039/b200623p.

(11) Sakakura, T.; Choi, J. C.; Saito, Y.; Masuda, T.; Sako, T.; Oriyama, T. Metal-Catalyzed Dimethyl Carbonate Synthesis from Carbon Dioxide and Acetals. *J. Org. Chem.* **1999**, *64* (12), 4506–4508. https://doi.org/10.1021/jo990155t.

(12) Kohno, K.; Choi, J.-C.; Ohshima, Y.; Hiroyuki, Y.; Sakakura, T. Synthesis of Dimethyl Carbonate from Carbon Dioxide Catalyzed by

Titanium Alkoxides with Polyether-Type Ligands. *ChemSusChem* **2008**, *1* (3), 186–188.

(13) Tomishige, K.; Kunimori, K. Catalytic and Direct Synthesis of Dimethyl Carbonate Starting from Carbon Dioxide Using CeO2-ZrO2 Solid Solution Heterogeneous Catalyst: Effect of H2O Removal from the Reaction System. *Appl. Catal. A Gen.* **2002**, *237* (1–2), 103–109. https://doi.org/10.1016/S0926-860X(02)00322-8.

(14) Aresta, M.; Dibenedetto, A.; Pastore, C.; Cuocci, C.; Aresta, B.; Cometa, S.; De Giglio, E.; Degiglio, E. Cerium(IV)Oxide Modification by Inclusion of a Hetero-Atom: A Strategy for Producing Efficient and Robust Nano-Catalysts for Methanol Carboxylation. *Catal. Today* **2008**, *137* (1), 125–131. https://doi.org/10.1016/j.cattod.2008.04.043.

(15) Li, A.; Pu, Y.; Li, F.; Luo, J.; Zhao, N.; Xiao, F. Synthesis of Dimethyl Carbonate from Methanol and CO2 over Fe-Zr Mixed Oxides. *J. CO2 Util.* **2017**, *19*, 33–39. https://doi.org/10.1016/j.jcou.2017.02.016.

(16) Ikeda, Y.; Sakaihori, T.; Tomishige, K.; Fujimoto, K. Promoting Effect of Phosphoric Acid on Zirconia Catalysts in Selective Synthesis of Dimethyl Carbonate from Methanol and Carbon Dioxide. *Catal. Letters* **2000**, *66* (1–2), 59–62. https://doi.org/10.1023/A:1019043422050.

(17) Jiang, C.; Guo, Y.; Wang, C.; Hu, C.; Wu, Y.; Wang, E. Synthesis of Dimethyl Carbonate from Methanol and Carbon Dioxide in the Presence of Polyoxometalates under Mild Conditions. *Appl. Catal. A Gen.* **2003**, *256* (1–2), 203–212. https://doi.org/10.1016/S0926-860X(03)00400-9.

(18) Wu, X. L.; Xiao, M.; Meng, Y. Z.; Lu, Y. X. Direct Synthesis of Dimethyl Carbonate on H3PO4 Modified V2O5. *J. Mol. Catal. A Chem.* **2005**, *238* (1–2), 158–162. https://doi.org/10.1016/j.molcata.2005.05.018.

(19) Lee, H. J.; Park, S.; Jung, J. C.; Song, I. K. Direct Synthesis of Dimethyl Carbonate from Methanol and Carbon Dioxide over H3PW12O40/CeXZr1-XO2 Catalysts: Effect of Acidity of the Catalysts. *Korean J. Chem. Eng.* **2011**, *28* (7), 1518–1522. https://doi.org/10.1007/s11814-011-0020-x.

(20) Lee, H. J.; Joe, W.; Song, I. K. Direct Synthesis of Dimethyl Carbonate from Methanol and Carbon Dioxide over Transition Metal Oxide/Ce0.6Zr0.4O2 Catalysts: Effect of Acidity and Basicity of the Catalysts. *Korean J. Chem. Eng.* **2012**, *29* (3), 317–322. https://doi.org/10.1007/s11814-011-0185-3.

(21) Dibenedetto, A.; Aresta, M.; Angelini, A.; Ethiraj, J.; Aresta, B. M. Synthesis, Characterization, and Use of Nb V/Ce IV-Mixed Oxides in the Direct Carboxylation of Ethanol by Using Pervaporation Membranes for Water Removal. *Chem. - A Eur. J.* **2012**, *18* (33), 10324–10334. https://doi.org/10.1002/chem.201201561.

(22) Zhang, Z. F.; Liu, Z. W.; Lu, J.; Liu, Z. T. Synthesis of Dimethyl Carbonate from Carbon Dioxide and Methanol over CexZr1-XO2 and

[EMIM]Br/Ce0.5Zr 0.5O2. *Ind. Eng. Chem. Res.* **2011**, *50* (4), 1981–1988. https://doi.org/10.1021/ie102017j.

(23) Yang, Q.; Wang, H.; Ding, X.; Yang, X.; Wang, Y. One-Pot Synthesis of Dimethyl Carbonate from Carbon Dioxide, Cyclohexene Oxide, and Methanol. *Res. Chem. Intermed.* **2015**, *41* (7), 4101–4111. https://doi.org/10.1007/s11164-013-1514-4.

(24) Cui, H.; Wang, T.; Wang, F.; Gu, C.; Wang, P.; Dai, Y. Kinetic Study on the One-Pot Synthesis of Dimethyl Carbonate in Supercritical CO2 Conditions. *Ind. Eng. Chem. Res.* **2004**, *43* (24), 7732–7739. https://doi.org/10.1021/ie049715r.

(25) Shi, M.; Shen, Y.-M. Synthesis of Mixed Carbonates via a Three-Component Coupling of Alcohols, CO2, and Alkyl Halides in the Presence of K2CO3 and Tetrabutylammonium Iodide. *Molecules* **2002**, *7* (4), 386–393. https://doi.org/10.3390/70400386.

(26) Ono, Y. Catalysis in the Production and Reactions of Dimethyl Carbonate, an Environmentally Benign Building Block. *Appl. Catal. A Gen.* **1997**, *155* (2), 133–166. https://doi.org/10.1016/S0926-860X(96)00402-4.

(27) Honda, M.; Tamura, M.; Nakagawa, Y.; Nakao, K.; Suzuki, K.; Tomishige, K. Organic Carbonate Synthesis from CO2 and Alcohol over CeO2 with 2-Cyanopyridine: Scope and Mechanistic Studies. *J. Catal.* **2014**, *318*, 95–107. https://doi.org/10.1016/j.jcat.2014.07.022.

(28) Chen, Y.; Wang, H.; Qin, Z.; Tian, S.; Ye, Z.; Ye, L.; Abroshan, H.; Li, G. TiXCe1-XO2 Nanocomposites: A Monolithic Catalyst for the Direct Conversion of Carbon Dioxide and Methanol to Dimethyl Carbonate. *Green Chem.* **2019**, *21* (17), 4642–4649. https://doi.org/10.1039/c9gc00811j.

(29) Honda, M.; Tamura, M.; Nakagawa, Y.; Sonehara, S.; Suzuki, K.; Fujimoto, K. I.; Tomishige, K. Ceria-Catalyzed Conversion of Carbon Dioxide into Dimethyl Carbonate with 2-Cyanopyridine. *ChemSusChem* **2013**, *6* (8), 1341–1344. https://doi.org/10.1002/cssc.201300229.

(30) Fu, Z.; Zhong, Y.; Yu, Y.; Long, L.; Xiao, M.; Han, D.; Wang, S.; Meng, Y. TiO2-Doped CeO2 Nanorod Catalyst for Direct Conversion of CO2 and CH3OH to Dimethyl Carbonate: Catalytic Performance and Kinetic Study. *ACS Omega* **2018**, *3* (1), 198–207. https://doi.org/10.1021/acsomega.7b01475.

(31) Liu, B.; Li, C.; Zhang, G.; Yan, L.; Li, Z. Direct Synthesis of Dimethyl Carbonate from CO2 and Methanol over CaO-CeO2 Catalysts: The Role of Acid-Base Properties and Surface Oxygen Vacancies. *New J. Chem.* **2017**, *41* (20), 12231–12240. https://doi.org/10.1039/c7nj02606d.

(32) Yoshida, Y.; Arai, Y.; Kado, S.; Kunimori, K.; Tomishige, K. Direct Synthesis of Organic Carbonates from the Reaction of CO2 with Methanol and Ethanol over CeO2 Catalysts. *Catal. Today* **2006**, *115* (1–4), 95–101. https://doi.org/10.1016/j.cattod.2006.02.027.

(33) Liu, B.; Li, C.; Zhang, G.; Yao, X.; Chuang, S. S. C.; Li, Z. Oxygen Vacancy Promoting Dimethyl Carbonate Synthesis from CO2 and Methanol over Zr-Doped CeO2 Nanorods. *ACS Catal.* **2018**, *8* (11), 10446–10456. https://doi.org/10.1021/acscatal.8b00415.

(34) Chen, L.; Wang, S.; Zhou, J.; Shen, Y.; Zhao, Y.; Ma, X. Dimethyl Carbonate Synthesis from Carbon Dioxide and Methanol over CeO2versus over ZrO2: Comparison of Mechanisms. *RSC Adv.* **2014**, *4* (59), 30968–30975. https://doi.org/10.1039/c4ra03081h.

(35) Zhang, M.; Xiao, M.; Wang, S.; Han, D.; Lu, Y.; Meng, Y. Cerium Oxide-Based Catalysts Made by Template-Precipitation for the Dimethyl Carbonate Synthesis from Carbon Dioxide and Methanol. *J. Clean. Prod.* **2015**, *103*, 847–853. https://doi.org/10.1016/j.jclepro.2014.09.024.

(36) Al-Darwish, J.; Senter, M.; Lawson, S.; Rezaei, F.; Rownaghi, A. A. Ceria Nanostructured Catalysts for Conversion of Methanol and Carbon Dioxide to Dimethyl Carbonate. *Catal. Today* **2020**, *350*, 120–126. https://doi.org/10.1016/j.cattod.2019.06.013.

(37) Stoian, D.; Bansode, A.; Medina, F.; Urakawa, A. Catalysis under Microscope: Unraveling the Mechanism of Catalyst de- and Re-Activation in the Continuous Dimethyl Carbonate Synthesis from CO2 and Methanol in the Presence of a Dehydrating Agent. *Catal. Today* **2016**, *283*, 2–10. https://doi.org/10.1016/j.cattod.2016.03.038.

(38) Arbeláez, O.; Orrego, A.; Bustamante, F.; Villa, A. L. Effect of Acidity, Basicity and ZrO2 Phases of Cu-Ni/ZrO2 Catalysts on the Direct Synthesis of Diethyl Carbonate from CO2 and Ethanol. *Catal. Letters* **2016**, *146* (4), 725–733. https://doi.org/10.1007/s10562-016-1699-4.

(39) Zhang, X.; Jia, D.; Zhang, J.; Sun, Y. Direct Synthesis of Diethyl Carbonate from CO2 and Ethanol Catalyzed by ZrO2/Molecular Sieve. *Catal. Letters* **2014**, *144* (12), 2144–2150. https://doi.org/10.1007/s10562-014-1403-5.

(40) Vivier, L.; Duprez, D. Ceria-Based Solid Catalysts for Organic Chemistry. *ChemSusChem* **2010**, *3* (6), 654–678. https://doi.org/10.1002/cssc.201000054.

(41) Jung, K. T.; Bell, A. T. An in Situ Infrared Study of Dimethyl Carbonate Synthesis from Carbon Dioxide and Methanol over Zirconia. *J. Catal.* **2001**, *204* (2), 339–347. https://doi.org/10.1006/jcat.2001.3411.

(42) Chen, L.; Wang, S.; Zhou, J.; Shen, Y.; Zhao, Y.; Ma, X. Dimethyl Carbonate Synthesis from Carbon Dioxide and Methanol over CeO_2 versus over ZrO_2 : Comparison of Mechanisms. *RSC Adv.* **2014**, *4* (59), 30968. https://doi.org/10.1039/C4RA03081H.

(43) Lee, H. J.; Park, S.; Song, I. K.; Jung, J. C. Direct Synthesis of Dimethyl Carbonate from Methanol and Carbon Dioxide over Ga2O3/Ce0.6Zr0.4O2 Catalysts: Effect of Acidity and Basicity of the Catalysts. *Catal. Letters* **2011**, *141* (4), 531–537. https://doi.org/10.1007/s10562-010-0544-4.

(44) Virtanen, P.; Gommers, R.; Oliphant, T. E.; Haberland, M.; Reddy, T.; Cournapeau, D.; Burovski, E.; Peterson, P.; Weckesser, W.; Bright, J.; et al. SciPy 1.0: Fundamental Algorithms for Scientific Computing in Python. *Nat. Methods* **2020**. https://doi.org/10.1038/s41592-019-0686-2.

(45) Millman, K. J.; Aivazis, M. Python for Scientists and Engineers. *Comput. Sci. Eng.* **2011**, *13* (2), 9–12. https://doi.org/10.1109/MCSE.2011.36.

(46) Oliphant, T. E. Python for Scientific Computing. *Comput. Sci. Eng.* **2007**, *9* (3), 10–20. https://doi.org/10.1109/MCSE.2007.58.

(47) Nelson, N. C.; Manzano, J. S.; Sadow, A. D.; Overbury, S. H.; Slowing, I. I. Selective Hydrogenation of Phenol Catalyzed by Palladium on High-Surface-Area Ceria at Room Temperature and Ambient Pressure. *ACS Catal.* **2015**, *5* (4), 2051–2061. https://doi.org/10.1021/cs502000j.

(48) Li, M.; Hu, Y.; Liu, C.; Huang, J.; Liu, Z.; Wang, M.; An, Z. Synthesis of Cerium Oxide Particles via Polyelectrolyte Controlled Nonclassical Crystallization for Catalytic Application. *RSC Adv.* **2014**, *4* (2), 992–995. https://doi.org/10.1039/c3ra44698k.

(49) Kim, N. W.; Lee, D. K.; Yu, H. Selective Shape Control of Cerium Oxide Nanocrystals for Photocatalytic and Chemical Sensing Effect. *RSC Adv.* **2019**, *9* (24), 13829–13837. https://doi.org/10.1039/c9ra01519a.

(50) Baqer, A. A.; Matori, K. A.; Al-Hada, N. M.; Shaari, A. H.; Kamari, H. M.; Saion, E.; Chyi, J. L. Y.; Abdullah, C. A. C. Synthesis and Characterization of Binary (CuO)0.6(CeO2)0.4 Nanoparticles via a Simple Heat Treatment Method. *Results Phys.* **2018**, *9*, 471–478. https://doi.org/10.1016/j.rinp.2018.02.079.

(51) Amadine, O.; Essamlali, Y.; Fihri, A.; Larzek, M.; Zahouily, M. Effect of Calcination Temperature on the Structure and Catalytic Performance of Copper–Ceria Mixed Oxide Catalysts in Phenol Hydroxylation. *RSC Adv.* **2017**, *7* (21), 12586–12597. https://doi.org/10.1039/c7ra00734e.

(52) Schuth, F.; Hesse, M.; Unger, K. K. Handbook of Heterogenous Catalysis. In *Handbook of Heterogenous Catalysis*; 1999; pp 100–119.

(53) Smith, P. J.; Kondrat, S. A.; Carter, J. H.; Chater, P. A.; Bartley, J. K.; Taylor, S. H.; Spencer, M. S.; Hutchings, G. J. Supercritical Antisolvent Precipitation of Amorphous Copper–Zinc Georgeite and Acetate Precursors for the Preparation of Ambient-Pressure Water-Gas-Shift Copper/Zinc Oxide Catalysts. *ChemCatChem* **2017**, *9* (9), 1621–1631. https://doi.org/10.1002/cctc.201601603.

(54) Di Monte, R.; Kašpar, J. Heterogeneous Environmental Catalysis - A Gentle Art: CeO 2-ZrO2 Mixed Oxides as a Case History. *Catal. Today* **2005**, *100* (1–2), 27–35. https://doi.org/10.1016/j.cattod.2004.11.005.

(55) Saada, R.; Kellici, S.; Heil, T.; Morgan, D.; Saha, B. Greener Synthesis of Dimethyl Carbonate Using a Novel Ceria-Zirconia Oxide/Graphene Nanocomposite Catalyst. *Appl. Catal. B Environ.* **2015**, *168–169*, 352–362. https://doi.org/10.1016/j.apcatb.2014.12.013.

(56) Cabañas, A.; Darr, J. A.; Lester, E.; Poliakoff, M. Continuous Hydrothermal Synthesis of Inorganic Materials in a Near-Critical Water Flow Reactor; the One-Step Synthesis of Nano-Particulate Ce1-XZrxO2 (X=0-1) Solid Solutions. *J. Mater. Chem.* **2001**, *11* (2), 561–568. https://doi.org/10.1039/b008095k.

(57) Gusain, D.; Singh, P. K.; Sharma, Y. C. Kinetic and Equilibrium Modelling of Adsorption of Cadmium on Nano Crystalline Zirconia Using Response Surface Methodology. *Environ. Nanotechnology, Monit. Manag.* **2016**, *6* (October 2017), 99–107. https://doi.org/10.1016/j.enmm.2016.07.002.

(58) Downs, R. T.; Hall-Wallace, M. The American Mineralogist Crystal Structure Database. *Am. Mineral.* **2003**, *88*, 247–250. https://doi.org/10.1007/978-3-642-00207-6_5.

(59) Kisi, H. E.; Howard, J. C.; Hill, J. R. Crystal Structure of Orthorhombic Zirconia in Partially Stabilized Zirconia. *J. Am. Ceram. Soc.* **1989**, *72*, 1757–1760.

(60) Persson, K. Materials Data on ZrO2 (SG:137) by Materials Project https://materialsproject.org/materials/mp-2574/. https://doi.org/10.17188/1200956.

(61) McCullough, J. D.; Trueblood, K. N. *Acta Crystallographica 12*; 1959.

Chapter 3 – Catalyst Testing with dehydrating agents

3.1 Introduction

In Chapter 2 multiple Ce and Zr based metal oxides were synthesised, including a number of Ce-Zr mixed metal oxides. In this chapter, their use in catalysing the direct synthesis of dialkyl carbonates will be investigated. The direct synthesis of dialkyl carbonates is of interest, as dialkyl carbonates are used in a number of organic transformations and solvent applications as discussed in Chapter 1. The investigation of this reaction will either utilise a dehydrating agent, providing a driving force for the reaction, or will be limited by the reaction's thermodynamics (Chapters 4 and 5).

Broadly speaking there are two types of dehydrating systems that can be used. The first physically removes the water from the system, by adsorption or membranes, which lowers the concentration of products pushing the equilibrium of the reaction towards products. This method of dehydration provides some driving force in terms of free energy of adsorption (or by Le Chatelier's principle), but this is typically not enough to make the reaction spontaneous.

The second type of dehydrating system is one in which the water is reacted with a dehydrating agent to produce a stable product. These reagents provide additional thermodynamic driving force as they essentially change the reaction from a reversible reaction shown below in Scheme 3.1A, to an irreversible reaction shown in Scheme 3.1B.

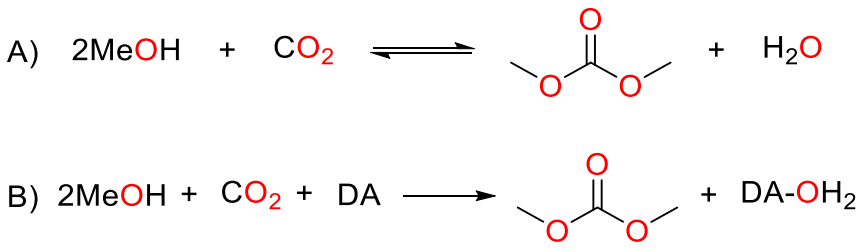

Scheme 3.1: Synthesis of dimethyl carbonate from CO_2 and methanol. A) Direct reaction between CO_2 and methanol to form DMC and water. B) Synthesis of dialkyl carbonates with a dehydrating agent (DA) to form DMC and a hydrated-DA.

This introduction will concentrate on reactions which use dehydrating agents. Firstly, how dehydrating agents change the thermodynamics of the reaction, along with the downsides to their use. It will then focus on a number of literature examples of dehydrating agents used in the reaction including carbodiimides, nitriles, acetals and orthoesters. The most promising of these dehydrating agents were selected for initial catalyst testing.

3.1.1 Direct synthesis with dehydrating agents

Dehydrating agents chemically bind to water to form stable hydrated products. This provides thermodynamic driving force, and the stability of the product ensures the reaction is not reversible. As a thermodynamically limited reaction, the formation of dialkyl carbonates has a Gibbs free energy greater than 0. In order for the reaction to become spontaneous, the reaction between water and the dehydrating agent needs to have a negative Gibbs free energy with a magnitude greater than the formation of the carbonate. Honda *et al.*[1] have observed this in the use of nitriles as dehydrating agents. Nitriles have a ΔH of hydration of around -90 kJ.mol^{-1} which when coupled to the formation of DMC provides an enthalpy change of ~-120 kJ.mol^{-1} (Figure 3.1).

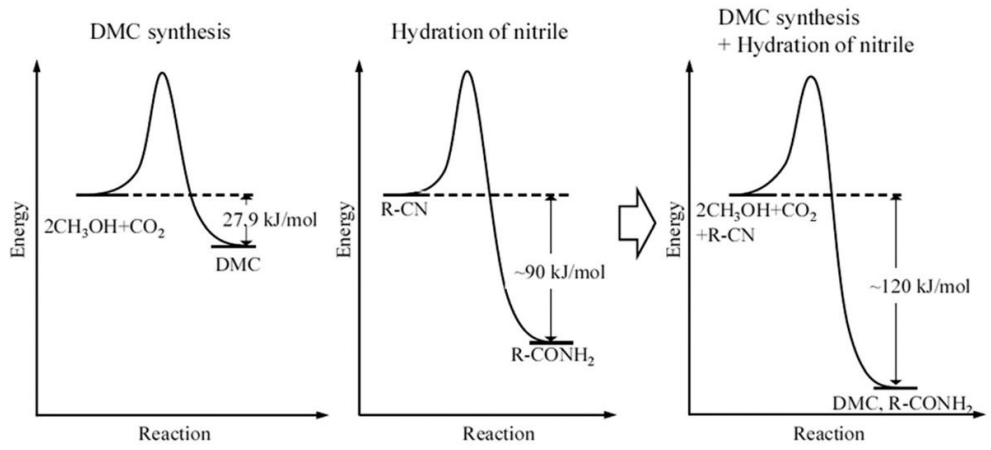

Figure 3.1. Enthalpy diagram for the formation of DMC with and without the presence of a nitrile. Reproduced with permission from Honda et al.[1]

Although dehydrating agents provide thermodynamic driving force, improving yields, they also have a number of drawbacks. The main issue with most of the dehydrating agents that have been investigated is that the cost of the dehydrating agent outstrips the value of the dimethyl carbonate generated (Table 3.1), making the economics less attractive.

Table 3.1: Cost per kilogram of commonly investigated dehydrating agents compared to DMC.

Compound	Cost ($/kg) [Alibaba]
2-cyanopyridine	20
Benzonitrile	65
Diisopropyl carbodiimide	65
Dicyclohexyl carbodiimide	1.2
Trimethoxy methane	7.5
Dimethyl carbonate	0.99

Aside from nitriles other utilised dehydrating agents include carbodiimides,[2] epoxides,[3,4] and orthoesters.[5,6] A decrease in selectivity due to side reactions is also observed. As nitrogen containing bases are often used as dehydrating agents, carbamates are formed as side products.[7–9] Dehydrating agent free reactions are much more attractive from a selectivity perspective but are limited by thermodynamics. This then becomes a question of how quickly a given catalyst system can reach equilibrium, as well as catalyst stability.

3.1.2 Catalyst testing with dehydrating agents

There has been much work reported that utilise various dehydrating agents in catalyst testing for the formation of dialkyl carbonates. However, there is also a lack of literature consensus when it comes to reaction conditions, with pressures ranging from atmospheric up to 300 bar, and temperatures range from 80–180 °C and reaction times from 1–80 h. Similarly, there is a wide variety of dehydrating agents, separation techniques, reactor designs, catalyst materials and promoters that has been tested.

3.1.2.1 Carbodiimides

It has been shown that carbodiimides react with the alcohols to form alkyl isoureas,[2] and both the alcohol and the isoureas can react further with CO_2 to form dialkyl carbonates. Aresta *et al.* demonstrated up to 60% yields for DMC and 15% for DEC using dicyclohexyl carbodiimide (DCC).[2] The by-product for these reactions are substituted ureas (Scheme 3.2-A) which precipitate out of the reaction mixture and have literature precedent for their conversion back to carbodiimides.[10–12] However, this regeneration may not be economically viable

due to the cost of the reagents involved, and as DMC is a bulk chemical, the use of expensive reagents in its production decreases the economic viability of the process. The overall reaction scheme for the formation of DMC in the presence of carbodiimides is shown in Scheme 3.2-B.

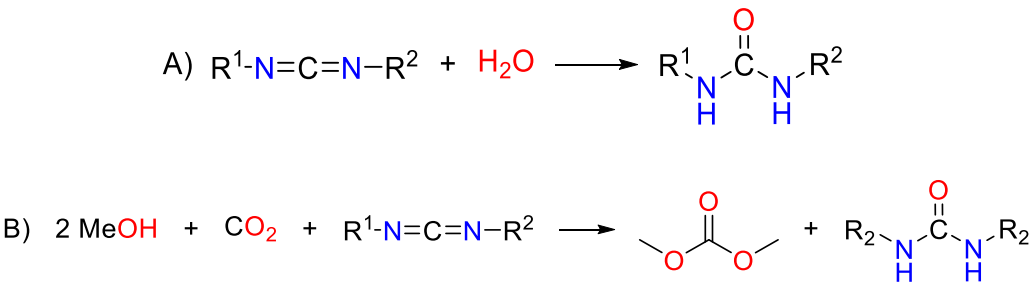

Scheme 3.2: Use of carbodiimides in the formation of dimethyl carbonate. A) The reaction of a disubstituted carbodiimide with water to form a disubstituted urea. B) The overall reaction scheme for the formation of dimethyl carbonate in the presence of a disubstituted carbodiimide.

Carbodiimides are also toxic reagents, that must be carefully handled. DIC is classified as fatal upon inhalation and DCC is classified as fatal upon skin contact. These features make the use of carbodiimides in large quantities much less appealing.

3.1.2.2 Nitriles

Several nitrile compounds have been tested as dehydrating agents for the formation of DMC. As shown in Figure 3.1 above, the hydration of nitrile compounds increases the overall enthalpy change of the reaction. Table 3.2 shows nitrile compounds investigated by Honda *et al.*[7–9] Acetonitrile shows the lowest performance at 120 °C with a DMC yield of 0.38%. Benzonitrile has a similarly low yield at the same temperature with 0.76%. Both of these reactions improve with an increase in temperature, up to 150 °C and reaction time. Acetonitrile sees a 23-fold increase in yield to 8.9%, and benzonitrile sees a 62-fold improvement in yield to 47%. The various cyanopyridines all perform differently, 3- and 4-cyanopyridine show yields of 2 and 4% respectively while 2-cyanopyridine shows a 94% yield. The difference indicates that the location of the nitrogen atom within the ring, in relation to the cyano-group is important for the reaction due to its role in the activation of the CO_2.[6]

Table 3.2: Nitrile compounds investigated for use a dehydrating agents in the synthesis of dimethyl carbonate.

Nitrile	Catalyst	Yield (%)	T (°C)	P (MPa)	t (h)	Ref
Acetonitrile	CeO_2	8.9	150	0.5	48	[7]
Acetonitrile	CeO_2	0.38	120	5	12	[8]
Benzonitrile	CeO_2	47	150	1	86	[9]
Benzonitrile	CeO_2	0.76	120	5	12	[8]
2-cyanopyridine	CeO_2	94	120	5	12	[8]
2-pyrimidinecarbonitrile	CeO_2	38.6	100	5	12	[8]
3-cyanopyridine	CeO_2	2.06	120	5	12	[8]
4-cyanopyridine	CeO_2	4.10	120	5	12	[8]
Pyrrole-2-carbonitrile	CeO_2	2.94	120	5	12	[8]
2-methyl-amino acetonitrile	CeO_2	n/d	120	5	12	[8]

The best performing of the nitrile compounds reported is 2-cyanopyridine, (Scheme 3.3), and it has been used to great effect in the synthesis of both dialkyl[8,13] and cyclic carbonates[6] with good conversion and selectivity for a wide range of alcohol substrates.

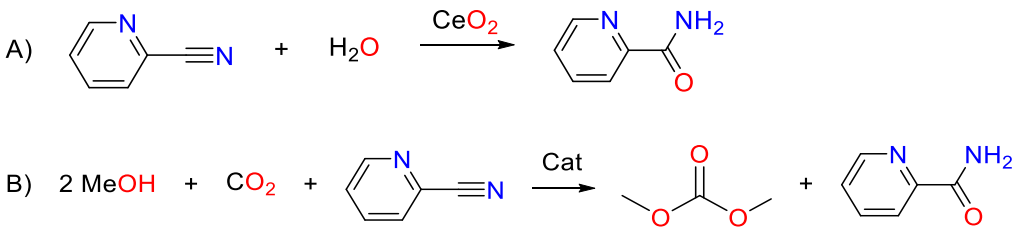

Scheme 3.3: Use of 2-cyanopyridine as a dehydrating agent A) the reaction of 2-cyanopyridine with water to form picolinamide in the presence of a cerium oxide catalyst B) The overall reaction scheme for the formation of dimethyl carbonate in the presence of 2-cyanopyridine.

Although the regeneration of 2-cyanopyridine from 2-picolinamide is possible over a Na_2O/SiO_2 catalyst[8], this reaction requires temperatures of 185 °C and 500 h of reaction time. This makes the regeneration of the dehydrating agent the limiting factor in this route being used industrially, as the cost of regeneration likely exceeds the value of the carbonate produced.

3.1.2.3 Orthoesters

Aside from nitrogen containing compounds, orthoesters and acetals have also been utilised as dehydrating agents.[5] These compounds are effectively anhydrides of the alcohol and produce more of the starting alcohol upon hydrolysis with water. This essentially makes the concentration of alcohol constant, whilst also removing water, driving the reaction to the right in favour of products by Le Chatelier's principle. Choi *et al*. also report the formation of DMC directly from 1,1,1-trimethoxy ethane.[14,15] The authors state that the orthoester is essentially pre-dehydrated methanol, which with their homogeneous methoxy-tin catalysts produces DMC and water as shown in Scheme 3.4.

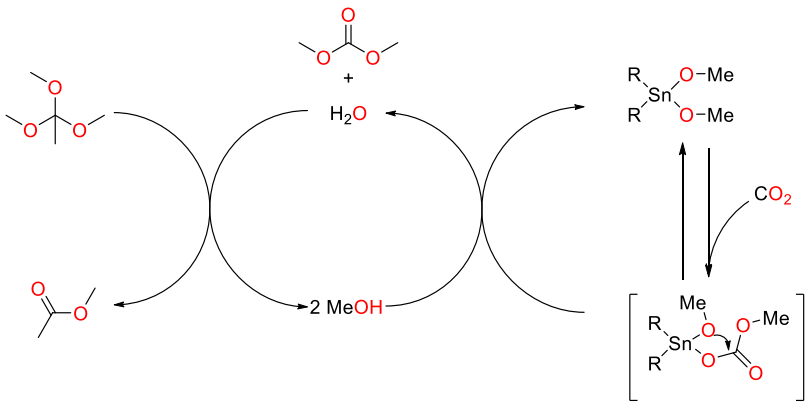

Scheme 3.4: Proposed catalytic cycle for the formation of DMC in the presence of an orthoester dehydrating agent with an alkyl-tin methoxide catalyst.[16]

Choi *et al.* have also reported the use of 2,2-dimethoxypropane[16] for the synthesis of DMC. The ketone products can be reacted with methanol to regenerate the dehydrating agent, which as stated above, essentially creates a pre-dehydrating step. Heterogeneous catalysts have also been used in conjunction with orthoesters. Saada *et al.*[17] used supported mixed metal oxides in conjunction with trimethoxy methane (TMM) achieving 40% DMC yields.

3.1.3 Summary

This introduction has investigated several classes of dehydrating agents in the direct synthesis of dialkyl carbonates. Based on this, three dehydrating agents were selected for investigation in the experimental work of this chapter. For a nitrile compound, 2-cyanopyridine was selected due to its good performance with ceria-based catalyst materials reported in the literature. For carbodiimides there is literature precedent for dicyclohexyl carbodiimide, however, this is a

solid powder with high toxicity and is allergenic. For this reason, diisopropyl carbodiimide was selected, as a liquid this compound can be used volumetrically. Finally, TMM was selected as the orthoester, this showed a good conversion in the work by Saada *et al.* with similar metal oxides to those produced in Chapter 2.

Although no consensus on reaction conditions has been reached in the literature, in this work we will initially perform reactions at 120 °C as this was the temperature used to achieve the greatest conversion by Honda *et al.* A range of pressure will be investigated both above and below the critical pressure of CO_2, however, initial pressures investigated will be 60 bar, as this is below the critical point of CO_2 and easily achievable with a liquid-withdrawal CO_2 cylinder and the equipment available.

The reaction conditions and dehydrating agents will help in the determination of which catalyst synthesised in Chapter 2 is the most active. Moreover, a comparison between dehydrating agents, and commercially available CeO_2 will help with choosing the most active and stable catalyst system for the reaction.

3.2 Experimental

3.2.1 General

Reagents were sourced from Merck, Fischer Scientific or Alfa Aesar. All reagents, except for 2-cyanopyridine, were used as received. The 2-cyanopyridine was discoloured and so was purified by distillation. Both the purified 2-cyanopyridine and DIC were kept under an argon atmosphere to prevent water ingress. Liquid CO_2 (99.8%) was obtained from BOC. Following reactions, reactors were cooled down to room temperature and slowly depressurised over the course of 1 h, the catalyst was filtered using a 2 µm PTFE syringe filter (Fischer Scientific). Samples were analysed by GD-FID to determine dimethyl carbonate concentration with trimethoxy benzene as a standard.

3.2.2 Analysis

Product analysis was performed on a Varian 3900 GC equipped with an FID detector at 300 °C with a H_2 flow rate of 40 $mL.min^{-1}$, air flow rate of 400 $mL.min^{-1}$, and argon makeup flow rate of 30 $mL.min^{-1}$. Helium was used as a

carrier gas at a constant linear velocity of 39.4 $cm.s^{-1}$ through a CP-Sil 5CB column from Agilent (50 m length, 0.32 mm ID, 5 µm film thickness). 0.5 µL of sample was injected with a split ratio of 100 and an injector temperature of 300 °C. The column was held at 50 °C for 5 min, then the temperature was ramped up to 70 °C at 3 $°C.min^{-1}$, then to 180 °C at 7 $°C.min^{-1}$, and finally up to 300 °C at 23 $°C.min^{-1}$. Retention times and calibration curve can be found in Appendix 3. Methanol conversion was based on DMC concentration. Minor products were not quantified.

3.2.3 Dehydrating agent screening

Custom-made 20 mL stainless steel autoclaves were loaded with a glass liner containing a magnetic stirrer bar and 0.03 g of catalyst, 1 mL methanol and 50 mol% dehydrating agent in air. Reactors were then sealed and pressurised to 50 bar at 40 °C with CO_2 using a JASCO PU-2088-CO2 pump. Reactors were placed into an aluminium heating block, preheated to the desired temperature, and heated to 120 °C under constant stirring at 400 RPM for 1-20 h.

3.2.4 Varied temperature experiments

Autoclaves were loaded with 0.03 g of commercial cerium oxide, 1 mL methanol and 2 mL DIC (corresponding to 50 mol% dehydrating agent) and pressurised with CO_2 to 50 bar at 40 °C. Autoclaves were then placed into an aluminium heating block at 80-120 °C for 1-6 h.

3.2.5 Variable CO_2 density experiments

For variable density experiments, 20 mL autoclaves were loaded with 0.03 g commercial cerium oxide, 1 mL methanol and 2 mL of DIC (corresponding to 50 mol% dehydrating agent). The autoclaves were weighed, then pressurised between 30 and 90 bar and weighed again. Density was calculated from the mass of CO_2 over the 20 mL autoclave. The autoclaves were then placed into a preheated aluminium heating block at 120 °C for 3 h with stirring.

3.2.6 Catalyst stability

Autoclaves were loaded with 0.03 g commercial cerium oxide, 1 mL methanol and 2 mL DIC. They were then pressurised to 50 bar at 40 °C and placed into a preheated aluminium heating block at 100 °C for 2 h. Following the reaction,

the reactors are depressurised. The catalyst was recovered by centrifugation, washed repeatedly with methanol before being allowed to dry at 120 °C for 1 h. The catalyst was then added back to the autoclave and this was repeated for 6 cycles. The initial supernatant from the centrifugation was recovered and analysed by GC-FID.

3.2.7 Calculation of CO_2 pressure-density isotherms

CO_2 density was calculated using the SRK equation (Equation 3.1) and physical component parameters (Table 3.3) reported by Camy *et al.*[18]

Equation 3.1 $$p = \frac{RT}{v-b} - \frac{a(T)}{v(v-b)}$$

Where a(T) and b are defined as:

Equation 3.2 $$a(T) = a_c . F(T)$$

Equation 3.3 $$a_c = 0.42748 \frac{R^2 T_c^2}{P_c}$$

Equation 3.4 $$b = 0.08664 \frac{RT_c}{P_c}$$

Equation 3.5 $$F(T) = \left[1 + (0.48 + 1.574\omega - 0.176\omega^2) \times \left(1 - \left(\frac{T}{T_c}\right)^{0.5}\right)\right]^2$$

Table 3.3: Physical component parameters for CO_2 reported by Camy et al. [18]

	T_c (°C)	P_c (bar)	ω
CO_2	31.2	73.83	0.223621

And density was calculated using Equation 3.6:

Equation 3.6 $$d = \frac{M_r}{v \times 1000}$$

The Equation 3.1 was solved for v with an iterative approach using python.[19]

Nomenclature:

ω = acentric factor
T = Temperature (K)
v = molar volume ($m^3.mol^{-1}$)
d = density ($g.mL^{-1}$)
p = Pressure (kPa)
a = mixture parameter ($m^6.bar^{-1}.mol^{-1}$)
b = mixture parameter ($m^3.mol^{-1}$)
R = ideal gas constant ($J.mol^{-1}.K^{-1}$)
Subscript $_c$ = critical

3.3 Results and discussion

3.3.1 Dehydrating agent screening

For the dehydrating agent screening a commercially available cerium oxide was selected, due to it being available in large quantities of consistent quality. The commercial cerium oxide was used to determine a baseline activity and to screen for the ideal dehydrating agent for further investigations. Each of the dehydrating agents was used in a 1:2 ratio of dehydrating agent: methanol, which allows for a theoretical maximum yield of 100%. Figure 3.2 shows the reaction profile of methanol with different dehydrating agents with commercial cerium oxide over 20 h.

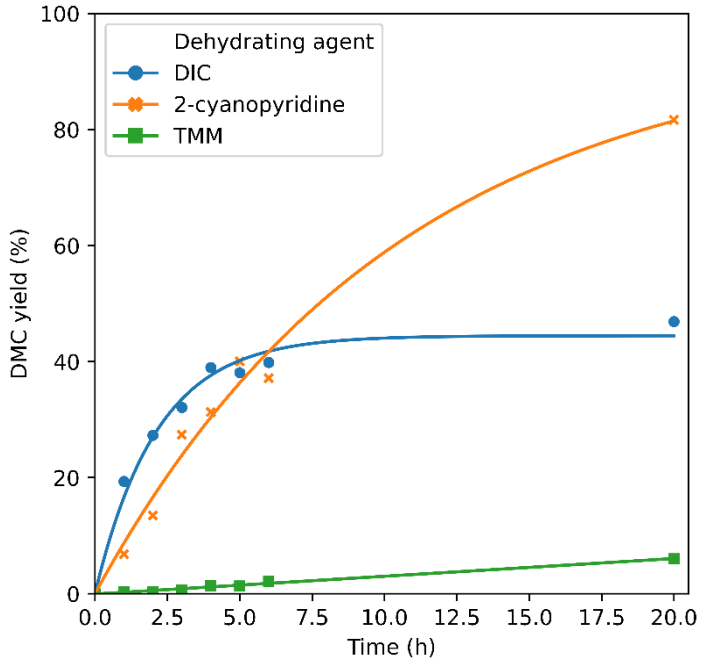

Figure 3.2: Reaction profiles of the formation of DMC in the presence of dehydrating agents. Conditions: 120 °C, 1 mL methanol, 50 mol% dehydrating agents, 0.03 g commercial CeO_2, 50 bar CO_2.

TMM achieved a DMC yield of around 2% after 6 h. Extending the reaction to 20 h increases the yield to 6%. The reaction of TMM with water relies on the presence of H^+ in the reactor and with the conditions investigated the pH of the reaction mixture is insufficient for a high rate of hydrolysis.[20] TMM was not investigated further due to its cost compared to DMC along with its poor performance. While a previous report by Saada *et al.* had achieved good yields using TMM (30%, 12 h),[17] Zhang *et al.* have reported yields around 6%, similar to those shown in Figure 3.2.[21] It is likely that for Saada *et al.* the source of H^+

for the hydrolysis of TMM was provided by the catalyst support material, as the catalyst composition between Zhang and Saada are similar Ce-Zr mixed metal oxides. The major difference being that the Ce-Zr utilised by Saada was supported on a graphene oxide support. It is likely then, that the commercial catalyst we have utilised does not provide a suitably acidic surface on which the TMM can react.

2-cyanopyridine initially gave a linear reaction profile, achieving over 40% DMC yield after 6 h (Figure 3.2). If the reaction continued in a linear fashion 100% would be expected after 20 h, however, 80% was observed. This indicates that the reaction follows first order reaction kinetics rather than the zero-order kinetics indicated by the initial linear profile. The greater conversion made 2-cyanopyridine a much more suitable candidate for further testing than TMM. The downside is that a cerium oxide catalyst is required for the reaction between 2-cyanopyridine and water, this would potentially lead to competition for active sites between the MeOH and 2-cyanopyridine. The rates observed here are similar to those obtained by Honda *et al.*[13] while also utilising a lower molar ratio of dehydrating agent to alcohol (1:2, as opposed to 100:1). Due to the unknown effect that a change in metal oxide would have on hydrolysis, 2-cyanopyridine was not investigated further, as a change in catalyst would likely not only affect the rate of DMC formation but also the rate of hydration of 2-cyanopyridine.

The conversion of methanol progressed more rapidly in the presence of DIC than the previous two dehydrating agents for the first 4 h of the reactions. However, the conversion began to plateau upon reaching 40% yield. Extending the reaction to 20 h, gave a 47% yield. This appeared to be due to the accumulation of the product of the hydration of DIC: diisopropyl urea (DIU). DIU is insoluble in the reaction medium and precipitates as crystalline material in the reaction vessel. This causes an increase in viscosity and likely leads to mass transfer limitations which caused the plateau in methanol conversion.

Initial rates of reaction were approximated using non-linear regression. For fitting, an exponential equation was used (Equation 3.7).

Equation 3.7: $$y = a \cdot e^{-b \cdot x} + c$$

Figure 3.3 shows the fit of the curve to the DMC concentration over time graph showing that the exponential equation has a good agreement with experimental data.

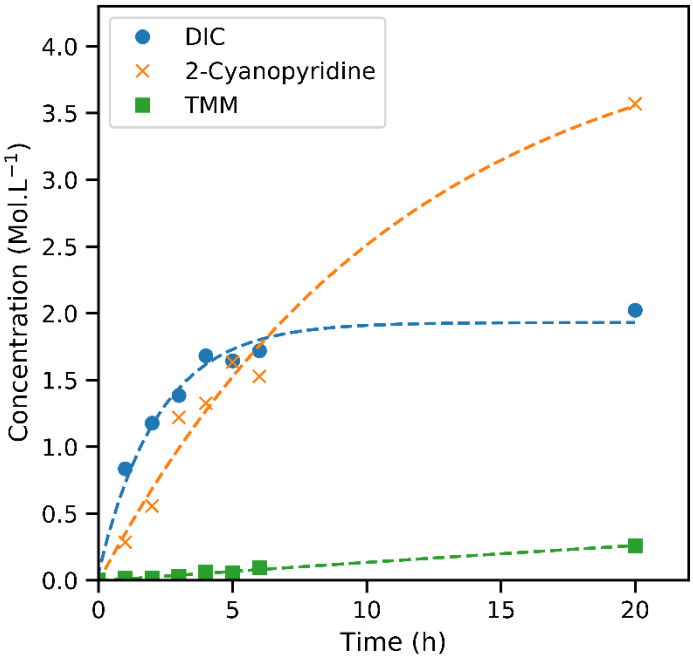

Figure 3.3: Concentration of DMC plotted against time with DIC (●), 2-cyanopyridine (x) and TMM (■) with fitted curves (---). Conditions: 120 °C, 1 mL methanol, 50 mol% dehydrating agents, 0.03 g commercial CeO_2, 50 bar CO_2.

Taking a derivative of the fitted curve (Equation 3.8), the rate of product formation could be determined.

Equation 3.8: $$\frac{dy}{dx} = -ab \cdot e^{-b \cdot x}$$

Plotting the rate against the concentration of DMC gives the observed catalytic rate constant and initial rate using Equation 3.9.

Equation 3.9: $$\frac{d[DMC]}{dt} = -k_{obs}[DMC]^1 + Rate_0$$

In the context of product formation -k_{obs} is the rate constant for the reverse reaction, while $Rate_0$ includes the forward rate constant and the concentrations of the reactants.

Figure 3.4 shows the rate against concentration plot for the three dehydrating agents at 140 °C. The y-intercept is the rate of reaction at a product concentration of 0 which is equivalent to the initial rate of reaction. The x-

intercept of these curves gives the concentration of DMC when the rate is 0, or plateau of the reaction.

In a reversible reaction this would be equal to the equilibrium concentration of DMC ($[DMC]_{eq}$). For these reactions utilising dehydrating agents, the plateau can be caused by factors including product inhibition, decreased rate caused by crystallisation and viscosity change, and thermodynamic equilibrium.

DIC had the highest initial rate at 0.95 $mol.L^{-1}.h^{-1}$ but we also see an $[DMC]_{eq}$ of 1.9 $mol.L^{-1}$ which is where the plateau for DIC occurs on Figure 3.3.

2-cyanopyridine had a lower initial rate, less than half of DIC at 0.39 $mol.L^{-1}.h^{-1}$. However, unlike DIC, 2-cyanopyridine allowed for a larger concentration of DMC to form with a calculated $[DMC]_{eq}$ of 4.29 $mol.L^{-1}$ or a DMC yield of 99.4%. This suggests that the reaction would go on to near completion, allowing for a long enough reaction time.

TMM had an initial rate an order of magnitude lower than both 2-cyanopyridine and DIC at 0.02 $mol.L^{-1}.h^{-1}$. The $[DMC]_{eq}$ calculated suggests that yield would be limited to 35%, although, as the fitted curve covers only a small range of concentrations this likely has a larger error than the other two dehydrating agents. The coefficients of the fitted curve also suggest that it would take 560 h to achieve this conversion.

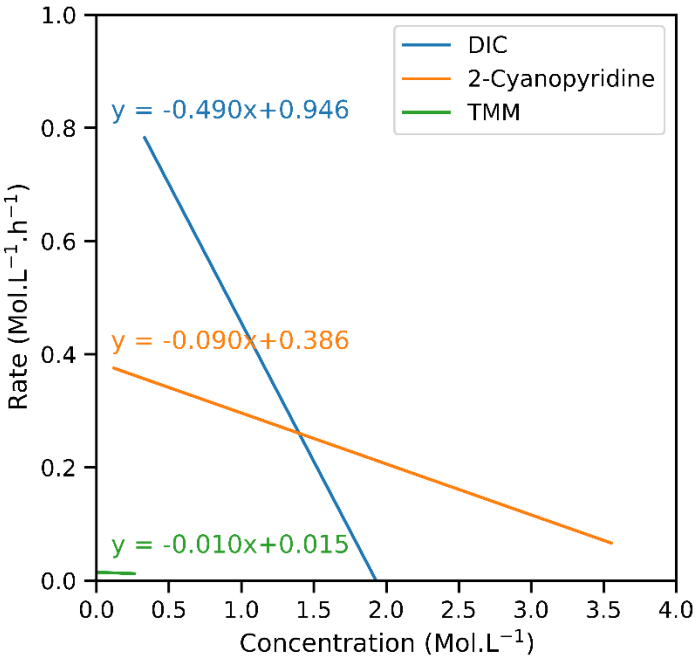

Figure 3.4: Rate against concentration for fitted reaction profiles with DIC, 2-cyanopyridine and TMM.

The goal of these experiments was to identify a dehydrating agent that would be suitable for testing the difference in activity between catalysts. Based on the data obtained (Figure 3.2), DIC was therefore selected for further investigations despite its toxicity and cost. The rationale behind this choice was twofold. Firstly, the reactions with DIC proceeded relatively quickly up to an appreciable conversion, allowing for more efficient screening of reaction conditions and catalyst materials. Secondly, and perhaps more importantly, the reaction between DIC and water is spontaneous. This means that, in principle, upon changing the catalyst material the only variable that is being changed is the rate of product formation. If 2-cyanopyridine were selected, the rate of hydration of 2-cyanopyridine could be affected with a change in catalyst. This would obfuscate the changes in the rate of DMC formation.

3.3.2 Variable temperatures experiments

After the selection of a viable dehydrating agent, suitable operating temperatures needed to be identified. As discussed above, typical temperatures for this reaction are at 140 °C or above, so determining how the reaction performs at lower temperatures was important. Reaction profiles for 120, 110 and 100 °C were obtained (Figure 3.5). As expected, as the temperature was decreased, the initial rate of the reaction also decreased. Reactions were also carried out for 2 and 3 h at 90 and 80 °C which saw a sharp decrease in DMC concentration when compared to the same timepoints at greater temperatures. One of the challenges in choosing an optimal temperature was considering the temperature dependence of the reaction between water and the dehydrating agent. That is to say, the sharp decrease may be caused either by a decrease in rate of DMC formation or due to a decrease in the reaction rate between the dehydrating agent and water.

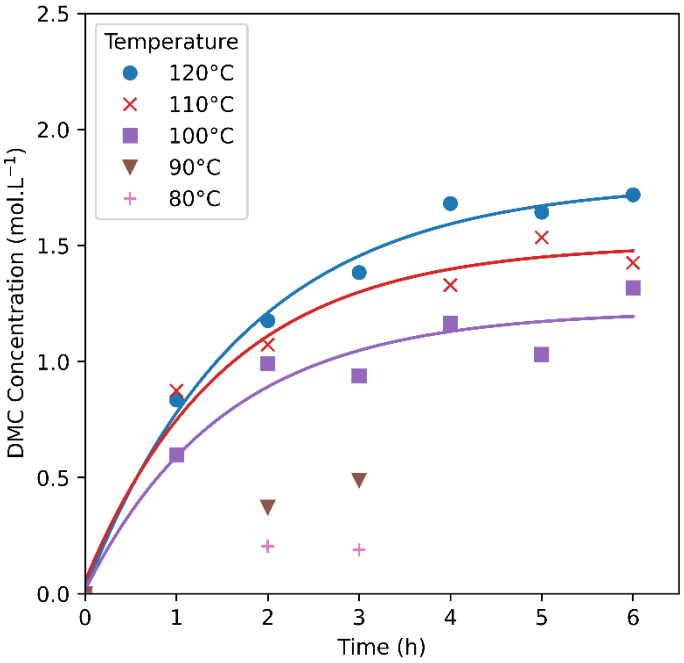

Figure 3.5: Effect of temperature on the rate of DMC formation in the presence of DIC. Conditions: 50 bar CO_2 (at 40 °C) 0.03 g commercial CeO_2, 2 mL DIC, 1 mL MeOH.

Unusually however, as the temperature was decreased the point at which the reaction began to plateau also decreased. This is unusual because if this were caused by an equilibrium being reached, we would expect the plateau to increase in an exothermic reaction. If it were caused by inhibition by DMC, we would expect it to plateau at the same point. What was observed was that the time taken to plateau appeared to remain constant, at 5 h. This implies that the plateau observed was not caused by DMC concentration, but due to another factor, such as the concentration of another product in the reactor, or catalyst deactivation.

In order to see what was occurring within the reactor, the starting mixture of a 2:1 methanol: DIC mixture was loaded into a view cell autoclave, without a catalyst and pressurised to 60 bar with CO_2. The autoclave was then heated to 120 °C and left undisturbed for 4 h. Figure 3.6 shows an image taken through a view-cell autoclave showing that all of the reaction mixture had solidified, when cooled down and depressurised this solid remained. Our hypothesis is that DIC and methanol react to form an isourea which precipitates out of solution. A Karl Fisher titration was performed on the methanol to determine water concentration, which was recorded as 210 ppm (0.02%) which is around 0.013 mmol of water, which was not enough water to fully react with the 15 mmol of

DIC present, and with no catalyst present we do not expect the reaction to progress.

This crystallisation only occurred under specific pressures (60 bar CO_2); when pressurised directly to higher pressures (90–200 bar at 120 °C) and held for as long as 16 h, no crystallisation occurred. This implies that CO_2 concentration or CO_2 density has an influence on the rate of crystallisation.

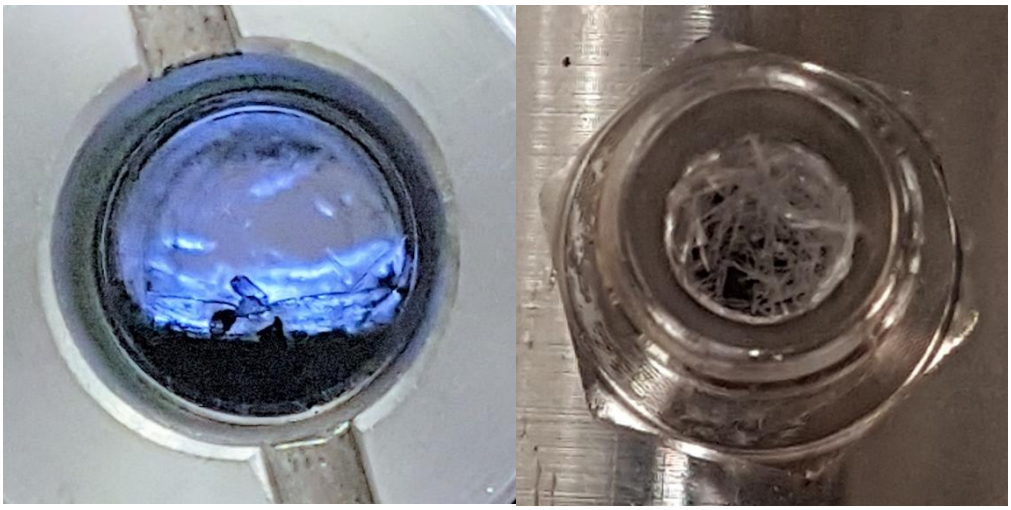

Figure 3.6: Solid formed within the view cell autoclave as a result of pressuring a typical reaction mixture of 3 mL 1:2 MeOH: DIC, and CO_2 to 60 bar. Left: Taken through the sapphire window at 60 bar CO_2 120 °C. Right: Shows what was seen through the removed Swagelok® fitting following cooling and depressurisation to room temperature and pressure.

An attempt was made to obtain a crystal structure of this material, though only a DIU crystal was found to scatter, likely formed from the low concentration of water present within the methanol. NMR of the dissolved crystals showed only starting materials. This indicates that this process is reversible and may also explain the plateau observed in variable temperature experiments.

For further experiments, pre-plateau time-points (2–3 h) were used to determine the effects of other parameters on the formation of DMC.

3.3.3 Effect of CO_2 density on DMC yield

Up to this point the reactions were all pressurised to 60 bar at 40 °C, which equates to a CO_2 density of 0.1 $g.mL^{-1}$. As the phase behaviour of CO_2 is dependent upon the density, an investigation into how density affected the reaction was undertaken. As the reaction goes from 3 moles of substrate to 2 moles of product, we therefore expected that an increase in pressure would lead to an increase in conversion by Le Chatelier's principle. Figure 3.7 shows that

a lower density of 0.05 g.mL^{-1} shows a 22% DMC yield after 3 h, which was 10% lower than at 0.1 g.mL^{-1} CO_2. The yield increased to a peak upon reaching 0.1 g.mL^{-1} CO_2 before decreasing, as density was raised further, to between 25-27% DMC yield. This decrease may have been due to the liquid phase expansion due to CO_2 dissolution, the increase in the liquid phase volume, with the same number of moles of methanol would lead to a decrease in methanol concentration.

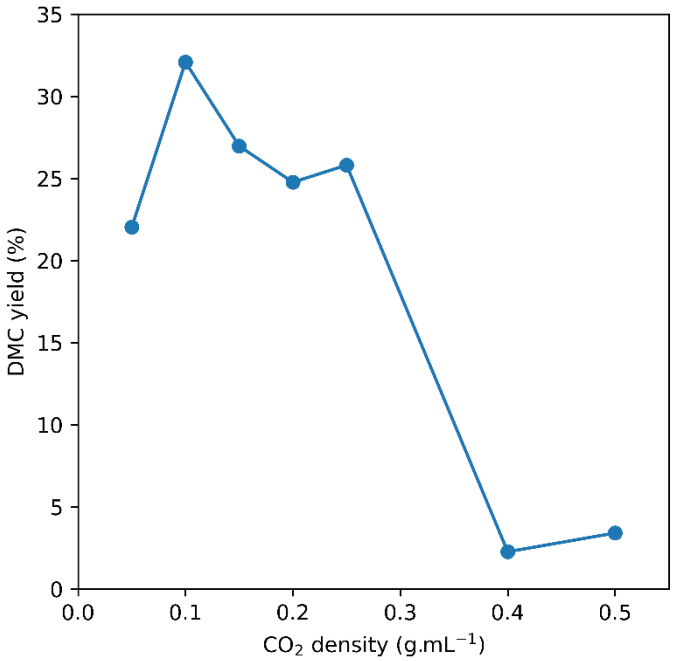

Figure 3.7: DMC yields over a range of CO_2 densities. Reaction conditions: 120 °C, 3 h, 2:1 mol ratio methanol to DIC, 0.03 g commercial CeO_2.

Upon reaching 0.4 g.mL^{-1}, DMC yield dropped sharply to around 2.5%. This density corresponds to the critical point of a CO_2 – methanol mixture. Once the critical point was reached, the methanol, rather than being contained in 3 mL, occupies the volume of the reactor. This resulted in a 6.5 fold decrease in concentration from 8.8 mol.L^{-1} to 1.3 mol.L^{-1}.

As rate is a function of concentration, this decrease in methanol concentration leads to lower rate. The design of batch reactors did not allow for an easy solution to investigate changes in methanol concentration. An increase in the amount of methanol would lower the reduction in concentration at the critical point but overfill the limited volume of the batch reactor. The expansion may also reduce rate due to lower contact with the catalyst which, once the mixture

has reached its critical point, is no longer suspended in the liquid phase (Figure 3.8).

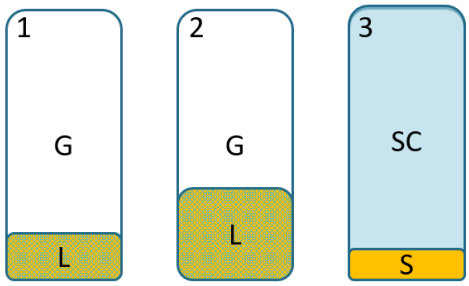

Figure 3.8: Representation of expansion of the liquid phase (L) at ambient pressure (1), pressurisation with CO_2 (2) and exceeding the critical density of the mixture (3). The solid catalyst is suspended in the liquid phase in 1 and 2. S = solid, L = liquid phase, G = gas phase, SC = supercritical phase.

Based on these batch experiments it was clear that CO_2 density had a great impact on DMC yield. Whilst initially it was expected that increasing the CO_2 density would lead to an increase in yield, it was the change in phase behaviour associated with the increase in density that had the bigger effect. Whilst in batch, lower CO_2 densities allowed for better contact with the catalyst, we would expect that the change in phase behaviour would be beneficial in a flow system, due to the improved mass transfer of a supercritical mixture.

Although much effort was dedicated to investigating additional CO_2 densities between 0.25 and 0.4 $g.mL^{-1}$, this was not possible due to the steep density curve at the pressurisation temperature of 40 °C. Figure 3.9 shows that a slight change in pressure between 70 and 90 bar, causes a much larger change in the density of CO_2. In theory, this curve can be made less steep by increasing the pressurisation temperature. However, preheating and loading the autoclaves at higher temperatures would introduce additional sources of error. For this reason, we continued pressurisation at 40 °C even though this made some densities inaccessible.

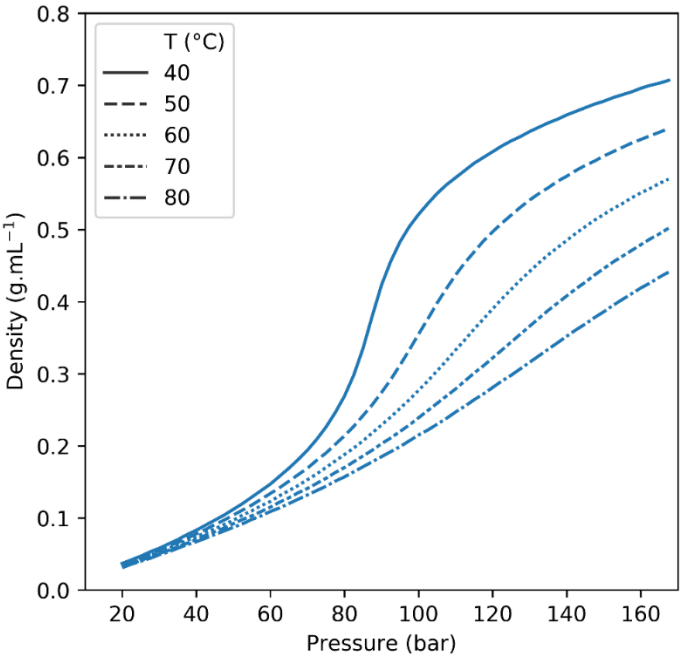

Figure 3.9: density - pressure isotherms for CO_2, calculated using the SRK equation.

The experiments presented so far have utilised the commercial cerium oxide material. We have shown that temperatures from 100–120 °C and CO_2 densities from 0.1–0.25 g.mL^{-1} (60-70 bar) are suitable for catalyst testing in batch. The spontaneous reaction between DIC and water makes this the ideal dehydrating agent for comparing catalysts. In the following section, we will be comparing several catalysts synthesised in Chapter 2 with the commercial CeO_2 used thus far.

3.3.4 Varying catalyst

As several catalysts were synthesised for use in this work, it was important that their activity be evaluated. Figure 3.10 shows the performance of a range of catalyst materials after 2 h reactions. In terms of yields the clear outlier was the commercial catalyst, with each of the catalysts synthesised in this work performing worse over the course of the reaction. Each of the catalysts synthesised achieved between 6.8% and 12.2% DMC yield, where the commercial material was closer to 23%.

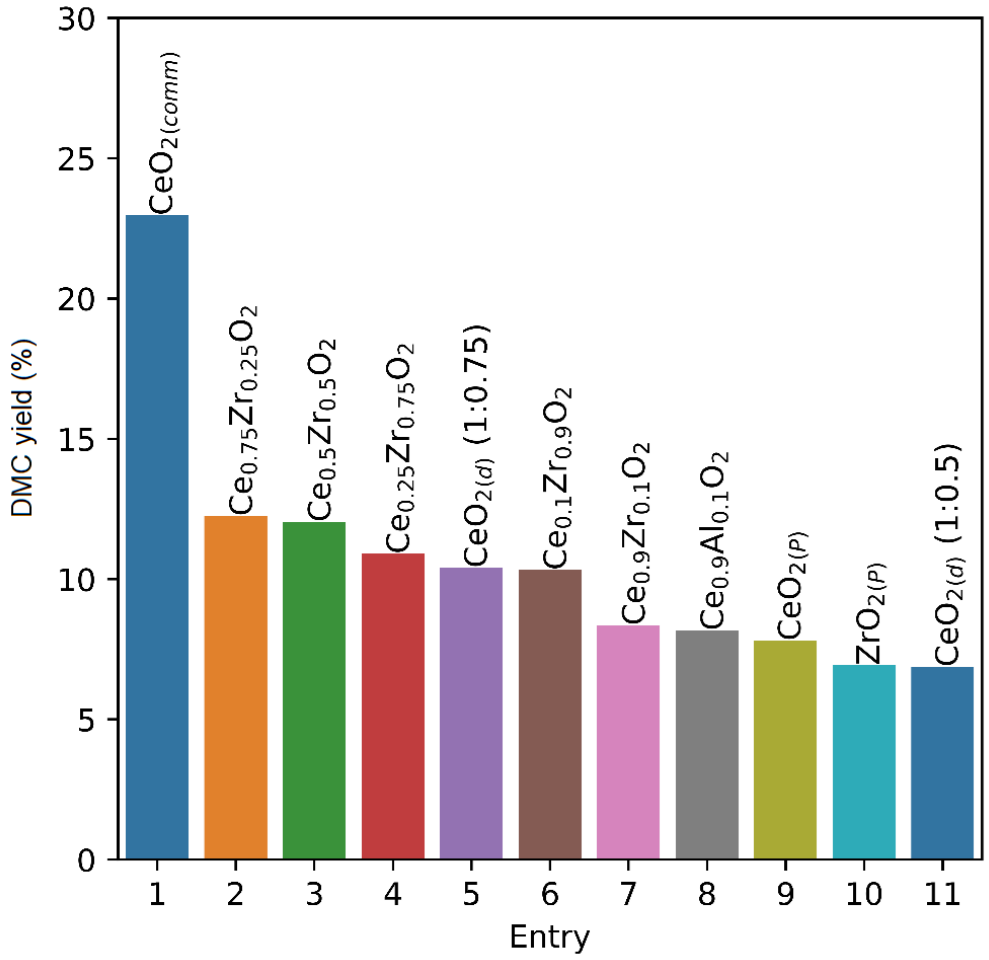

Figure 3.10: DMC yields observed after 2 h with a range of catalyst materials. Conditions: 100 °C, 50 bar CO_2 (at 40 °C), 1 mL methanol, 2 mL DIC, 2 h, 0.03 g catalyst. Entries relates to Table 3.4.

A correlation between surface area and DMC yield was expected. As such CeO_2 (1:0.75) with a surface area of 423 $m^2.g^{-1}$ was expected to perform best. Table 3.4 however, shows that this is not the case. The higher surface area CeO_2 (Entry 5) performed marginally better than pure CeO_2 with a lower surface area (Entry 9). Of the catalysts synthesised in this work, it appeared that composition had more of an impact on DMC yields, with the mixed Ce-Zr metal oxides performing best. $Ce_{0.9}Al_{0.1}O_2$ produced in this work had a lower-than-expected activity. This despite showing the greatest signal in the CO_2 TPD, implying a high degree of basic sites, as well as having the highest surface area of the precipitation catalysts.

*Table 3.4: Comparison of DMC yield, surface area and synthesis method for each catalyst tested. *Numbers in brackets refers to ratio of precursor to polymer template (see Chapter 2).*

Entry	Catalyst	DMC yield (%)	Surface area ($m^2.g^{-1}$)	Synthesis method
1	Commercial CeO_2	23	50	Commercial
2	$Ce_{0.75}Zr_{0.25}O_2$	12	103	Precipitation
3	$Ce_{0.50}Zr_{0.50}O_2$	12	102	Precipitation
4	$Ce_{0.25}Zr_{0.75}O_2$	11	88	Precipitation
5	CeO_2 (1:0.75)*	10	425	Decomposition
6	$Ce_{0.10}Zr_{0.90}O_2$	10	59	Precipitation
7	$Ce_{0.90}Zr_{0.10}O_2$	8.4	108	Precipitation
8	$Ce_{0.9}Al_{0.1}O_2$	8.2	166	Precipitation
9	CeO_2	7.8	108	Precipitation
10	ZrO_2	6.9	57	Precipitation
11	CeO_2 (1:0.5)*	6.9	172	Decomposition

The low surface area of the commercial CeO_2 clearly had little impact on its activity. Whilst this catalyst was the most active, further studies into its stability were performed.

3.3.5 Catalyst stability

Commercial CeO_2 performed best in the initial activity studies, showing the highest conversion. However, with the aim of utilising a catalyst in a flow system, the stability of the catalyst was equally important. In this section, the catalysts were recovered by centrifugation after each reaction and reused in subsequent experiments. Catalyst recovery was around 98% however, absolute yields have been used rather than normalising to catalyst mass.

While the commercial CeO_2 had the greatest conversion in the initial reaction, upon repeated cycles it became clear that the performance was short-lived (Figure 3.11). The commercial catalyst achieved a high yield only on the first cycle before dropping off to similar levels to the other catalysts synthesised in this work.

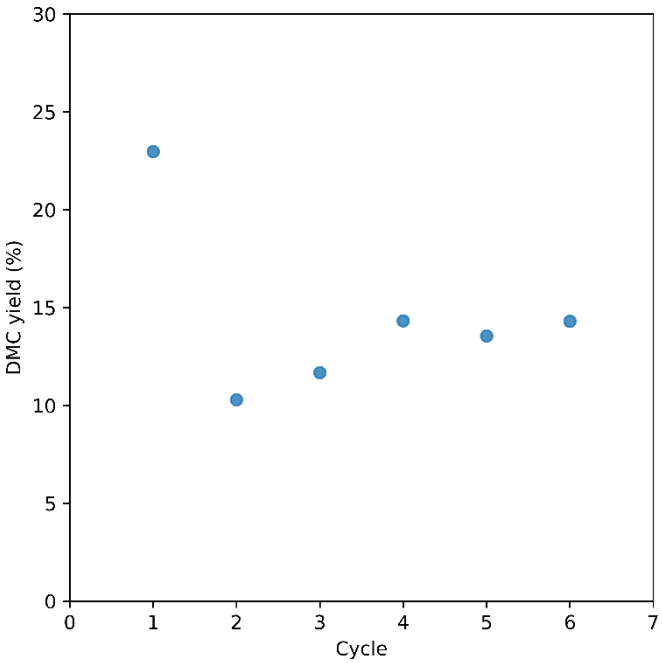

Figure 3.11: DMC yield with each reuse cycle with commercial CeO_2. Conditions: 120 °C, 50 bar CO_2 (at 40 °C), 1 mL methanol, 2 mL DIC, 2 h per cycle, 0.03 g initial catalyst loading. Cycle 1 utilised fresh catalyst.

While a decrease in activity was expected for a commercial cerium oxide, this occurred more rapidly than is shown in similar work by Aresta *et al.*[22] though remained more stable after the initial decrease. This may be due to the use of dehydrating agent in this work, compared to the dehydrating agent free reaction performed by Aresta *et al*. The reactions were also performed at a lower temperature (120 °C compared to 135 °C) which would affect the rate of catalyst deactivation. As the authors also demonstrated, different sources of CeO_2 have different stabilities, likely due to the difference in synthesis methods, which is unreported for the commercial CeO_2 used in this work.

The other catalysts synthesised for this work did not see this decrease after the first recycle, and when plotted as cumulative turnover number, calculated using Equation 3.10, each of the catalysts formed a straight line as shown in Figure 3.12, implying that deactivation was not occurring over these 6 cycles.

Equation 3.10 $$TON = \frac{n_{DMC}}{n_{cat}}$$

Where:

TON = Turnover number

n_{DMC} = total moles of DMC formed

n_{cat} = total moles of catalyst

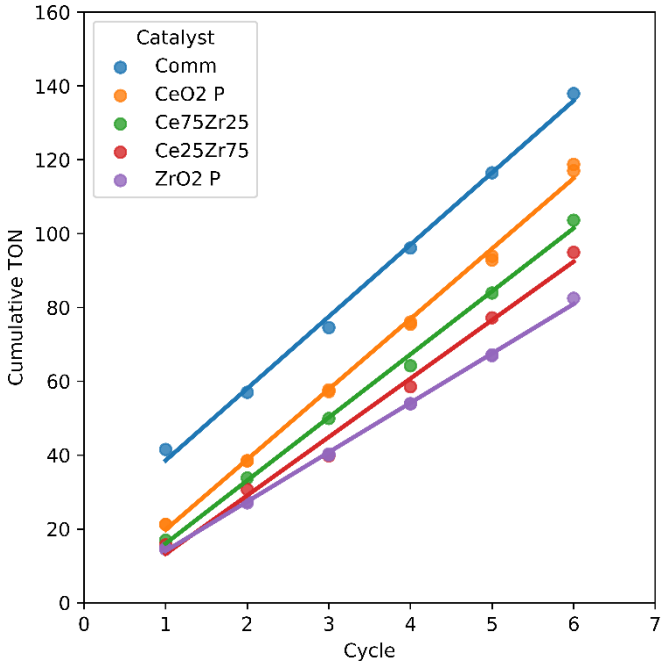

Figure 3.12: Cumulative turnover of catalysts over successive cycles of catalyst reuse. Conditions: 120 °C, 50 bar CO_2 (at 40 °C), 1 mL methanol, 2 mL DIC, 2 h per cycle, 0.03 g initial catalyst loading.

An intercept of zero would be expected for each of the catalysts, as this would indicate that there was no change in the number of turnovers with each cycle. Table 3.5 shows that the commercial CeO_2 had an intercept of 19.04, which indicated that the initial cycle, with fresh catalyst, had a greater turnover than subsequent cycles (around 40 turnovers on cycle 1 compared to around 19 turnovers from cycle 2 onwards). $CeO_{2(P)}$, $ZrO_{2(P)}$ and $Ce_{0.75}Zr_{0.25}O_2$ all had intercepts close to 0. This showed that these catalysts each had a consistent turnover with each cycle. The negative intercept observed for $Ce_{0.25}Zr_{0.75}O_2$ was likely due to cycle 3 (which is behind cycle 3 of ZrO_2 in Figure 3.12), where a decrease in activity was observed, though this was not sustained in subsequent cycles, implying that this was an error in the experiment, rather than a real deactivation.

Table 3.5: Turnovers per cycle and intercept for catalysts tested for stability.

Catalyst	Turnovers per cycle	Intercept
$Ce_{0.25}Zr_{0.75}O_2$	15.84	-2.63
$Ce_{0.75}Zr_{0.25}O_2$	16.43	0.47
$CeO_{2(P)}$	19.04	0.71
$ZrO_{2(P)}$	13.38	0.62
Commercial CeO_2	19.49	19.04

However, turnover does not give the complete story. The higher the molecular mass of the catalyst, the more turnovers were calculated per mole of product formed. We can see in Figure 3.12 that with decreasing molecular mass, we observe decreasing TON.

When the same data is instead plotted as cumulative product formation (Figure 3.13), it becomes evident that each of the catalysts synthesised in this work produced a similar quantity of DMC. Each of the catalysts had very similar gradients, producing around 1.6 mmol of DMC per cycle, including the commercial sample. This indicated that across multiple runs all the catalysts perform similarly. Over a number of cycles no catalyst stood out as being more productive save for the commercial sample due to an initial boost to its productivity in its first cycle when fresh catalyst is used.

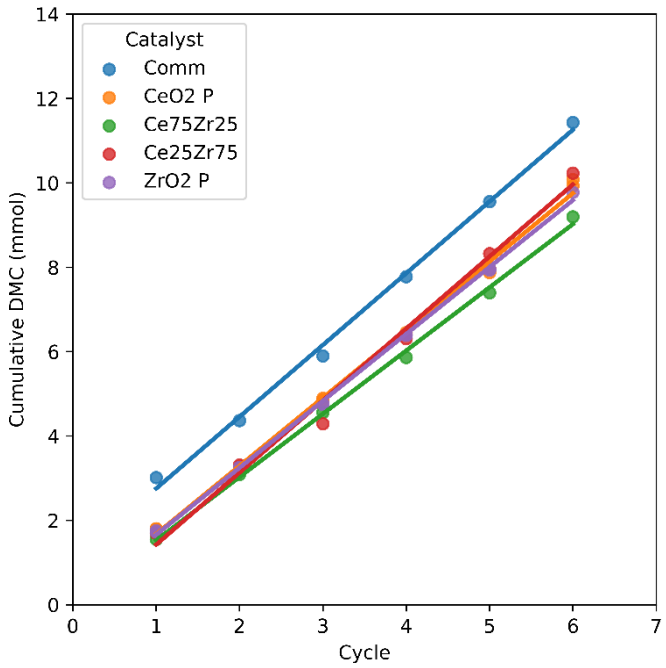

Figure 3.13: Cumulative DMC formed over successive cycles of catalyst reuse. Conditions: 120 °C, 2 h per cycle, 0.03 g initial catalyst loading.

However, this method of testing catalyst stability is not without its weaknesses. Though every effort was made, recovery of catalyst material was not 100 %. This then makes it difficult to postulate a mechanism for the initial decrease in the commercial sample. A number of options exist; a deactivation of the most reactive sites which leaves behind less active, but more stable sites. Another possibility is the loss of the smallest and most active particles upon recovery, the commercial powder is a much finer mesh than the catalysts synthesised in this work.

As a result, an attempt was made to grind the catalysts synthesised in this work to a finer mesh to improve dispersion in the liquid phase. This did not lead to an increase in yield. The synthesised catalysts were also washed in hot nitric acid, in an attempt to activate the surface, which again did not improve the yield. The opposite was attempted, the commercial catalyst was pressed into a pellet, decreasing its dispersion in the liquid phase, this decreased its performance. Similarly calcining the commercial catalyst at 450 °C also decreased its performance to the same level as the synthesised catalysts. This was a less than ideal situation; we had found several ways to decrease the performance of the commercial catalyst, but no way to increase the performance of the synthesised catalysts.

3.4 Conclusions

In this chapter we have evaluated a number of catalysts for their activity towards dialkyl carbonate synthesis utilising a dehydrating agent. Three dehydrating agents were tested and DIC was shown to be the most suitable for further testing due to its spontaneous reaction with water. However, 2-cynopyridine showed the highest yields after long reaction times, though due to the reaction of 2-cyanopyridine and water being catalysed by CeO_2, it was not selected for testing of other pure and mixed metal oxides synthesised in this work.

Variations on temperature were then investigated, showing that a decrease in initial rate and also in the point of plateau was observed. It was not clear if the decrease was caused by the decrease in rate of DMC synthesis, the rate of DIC conversion to DIU, or another factor such as the crystallisation that was observed. Additional experiments on the effect of temperature on the hydration of DIC, and the cause of the crystallisation within the reactor should be conducted should work with DIC continue. Another experiment such as starting the reaction with 40% DMC and fresh DIC would aid in the determination of what causes the early plateau. This was beyond the scope of this work, as the objective of this work was to develop a dehydrating agent-free synthesis.

The effect that changing CO_2 density had on DMC yields were also investigated. Initial assumptions that a simple relationship where an increase in pressure would lead to an increase in conversion were not observed. As pressure increased the reaction phase behaviour changed, at a CO_2 density of 0.4 $g.mL^{-1}$, a supercritical mixture of methanol and CO_2 was formed, which decreased the methanol concentration and the contact with the catalyst, lowering DMC yield. Whilst this had a negative effect in a batch reactor, the same mixing was expected to be beneficial in a different reactor type, such as packed bed flow reactor.

With the conditions and dehydrating agents investigated, the performance of several catalysts synthesised in Chapter 2 were investigated. The commercial CeO_2 proved to have the highest activity, though catalyst stability studies show that the higher DMC yields are only observed when the catalyst is fresh. After the initial reaction the activity decreased to a similar level as the other catalysts

investigated. Although the catalysts produced in this work had a lower initial activity, this activity was stable for 6 reuse cycles. Each of the catalysts tested produce a similar amount of DMC with each cycle, with gradients of around 1.6 mmol.cycle^{-1}.

The results obtained here would be used as temperature and pressure starting points in the calculation of the thermodynamics for the dehydrating agent-free reactions.

3.5 References

(1) Honda, M.; Tamura, M.; Nakagawa, Y.; Tomishige, K. Catalytic CO 2 Conversion to Organic Carbonates with Alcohols in Combination with Dehydration System. *Catal. Sci. Technol.* **2014**, *4* (9), 2830. https://doi.org/10.1039/C4CY00557K.

(2) Aresta, M.; Dibenedetto, A.; Fracchiolla, E.; Giannoccaro, P.; Pastore, C.; Pápai, I.; Schubert, G. Mechanism of Formation of Organic Carbonates from Aliphatic Alcohols and Carbon Dioxide under Mild Conditions Promoted by Carbodiimides. DFT Calculation and Experimental Study. *J. Org. Chem.* **2005**, *70* (16), 6177–6186. https://doi.org/10.1021/jo050392y.

(3) Eta, V.; Mäki-Arvela, P.; Wärn, J.; Salmi, T.; Mikkola, J. P.; Murzin, D. Y. Kinetics of Dimethyl Carbonate Synthesis from Methanol and Carbon Dioxide over ZrO2-MgO Catalyst in the Presence of Butylene Oxide as Additive. *Appl. Catal. A Gen.* **2011**, *404* (1–2), 39–46. https://doi.org/10.1016/j.apcata.2011.07.004.

(4) Tian, J. S.; Miao, C. X.; Wang, J. Q.; Cai, F.; Du, Y.; Zhao, Y.; He, L. N. Efficient Synthesis of Dimethyl Carbonate from Methanol, Propylene Oxide and CO2 Catalyzed by Recyclable Inorganic Base/Phosphonium Halide-Functionalized Polyethylene Glycol. *Green Chem.* **2007**, *9* (6), 566–57. https://doi.org/10.1039/b614259a.

(5) Choi, J.-C. C.; He, L.-N. N.; Yasuda, H.; Sakakura, T.; Yasudaa, H.; Sakakura, T. Selective and High Yield Synthesis of Dimethyl Carbonate Directly from Carbon Dioxide and Methanol. *Green Chem.* **2002**, *4* (3), 230–234. https://doi.org/10.1039/b200623p.

(6) Su, X.; Lin, W.; Cheng, H.; Zhang, C.; Wang, Y.; Yu, X.; Wu, Z.; Zhao, F. Metal-Free Catalytic Conversion of CO2 and Glycerol to Glycerol Carbonate. *Green Chem.* **2017**, *19* (7), 1775–1781. https://doi.org/10.1039/c7gc00260b.

(7) Honda, M.; Kuno, S.; Begum, N.; Fujimoto, K. I.; Suzuki, K.; Nakagawa, Y.; Tomishige, K. Catalytic Synthesis of Dialkyl Carbonate from Low Pressure CO2 and Alcohols Combined with Acetonitrile Hydration Catalyzed by CeO2. *Appl. Catal. A Gen.* **2010**, *384* (1–2), 165–170. https://doi.org/10.1016/j.apcata.2010.06.033.

(8) Honda, M.; Tamura, M.; Nakagawa, Y.; Sonehara, S.; Suzuki, K.; Fujimoto, K. I.; Tomishige, K. Ceria-Catalyzed Conversion of Carbon Dioxide into Dimethyl Carbonate with 2-Cyanopyridine. *ChemSusChem* **2013**, *6* (8), 1341–1344. https://doi.org/10.1002/cssc.201300229.

(9) Honda, M.; Kuno, S.; Sonehara, S.; Fujimoto, K. I.; Suzuki, K.; Nakagawa, Y.; Tomishige, K. Tandem Carboxylation-Hydration Reaction System from Methanol, CO2 and Benzonitrile to Dimethyl Carbonate and Benzamide Catalyzed by CeO2. *ChemCatChem* **2011**, *3* (2), 365–370. https://doi.org/10.1002/cctc.201000339.

(10) Ohmori, H.; Saka, K.; Naga, N.; Mizuki, Y.; Masui, M. Reaction of Electrochemically Generated Triphenylphosphine Radical Cation with Amides and Ureas. *Chem. Pharm. Bull.* **1985**, *33* (1), 373–376. https://doi.org/10.1248/cpb.33.373.

(11) Duangkamol, C.; Pattarawarapan, M.; Phakhodee, W. Ultrasonic-Assisted Synthesis of Carbodiimides from N,N′-Disubstituted Thioureas and Ureas. *Monatshefte fur Chemie* **2016**, *147* (11), 1945–1949. https://doi.org/10.1007/s00706-016-1761-3.

(12) Schlama, T.; Gouverneur, V.; Mioskowski, C.; Pii, P.; Science, E.; Bioorganique, C.; Pasteur, L. A New and Efficient Preparation of Carbodiimides from Ureas Using Dimethylphosgeniminium Chloride as a Dehydrating Agent. *Tetrahedron Lett.* **1996**, *37* (39), 7047–7048. https://doi.org/10.1016/0040-4039(96)01593-6.

(13) Honda, M.; Tamura, M.; Nakagawa, Y.; Nakao, K.; Suzuki, K.; Tomishige, K. Organic Carbonate Synthesis from CO2 and Alcohol over CeO2 with 2-Cyanopyridine: Scope and Mechanistic Studies. *J. Catal.* **2014**, *318*, 95–107. https://doi.org/10.1016/j.jcat.2014.07.022.

(14) Sakakura, T.; Saito, Y.; Okano, M.; Choi, J.-C. C.; Sako, T.; Choi, J.-C. C.; Sakakura, T. Selective Conversion of Carbon Dioxide to Dimethyl Carbonate by Molecular Catalysis. *J. Org. Chem.* **2002**, *63* (20), 7095–7096. https://doi.org/10.1021/jo980460z.

(15) Choi, J. C.; Sakakura, T.; Sako, T. Reaction of Dialkyltin Methoxide with Carbon Dioxide Relevant to the Mechanisms of Catalytic Carbonate Synthesis. *J. Am. Chem. Soc.* **1999**, *121* (15), 3793–3794. https://doi.org/10.1021/ja9900499.

(16) Sakakura, T.; Choi, J. C.; Saito, Y.; Masuda, T.; Sako, T.; Oriyama, T. Metal-Catalyzed Dimethyl Carbonate Synthesis from Carbon Dioxide and Acetals. *J. Org. Chem.* **1999**, *64* (12), 4506–4508. https://doi.org/10.1021/jo990155t.

(17) Saada, R.; Kellici, S.; Heil, T.; Morgan, D.; Saha, B. Greener Synthesis of Dimethyl Carbonate Using a Novel Ceria-Zirconia Oxide/Graphene Nanocomposite Catalyst. *Appl. Catal. B Environ.* **2015**, *168–169*, 352–362. https://doi.org/10.1016/j.apcatb.2014.12.013.

(18) Camy, S.; Pic, J. S.; Badens, E.; Condoret, J. S. Fluid Phase Equilibria of the Reacting Mixture in the Dimethyl Carbonate Synthesis from

Supercritical CO2. *J. Supercrit. Fluids* **2003**, *25* (1), 19–32. https://doi.org/10.1016/S0896-8446(02)00087-6.

(19) Python Software Foundation. Python https://www.python.org/.

(20) Clayden, Jonathan; Greeves, Nick; Warren, Stuart; Wothers, P. *Organic Chemistry*; Oxford University Press, 2001.

(21) Zhang, Z. F.; Liu, Z. W.; Lu, J.; Liu, Z. T. Synthesis of Dimethyl Carbonate from Carbon Dioxide and Methanol over CexZr1-XO2 and [EMIM]Br/Ce0.5Zr 0.5O2. *Ind. Eng. Chem. Res.* **2011**, *50* (4), 1981–1988. https://doi.org/10.1021/ie102017j.

(22) Aresta, M.; Dibenedetto, A.; Pastore, C.; Cuocci, C.; Aresta, B.; Cometa, S.; De Giglio, E.; Degiglio, E. Cerium(IV)Oxide Modification by Inclusion of a Hetero-Atom: A Strategy for Producing Efficient and Robust Nano-Catalysts for Methanol Carboxylation. *Catal. Today* **2008**, *137* (1), 125–131. https://doi.org/10.1016/j.cattod.2008.04.043.

Chapter 4 – Thermodynamic calculations

This chapter includes quantum chemical calculations performed by Dr Theo Keane, The University of Sheffield, see Section 4.2.5.

4.1 Introduction

The work shown thus far in this thesis has focused on the direct synthesis of dimethyl carbonate in the presence of a dehydrating agent (DA) (Scheme 4.1). The stable product formed by the reaction of water with the dehydrating agent prevents the reverse reaction from occurring and provides additional thermodynamic driving force which can take this reaction from being thermodynamically limited (a positive Gibbs free energy) to spontaneous (a negative Gibbs free energy).

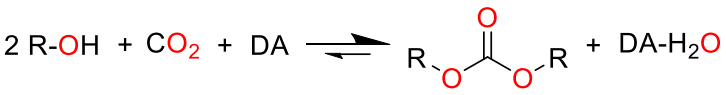

Scheme 4.1: Direct synthesis of dialkyl carbonates in the presence of a dehydrating agent (DA).

As discussed before, without a dehydrating agent, the reaction favours the starting materials and becomes thermodynamically limited (Scheme 4.2). The use of dehydrating agents in the literature has enabled high conversions and selectivity towards DMC.[1] However, work conducted without the use of a DA showed much lower conversions. It is rare for the plateau of the reaction in these reports to be compared to the theoretical calculated equilibrium conversions, and the common assumption is that the plateau is caused by thermodynamics, and not by other factors, such as catalyst deactivation.

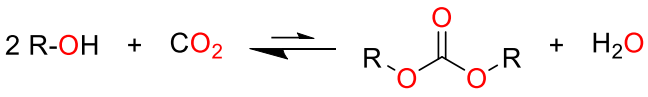

Scheme 4.2: Direct synthesis of dialkyl carbonates from CO_2 and alcohols without a dehydrating agent.

The theoretical conversion of MeOH to DMC can be calculated using the van't Hoff equation (Equation 4.1) and the equilibrium equation (Equation 4.2).

Equation 4.1 $$K_{eq} = e^{\left(-\frac{\Delta H}{RT}-\frac{\Delta S}{R}\right)}$$

Where:

K_{eq} = Equilibrium constant (-)

ΔH = Enthalpy change ($J \cdot mol^{-1}$)

ΔS = Entropy change ($J \cdot mol^{-1} \cdot K^{-1}$)

R = Ideal Gas constant ($J \cdot mol^{-1} \cdot K^{-1}$)

T = absolute Temperature (K)

Equation 4.2 $$K_{eq} = \frac{[DAC][H_2O]}{[CO_2][ROH]^2}$$

The equilibrium equation can be simplified to Equation 4.3, as DAC and H_2O are produced in equal amounts.

Equation 4.3 $$k_{eq} = \frac{[DAC]^2}{[CO_2][ROH]^2}$$

Which rearranged gives DAC and H_2O concentration in Equation 4.4

Equation 4.4 $$[H_2O] = [DAC] = \sqrt{k_{eq}[CO_2][ROH]^2}$$

Values for ΔH and ΔS of reaction can be calculated using literature values for ΔH_f^0 and S^0 (Methods section, Table 4.1). The Gibbs free energy of the reaction (ΔG) can then be calculated using the Gibbs equation (Equation 4.5)

Equation 4.5 $$\Delta G = \Delta H - T\Delta S$$

This then enables the calculation of the equilibrium conversion of ROH for those reactions using the Equation 4.6.

Equation 4.6 $$Conv_{eq} = \frac{[ROH]_{eq}}{[ROH]_0} = \frac{2[DAC]_{eq}}{[ROH]_0} = \frac{2\sqrt{k_{eq}[CO_2]_{eq}[ROH]_{eq}^2}}{[ROH]_0}$$

The van't Hoff equation provides the simplest method of calculation of equilibrium conversion. However, it assumes that the ΔH and ΔS terms are temperature independent (so-called van't Hoff approximation). In practice these values are often temperature dependant, however, and are proportional to the heat capacity (C_p) of the substance as given by Equation 4.7 and Equation 4.8

Equation 4.7 $$\Delta H_T = \Delta H_{T_0} + \Delta C_p (T - T_0)$$

Equation 4.8 $$\Delta S_T = \Delta S_{T_0} + \Delta C_p ln\left(\frac{T}{T_0}\right)$$

Where:

$$\Delta C_p = \sum nC_{p(products)} - \sum nC_{p(reactants)}$$

ΔH_T = Enthalpy change at temperature T ($J \cdot mol^{-1}$)

ΔS_T = Entropy change at temperature T ($J \cdot mol^{-1} \cdot K^{-1}$)

n = moles of substance

Cp = molar isobaric heat capacity ($J \cdot mol^{-1} \cdot K^{-1}$)

ΔCp = Change in heat capacity ($J \cdot mol^{-1} \cdot K^{-1}$)

T = Temperature of interest (K)

T_0 = Temperature of the measured value (K)

The value of the heat capacity at constant pressure (C_p) is also temperature dependant according to the Shomate equation (Equation 4.9) and polynomials (Methods section, Table 4.3).

Equation 4.9 $$C_p = A + Bt + Ct^2 + Dt^3 + \frac{E}{t^2}$$

Where:

$$t = \frac{T}{1000} (K \cdot 10^{-3})$$

A-E = Shomate coefficients

This chapter aims to provide a theoretical basis for the practical work presented in Chapter 5 by determining the equilibrium position of the reaction showing in Scheme 4.2 at relevant temperatures and pressures; determining how the purity of starting materials affect that equilibrium position; and calculating the effect of separating the products from the reactants on the equilibrium position. As Chapter 5 investigates both ethanol and methanol in batch and flow, the equilibrium conversions for both alcohols have been calculated.

4.2 Methods

4.2.1 Calculation of K_{eq}

Values for ΔH^0 and ΔS^0 for DEC and DMC were calculated from enthalpy change of formation (ΔH_f) and standard entropy (S) of each component in its standard state using Equation 4.10 and Equation 4.11.

Equation 4.10 $$\Delta H_{reac} = \sum \Delta H_{f\ products} - \sum \Delta H_{f\ reactants}$$

Equation 4.11 $\Delta S_{reac} = \sum S_{products} - \sum S_{reactants}$

Values of ΔH_f and S were obtained from several sources (Table 4.1).

ΔG was then calculated for a range of temperatures from 40 °C to 160 °C using Equation 4.12.

Equation 4.12 $\Delta G^0 = \Delta H^0 - T\Delta S^0$

Using Equation 4.13 the equilibrium constant K_{eq} was calculated for each temperature.

Equation 4.13 $ln(K_{eq}) = \frac{\Delta H}{RT} - \frac{\Delta S}{R}$

Equation 4.14 was used to calculate product equilibrium concentrations from K_{eq}

Equation 4.14 $K_{eq} = \frac{[DMC]_{eq}[H_2O]_{eq}}{[CO_2]_{eq}[ROH]^2_{eq}}$

A numerical optimisation of Equation 4.14 was implemented in python,[2] using only the standard library. (code is freely available on GitHub).[3] CO_2 densities were calculated from CO_2 concentrations using Equation 4.15.

Equation 4.15 $d = [CO_2] \cdot 44.01(g \cdot mol^{-1})$

Where: d = density ($g \cdot mL^{-1}$)

$[CO_2]$ = CO_2 concentration ($mol \cdot mL^{-1}$)

Table 4.1: Enthalpies of formation (ΔH_f^0) in standard state for each component investigated in this work. [a]Calculated from reaction enthalpy of the alcolysis of propylene carbonate. [b]calculated from the reaction enthalpy of the hydrolysis of tetramethyl orthocarbonate. The number of decimal places shown were taken directly from the published values and are meant to refelect the accuracy of the original calculation.

Component	ΔH_f^o (kJ·mol^{-1})	Year published	Source	S^o (J·K^{-1}·mol^{-1})	Year published	Source
Dimethyl Carbonate $DMC_{(l)}$	-607.27	-	DIPPR project[4]	218.7	-	DIPPR project[4]
	-608.76	2015	NIST TDE 2015 (Knovel)[5]			
	-613.78	2010	Lieno et al.[6]			
	-614.53[a]	1991	NIST[7–10]			
	-595.73[a]	1991	NIST[7–9,11]			
	-607.60[b]	1972	NIST[7,12]			
Diethyl Carbonate $DEC_{(l)}$	-682.65	-	DIPPR project[4]	293.3	-	DIPPR project[4]
	-681.58	2015	NIST TDE 2015 (Knovel)[13]			
	-681.5	1972	NIST[7,14]			
	-724.17	1971	NIST[7,11]			
Methanol $MeOH_{(l)}$	-239.45	2015	NIST TDE 2015 (Knovel)[15]	127.19	1971	NIST[16,17]
	-238.4	1972	NIST[7,18]	126.8	1929	NIST[16,19]
	-239.5	1965	NIST[7,20]			
	-238.9	1960	NIST[7,21]			
Ethanol $EtOH_{(l)}$	-276.93	2015	NIST TDE 2015 (Knovel)[22]	159.86	1977	NIST[16,23]
	-277	1965	NIST[7,20]	161.21	1961	NIST[16,24]
	-277.6	1960	NIST[7,21]	160.7	1929	NIST[16,25]
Carbon dioxide $CO_{2(g)}$	-393.51	2015	NIST TDE 2015 (Knovel)[26]	213.79	1998	NIST[16,27]
	-393.52	1998	NIST[7,21]	213.785	1984	NIST[16,28]
Water $H_2O_{(l)}$	-285.83	2015	NIST TDE 2015 (Knovel)[29]	69.95	1984	NIST[16,27]
	-285.83	1998	NIST[7,30]			
	-285.83	1984	NIST[7,31]			

4.2.2 Quantum chemical calculations (QCC)

The thermodynamic values for this work were calculated using previously reported values of enthalpy of formation (ΔH_f) and standard entropy (S). The use of computational methods is now a more common way to calculate these values. To compare the values obtained computationally with those obtained experimentally, quantum chemical calculations were performed.

These were provided by Dr Theo Keane, The University of Sheffield.

A composite scheme was used to obtain theoretical thermochemical data. First, density functional theory calculations were performed using Gaussian 09, revision D.01,[32] using the ωB97XD exchange-correlation functional[33] and the def2-QZVPP[34] basis set, in vacuo. This functional has been found to perform well for a wide variety of chemical problems.[35] Following geometry optimisations, frequency calculations were performed in order to obtain thermochemical corrections to the internal (electronic) energy. The thermochemical corrections were calculated using Grimme's quasi-harmonic approach,[36] as implemented in the goodvibes package, version 2.0.3.[37] No frequency scaling factor was applied in the free energy calculations and the rigid-rotor cut-off was set to 100 cm^{-1}. In the case of DMC, a search for local minima was conducted and three different stable conformations were found with differing symmetries: one C2v, one Cs and one C2 (Figure 4.1).

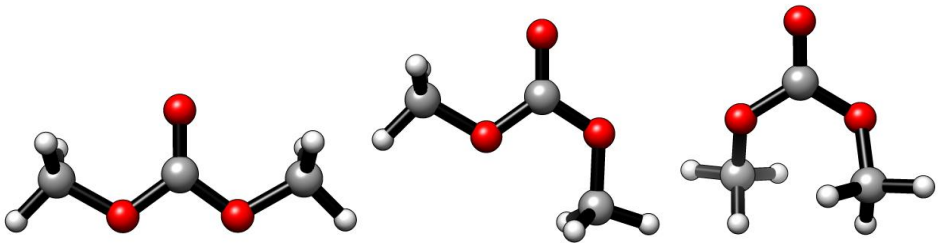

Figure 4.1: C2v isomer (left), Cs isomer (middle) and C2 isomer (right) of DMC, optimised with ωB97XD/def2-QZVPP. All other rotamers were found to be saddle points.

All three stable rotamers were considered in the calculations and in the analysis, a Boltzmann-weighted distribution at each temperature of the thermochemical data of the three rotamers was used.

Second, explicitly correlated coupled cluster singles and doubles with perturbative triples (CCSD(T)-F12b) calculations were performed at these

geometries using Molpro, version 2012.1.[38–41] A two-point, Schwenke-type complete basis set (CBS) extrapolation using the formula of Hill and co-workers[42] was performed, using the cc-pVDZ-F12 and cc-pVTZ-F12 orbital basis sets.[43] The geminal Slater exponent, β, was set to 0.9 and 1.0 in the DZ and TZ calculations, respectively.[42] Density fitting of the relevant matrices was performed using the cc-pV(n + 1)Z/JKFit,[44] the cc-pVnZ-F12/MP2Fit and cc-pVnZ-F12/OptRI+ auxilliary basis sets,[45,46] where n is the cardinal number of the orbital basis set. The resulting CCSD(T)-F12b/CBS energies were used to obtain final theoretical thermochemical values by adding the thermochemical corrections from the DFT calculations to the internal energies from the correlated wavefunction calculations.

These values provided by Dr Keane were then compared with other methods for correcting the value of ΔG at a given temperature. ΔG was calculated from 250-500 K in 10 K increments. Values for select temperatures are shown in Table 4.2. A linear regression of ΔG *versus* T gives a ΔH^0 of -20.76 kJ·mol^{-1}, a ΔS^0 of -0.177 kJ.K^{-1}·mol^{-1} and a ΔG^0 of +31.84 kJ·mol^{-1}.

Table 4.2: ΔG calculated by the QCC methods. The gradient of the ΔG vs T gives a ΔS^0 of -0.177 kJ·K^{-1}·mol^{-1} and the intercept a ΔH^0 of -20.76 kJ·mol^{-1}

Temperature (K)	ΔG (kJ·Mol^{-1})
250	23.457
300	32.193
410	51.611
500	67.530

4.2.3 Effect of Temperature on ΔH and ΔS

The correction for ΔH, ΔS (Equation 4.7 and Equation 4.8) and the correction for heat capacities have been used to show the effect temperature has on the entropy and enthalpy changes of the reaction. Heat capacities at 298 K and the equations and coefficients for calculation of heat capacity are shown in Table 4.3. The resulting corrected values were then used to calculate ΔG and K_{eq} to determine how the temperature correction affects the calculated equilibrium.

Table 4.3: Heat capacities at 298 K, along with the coefficients and equation for the temperature dependence of C_p. Decimal places used are the same as those quoted in the literature with no rounding.

Substance	C_p^{298} ($J \cdot K^{-1} \cdot mol^{-1}$)	Heat capacity coefficients		Equation	Ref
$DMC_{(g)}$	99.9	A	87.96135349	$C_p = A + BT + CT^2 + DT^3 + ET^4 + FT^5 + GT^6$	[47]
		B	-0.372153229		
		C	0.002398124		
		D	$-4.47228 \cdot 10^{-6}$		
		E	$4.09941 \cdot 10^{-9}$		
		F	$-1.87146 \cdot 10^{-12}$		
		G	$3.38886 \cdot 10^{-16}$		
$MeOH_{(g)}$	45.2	A	40.046	$C_p = A + BT + CT^2 + DT^3 + ET^4$	[48]
		B	-0.038287		
		C	0.00024529		
		D	$-2.1679 \cdot 10^{-7}$		
		E	$5.9909 \cdot 10^{-11}$		
$H_2O_{(l)}$	75.3	A	-203.6060	$C_p = A + Bt + Ct^2 + Dt^3 + \frac{E}{t^2}$ t = T/1000	[28,49]
		B	1523.290		
		C	-3196.413		
		D	2474.455		
		E	3.855326		
$CO_{2(g)}$	81.9	A	24.99735	$C_p = A + Bt + Ct^2 + Dt^3 + \frac{E}{t^2}$ t = T/1000	[28,50]
		B	55.18696		
		C	-33.69137		
		D	7.948387		
		E	-0.136638		

4.2.4 Effect of product removal on equilibrium position

In order to calculate the effect of product removal on equilibrium position, the numerical optimisation was performed for a set number of cycles (500-10,000). At the end of each cycle the concentrations of reagents gives the equilibrium constant (by Equation 4.14). This equation was modified to include a product removal factor for one or both products (Equation 4.16) and the numerical optimisation was then performed again.

Equation 4.16

$$\frac{[DMC]_{start}[H_2O]_{start}}{[CO_2]_{start}[ROH]^2_{start}} = \frac{x[DMC]_{eq}\, y[H_2O]_{eq}}{[CO_2]_{eq}[ROH]^2_{eq}}$$

Where:

x, y = product removal factor where a 10% product removal has a value of 0.9

These calculations simulated the physical removal of a product from the reactor, such as by a membrane or molecular sieves downstream of the reactor bed. The removal can be calculated in two modes:

1. Constant starting material, where the concentrations of CO_2 and/or alcohol remained constant with each cycle, which is analogous to continuously replenishing the CO_2, alcohol, or both.

Note: In constant starting material mode, the starting material concentration decreased during the iteration process, but between cycles was restored to the initial starting concentration. For 0% product removal, this took around 6 cycles to stabilise at the final conversion.

2. Decreasing starting material, where the CO_2 and alcohol were depleted with each cycle as in a closed reactor with no continuous substrate feed. In this mode the denominator of Equation 4.16 decreases, which means the total amount of product that could be generated each cycle decreased.

4.3 Results and discussion

4.3.1 Equilibrium conversions

As mentioned in the introduction above, the formation of DAC without a dehydrating agent is thermodynamically limited. To determine whether the plateau in the reaction was caused by the reaction reaching equilibrium or by

some other factor, such as catalyst deactivation, it was important to calculate the equilibrium conversion. As described in the methods above, this was done by first calculating ΔG of reaction, and calculating K_{eq} using the van't Hoff equation and then iteratively solving the equilibrium equation.

For DEC the values of ΔH_f from NIST TDE (Methods section Table 4.1) were used as these are the most recent:

$$\Delta H^0_{DEC} = (-681.58 - 285.83) - (2(-276.93) - 393.51)$$
$$= -20.04\ kJ \cdot mol^{-1}$$

$$\Delta S^0_{DEC} = (293.3 + 69.95) - (2(159.86) + 213.79)$$
$$= -170.26 J \cdot \mathrm{K}^{-1} \cdot mol^{-1}$$

For DMC, the difference in the reported values lead to a significant variation in ΔG. Using the ΔH_f of DMC reported by NIST TDE gave a ΔG^0 of +31.32 $kJ \cdot mol^{-1}$, the value reported by Lieno *et al.* however gave a ΔG^0 of +26.29 $kJ \cdot mol^{-1}$. Calculating K_{eq} at 413 K for both gave an order of magnitude difference, using these to calculate methanol conversions gave a 0.207% and 0.427% with NIST TDE and Lieno *et al.* respectively (Table 4.4).

Table 4.4: Difference between ΔG, K_{eq} and methanol conversion with different reported values of ΔH_f DMC.

Reference	DMC ΔH_f ($kJ \cdot Mol^{-1}$)	ΔG_{413K} ($kJ \cdot Mol^{-1}$)	K_{eq}	MeOH conversion (%)
NIST TDE[5]	-608.76	+51.96	2.68 x10^{-7}	0.207
Lieno *et al.*[6]	-613.78	+46.94	1.16 x10^{-6}	0.427

Since the value reported by Lieno *et al.* was in closer agreement with experimental data in Chapter 5 and the literature, as well as its precedent in calculating thermodynamics for the formation of DMC,[6] this value was used to calculate the ΔH for DMC:

$$\Delta H^0_{DMC} = (-613.78 - 285.83) - (2(-239.45) - 393.51)$$
$$= -27.20\ kJ \cdot mol^{-1}$$

$$\Delta S^0_{DMC} = (218.7 + 69.95) - (2(127.19) + 213.79)$$
$$= -179.52\ J \cdot \mathrm{K}^{-1} \cdot mol^{-1}$$

Scheme 4.3 and Scheme 4.4 show the enthalpy, and entropy changes for the synthesis of DMC and DEC at 298 K. The reaction to form DMC has a ΔG° of +26.29 kJ·mol^{-1} and for DEC ΔG° is +30.69 kJ·mol^{-1}. The negative values for ΔS means that, with increasing temperature, the entropic contribution to the reaction becomes greater, resulting in a more positive ΔG. This in turn means that the value of K_{eq} (by Equation 4.13) becomes smaller, and thus the concentration of products also decreases with increasing temperature (Equation 4.14).

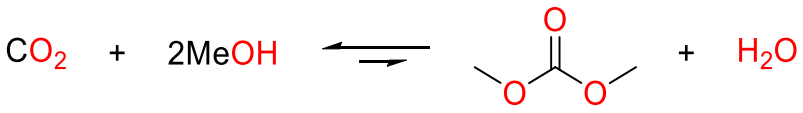

Scheme 4.3: Reaction between CO_2 and methanol to form DMC and water, ΔG_{298} = +26.2 kJ·mol^{-1}, ΔH_{298} = -27.2 kJ·mol^{-1} and ΔS_{298} = -179.52 J·K^{-1}·mol^{-1}.

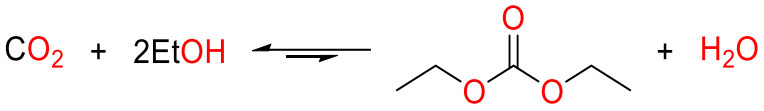

Scheme 4.4: Reaction between CO_2 and ethanol to form DEC and water, ΔG_{298} = +30.69 kJ·mol^{-1}, ΔH_{298} = -20.04 kJ·mol^{-1} and ΔS_{298} = -170.26 J·K^{-1}.mol^{-1}.

Table 4.5 shows a comparison of different reported thermodynamics for the formation of DMC and DEC. The value ΔG value for DMC calculated in this work aligns closely with other work that calculate their thermodynamics in the standard state.[6,51] However, Chiang *et al.*[51] calculate different values for ΔH and ΔS (-142 J·K^{-1}·mol^{-1} for Chiang compared to -179.52 J·K^{-1}·mol^{-1} calculated in this work). This difference in ΔS and ΔH would affect how much ΔG grows with increasing temperature, with Chiang's ΔG growing less. When values are calculated with each component in the gas phase rather than standard state, ΔG increases for both DMC[52] and DEC.[53] The purpose of these calculations, however, is utility and the value which best aligns with experimental work is the most useful.

Table 4.5: Comparison of calculated thermodynamics for DMC and DEC. The number of decimal places are used as reported.

Product	State	ΔG^0 (kJ·mol^{-1})	ΔH^0 (kJ·mol^{-1})	Ref
DMC	Standard	+26.29	-27.20	This work
DMC	Standard	+26.21	-27.90	[6]
DMC	Standard	+25.34	-16.98	[51]
DMC	Gas phase	+32	-22	[52]
DEC	Standard	+30.69	-20.04	This work
DEC	Gas phase	+35.84	-16.60	[53]

An extended equilibrium was also investigated, taking into account the possibility of excess CO_2 and water reacting to give carbonic acid as shown in Scheme 4.5. An equilibrium constant of 1.7×10^{-3} was reported for the formation of carbonic acid from CO_2 and water at 298 K.[54] The effect that the carbonic acid equilibrium had on the conversion of methanol was minimal with a change in conversion between 0.01% and 0.05% at 298 K, depending on starting concentrations of methanol and CO_2. This shows that the formation of carbonic acid has a negligible effect on the amount of DAC formed, and so the simpler equilibria shown above were used for all thermodynamic calculations going forward.

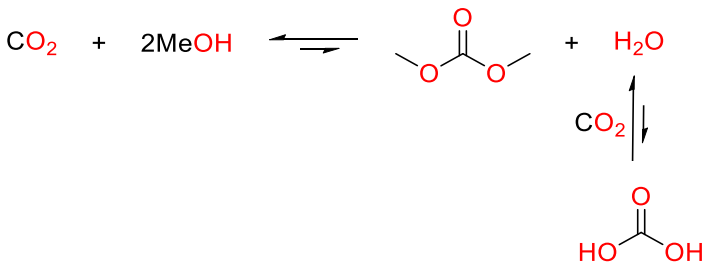

Scheme 4.5: Extended equilibrium for DMC, including carbonic acid equilibrium formed between CO_2 and H_2O.

Figure 4.2 shows the equilibrium conversion of methanol across a range of temperatures, from 297–413 K, and CO_2 densities, from 0.01–0.96 g·mL^{-1}, in a closed system. As expected from the negative entropy change, the equilibrium conversion of methanol decreased with increasing temperature. Increasing CO_2 density increased methanol conversion due to the higher CO_2 concentration. Based on thermodynamic calculations, the highest equilibrium conversion of

methanol was 4.42% at 297 K in liquid CO_2 (56 bar). At temperatures between 373 and 413 K, where many catalytic reactions are actually performed for kinetic reasons, the maximum calculated conversion was 1.45% at 0.96 $g \cdot ml^{-1}$ of CO_2 at 373 K. In order to achieve this CO_2 density at 373 K, a pressure of 1000 bar was required which is extremely high for an industrial process. More reasonable CO_2 densities of 0.5 $g.mL^{-1}$ (200 bar at 373 K) gave an equilibrium conversion of methanol of 1.01%.

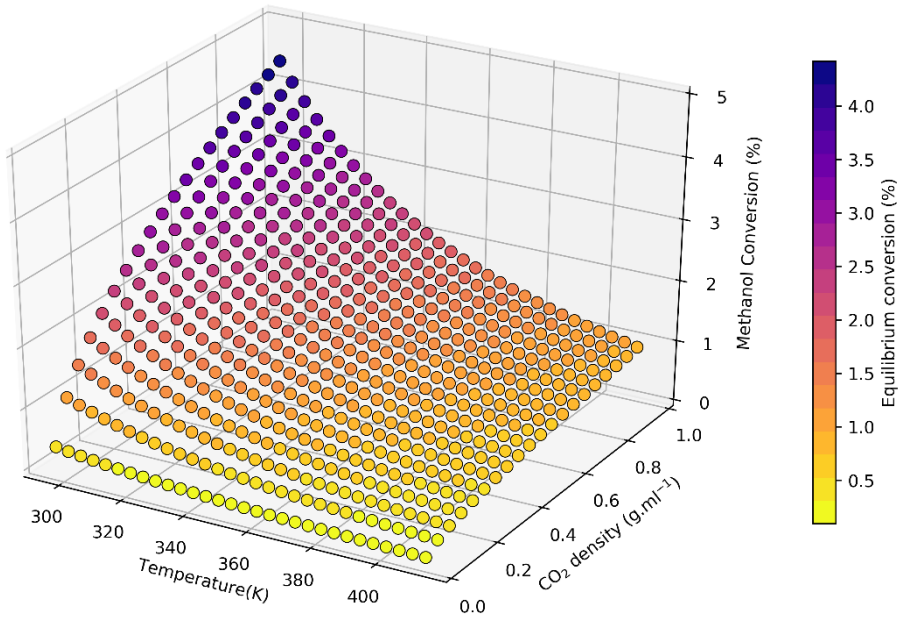

Figure 4.2: Calculated equilibrium methanol conversions for the formation of DMC from CO_2 and methanol across multiple temperatures and CO_2 densities. Methanol starting concentration: 24.72 $mol \cdot L^{-1}$.

A similar trend was seen for the conversion of ethanol to DEC. Figure 4.3 shows that due to the higher ΔG of this reaction, the equilibrium conversions at the same conditions are around 50% lower than for methanol. The highest equilibrium conversion for ethanol was 2% with liquid CO_2 at 298 K. At typical reaction temperatures 373–413 K the highest equilibrium conversion was 0.6% at 1000 bar CO_2. Equilibrium conversions at more reasonable pressures (200 bar) are around 0.3%.

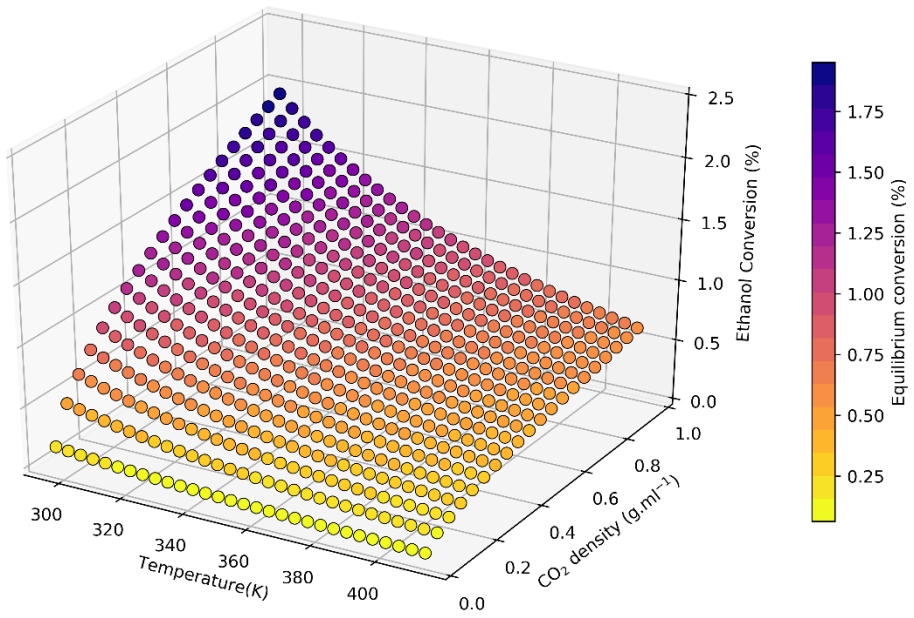

Figure 4.3: Calculated equilibrium conversions for the condensation of CO_2 with ethanol across multiple temperatures and CO_2 densities. Ethanol starting concentration: 17.13 Mol·L^{-1}.

From these calculations we can infer that the optimal conditions for high alcohol conversions are a low temperature and a high CO_2 density (and thus pressure or concentration). Optimal conditions for the reaction thermodynamics do not necessarily provide optimal kinetics, and experimentally a compromise between thermodynamics and kinetics must be achieved.

4.3.2 Temperature dependence of ΔH and ΔS

The conversions presented above are based on the van't Hoff equation and assume that ΔH and ΔS remain constant with increasing temperature. However as shown in Equation 4.7–Equation 4.9, changing temperature causes a change in ΔH and ΔS proportional to the heat capacity of the system.

Figure 4.4 shows 4 methods of calculating ΔG; these values will be used to determine which method corresponds most closely to experimental values obtained in Chapter 5. If experimental values far exceed the calculated equilibrium, then it is unlikely that the method is accurate at those temperatures. The uncorrected ΔG values (●) and the temperature corrected ΔH and ΔS (●) follow the same linear trend with little deviation. This was to be expected, as the ΔC_p of the reaction mixture was 0.0029 kJ·mol^{-1}·K^{-1} causing very little change in ΔH and ΔS. Temperature correction of C_p as well as ΔH and ΔS (●)

caused a larger deviation from the uncorrected ΔG value as temperature increased, with a ΔG 3.8 kJ.mol^{-1} lower than the uncorrected ΔG at 500 K. There was reasonable agreement of the uncorrected (●) and corrected values (●) between 280 and 350 K, which was expected due to the correction terms of Equation 4.7 and Equation 4.8 being equal at 298 K. The values calculated by QCC (●) followed a similar linear trend as the uncorrected, though offset by an average of 5.16 kJ·mol^{-1}. The QCC calculated the ΔH° to be 7 kJ·mol^{-1} higher than Lieno *et al.* estimating that the reaction is less exothermic. This then gives a lower K_{eq} and thus predicted a lower equilibrium conversion.

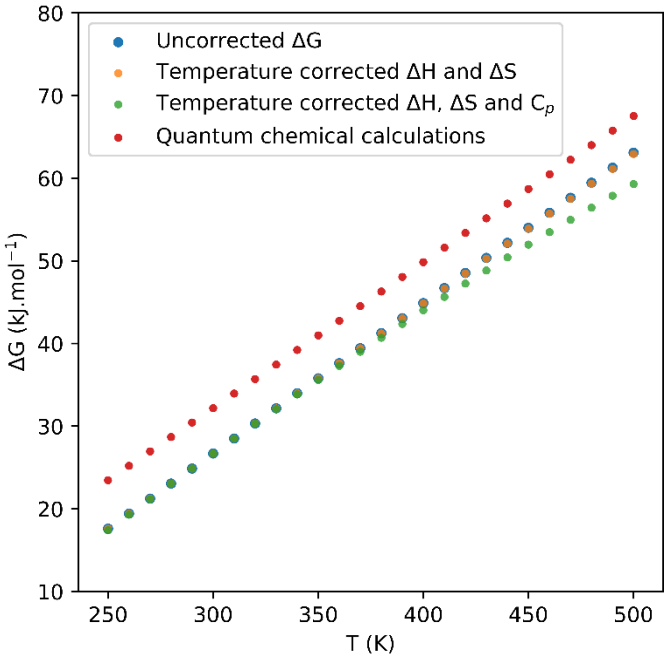

Figure 4.4: Change in ΔG with increasing temperature, with uncorrected ΔG being values calculated with Equation 4.12, temperature corrected being values calculated with Equation 4.7 - Equation 4.9 and QCC being values calculated as described in the Methods section above.

Figure 4.5 shows how K_{eq} changes with temperature for each of the methods used to calculate the temperature dependence of ΔG. The uncorrected values (●) were slightly lower than the corrected values of ΔH and ΔS (●) throughout, from 250–500 K. The C_p corrected values (●) gave higher values of K_{eq} both at lower (below 280 K) and again at higher temperatures (above 350 K), overlapping with the uncorrected and ΔH and ΔS corrected values between 280–350 K. The QCC ΔG (●) gave lower values of K_{eq} for all the temperature range, which in turn translates to a lower equilibrium conversion. The values calculated by QCC show good agreement to the NIST TDE values, however as

discussed above, these correlate poorly to experimental values both in the literature and presented Chapter 5.

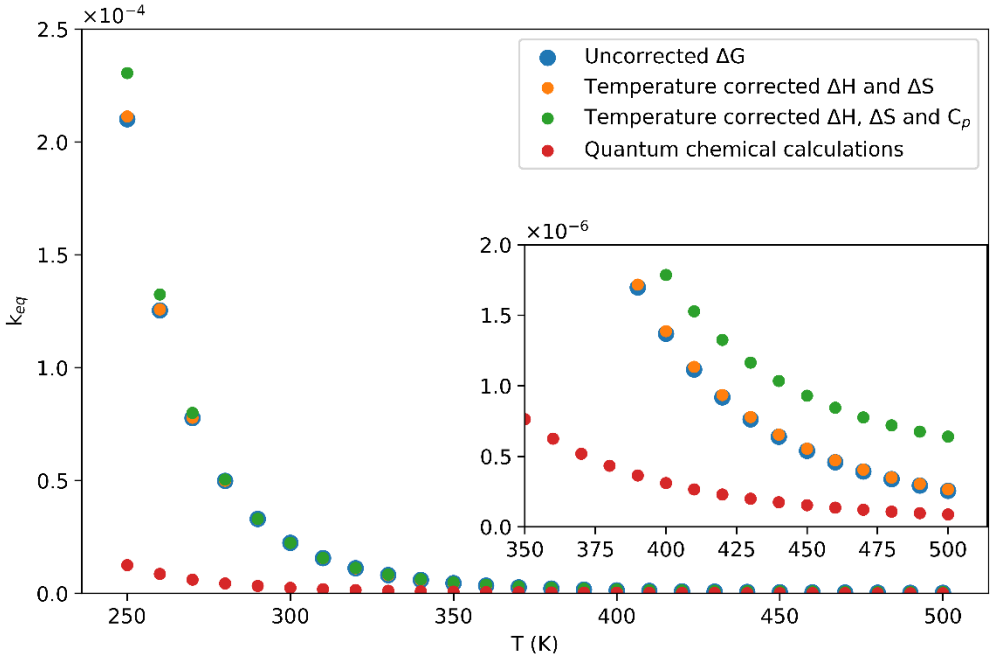

Figure 4.5: Shows the change in K_{eq} with increasing temperature for different methods of calculating the change in ΔG with increasing temperature. Inset: Zoomed on higher temperature region to show the effect of temperature correction on K_{eq}.

A comparison of equilibrium conversions between these methods are shown in Table 4.6 at three experimentally relevant temperatures. Uncorrected and ΔH and ΔS corrected had the same equilibrium conversion to 2 decimal places due to the small change in ΔG calculated between the methods. For example, at 413 K the uncorrected ΔG was +47.26 kJ·mol^{-1}, and the corrected was +47.21 kJ·mol^{-1} giving an equilibrium conversion of 0.785% and 0.792% respectively. The method correcting ΔH, ΔS and C_p calculated a decreased ΔG, causing increased equilibrium conversions from 1.21% to 1.30% at 373 K and 0.79% to 0.92% at 413 K. QCC predicted less than half of the conversion of the other methods at each temperature decreasing from 0.52% at 373 K down to 0.38% at 413 K.

Table 4.6: Equilibrium methanol conversions for each method of calculating ΔG at 373,393 and 413 K. Initial concentrations: 24.72 mol·L^{-1}methanol, 15 mol·L^{-1}CO_2 (0.66 g.mL^{-1}), 0 mol·L^{-1} DMC and water.

	Methanol conversion (%)			
Temperature (K)	Uncorrected	ΔH and ΔS corrected	ΔH, ΔS and C_p corrected	QCC
373	1.21	1.21	1.30	0.52
393	0.97	0.97	1.08	0.44
413	0.79	0.79	0.92	0.38

The differences found between each method was due to the assumptions used in each calculation. The uncorrected method uses only the Gibbs and van't Hoff equations and only rely on calculated values for ΔH and ΔS, which were themselves not without variation. This method did not account for changes in ΔH and ΔS that occur with increasing temperature. However, the method gives a good approximation with the fewest assumptions.

The ΔH and ΔS temperature correction relies on accurate values for C_p for the conditions being investigated. In the work above, gas phase values were used for each component aside from water. This was due to the Shomate equation for water not covering the full temperature range in the gas phase. The value for C_p will vary depending on the phase that the component is in at a given temperature. This meant that whilst the ΔH and ΔS correction method assumed C_p remains constant with temperature, the selection of an appropriate starting C_p is still vital for producing useful results. This ultimately relies on assuming the phase behaviour of the components and their mixtures. Figure 4.6 shows the difference of heat capacity of water between the liquid and vapour phase at 1 bar. The phases have mean C_p of 75.5 and 36.0 J·K^{-1}·mol^{-1} in the liquid and vapour phases respectively. Notably, the phase changes halfway through the range of temperatures investigated in this work, making either value accurate for part of the range. Leino *et al.*, used both values for water: 33.6 J·K^{-1}·mol^{-1} in their DMC[6] paper and 75.30 J·K^{-1}·mol^{-1} in their DEC[53] paper.

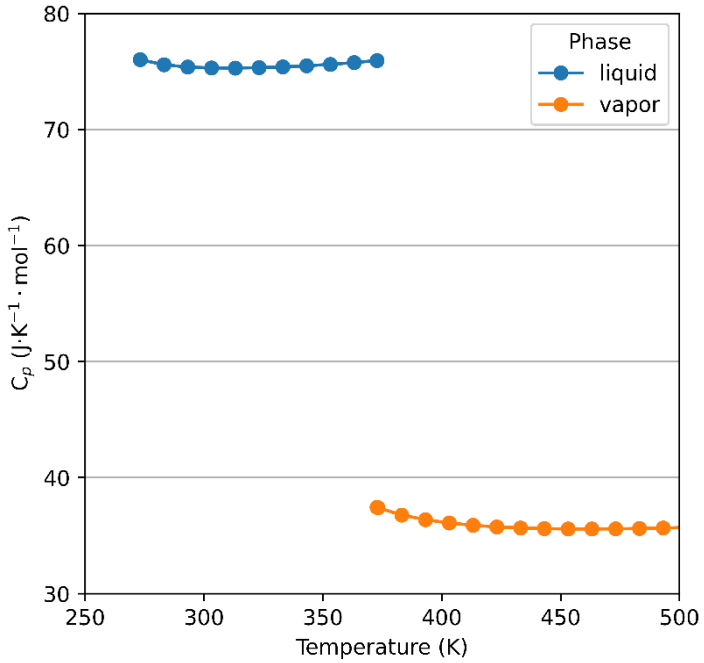

Figure 4.6: Changing isobaric heat capacity (Cp) and phase of water with changing temperature at 1 bar (Data retrieved from NIST isobaric properties[55]).

As shown in Figure 4.2 and Figure 4.3, the high conversions of dialkyl carbonates requires high pressures and temperatures. Figure 4.7 shows the change in C_p of water at 100 bar across the temperature range. At this pressure water remains in the liquid phase, and as temperature increases from 300–500 K C_p also increases, the mean C_p across the temperature range is 77.0 J·K^{-1}·mol^{-1} though this will underestimate the C_p at low temperatures and overestimate it at high temperatures. Therefore, for the ΔH and ΔS correction to be useful, the correct phase should be chosen, and a C_p chosen from within a narrow temperature range.

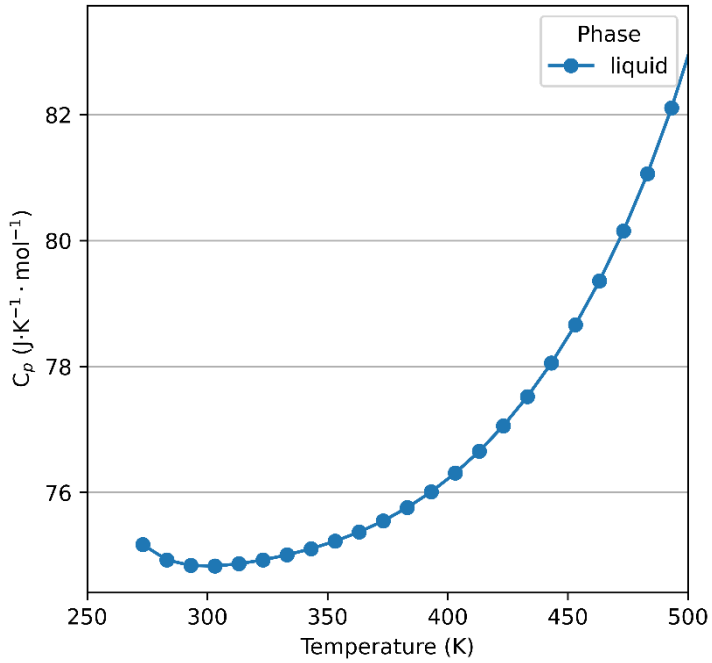

Figure 4.7: Changing isobaric heat capacity (Cp) and phase of water with changing temperature at 100 bar (Data retrieved from NIST isobaric properties[55]).

The temperature correction of ΔH, ΔS and C_p introduce additional equations and variables. For C_p correction, the equations vary based on the polynomial fit chosen for the data, giving different values of C_p for different temperatures (with the pressure not reported[48]). Additional complexity is added when considering the phase behaviour; the polynomial equations are for a single phase and a range of temperatures, therefore when changing phase, a separate equation would be needed. NIST utilises an equation of state[56] in order to calculate C_p across temperature, pressure and phase boundaries which adds additional complexity and assumptions. Another consideration is that the phase behaviour of a pure substance and a mixture are not interchangeable. With CO_2 acting as a solvent, methanol may exist in the vapour phase at a temperature and pressure where one would expect methanol alone to exist in the liquid phase. A model of the phase behaviour of the quaternary mixture of CO_2, methanol, DMC and water has been reported[57] and utilises the SRK equation of state along with a complex series of mixing rules.

The final method, QCC, appears to over-estimate ΔG between 250–500 K, which could be due to the conditions used to calculate it, such as being calculated *in vacuo*. This may be the cause of the increase in ΔH and ΔS for this method. The value of ΔH calculated by QCC was close to the -608.78 kJ·Mol^{-1}

value of ΔH_f reported by NIST TDE. Using the ΔH_r calculated by QCC (-20.76 kJ.mol^{-1}) and the ΔH_f of the other components, the $\Delta H_{f\ (DMC)}$ could be calculated:

$$\Delta H_{DMC} = -20.76 + (2(-239.45) - 393.51) + 285.83 = -607.34 \text{kJ·mol}^{-1}$$

Whilst there is a greater effect on the equilibrium conversions with temperature in the corrected versions, the lack of agreement between sources undermines the confidence in the calculated values. The change in phase behaviour and pressure in actual experiments may also affect the actual values for C_p in the system, meaning that no single method is accurate in all scenarios. Using the uncorrected values relies upon the fewest assumptions and was therefore chosen for further studies.

4.3.3 Wet starting material

With the uncorrected method chosen for further calculations, this was then used to calculate the effect that a non-zero water content in the starting material has on the equilibrium conversion of methanol and ethanol.

The equilibrium conversions calculated in the previous section assume that both the methanol (Figure 4.2) and ethanol (Figure 4.3) are completely water free upon initiation of the reaction. However, both methanol and ethanol are hygroscopic and will have some level of residual water. The alcohols therefore need to be dried to ensure that the concentration of water is as low as possible at the start of the reaction.

The numerical optimisation was applied to a system with concentrations corresponding to the pure alcohols (24.7 mol·L^{-1} for methanol and 17.1 mol·L^{-1} for ethanol) and 15 mol·L^{-1} CO_2 (corresponding to a CO_2 density of 0.66 g·ml^{-1}). A concentration of water corresponding to between 0–500 ppm was given at the beginning of each calculation as shown in Table 4.7. The optimisation of Equation 4.14 (Section 4.2.1) was then performed, allowing us to determine the effect that residual water had on the equilibrium conversion as alcohols purchased without molecular sieves could have several hundred ppm of water present.[58]

The following assumptions were made in these calculations:

1. Ideal solutions with zero excess molar volume, referenced to a constant 1 L volume.
2. Single phase, homogeneous conditions were maintained at all temperatures.

Table 4.7: Starting concentrations used in the wet starting material calculations.

H_2O ppm [mM]	[DMC] (mM)	[MeOH] (M)	[CO_2] (M)
0 [0]	0	24.700	15.000
100 [4.39]	0	24.698	15.000
200 [8.79]	0	24.695	15.000
300 [13.2]	0	24.693	15.000
400 [17.6]	0	24.690	15.000

Calculating the equilibrium concentrations using the iterative approach, with 100 ppm water at 298 K, gave values for $[DMC]_{eq}$ and $[H_2O]_{eq}$ of 0.429 and 0.473 M respectively, a difference of 4.39 mM. This was the expected result based on the stoichiometry of the reaction and the starting concentration of H_2O. Figure 4.8 shows the effect of increasing ppm of water on methanol conversion at each temperature and water concentration.

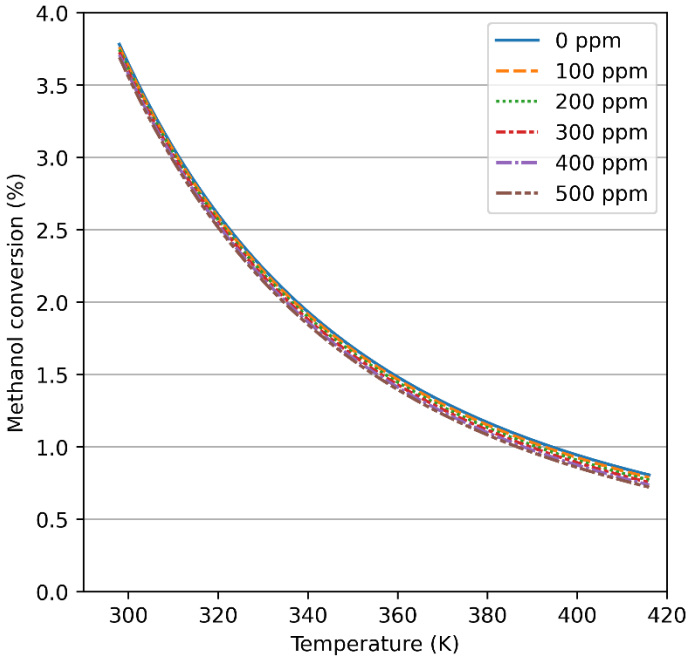

Figure 4.8: Effect of increasing starting concentrations of water, from 0–500 ppm, on the equilibrium conversion of methanol. Initial concentrations: 15 mol.L^{-1} CO_2 (0.66 g.ml^{-1}), 0 mol.L^{-1} DMC.

With increasing concentrations of water, the equilibrium conversion of methanol decreases. However, the effect was rather small for methanol: at 300 K a decrease from 3.65% to 3.56% methanol conversion was expected from a dry 0 ppm to 500 ppm of water, a relative decrease of 2.5%. The effect of wet starting material becomes more pronounced at higher temperatures when the equilibrium conversions are lower due to entropic contributions, decreasing the equilibrium conversion from 0.81% to 0.72% at 416 K, a relative 12% decrease.

Wet starting material had a more pronounced effect on the conversion of ethanol to DEC (Figure 4.9). This is because the ethanol to DEC reaction has a lower K_{eq} at any given temperature than methanol, and any starting concentration of water hinders the reaction more so than for methanol. As described for methanol above, increased temperature increases the predicted discrepancies. At 300 K a 1.53% conversion is predicted at equilibrium with the dry ethanol, compared with 1.41% at 500 ppm of water, decreasing conversion by a relative 8%. At 416 K with 0 ppm of water a 0.50% ethanol conversion is calculated at equilibrium, compared to 0.38% at 500 ppm, a relative 24% decrease.

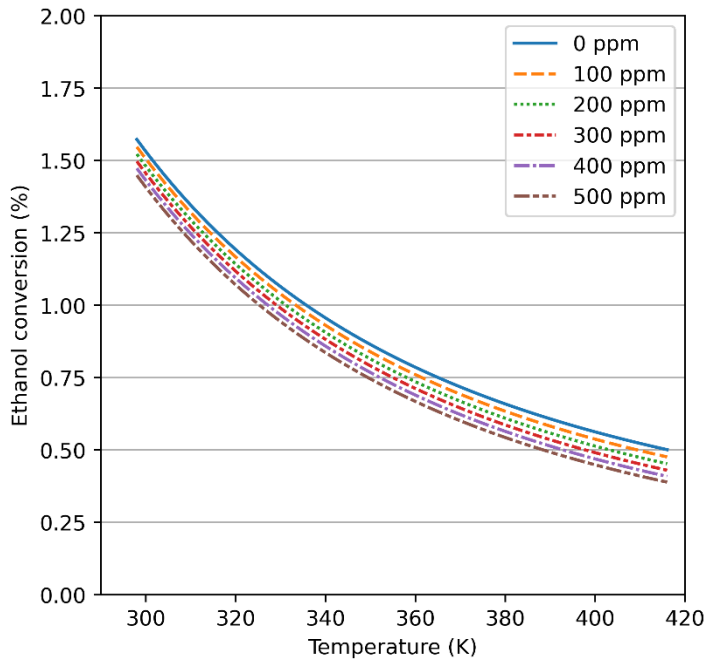

Figure 4.9: Effect of increasing concentrations of water, from 0–500 ppm, on the equilibrium conversion of ethanol. Initial concentrations: 15 mol·L^{-1} CO_2 (0.66 g·ml^{-1}), 0 mol·L^{-1} DEC

The synthesis of dialkyl carbonates from methanol and ethanol obviously benefits from using water free substrates. The effect of initial water concentration on the equilibrium conversion of ethanol is much more pronounced, due to the lower overall conversions. The calculations for methanol suggest that for water concentrations below 500 ppm the decrease in equilibrium conversion is acceptable. For ethanol, concentrations of water below 100 ppm appears to be ideal. The use of a dry substrate is therefore recommended, and appropriate storage conditions are vital to maintaining the quality of the starting material. With the addition of a water removal system, wet starting materials become less of an issue.

4.3.4 Removal of products

The removal of products from the reactor prevents the reaction from being limited by the initially established equilibrium. It is common in the formations of DACs for water to be removed from the reactor, either by dehydrating agents (Chapter 3) or by non-reactive physical water removal strategies.[59–62] Removing water shifts the equilibrium towards products, allowing for higher conversions of the starting material. As discussed in Chapter 3, the dehydrating agents not only remove water, but provide a thermodynamic driving force in the form of a

negative ΔG which, when coupled with the formation of DAC, can make the reaction spontaneous.

For non-reactive dehydrating agents their utility comes from removal of water preventing the backwards reaction, rather than providing thermodynamic driving force, as they are typically used downstream of the reactor. The resulting mixture of DAC, alcohol and CO_2 can then be cycled back into the reactor. In this case the enthalpy of adsorption will not play much of a role in the reaction due to the order of magnitude larger ΔG of reaction. To determine how much of an effect product removal can have on the equilibrium position, the same iterative approach as the wet starting material section, described above, was used. For product removal, upon reaching equilibrium, a percentage of the product is removed. By Le Chatelier's principle the equilibrium would then shift to minimise the change, producing more products.

Most publications focus upon the removal of the unwanted product: water. This is because water in the reactor allows the backwards reaction to methanol and CO_2. However, as Equation 4.2 clearly shows, the concentrations of both products limit the equilibrium conversion. This means that the removal of one product leads to the accumulation of the other and, due to stoichiometry of the reaction, neither product can be made without an equimolar amount of the other. To model the effect of iteratively removing either one or both products the program follows the flow shown in Figure 4.10.

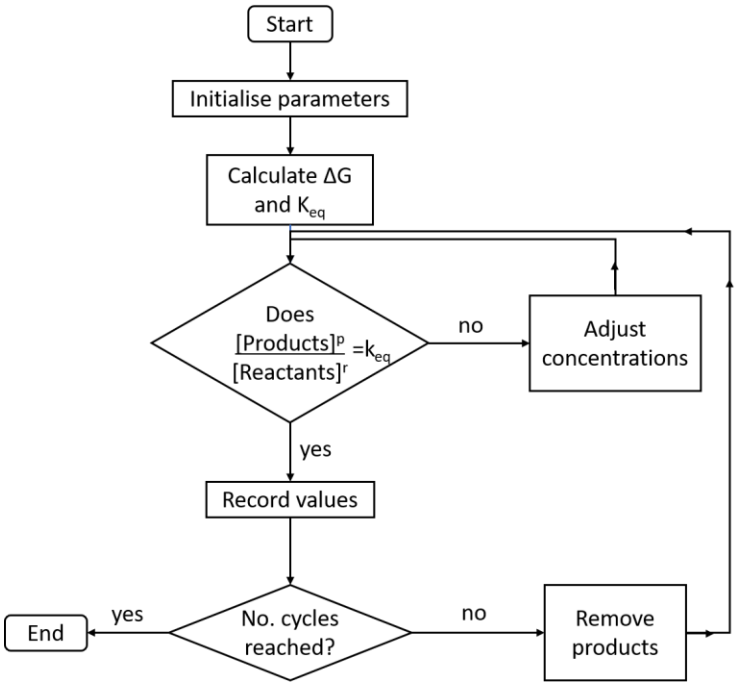

Figure 4.10: Flow chart describing the iteration process used by the software. Implementation can be found in Appendix 4.

This is modelled using the same numeric optimisation as described above, with the following additional assumptions:

The reactor was allowed to achieve equilibrium before any product was removed.

The model assumes that the reaction reaches equilibrium, a certain percentage of each product is removed, and the reaction can proceed to equilibrium again. The kinetics are not taken into account and each cycle is likely to require a different amount of time in practice.

Single phase, homogeneous conditions are maintained at all temperatures in a volume of 1 L.

This assumption allows for ease of calculation, as without this, as products are removed the volume and concentrations would change. A homogeneous 1 L reactor also means that concentrations were equal to the number of moles in the reactor for calculation of the amount of product removed. This assumption may be accurate with a supercritical flow reactor but may be less accurate for batch or low-pressure flow reactions where phase changes are likely to occur.

With 20% water removal, the system was allowed to reach equilibrium, 20% of the water was removed and the system was allowed to reach equilibrium again. This is repeated for a number of cycles, so at 393 K the equilibrium equation with 20% removal is as follows:

Cycle 1 (at equilibrium):

$$1.58982 \cdot 10^{-6} = \frac{0.112 \cdot 0.112}{14.88 \cdot 24.48^2}$$

20% of [H_2O] is removed making the starting concentrations in Cycle 2:

CO_2 = 14.88 (mol·L^{-1})

MeOH = 24.48 (mol·L^{-1})

DMC = 0.112 (mol·L^{-1})

H_2O = 0.090 (mol·L^{-1})

Cycle 2 (at equilibrium):

$$1.58982 \cdot 10^{-06} = \frac{0.131 \cdot 0.108}{14.87 \cdot 24.46^2}$$

Due to the growing numerator and shrinking denominator (as starting materials are consumed), the amount of product made also decreases over time. Each "cycle" in this context refers to an equilibrium-removal cycle; equilibrium calculation followed by removal of products. What each cycle means in terms of real time would depend upon the kinetics, separation method, catalyst stability and other details of the experimental setup.

Table 4.8 shows the first 5 cycles with 20% water removal. Equilibrium concentration of DMC and water are equal initially as they are made in a 1:1 ratio in the reaction. Upon reaching equilibrium, 20% of the water is removed. With each cycle the Δ[DMC] decreases as DMC accumulates in the reactor, this in turn causes the amount of [H_2O] removed to decrease which leads to diminishing returns.

Table 4.8: First 5 cycles of a modelled 20% water removal at 393 K.

Cycle	$[CO_2]$ $(mol \cdot L^{-1})$	[MeOH] $(mol \cdot L^{-1})$	[DMC] $(mol \cdot L^{-1})$	$[H_2O]$ $(mol \cdot L^{-1})$	Cumulative $[H_2O]$ removed	Δ[DMC] $(mol \cdot L^{-1})$
0	15.000	24.720	0.000	0.000	0.000	-
1	14.88	24.472	0.124	0.124	0.000	0.124
2	14.86	24.446	0.137	0.112	0.025	0.013
3	14.85	24.420	0.150	0.102	0.047	0.013
4	14.84	24.396	0.162	0.094	0.068	0.012
5	14.83	24.372	0.174	0.088	0.087	0.012

Some degree of error is allowed in the calculation, the K_{eq} was considered to be reached once it is within 10^{-13} of the value calculated with Equation 4.13, which is due to the computer's internal representation of floating-point numbers.

Figure 4.11 shows diagrammatic representations of the calculations performed. Figure 4.11A depicts the removal of a single product, which in this work was water. This represents a reactor with a closed loop: the reaction progresses to equilibrium; the system then removes water and the system is allowed to proceed to equilibrium again. Figure 4.11B depicts removal of both products. This can be performed asymmetrically and symmetrically. In the asymmetric calculations a constant amount of DAC is removed, along with a variable amount of water. This is intended to mimic a system where removal of one product is more efficient than removal of another. In this case, water removal is more efficient than DAC removal. Figure 4.11C and D depict the removal of both products with constant CO_2 concentration with D also having constant alcohol concentration. C and D could also be simulated with asymmetric product removal, though this has not been done here for the sake of conciseness.

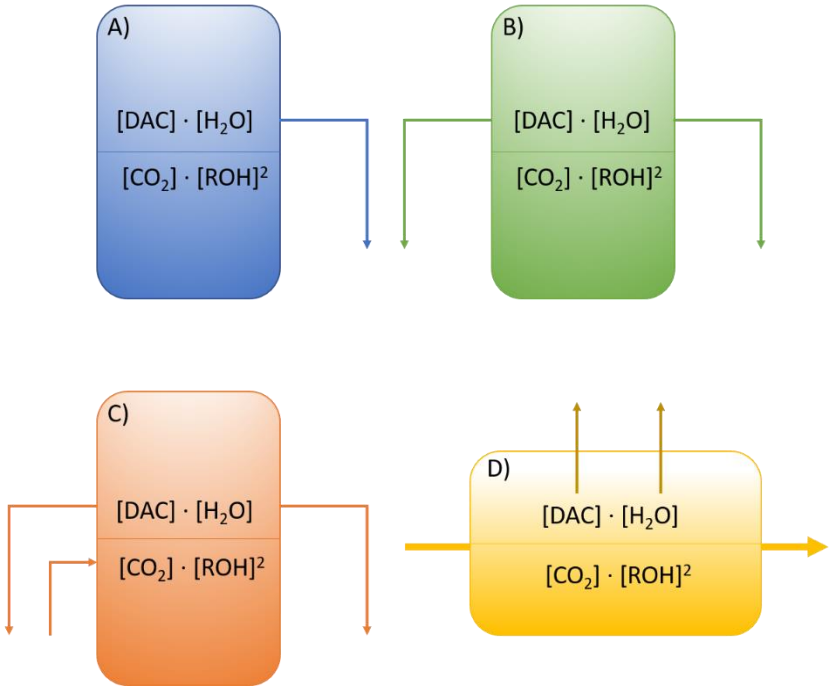

Figure 4.11: Four diagrams used to represent the different product removal models. A) Removal of a single product B) Removal of both products C) Removal of both products with constant CO_2 concentration D) Removal of both products with constant CO_2 and alcohol concentrations.

4.3.5 Single product removal

These calculations were conducted to determine the effect of water removal on equilibrium conversion. 500 equilibrium-water removal cycles were calculated at 6 different water removal efficiencies, from 0–100%. Figure 4.12 shows that a cumulative 25% methanol conversion is possible with a 100% water removal in each cycle. Practically however, we would expect the rate of product formation to decrease with both increasing concentrations of products and decreasing concentrations of starting materials.

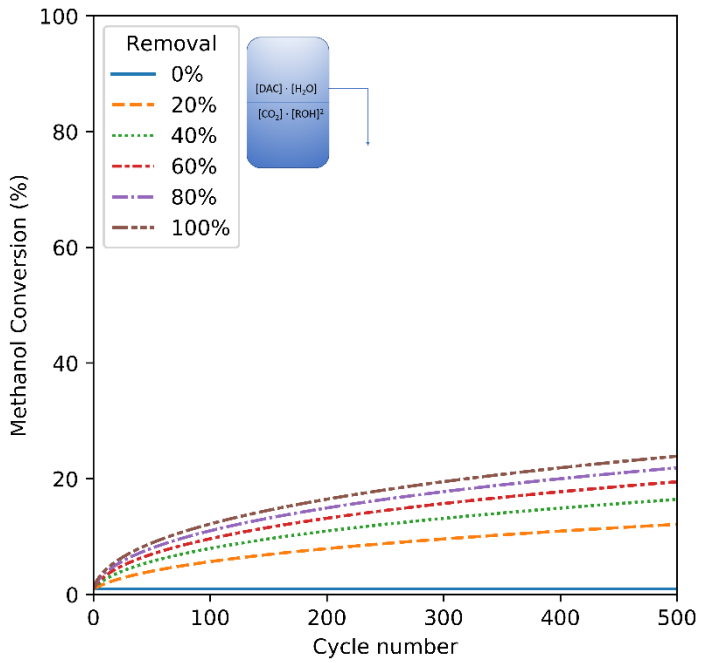

Figure 4.12: Calculated methanol conversion with removal of water, each line represents a water removal percentage from 0–100%..Conditions: 393 K, 15 mol·L^{-1} CO_2 (0.66 g·mL^{-1}), 24.72 mol·L^{-1} methanol, 0 mol·L^{-1} DMC and water.

Figure 4.13 shows how the concentrations of DMC and water diverge once water is removed from the system. As expected, where no water is removed both DMC and water concentration remains at 0.121 M. At 20% water removal, both DMC and water reach 0.121 M at the first cycle, then they diverge. After 50 cycles DMC has accumulated in the reactor achieving a 0.5 M concentration while H_2O is at 0.027M.

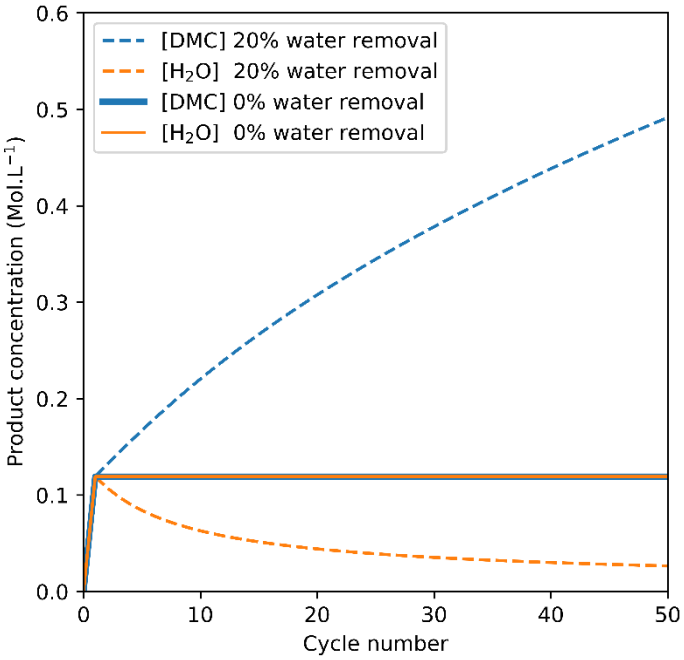

Figure 4.13: Comparison of the influence of 0% (—) and 20% (---) water removal on product concentration for 50 cycles Conditions: 393 K, initial concentrations: 15 mol·L^{-1} CO_2, 24.72 mol·L^{-1} methanol, 0 mol·L^{-1} DMC and water.

Multiplying the concentrations of DMC and water together gives the numerator of the equilibrium equation. Table 4.9 shows that K_{eq} remains constant as product is removed, as expected. The decreasing denominator means that the amount of DMC made with each cycle also decreases as shown in Table 4.8.

Table 4.9: Comparison of component concentrations and K_{eq} after 5 and 50 cycles with 0 and 20% water removal.

Equilibrium equation $k_{eq} = \frac{[DMC][H_2O]}{[CO_2][MeOH]^2}$				
Water removal (%)	[DMC] (M)	[H_2O] (M)	[CO_2][MeOH]^2 (M^3)	K_{eq} (10^{-6})
0	0.1241	0.1241	8908.68	1.729
20 (5 cycles)	0.1740	0.0875	8806.43	1.729
20 (50 cycles)	0.5117	0.0275	8135.69	1.729

Using water removal alone, Choi *et al.*[63] demonstrated that a 40% yield was possible using molecular sieves downstream of the reactor bed. Figure 4.14 shows a comparison of our model compared to data digitised from Choi *et al.* Their reaction was performed at 453 K so the parameters of the model were adjusted.

Choi *et al.* utilised a loop reactor which circulated the contents through a bed of molecular sieves before returning to the reactor, the flow-rate for this step is not reported. Depending on the efficiency of their water removal, our model predicts that it may have taken Choi *et al.* a minimum of 10,000 cycles or circulation of the reactor volume. From their experimental data Figure 4.14 (right) we can see the same benefit to conversion as seen in our model Figure 4.14 (left), when moving from 0% removal to 20% water removal. In our model, water removal was only applied once the system had reached equilibrium, though in their experiment, water removal was applied constantly over the course of the reaction.

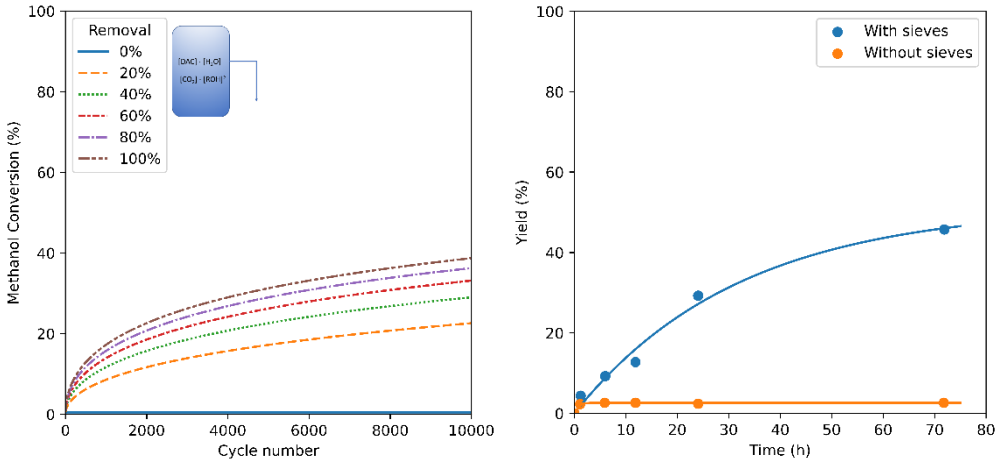

Figure 4.14: Comparison of modelled water removal with reported data. Left: Calculation of conversion for 10,000 cycles with varying removal from 0–100% at 453 K 9.78 mol.L^{-1} CO_2 (0.43 g.mL^{-1}), 24.72 mol.L^{-1} methanol, 0 mol.L^{-1}DMC and water. Right: Yield of DMC with, and without, molecular sieves in a recycling reactor, adapted from Choi et al.[63] *lines added as a guide to the eye. Conditions: 453 K, 300 bar CO_2.*

This same method could be applied with ethanol under the same conditions. With 10,000 cycles modelled (Figure 4.15) just under 30% conversion was predicted with 100% water removal after 10,000 cycles. This was 10% lower than that calculated for methanol conversion in Figure 4.14. However, compared to the equilibrium conversion with no water removal, 0.32%, this represents a 100-fold increase in ethanol conversion. The increase in carbonate concentration of both DMC and DEC, from water removal also allows for easier processing, such as by distillation, that are unfeasible at equilibrium concentrations. Aresta *et al.*[60] determined that separation of DMC by distillation becomes feasible at around 6% alcohol conversion, so a system that allows this conversion to be reached would make further downstream processing more

efficient. Therefore, a compromise between the energy cost of continuing the reaction past 6% and the energy required to separate the DAC by distillation would have to be found.

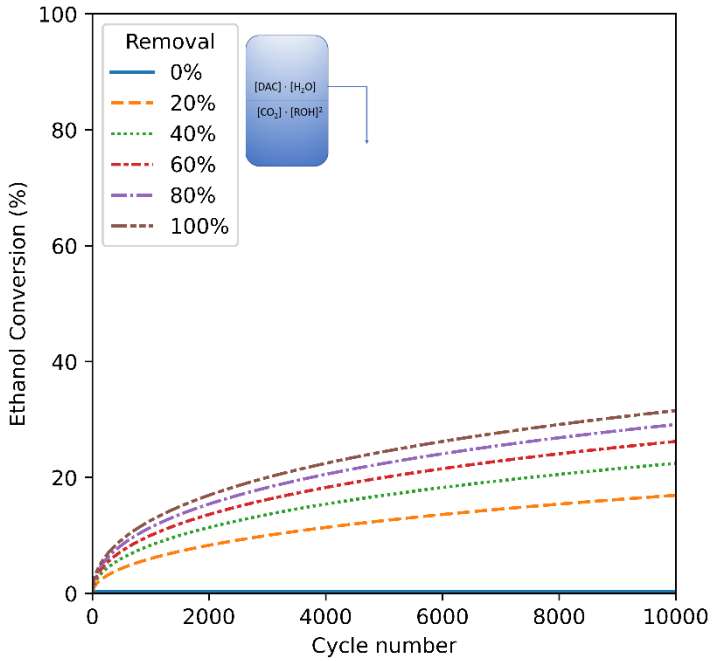

Figure 4.15: Ethanol to DEC conversion over 10,000 removal cycles with varying water removal from 0–100%. Conditions: 453 K, initial concentrations: 15 mol·L^{-1} CO_2, 17.126 mol·L^{-1} ethanol, 0 mol·L^{-1} water and DEC.

Diminishing DAC returns can be observed for both methanol and ethanol, with increasing water removal. The largest improvement in conversion is observed when moving from 0–20% water removal. An increase from 80–100% gives a smaller benefit to conversion.

Keeping the concentration of CO_2 constant is a more likely scenario in a real experiment. With just water removal alone, keeping CO_2 constant does lead to some improvement in methanol conversion, 25.4% conversion after 500 cycles compared to 23.9% (at 100% water removal, 393 K). Keeping the concentration of CO_2 and methanol constant also leads to an improvement in conversion, 30.8% conversion after 500 cycles.

In order to improve the conversion further, the DAC can be removed from the reactor at the same time. The reason for the lack of removal of both DAC and water in the literature may be due to the difficulties in separating it from the

reaction mixture, or the focus on by-product removal. Separation of DMC from methanol has been demonstrated using pervaporation membranes.[64] Therefore a two-step separation may be a solution to this: enrichment of DMC by water removal, followed by pervaporation to remove DMC.

4.3.6 Removal of both products

As demonstrated in the previous section, removal of water enhanced the conversion of methanol and ethanol to their respective DAC. Removal of both products should give a greater cumulative conversion. Initially a 2% DMC removal, with variable water removal from 0–100%, was calculated.

Figure 4.16 (left) shows that, with the removal of 2% of DMC with each cycle, calculated methanol conversion reached 40% in just 500 cycles, compared to 20% with water removal alone (Figure 4.12). This shows that even a low-level removal of DMC, coupled with higher water removal, gives a much greater conversion of alcohol over the same number of equilibrium-product removal cycles.

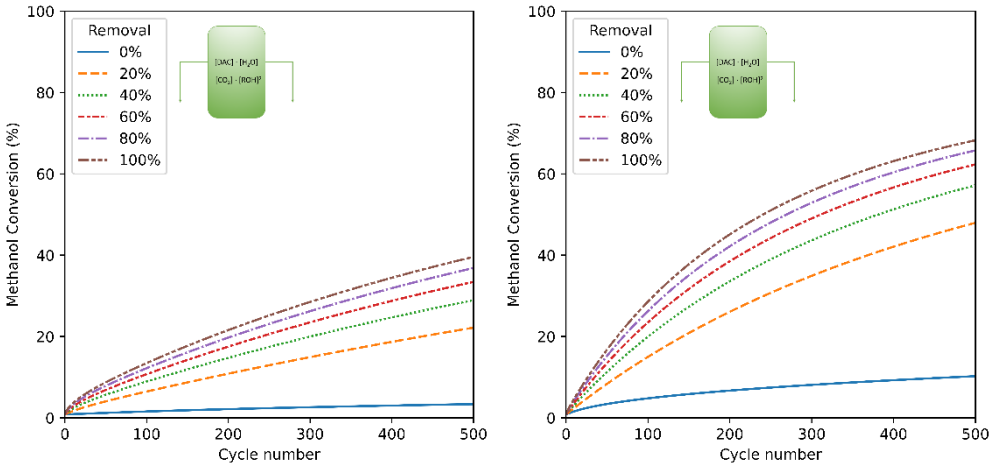

Figure 4.16: Calculated methanol conversions in a reaction system utilising a constant 2% DMC removal (left) and 20% DMC removal (right) for 500 cycles with varying water removal, from 0–100%. Conditions: 393 K, initial concentrations: 9.78 mol·L^{-1} CO_2, 27.72 mol·L^{-1} methanol, 0 mol·L^{-1}DMC and water.

With a fixed 20% DMC removal, along with water removal from 0–100% effective (Figure 4.16 right), over 80% methanol conversion is predicted in the same number of cycles. It is also worth noting that there were still diminishing returns on increasing water removal. This may help to determine where optimisation efforts could be focused: the increase in conversion from of 20%

of a single product to 20% DMC and 20% water was greater than further increasing water removal percentage.

We would expect, in practice, that both DAC and water removal are able to be optimised independantly, Figure 4.17 shows the effect that equal removal of both DAC and water would have on alcohol conversions for methanol and ethanol (left and right respectively). For methanol over 90% conversion is expected with 100% product removal. With a more realistic 40% removal this fell to just under 80% conversion. Similarly with ethanol 90% conversion is predicted with 100% product removal each cycle though ethanol has a noticibly shallower curve due to the lower conversion per cycle. CO_2 concentration was increased for the models shown in Figure 4.17 as at 9.78 M it became the limiting reagent in the conversion.

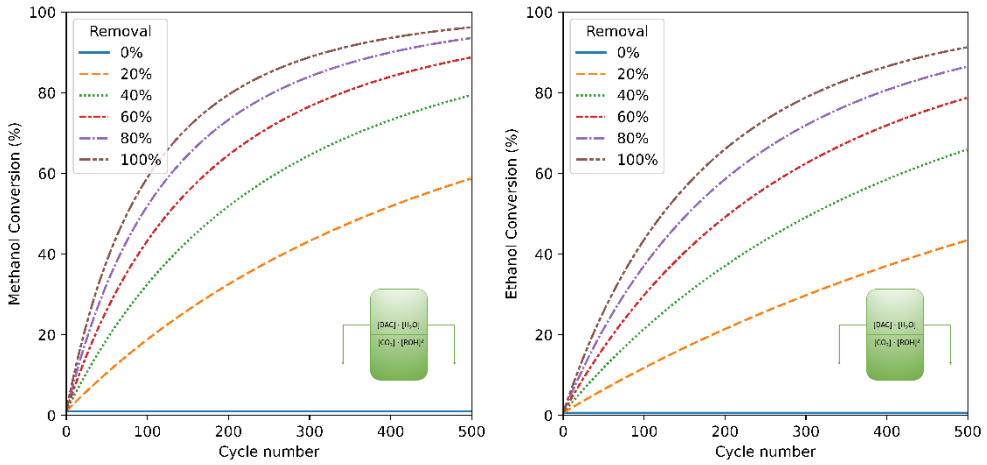

Figure 4.17: Calculated methanol (left) and ethanol (right) conversions with equal DAC and water removal ranging from 0–100%. Conditions: 393 K initial concentrations: 15.78 mol·L^{-1} CO_2, 27.72 mol·L^{-1} methanol (left) 17.126 mol·L^{-1} ethanol (right), 0 mol·L^{-1} water and DAC.

This shows that with removal of both products, the number of cycles it takes to achieve high conversions drops dramatically compared to water removal alone. Whilst water is considered a byproduct of the reaction, and is naturally the target for removal, in reality both products inhibit the forward reaction. Removal of both products, in equal or unequal amounts, is therefore expected to give a more productive system than one that removes water alone.

4.3.7 Constant starting material

The above figures show how removing products from a closed system can impact the conversion and accumulate. Another way to improve conversions is to keep the concentrations of one, or both, starting materials constant. In practice it is likely that CO_2 pressure would be maintained over the course of the reaction. Figure 4.18 shows the effect that maintaining a constant CO_2 concentration has on methanol conversion, with the same equal product removal as in the previous section. Keeping CO_2 constant allows for close to 100% methanol conversion in 500 cycles and even with a 20% removal of both products, a 60% conversion is calculated.

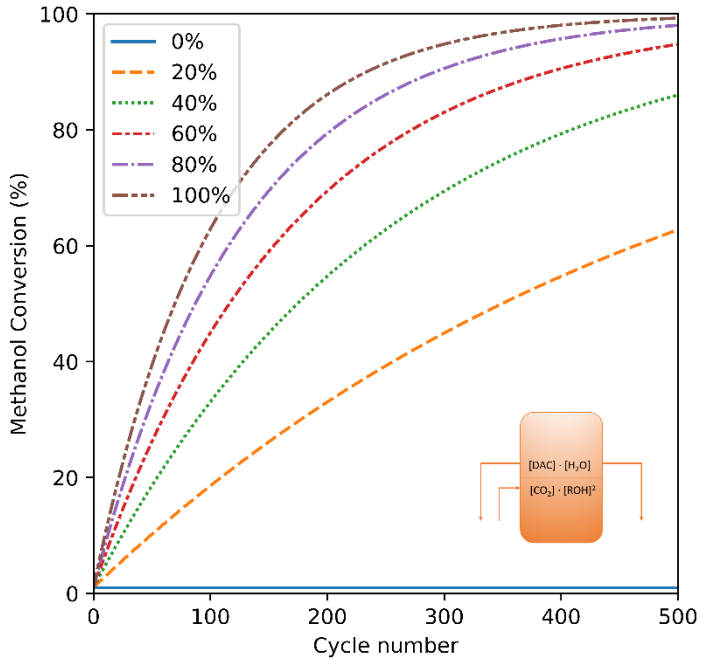

Figure 4.18: Calculated methanol conversion in a reaction system utilising equal product removal for 500 cycles with varying removal percentages, with constant CO_2 concentration. Conditions: 393 K, initial concentrations: 15 mol·L^{-1} CO_2, 27.72 mol·L^{-1} methanol, 0 mol·L^{-1}DMC and water.

Finally, a continuous system can also be modelled in this way, by maintaining a constant concentration of both methanol and CO_2. With an equal separation of both water and DMC, the number of mols of DMC (and by extension water) produced from the system could be modelled. Conversion was not a particularly useful metric for this model as the number of moles of methanol remain constant. Therefore Figure 4.19 shows the number of moles of DMC that would be obtained from a 1 L reactor with constant methanol and CO_2 concentration. With 27 moles of methanol in the reactor, the equivilent of 100% conversion in

a closed system would lead to 13.5 moles of DMC. This was exceeded within 100 cycles. By maintaining reactant concentrations the total amount of product remained constant across each cycle, and the amount of DMC and water produced with each cycle increased linearly.

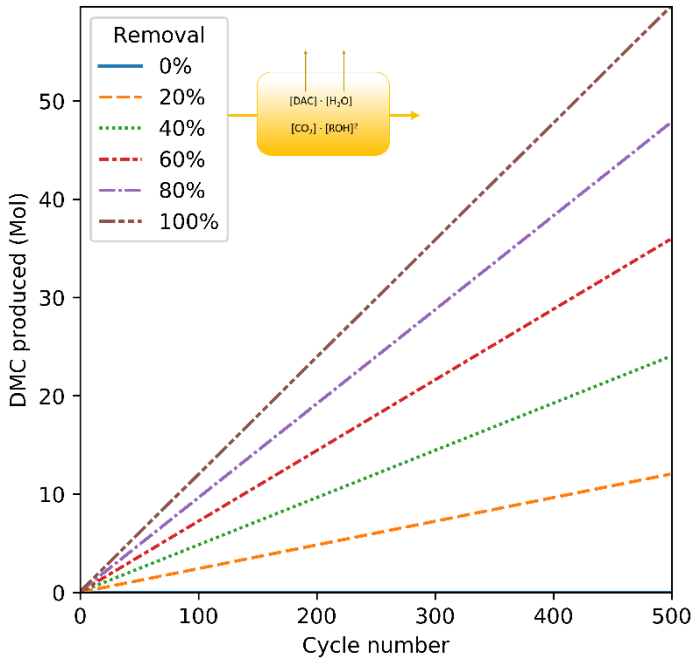

Figure 4.19: Calculated DMC production with a constant CO_2 and methanol feed along with equal removal of DMC and water. Conditions: 393 K, initial concentrations: 15 mol·L^{-1} CO_2, 27.72 mol·L^{-1} methanol, 0 mol·L^{-1}DMC and water.

All product removal models in this section assume ideal product removal techniques. These do not account for factors such as decreasing performance over time caused by effects such as membrane fouling or saturation of molecular sieves.

The thermodynamic modelling presented here allows for the prediction of conversion given a known product removal efficiency and reaction conditions. Poliakoff *et al*. state that while thermodynamics cannot be beaten, avoiding equilibrium situations in order to sidestep thermodynamic barriers may be used.[65] The theoretical computational modelling presented in this chapter shows that by removing products and continually shifting the equilibrium, an improvement in alcohol conversion can be achieved.

Figure 4.20 shows a comparison of the different product removals presented in this section. Removing multiple products from the reactor gives the greatest boost to predicted conversion.

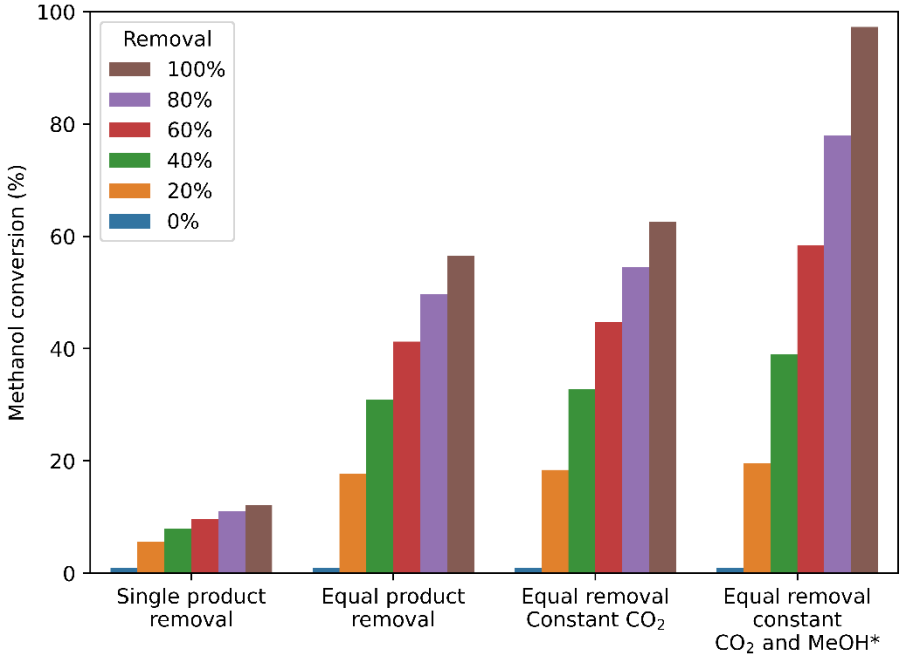

*Figure 4.20: Comparison of conversions at 100 cycles with different product removal strategies. *equivalent conversion is used for constant CO_2 and MeOH. Conditions: 393 K, initial concentrations: 15 mol·L^{-1} CO_2, 27.72 mol·L^{-1} methanol, 0 mol·L^{-1}DMC and water.*

By keeping reactant concentrations constant over the course of a reaction, we have also shown that a much more efficient system could be achieved than a batch system with perfect product removal.

4.4 Conclusions

The work in this chapter uses first principle thermodynamics with a numerical optimisation to calculate equilibrium conversions for methanol and ethanol to their corresponding DACs under a variety of reaction conditions. From the methods of temperature correction that were evaluated, the simplest model based on the van't Hoff approximation was chosen. This method reduced the number of physical constants required, reducing the errors associated with variations in reported values. The other methods show that the decrease in ΔG with increasing temperature was less than would be predicted with the Gibbs equation alone. Though due to the lack of confidence in the values of C_p obtained, the Gibbs equation was used for further calculations.

Using the van't Hoff approximation, a range of reaction conditions was evaluated. This included a temperature range from 298–416 K and CO_2 densities from 0.01–0.95 $g \cdot mL^{-1}$. These calculations showed that the ideal conditions for high alcohol conversion are low temperatures and high CO_2 density. We calculated that an equilibrium methanol conversion of 4.3% and for ethanol a conversion of 1.9% was expected at 298 K and 0.98 $g \cdot mL^{-1}$. Under more relevant conditions, a methanol conversion around 0.4%, and an ethanol conversion of 0.3% are calculated.

Calculations were performed investigating the influence of wet starting materials on alcohol conversion, as well as the effect of product removal. The wet starting material calculations show a relatively small influence that wet starting material has on final methanol conversions. Up to water concentrations of 500 ppm a maximum of a 12% relative decrease was calculated, from 0.81% to 0.72% methanol conversion. The effect on ethanol conversion was more pronounced, with a 24% relative decrease at 500 ppm from 0.50% to 0.38% ethanol conversion.

The product removal calculations, removing a percentage of products upon reaching equilibrium, have demonstrated that an improvement in alcohol conversion can be achieved with a water removal system in place. The benefit of the addition of a water removal system is large but has diminishing returns as K_{eq} remains constant and DAC accumulates in the reactor. To further improve alcohol conversion, we have shown that removal of both water and DAC will give a much more productive system. With just a 2% removal of DMC, we calculated that double the methanol conversion can be achieved in the same number of removal cycles, compared to water removal alone.

4.5 References

(1) Honda, M.; Tamura, M.; Nakagawa, Y.; Nakao, K.; Suzuki, K.; Tomishige, K. Organic Carbonate Synthesis from CO2 and Alcohol over CeO2 with 2-Cyanopyridine: Scope and Mechanistic Studies. *J. Catal.* **2014**, *318*, 95–107. https://doi.org/10.1016/j.jcat.2014.07.022.

(2) Python Software Foundation. Python https://www.python.org/.

(3) O'Neill, M. Thermodynamics_class. *Github*. 2019.

(4) Design Institute for Physical Properties. DIPPR Project 801 - Full

Version. Design Institute for Physical Property Research/AIChE https://app.knovel.com/hotlink/toc/id:kpDIPPRPF7/dippr-project-801-full/dippr-project-801-full.

(5) Knovel; National Institute of Standards and Technology. KDA - dimethyl carbonate https://app.knovel.com/web/poc/ms/profile.html?cid=kcE6MU25U9&prop=prEFO (accessed Jul 2, 2020).

(6) Leino, E.; Mäki-Arvela, P.; Eta, V.; Murzin, D. Y.; Salmi, T.; Mikkola, J. P. Conventional Synthesis Methods of Short-Chain Dialkylcarbonates and Novel Production Technology via Direct Route from Alcohol and Waste CO2. *Appl. Catal. A Gen.* **2010**, *383* (1–2), 1–13. https://doi.org/10.1016/j.apcata.2010.05.046.

(7) Afeefy, H. Y.; Liebman, J. F.; Stein, S. E. Neutral Thermochemical Data. In *NIST Chemistry WebBook, NIST Standard Reference Database Number 69*; Linstrom, P. J., Mallard, W. G., Eds.; National Institute of Standards and Technology: Gaithersburg MD, 20899. https://doi.org/10.18434/T4D303.

(8) Knauth, P.; Sabbah, R. Energetics of Inter. and Intramolecular Bonds in Alkanediols. Iv. the Thermochemical Study of 1,2-Alkanediols at 298.15 K. *Thermochim. Acta* **1990**, *164* (C), 145–152. https://doi.org/10.1016/0040-6031(90)80431-W.

(9) Zhang, S.; Luo, Y. Studies on Kinetics and Technological Conditions of Synthesis of Dimethyl Carbonate. *huaxue fanying gongcheng yu gongyi* **1991**, *7* (1), 10–19.

(10) Vasil'eva, T. F.; Zhil'tosova, E. N.; Vvedenski, A. A. Enthalpies of Combustion of Alkylene Carbonates. *Russ. J. Phys. Chem. (Engl. Transl.)* **1972**, *46*, 316.

(11) Joncich, M. J.; Choi, J. K. Heats of Combustion, Heats of Formation and Vapor Pressures of Some Organic Carbonates Estimation of Carbonate Group Contribution to Heat of Formation. *J. Chem. Eng. Data* **1971**, *16* (1), 87–90. https://doi.org/10.1021/je60048a026.

(12) Wiberg, K. B. *Energies of Organic Compounds*; 1989.

(13) Knovel; National Institute of Standards and Technology. KDA - diethyl carbonate https://app.knovel.com/web/poc/ms/profile.html?cid=kcNK0LV7BQ (accessed Jul 2, 2020).

(14) Månsson, M. Enthalpies of Combustion and Formation of Ethyl Propionate and Diethyl Carbonate. *J. Chem. Thermodyn.* **1972**, *4* (6), 865–871. https://doi.org/10.1016/0021-9614(72)90008-0.

(15) Knovel; National Institute of Standards and Technology. KDA - methanol https://app.knovel.com/web/poc/ms/profile.html?cid=kcY4PHE01W (accessed Jul 2, 2020).

(16) Domalski, E. S.; Hearing, E. D. Condensed Phase Heat Capacity Data. In *NIST Chemistry WebBook, NIST Standard Reference Database Number 69*; Linstrom, P. J., Mallard, W. G., Eds.; National Institute of Standards and Technology: Gaithersburg MD, 20899. https://doi.org/10.18434/T4D303.

(17) Carlson, H. G.; Westrum, E. F. Methanol: Heat Capacity, Enthalpies of Transition and Melting, and Thermodynamic Properties from 5-300°K. *J. Chem. Phys.* **1971**, *54* (4), 1464–1471. https://doi.org/10.1063/1.1675039.

(18) Baroody, E E; Carpenter, G. A. Heat of Formation of Propellant Compounds (U). *Rpt. Nav. Ordanance Syst. Command Task No. 331-003/067-1/UR2402-001* **1972**, 1–9.

(19) Kelley, K. K. The Heat Capacity of Methyl Alcohol from 16K to 298K and the Corresponding Entropy and Free Energy. *J. Am. Chem. Soc.* **1929**, *51* (9), 180–187. https://doi.org/10.1021/ja01384a018.

(20) Chao, J.; Rossini, F. D. Heats of Combustion, Formation, and Isomerization of Nineteen Alkanols. *J. Chem. Eng. Data* **1965**, *10* (4), 374–379. https://doi.org/10.1021/je60027a022.

(21) Green, J. H. S. Revision of the Values of the Heats of Formation of Normal Alcohols. *Chem. Ind.* **1960**, 1215–1216.

(22) Knovel; National Institute of Standards and Technology. KDA - ethanol https://app.knovel.com/web/poc/ms/profile.html?cid=kcQ0NB21PG (accessed Jul 2, 2020).

(23) Haida, O.; Suga, H.; Seki, S. Calorimetric Study of the Glassy State XII. Plural Glass-Transition Phenomena of Ethanol. *J. Chem. Thermodyn.* **1977**, *9* (12), 1133–1148. https://doi.org/10.1016/0021-9614(77)90115-X.

(24) Green, J. H. S. Thermodynamic Properties of Organic Oxygen Compounds. *Q. Rev. Chem. Soc.* **1961**, *15* (2), 125–152. https://doi.org/10.1039/qr9611500125.

(25) Kelley, K. K. The Heat Capacities of Ethyl and Hexyl Alcohols from 16°K to 298°K and the Corresponding Entropies and Free Energies. *J. Am. Chem. Soc.* **1929**, *51* (4), 779–786. https://doi.org/10.1021/ja01379a022.

(26) Knovel; National Institute of Standards and Technology. KDA - carbon dioxide https://app.knovel.com/web/poc/ms/profile.html?cid=kcN22FE3G5 (accessed Jul 2, 2020).

(27) Cox, J. D.; Wagman, D. D.; Medvedev, V. A. CODATA Key Values for Thermodynamics. **1984**, 1.

(28) Chase, M.W., J.; Chase, M. W. . J.; Chase, M.W., J. NIST-JANAF Themochemical Tables, Fourth Edition. *J. Phys. Chem. Ref. Data, Monogr. 9* **1998**, 1–1951.

(29) Knovel; National Institute of Standards and Technology. KDA - water https://app.knovel.com/web/poc/ms/profile.v?cid=kcC4EC6H01&prop=prEFO (accessed Jul 2, 2020).

(30) Cox, J. D.; Wagman, D. D.; Medvedev, V. A. CODATA Key Values for Thermodynamics. *Netsu Sokutei* **1976**, *3* (2), 61–62. https://doi.org/10.11311/jscta1974.3.61.

(31) Chase, M.W., J. NIST-JANAF Themochemical Tables, Fourth Edition. *J. Phys. Chem. Ref. Data, Monogr. 9* **1998**, 1–1951.

(32) Frisch, M. J.; Trucks, G. W.; Schlegel, H. B.; Scuseria, G. E.; Robb, M. A.; Cheeseman, J. R.; Scalmani, G.; Barone, V.; Mennucci, B.; Petersson, G. A.; et al. Gaussian 09, Revision D.01. Gaussian, Inc.: Wallingford CT 2013.

(33) Chai, J. Da; Head-Gordon, M. Long-Range Corrected Hybrid Density Functionals with Damped Atom-Atom Dispersion Corrections. *Phys. Chem. Chem. Phys.* **2008**, *10* (44), 6615–6620. https://doi.org/10.1039/b810189b.

(34) Weigend, F.; Ahlrichs, R. Balanced Basis Sets of Split Valence, Triple Zeta Valence and Quadruple Zeta Valence Quality for H to Rn: Design and Assessment of Accuracy. *Phys. Chem. Chem. Phys.* **2005**, *7* (18), 3297–3305. https://doi.org/10.1039/b508541a.

(35) Goerigk, L.; Hansen, A.; Bauer, C.; Ehrlich, S.; Najibi, A.; Grimme, S. A Look at the Density Functional Theory Zoo with the Advanced GMTKN55 Database for General Main Group Thermochemistry, Kinetics and Noncovalent Interactions. *Phys. Chem. Chem. Phys.* **2017**, *19* (48), 32184–32215. https://doi.org/10.1039/c7cp04913g.

(36) Grimme, S. Supramolecular Binding Thermodynamics by Dispersion-Corrected Density Functional Theory. *Chem. - A Eur. J.* **2012**, *18* (32), 9955–9964. https://doi.org/10.1002/chem.201200497.

(37) Funes-Ardoiz, I.; Paton, R. S. *GoodVibes, Version 2.0.3*; 2018. https://doi.org/10.5281/zenodo.1435820.

(38) Werner, H.-J.; Knowles, P. J.; Knizia, G.; Manby, F. R.; Schütz, M.; Celani, P.; Korona, T.; Lindh, R.; Mitrushenkov, A.; Rauhut, G.; et al. MOLPRO, Version 2012.1, a Package of Ab Initio Programs.

(39) Werner, H.-J.; Knowles, P. J.; Knizia, G.; Manby, F. R.; Schütz, M. Molpro: A General-Purpose Quantum Chemistry Program Package. *Wiley Interdiscip. Rev. Comput. Mol. Sci.* **2012**, *2* (2), 242–253. https://doi.org/10.1002/wcms.82.

(40) Adler, T. B.; Knizia, G.; Werner, H. J. A Simple and Efficient CCSD(T)-F12 Approximation. *J. Chem. Phys.* **2007**, *127* (22). https://doi.org/10.1063/1.2817618.

(41) Werner, H. J.; Knizia, G.; Manby, F. R. Explicitly Correlated Coupled Cluster Methods with Pair-Specific Geminals. *Mol. Phys.* **2011**, *109* (3), 407–417. https://doi.org/10.1080/00268976.2010.526641.

(42) Hill, J. G.; Peterson, K. A.; Knizia, G.; Werner, H. J. Extrapolating MP2 and CCSD Explicitly Correlated Correlation Energies to the Complete Basis Set Limit with First and Second Row Correlation Consistent Basis Sets. *J. Chem. Phys.* **2009**, *131* (19). https://doi.org/10.1063/1.3265857.

(43) Peterson, K. A.; Adler, T. B.; Werner, H. J. Systematically Convergent Basis Sets for Explicitly Correlated Wavefunctions: The Atoms H, He, B-Ne, and Al-Ar. *J. Chem. Phys.* **2008**, *128* (8). https://doi.org/10.1063/1.2831537.

(44) Weigend, F. A Fully Direct RI-HF Algorithm: Implementation, Optimised Auxiliary Basis Sets, Demonstration of Accuracy and Efficiency. *Phys. Chem. Chem. Phys.* **2002**, *4* (18), 4285–4291. https://doi.org/10.1039/b204199p.

(45) Kritikou, S.; Hill, J. G. Auxiliary Basis Sets for Density Fitting in Explicitly Correlated Calculations: The Atoms H–Ar. *J. Chem. Theory Comput.* **2015**, *11* (11), 5269–5276. https://doi.org/10.1021/acs.jctc.5b00816.

(46) Shaw, R. A.; Hill, J. G. Approaching the Hartree–Fock Limit through the Complementary Auxiliary Basis Set Singles Correction and Auxiliary Basis Sets. *J. Chem. Theory Comput.* **2017**, *13* (4), 1691–1698. https://doi.org/10.1021/acs.jctc.7b00140.

(47) Yaws' Critical Property Data for Chemical Engineers and Chemists - Table 40. Heat Capacity of Gas - Organic Compounds, CP = A + BT + CT 2 + DT 3 + ET 4 + FT 5 + GT 6 - Knovel https://app.knovel.com/web/view/itable/show.v/rcid:kpYCPDCECD/cid:kt009ZN3A4/viewerType:eptble//root_slug:table-40-heat-capacity-of-gas---organic-compounds-csubpsub--a--bt--ct-sup2sup--dt-sup3sup--et-sup4sup--ft-sup5sup--gt-sup6sup/url_slug:table-40-heat- (accessed Jun 13, 2020).

(48) Ludwig's Applied Process Design for Chemical and Petrochemical Plants, Volume 2 (4th Edition) - Table C-4. Heat Capacity of Gas, Cp = A + BT + CT2 + DT3 + ET4 - Knovel https://app.knovel.com/web/view/itable/show.v/rcid:kpLAPDCP02/cid:kt00XRAY24/viewerType:eptble//root_slug:table-c-4-heat-capacity-of-gas-csubpsub--a-43-bt-43-ctsup2sup-43-dtsup3sup-43-etsup4sup/url_slug:physical-p-table-c-4-heat?q=methanol cp&b-q=methan (accessed Jun 13, 2020).

(49) NIST Chemistry WebBook Water https://webbook.nist.gov/cgi/cbook.cgi?ID=C7732185&Mask=2#Thermo-Condensed (accessed Jun 13, 2020).

(50) NIST Chemistry WebBook Carbon dioxide https://webbook.nist.gov/cgi/inchi?ID=C124389&Mask=1#Thermo-Gas (accessed Jun 13, 2020).

(51) Chiang, C. L.; Lin, K. S.; Yu, S. H. Improvement of Dimethyl Carbonate Formation via Methanol Carbonation over Vanadium-Doped Cu–Ni/AC Catalyst. *J. Taiwan Inst. Chem. Eng.* **2019**, *98*, 132–149.

https://doi.org/10.1016/j.jtice.2018.08.001.

(52) Santos, B. A. V.; Pereira, C. S. M.; Silva, V. M. T. M.; Loureiro, J. M.; Rodrigues, A. E. Kinetic Study for the Direct Synthesis of Dimethyl Carbonate from Methanol and CO2 over CeO2 at High Pressure Conditions. *Appl. Catal. A Gen.* **2013**, *455*, 219–226. https://doi.org/10.1016/j.apcata.2013.02.003.

(53) Leino, E.; Mäki-Arvela, P.; Eränen, K.; Tenho, M.; Murzin, D. Y.; Salmi, T.; Mikkola, J. P. Enhanced Yields of Diethyl Carbonate via One-Pot Synthesis from Ethanol, Carbon Dioxide and Butylene Oxide over Cerium (IV) Oxide. *Chem. Eng. J.* **2011**, *176–177*, 124–133. https://doi.org/10.1016/j.cej.2011.07.054.

(54) Sadhukhan, T.; Latif, I. A.; Datta, S. N. Solvation of CO2 in Water: Effect of RuBP on CO2 Concentration in Bundle Sheath of C4 Plants. *J. Phys. Chem. B* **2014**, *118* (29), 8782–8791. https://doi.org/10.1021/jp505237s.

(55) Lemmon, E. W.; McLinden, M. O.; Friend, and D. G. *NIST Chemistry WebBook, NIST Standard Reference Database*; 2017. https://doi.org/10.18434/T4D303.

(56) Wagner, W.; Pruss, A. The IAPWS Formulation 1995 for the Thermodynamic Properties of Ordinary Water Substance for General and Scientific Use. *J. Phys. Chem. Ref. Data* **2002**, *31* (2), 387–535.

(57) Camy, S.; Pic, J. S.; Badens, E.; Condoret, J. S. Fluid Phase Equilibria of the Reacting Mixture in the Dimethyl Carbonate Synthesis from Supercritical CO2. *J. Supercrit. Fluids* **2003**, *25* (1), 19–32. https://doi.org/10.1016/S0896-8446(02)00087-6.

(58) Bradley, D.; Williams, G.; Lawton, M. Drying of Organic Solvents: Quantitative Evaluation of the Efficiency of Several Desiccants. *J. Org. Chem* **2010**, *75*, 8351. https://doi.org/10.1021/jo101589h.

(59) Li, C.; Zhong, S. Study on Application of Membrane Reactor in Direct Synthesis DMC from CO 2 and CH 3 OH over Cu – KF / MgSiO Catalyst. **2003**, *82*, 83–90. https://doi.org/10.1016/S0920-5861(03)00205-0.

(60) Aresta, M.; Dibenedetto, A.; Dutta, A. Energy Issues in the Utilization of CO2 in the Synthesis of Chemicals: The Case of the Direct Carboxylation of Alcohols to Dialkyl-Carbonates. *Catal. Today* **2017**, *281*, 345–351. https://doi.org/10.1016/j.cattod.2016.02.046.

(61) Wang, J.; Hao, Z.; Wohlrab, S. Continuous CO2 Esterification to Diethyl Carbonate (DEC) at Atmospheric Pressure: Application of Porous Membranes for in-Situ H2O Removal. *Green Chem.* **2017**. https://doi.org/10.1039/C7GC00916J.

(62) Santos, B. a. V.; Pereira, C. S. M.; Silva, V. M. T. M.; Loureiro, J. M.; Rodrigues, a. E. Design of a True Moving Bed Reactor for the Direct Synthesis of Dimethyl Carbonate. *Chem. Eng. Sci.* **2015**, *123*, 406–419. https://doi.org/10.1016/j.ces.2014.11.017.

(63) Choi, J.-C. C.; He, L.-N. N.; Yasuda, H.; Sakakura, T.; Yasudaa, H.; Sakakura, T. Selective and High Yield Synthesis of Dimethyl Carbonate Directly from Carbon Dioxide and Methanol. *Green Chem.* **2002**, *4* (3), 230–234. https://doi.org/10.1039/b200623p.

(64) Wang, L.; Han, X.; Li, J.; Zhan, X.; Chen, J. Separation of Azeotropic Dimethylcarbonate/Methanol Mixtures by Pervaporation: Sorption and Diffusion Behaviors in the Pure and Nano Silica Filled Pdms Membranes. *Sep. Sci. Technol.* **2011**, *46* (9), 1396–1405. https://doi.org/10.1080/01496395.2011.571227.

(65) Poliakoff, M.; Leitner, W.; Streng, E. S. The Twelve Principles of CO2 CHEMISTRY. *Faraday Discuss.* **2015**, *183*, 9–17. https://doi.org/10.1039/c5fd90078f.

Chapter 5 – Dehydrating agent free synthesis of dialkyl carbonates

5.1 Introduction

As has been discussed in Chapter 4, the direct syntheses of dialkyl carbonates from CO_2 and alcohols are thermodynamically limited reactions. Strategies to overcome the thermodynamic limitations include the physical or chemical removal of products. Chapter 3 demonstrated the use of dehydrating agents to chemically remove water from the reaction system. In this chapter we will focus on the dehydrating agent free synthesis of dialkyl carbonates. Much of the literature in this area focuses on novel catalytic systems, with a small portion also focusing on physical product separation.[1–4]

5.1.1 Dehydrating agent free batch reactions

Dehydrating agent free reactions have been explored in the literature and, while a number of papers mention the thermodynamic limitations of the reaction, only a small number undertake calculations to compare the experimental conversions to a theoretical equilibrium conversion.[5–8] Kabra *et al.*[9] undertake a thermodynamic and experimental study on DMC formation, which led to them calculating a ΔG of +38 kJ.mol^{-1} which is greater than that reported by Leino *et al.*[5] (+26.2 kJ.mol^{-1}) and the two values calculated in Chapter 4 (31.3 and 26.2 kJ.mol^{-1}). It is worth noting that the reported conversions are greater than their calculated conversions, which may be due to their use of an ionic liquid as a promotor, which can sequester water from the reaction.[10,11] Similarly, Jiang *et al.*[12] report that their plateaued methanol conversions of 4% indicate that the equilibrium of the reaction has been reached, but no thermodynamic calculations, nor confirmatory reactions, were conducted.

Table 2.3 shows a comparison of the reported conversions at their reaction plateau alongside the theoretical values calculated in Chapter 4. The calculated equilibrium conversions given are the best-case scenario, with the concentration of pure alcohol being used and zero starting water. The concentrations of CO_2 are calculated based on the density of the CO_2 in the reactor. This leads to

several interesting results. For example, entry 7 has a slightly higher equilibrium conversion than entries 10–13, despite being at a higher temperature, due to the higher CO_2 concentration (5.85 mol·L^{-1} vs 3.00 mol·L^{-1}). Entry 14 has a lower equilibrium conversion than entry 7, because the reactor was pressurised at reaction temperature, leading to a lower CO_2 concentration than entry 7 which was pressurised at RT. In reality, we would also expect that the alcohol concentration is likely to be lower under reaction conditions, as the CO_2 dissolves into the liquid phase. Reasons for the discrepancies between calculated and experimental conversions may be due to the assumptions made in the equilibrium calculation, the effect of pressure on Gibbs free energy, which Lieno *et al.*[5,6] corrected for in their work using Equation 5.1.

Equation 5.1
$$\Delta_r G_p = \Delta_r G^0 - RT ln\left(\frac{P}{P^0}\right)$$

Other corrections that could have been applied, such as the effect of temperature on ΔH, ΔS and C_p may explain the discrepancy at higher temperatures as shown in Chapter 4.

Table 5.1: Comparison of reported plateau conversions with calculated equilibrium conversions, using the method reported in Chapter 4, for literature reported reactions. CO_2 density is calculated at the temperature and pressure at which the reactor was loaded. [a]ref 13 and 16 are specified to have been loaded with 200 mmol CO_2 in a 17 mL reactor, CO_2 concentration was calculated accordingly.

Entry	Catalyst	T (°C)	p (Bar)	Conversion (%)	Calculated equilibrium conversion (%)	Ref
1	ZrO_2	110	60[a]	0.00	0.49	13
2	Fe_2O_3	110	50	0.02	0.50	14
3	CeO_2	110	60	0.05	0.49	13
4	ZrO_2	110	50	0.06	0.50	14
5	$Ce_{0.5}Zr_{0.5}O_2$	110	60	0.13	0.49	13
6	Fe-Zr	110	50	0.23	0.50	14
7	$H_3PW_{12}O_{40}$/ $Ce_{0.6}Zr_{0.4}O_2$	170	60	0.26	0.40	15
8	Nb_2O_5/CeO_2	135	300	0.30 (ethanol)	0.24	4

9	H_3PO_4/ZrO_2	130	50[a]	0.32	0.40	[16]
10	CeO_2	135	50	0.35	0.39	[17]
11	Al-CeO_2 (3%Al)	135	50	0.40	0.39	[17]
12	Al-CeO_2 (10%Al)	135	50	0.42	0.39	[17]
13	Fe-CeO_2 (7% Fe)	135	50	0.45	0.39	[17]
14	$Ga_2O_3/Ce_{0.6}Zr_{0.4}O_2$	170	60	0.45	0.22	[18]
15	$Ce_{0.2}Zr_{0.8}O_2$	110	60	0.74	0.49	[13]
16	$Ce_{0.33}Zr_{0.67}O_2$	110	60	0.76	0.49	[13]
17	H_3PO_4/V_2O_5	140	6	1.80	0.09	[19]
18	$H_3PW_{12}O_{40}/ZrO_2$	100	40	4.04	1.3	[12]

Another factor contributing to the higher conversions may be due to the low rate of cooling following a reaction, as the reactor cools the equilibrium conversion increases. Liu *et al.*[20] achieved a 0.6% methanol conversion at 140 °C at 30 bar (~0.04 $g.mL^{-1}$ CO_2) which has a predicted equilibrium conversion, of 0.25%. Liu *et al.*, however, uses a larger reactor with a greater volume of methanol (35 mL). Due its larger size, a temperature gradient within the reactor may have an impact on the achieved conversion.

Jiang *et al.*[12] report a 4% methanol conversion where a conversion between 0.46–1.3% would be expected for the conditions reported. Assuming their analytical methods were accurate, this result could imply some level of water sequestration, possibly by their catalyst material.

Without the calculated equilibrium values, it is difficult to know how close to equilibrium the reaction has come. With the wide range of conversions reported, along with the variation in reaction conditions, it is clear that thermodynamic calculations are required in order to further develop the understanding of these reactions. The plateaus of reaction profiles may be due to a number of factors: equilibrium, product inhibition, catalyst deactivation and may plateau early due to wet starting material. Comparison of the achieved value with the calculated value, or as we demonstrate below: the reverse reaction, can give further insights into the reaction.

5.1.2 Loop reactors

Choi *et al.*[21] report a loop reactor (Figure 5.1), with sequential reaction and drying units. This system makes use of molecular sieves in a drying bed following on from the catalyst bed, before passing the dehydrated reaction mixture back into reactor to allow the reaction to progress further.

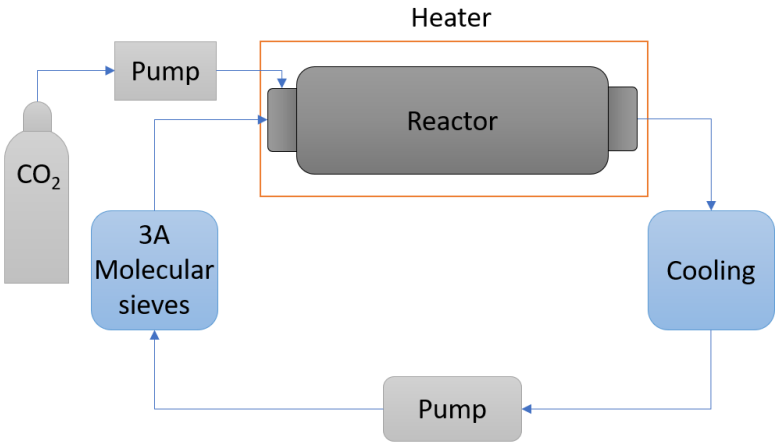

Figure 5.1: Schematic of the batch reactor with Internal recycle (adapted from Choi et al.[21]).

This system leads to a high yield when compared to other easily regenerable dehydrating agents, achieving a 30% yield in 24 h and achieving around 45% after 80 h. The drawback of this system is that it is also energy intensive, as it is necessary to cool the reaction mixture before passing it over the molecular sieves and reheat the mixture upon re-entry to the reactor. Molecular sieves have an advantage over the more reactive dehydrating agents discussed in Chapter 3 as the regeneration by calcination is facile.

5.1.3 Continuous flow synthesis

There are a number of reported uses of continuous flow for the synthesis of dialkyl carbonates. Zhang *et al.*[22] report a 4% methanol conversion in flow using a Cu-Ni@VSiO catalyst with a 2.8% DMC yield without dehydrating agents. Pimprom *et al.*[23] report a 30% methanol conversion using a Cu-Ni/SBA-15 catalyst in flow, however their selectivity towards DMC is lower than Zhang *et al*. resulting in a yield of 3%. It is possible that the SBA-15 support acts as to remove water from the reaction.

Water removal has also been explored in flow systems, as discussed in Chapter 3 and 4, the removal of products from the reactor enables higher conversions. The use of membranes have been reported by Li and Zhong.[2] allowing for an

improved reactor system which allows them to achieve more than 9% conversion of methanol to DMC under relatively mild conditions (130 °C and 4 bar CO_2), more than double that reported by Zhang *et al.* under higher pressure conditions (140 °C, 16 bar).[22] There are also several reports that utilise membranes for water separation for diethyl carbonate synthesis. Aresta *et al.*[4] report the use of pervaporation membranes coupled with a distillation in order to obtain DEC at a >90% purity following distillation. In this reaction the use of a membrane gave an increase in conversion from 0.9% up to 3% at 300 bar. Another example has been reported by Wang *et al.*,[1] which demonstrates that separation of products is possible even under milder conditions, they report that a 25-35% enrichment of products is possible using an MFI-57 membrane. More interestingly the initial pressure of the CO_2 used in this experiment is 1 bar at 100 °C.

Another design for continuous synthesis is the moving bed reactor, the design of which was reported by Santos *et al.*[24] This reactor uses multiple zones, along with molecular sieves for dehydration. This report only includes simulation data with no experimental results to date. The simulations led to an expected methanol conversion of 4%.

Continuous strategies utilising a dehydrating agent have been reported also. Bansode and Urakawa[25,26] reported a continuous reactor system that utilises 2-cyanopyridine as a dehydrating agent. This system enables the authors to reach a methanol conversion >95% with a 99% selectivity to DMC using a cerium oxide catalyst and a fixed bed reactor. They mention that the regeneration of the 2-cyanopyridine is slow, however, and requires optimisation.

The aim of this chapter is to show the benefit of having conducted thermodynamic calculations for comparison with reaction data both in batch and continuous operation. In flow, the effect of different reaction conditions on the rate of reaction, and the rate of catalyst deactivation, can be examined. Finally, the stability of dimethyl carbonate, once removed from a catalyst, is investigated along with preliminary experiments for the separation of products using supercritical CO_2.

5.2 Materials and methods

5.2.1 Analysis

Quantitative analysis of samples from catalytic experiments without dehydrating agents was performed on a Shimadzu GC-2010 Plus equipped with an FID detector at 300 °C with a H_2 flow rate of 40 mL.min^{-1}, air flow rate of 400 mL.min^{-1}, and argon makeup flow rate of 30 mL.min^{-1}. Helium was used as a carrier gas at a constant linear velocity of 39.4 cm.s^{-1} through a BP20 capillary column from SGE analytical science (30 m length, 0.25 mm ID, 0.5 µm film thickness). 1 µL of sample was injected with a split ratio of 50 and an injector temperature of 250 °C. The column was held at 50 °C for 1 min, then the temperature ramped up to 70 °C at 3 °C.min^{-1}, then to 180 °C at 7 °C.min^{-1}, and finally up to 240 °C at 23 °C.min^{-1}.

5.2.2 Direct batch synthesis of DMC and DEC

Batch experiments were conducted in custom made stainless-steel autoclaves with a total volume of 20 mL. 5 mL of dry alcohol was added to 0.3 g of catalyst in a glass liner containing a Teflon-coated magnetic stir bar. The glass liner was inserted into an autoclave preheated to 40 °C, sealed and pressurised with 70 bar of CO_2. The autoclaves were then placed into aluminium heating blocks set to the desired reaction temperature with stirring at 400 rpm. At the end of the reaction the autoclaves were cooled to room temperature before being slowly depressurised. The liquid remaining in the glass liner was filtered with a 0.45 µm syringe filter, a mesitylene internal standard solution was added. The mixtures were then analysed by GC-FID.

5.2.3 Continuous flow synthesis of DMC and DEC

A 10 cm piece of ½ inch stainless steel tubing was packed with 0.3 g of cerium oxide between two beds of glass wool. This was attached to a pre-heated continuous flow rig[27] (Figure 5.2). The reactor was wrapped in resistive heating tape (200 W, 120 cm) and temperature-controlled using a Eurotherm 2216 PID control box. The system was purged with 2 mL.min^{-1} of CO_2 at 200 bar and 40 °C for 10 min. Then the reactor containing the catalyst bed was heated up to the desired reaction temperature, the reaction was started by the addition of alcohol flow from the reservoir under an inert atmosphere of argon, maintained at room temperature and pumped at 0.2 mL.min^{-1}. The back-pressure regulator (JASCO BP-2080 Plus) was connected to an autosampler (GE Frac920) which collected

6 mL samples (at 30-minute intervals for 0.2 mL.min^{-1}). 1 mL aliquots were taken, 0.12 mmol mesitylene was added, and the mixtures were analysed by GC-FID. Productivity was calculated using Equation 5.2 where p is productivity, nDAC is the number of moles of dialkyl carbonate formed, v is volume of catalyst bed and t is time.

Equation 5.2 $$p = \frac{nDAC}{v.t}$$

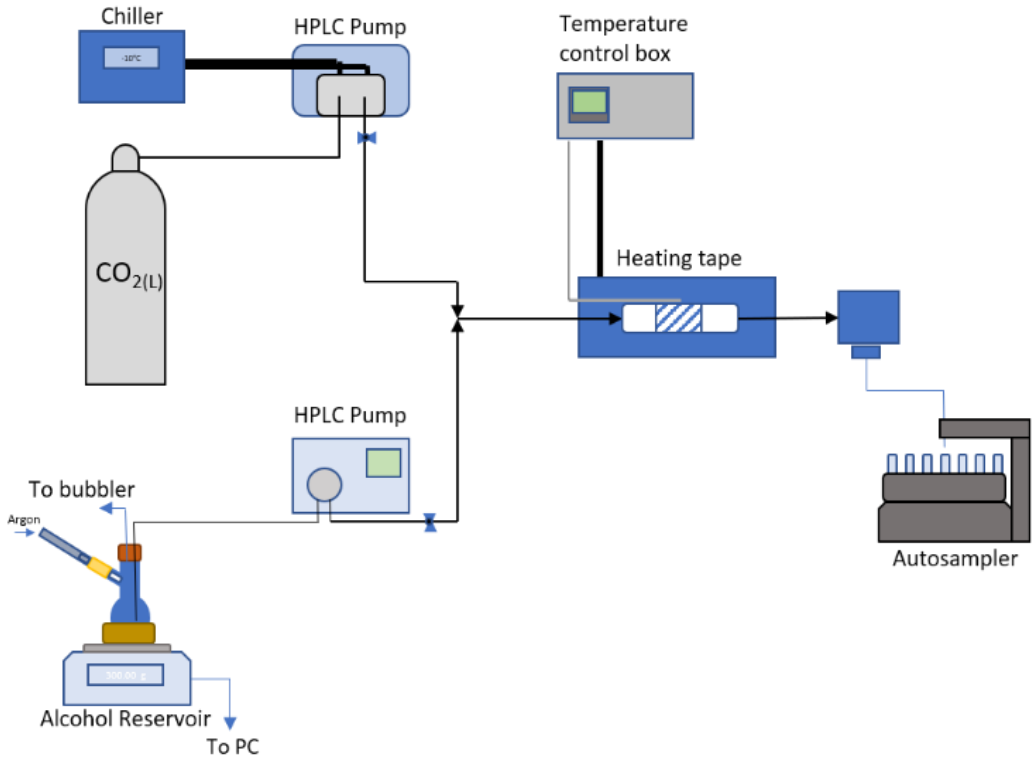

Figure 5.2: Flow experimental setup. Alcohol was pumped from a reservoir held under argon. Change of mass over time was logged using custom software written in python. The alcohol was mixed with CO_2 pumped from a liquid withdrawal cylinder before entering the reactor, which was held at constant temperature with a PID controller. Reactants and products exited the reactor via a back-pressure regulator where the sample was collected by an autosampler.

Flow rate was monitored using an RS-232 connection between the balance and PC. For the data logging, Python[28] and the pyserial module[29] were used, allowing continuous reading of the mass of alcohol in the reservoir which was then converted into flowrate using the density of the alcohol (0.792 g.mL^{-1} for methanol, 0.789 g.mL^{-1} for ethanol). Figure 5.3a shows the mass/volume over a 2 h period which is then converted to flowrate by taking the change in volume over a 3 min interval (Figure 5.3b).

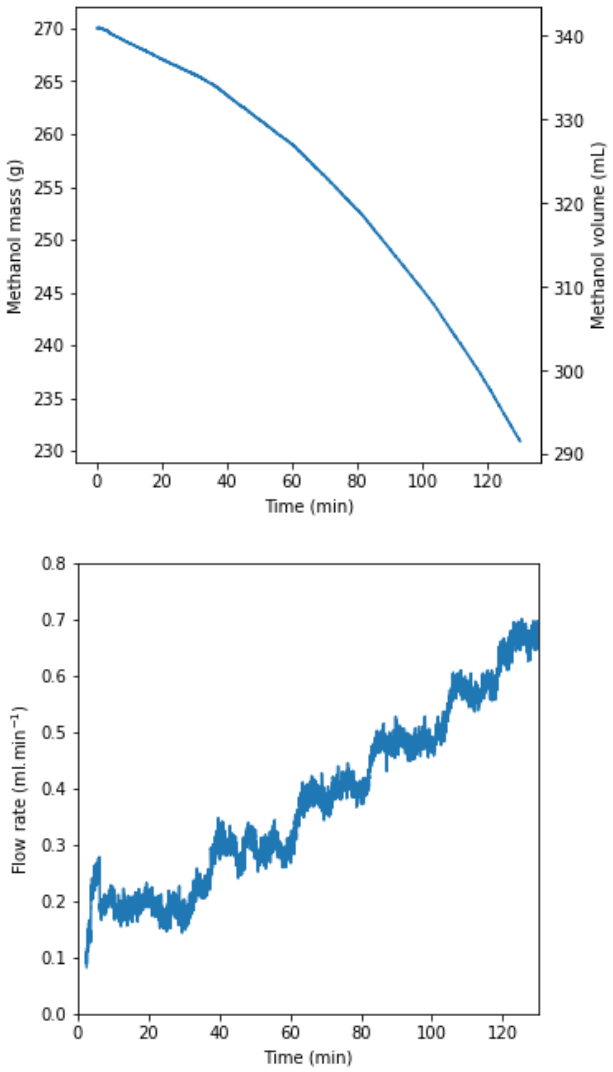

Figure 5.3: Example of the mass/volume data collected(top) and the corresponding flow rates calculated from a 3 min moving average(bottom).

5.2.4 DMC hydrolysis

Hydrolysis experiments of DMC were performed using a stock solution consisting of 1 mL DMC, 0.236 mL H_2O (adjusted to pH 3 with 1 M H_2NO_3), 1 mL DMSO (to homogenise the mixture), and 0.05 mL d_6-DMSO. Sealed J-Young's NMR tubes were then loaded with 1 mL of the homogeneous stock solution and placed into a custom-made aluminium heating block set to the desired hydrolysis temperature. The mixture was periodically analysed by quantitative ^{1}H NMR (zg30, D1 = 1s, NS = 16), and the MeOH peak at 3.18 ppm was monitored to measure DMC hydrolysis.

5.2.5 XPS

XPS analysis was performed by Dr David Morgan, Cardiff University.

X-ray photoelectron spectroscopy (XPS) was performed on a Thermo Fisher Scientific K-α+ spectrometer. Samples were analysed using a micro-focused monochromatic Al x-ray source (72 W) using the 400 µm spot option, which is an ellipse of ca. 400 x 600 µm. Data was recorded at pass energies of 150 eV for survey scans and 40 eV for high resolution scan with 1 eV and 0.1 eV step sizes respectively. Charge neutralisation of the sample was achieved using a combination of both low energy electrons and argon ions.

Data analysis was performed in CasaXPS using a Shirley type background and Scofield cross sections, with an energy dependence of -0.6.

5.2.6 Phase behaviour experiments

For phase behaviour experiments, a 10 mL internal volume view cell autoclave was loaded with 2 mL of a 4% equimolar mixture of DMC, and water in methanol. This was wrapped in resistive heating tape set to 50 °C, based on an internal thermocouple, and pressurised with CO_2. Pressure was adjusted using a HPLC pump and back pressure regulator and images were taken periodically using a Samsung galaxy S7 edge. A calibration of the volume was produced using known volumes, allowing for an approximate volume estimation of each phase under each condition.

High pressure NMR was performed on a 500 MHz instrument at 50 °C using a sapphire NMR tube with titanium fittings. The NMR tube was loaded with approximately 0.2 mL of 0.4 % DMC/water in methanol with sodium trimethylsilylpropanesulfonate (DSS) as an internal standard. The tube was pressurised with CO_2 (as described in Section 5.2.2) at 50 °C inside a polycarbonate sleeve.

5.3 Results and discussion

5.3.1 Batch synthesis

Firstly, a catalyst candidate needed to be identified. Although a similar test was performed in Chapter 3, testing the same catalysts without a dehydrating agent present allowed us to determine if the catalysts perform the same with and without a dehydrating agent present. Table 5.2 shows a comparison of 6 catalysts in a 24 h reaction. The commercial cerium oxide (Entry 1) outperformed the other catalysts showing better performance than the other

catalysts without a dehydrating agent, just as it outperformed other materials tested in experiments with dehydrating agents (Chapter 3).

Table 5.2: Catalysts trialed for batch reactions without a dehydrating agent. Functionalised catalysts were CeO_2 synthesised by precipitation functionalised with perfluorooctyltriethoxysilane (Appendix 5). Conditions: 24 h, 90 bar CO_2, 3 mL methanol, 0.03 g catalyst, 100 °C.

Entry	Catalyst	DMC Concentration (mM)	Conversion (%)
1	Commercial CeO_2	18.7	0.151
2	$Ce_{0.5}Zr_{0.5}O_2$	10.9	0.088
3	Functionalised CeO_2 50%	8.50	0.069
4	$Ce_{0.9}Al_{0.1}Ox$	7.56	0.061
5	CeO_2 (Precipitation)	7.01	0.057
6	Functionalised CeO_2 100%	6.58	0.053

Each of the achieved DMC concentrations fell far below the equilibrium concentration of 130 mM (1.0% methanol conversion) at this temperature and pressure. This suggests that the rate of the reaction at 100 °C is low and while this temperature showed appreciable rates with dehydrating agent present (Chapter 3), without a dehydrating agent there is likely to be a change in the reaction kinetics as well as the reaction thermodynamics. Therefore, more catalyst is required for similar rates. As discussed in Chapter 3, 90 bar at 40 °C is above the critical density of a CO_2-methanol mixture. This may lead to a decrease in methanol concentration in the reactor, and a lower contact with the catalyst.

For these reasons, further experiments lowered the pressure to 70 bar (at 40 °C) and catalyst loading increased to 0.3 g. With these changes reaction profiles at three temperatures were obtained, and the reactions approach the calculated equilibrium conversions in less than 24 h.

Due to the nature of these experiments, there was potential for a larger experimental error. Each datum represents a reactor loaded and pressurised independently to each other. Slight variations in mass of reagents loaded and cooling time as well as other errors such as minor leaks or loss of reaction mixture due to speed of depressurisation can also affect the outcome of an experiment and longer reaction times can compound these errors. Whilst some

errors are also present with the dehydrating agent reactions in Chapter 3, the lower conversions and thus concentrations of products in these equilibrium-limited reactions increased the impact these errors have. As a result, reactions were conducted in triplicate for Figure 5.4 and Figure 5.5. The errors appeared to affect the higher temperature, and longer reactions more, with the 3 and 6 h experiments at 140 °C showing the largest standard deviation. However, the trend of the mean conversions gave an acceptable picture of the reaction profiles.

Figure 5.4 shows the reaction profiles for the conversion of methanol at 140, 120 and 100 °C. At 140 °C the reaction progressed rapidly over the first three hours, and then began to plateau at around 0.4% conversion, a trend that has been previously reported by Tomishige *et al.* and again by Aresta *et al.*[13,17] The reaction at 120 °C progressed more slowly and a 0.32% conversion was reached after 6 h. The reaction at 100 °C was the slowest, achieving around 0.1% conversion after 6 h. A compromise between kinetics and thermodynamics was observed, with higher temperatures equilibrium can be reached over shorter timescales, but the amount of product made is lower.

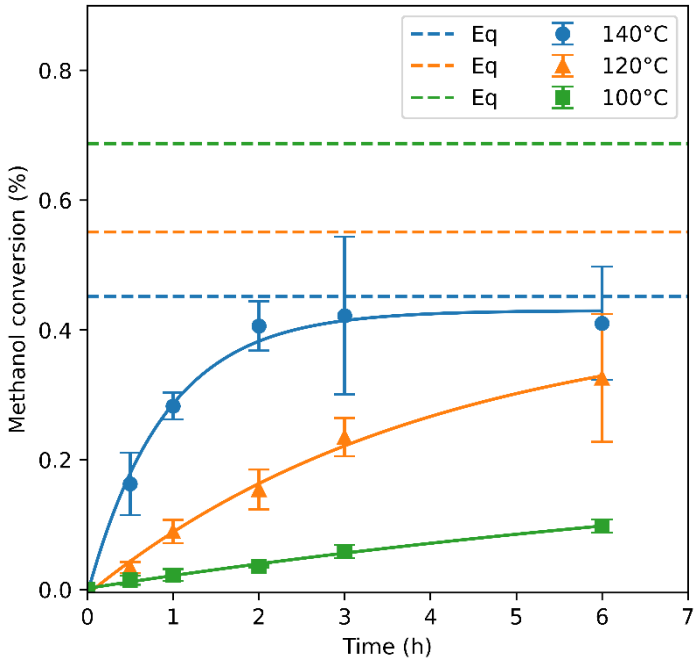

Figure 5.4:. Methanol conversion profiles at different temperatures at 140 (●), 120(▲) and 100 (■) °C plotted with calculated equilibrium conversions (--) with the corresponding colour. Reaction conditions:

0.3 g CeO_2, 70 bar CO_2 at 40 °C, 5 mL dry methanol. Lines added as a guide to the eye. Error bars show standard deviation (n=3).

Table 5.3 shows that after 20 h the reaction at 140 °C had reached the calculated equilibrium and after 30 h the reaction at 120 °C had slightly exceeded the calculated equilibrium. The reaction at 100 °C achieved 55% of the calculated equilibrium after 30 h. Based on the increasing standard deviations with increasing reaction time, it is likely that these results were within experimental error.

Table 5.3: Comparison of methanol conversion at different temperatures and timepoints, along with how close to the calculated equilibrium the reaction reached.

Alcohol	Temperature (°C)	Time (h)	Conversion (%)	% of equilibrium
Methanol	100	0.5	0.0068	1
Methanol	100	30	0.38	56
Methanol	120	0.5	0.0281	5
Methanol	120	30	0.63	115
Methanol	140	0.5	0.0795	18
Methanol	140	20	0.45	101

Figure 5.5 shows the conversion profile of ethanol under the same conditions. The reaction reached its calculated equilibrium after 2 h and then plateaued at around 0.27%, just below the calculated equilibrium for DEC under the reaction conditions of 0.28%. The agreement between the experimental results and the calculated equilibrium helps to give confidence that the reason for the plateau was the reaction equilibrium.

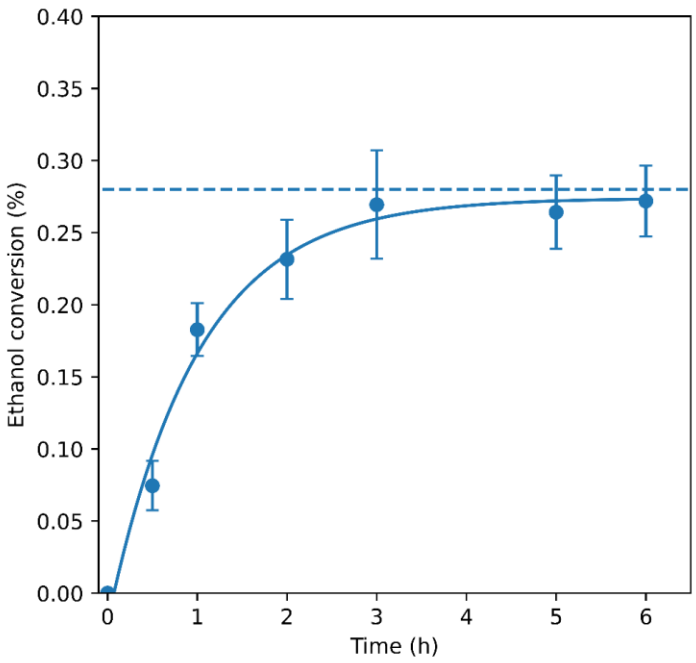

Figure 5.5: Ethanol conversions profile, with experimental points (●) and calculated equilibrium conversion (--). Reaction conditions: 140 °C, 5 mL dry ethanol, 0.3 g cerium oxide, 70 bar CO_2 at 40 °C. lines added as a guide to the eye. Error bars show standard deviation (n=3).

To further confirm that equilibrium was the reason for the plateau in this work, and not as a result of other phenomena such as product inhibition, reverse reactions starting from twice the equilibrium concentration were conducted. A stock solution with an equimolar concentration of water and DMC were added to the reactors with catalyst and pressurised to 70 bar.

Figure 5.6 shows the hydrolysis of DMC at reaction temperatures in the presence of a catalyst. The reverse reactions showed similar profiles to the corresponding forward reaction. It was expected that the forward and reverse reactions would converge upon an equilibrium concentration, however, for 140 °C the reverse reaction plateaued at a concentration slightly above the forward reaction. Even with this minor discrepancy we can have confidence that the equilibrium concentration lies between 58 and 65 mM. Reasons for this discrepancy could be down to a number of factors. A non-zero water concentration can cause an early plateau in the forward reaction, and in the reverse reactions, water concentration below the concentration of DMC will raise the plateau.

Another factor may be CO_2 concentration, in the reverse reaction the same CO_2 density was used as the forward reaction, a more accurate experiment would lower the CO_2 pressure in the reverse reaction to account for the CO_2 released by the hydrolysis of DMC. Variance in experimental values may be another factor, as the standard deviation of the forward reactions approached the reverse values, and the reverse reactions were not conducted in triplicate. The reverse reactions for 120 and 100 °C did not reach equilibrium in 6 h. Based on the forward reactions 30 h or more may be required to achieve this.

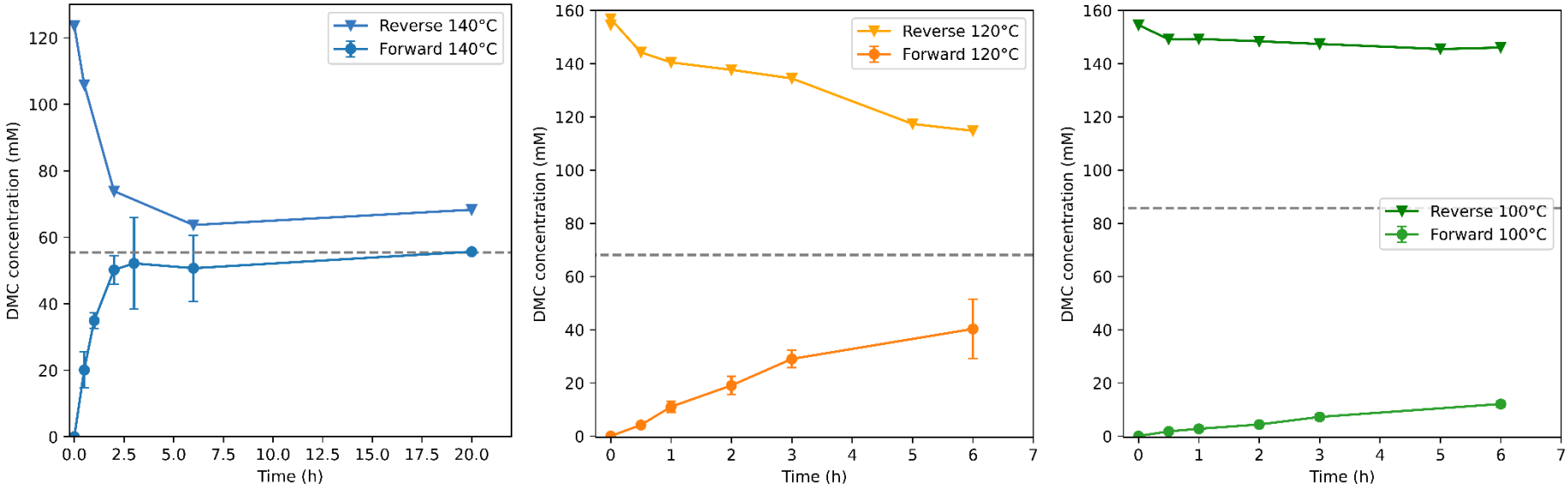

Figure 5.6: Formation and decomposition of dimethyl carbonate at various reaction temperatures. From left to right: 140, 120 and 100 °C, the dashed line indicates the calculated equilibrium conversion at each temperature. Reaction conditions, forward: 0.3 g CeO_2, 70 bar CO_2 at 40 °C, 5 mL dry methanol. Reverse: 0.3 g CeO_2, 5 mL stock solution, 70 bar CO_2 at 40 °C. Lines added as a guide to the eye. Error bars show standard deviation (n=3).

5.3.2 Modelling of batch kinetic parameters

The batch reaction setup made traditional kinetic analysis difficult, due to being unable to sample from the same reaction mixture over time. A more convenient method for gathering concentration data over time would be some form of in-situ analysis, such as headspace GC, in-situ ATR-IR or similar. In the absence of these techniques, an approximation was made to obtain the rate of reaction from a non-linear regression. Due to the shape of the profiles, with rate decreasing with increasing conversion, a first order kinetic model was assumed. An exponential growth equation and SciPy[30] was used to fit the batch data (Equation 5.3). This followed the form of the reversible first order reaction equation (Equation 5.4).[31]

Equation 5.3 $$[DMC] = a \cdot e^{(-b \cdot t)} + c$$

Equation 5.4 $$[DMC] = ([DMC]_0 - [DMC]_{eq}) \cdot e^{-k_{obs} \cdot t} + [DMC]_{eq}$$

Where:

t = time

a,b,c are coefficients of fitting

$[DMC]_0$ = Starting concentration

$[DMC]_{eq}$ = Equilibrium concentration

k_{obs} = observed catalytic rate constant

The equation in this form allowed for fitting both the forward and reverse reactions as, theoretically, the only variable that changes between the reactions is $[DMC]_0$. This also allowed for constraints to be applied during the fitting, in the work presented $[DMC]_0$ was constrained to 0.

Figure 5.7 shows the curves fitted to the experimental data with excellent agreement.

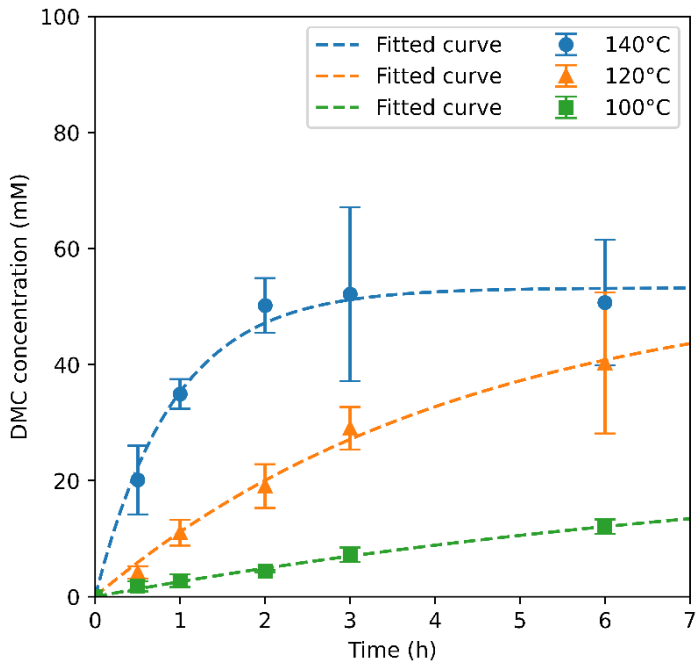

Figure 5.7: Fitted exponential curves (--) to experimental data at 140 (●), 120(▲) and 100 (■) °C. Error bars show standard deviation (n=3).

Taking the derivative of Equation 5.3 gives Equation 5.5:

Equation 5.5

$$\frac{d[DMC]}{dt} = -ab \cdot e^{(-b \cdot t)}$$

Which allows for the calculation of the rate of change in DMC concentration with time.

When this rate is plotted against concentration, a first order reaction will give a straight line with a slope of k_{obs} and an intercept of the initial rate (Equation 5.6).

Equation 5.6

$$\frac{d[DMC]}{dt} = -k_{obs}[DMC]^1 + Rate_0$$

Where $Rate_0$ is the rate when [DMC] = 0

Figure 5.8 shows the plotted rate *versus* concentration for the three fitted reaction profiles. Due to DMC being a product an intercept is observed that gives the rate of reaction where [DMC] = 0, which for the forward reaction is the initial rate. Where the lines intersect also tells us at which concentration it would be advantageous to decrease the reaction temperature; For example, at 0.052 M the 140 and 120 °C lines intersect, so that for concentrations exceeding this, the reactions progress faster at 120 °C than at 140 °C.

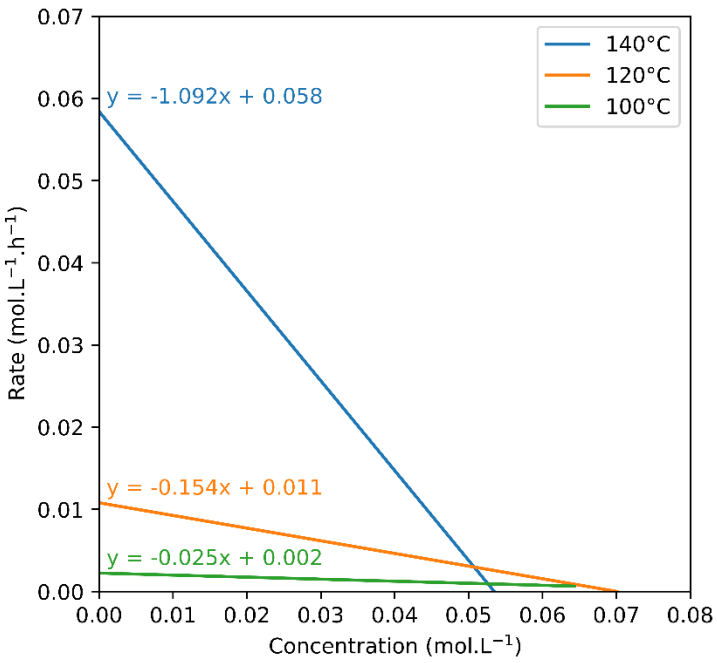

Figure 5.8: Modelled rate versus concentration data for fitted curves giving a gradient of k_{obs}, and an intercept of initial rate.

Table 5.4 shows the kinetic parameters (k_{obs}, $Rate_0$), obtained using this analysis, as well as equilibrium concentration obtained from the x-intercept or the curve fitting parameter *c*. The equilibrium concentrations from this analysis were compared to those calculated using our thermodynamic model and gave good agreement for both DMC and DEC, with the greatest observed error of 6.5% at 100 °C, which was likely due to the lack of experimental data closer to the equilibrium. Overall, the DEC reactions show the smallest error of 1.7%, which may be due to having a greater number of data closer to the equilibrium, which required less extrapolation from the data to the plateau.

Table 5.4: Kinetic parameters approximated by fitted curve with calculated equilibrium concentration of DMC.

Temperature (°C)	k_{obs} (h^{-1})	$Rate_0$ ($Mol.L^{-1}.h^{-1}$)	Kinetic $[DMC]_{eq}$ (mM)	Thermodynamic calculated $[DMC]_{eq}$ (mM) {% error}
140	1.092	5.84×10^{-2}	53.5	55.4 {3.4}
120	0.154	1.08×10^{-2}	70.1	68.1 {2.9}
100	0.025	2.24×10^{-3}	90.5	84.6 {6.5}
140 Ethanol	0.918	2.17×10^{-2}	23.6 (DEC)	24.0 {1.7} (DEC)

This approximation can be used to predict the rate of reaction at a given concentration. Furthermore, using Equation 5.4 an expected reaction profile can be constructed. This can be seen in Figure 5.9 where the approximated k_{obs} have been used. This allowed us to predict that the reactions would plateau after 4, 30 and 160 h at 140, 120 and 100 °C respectively.

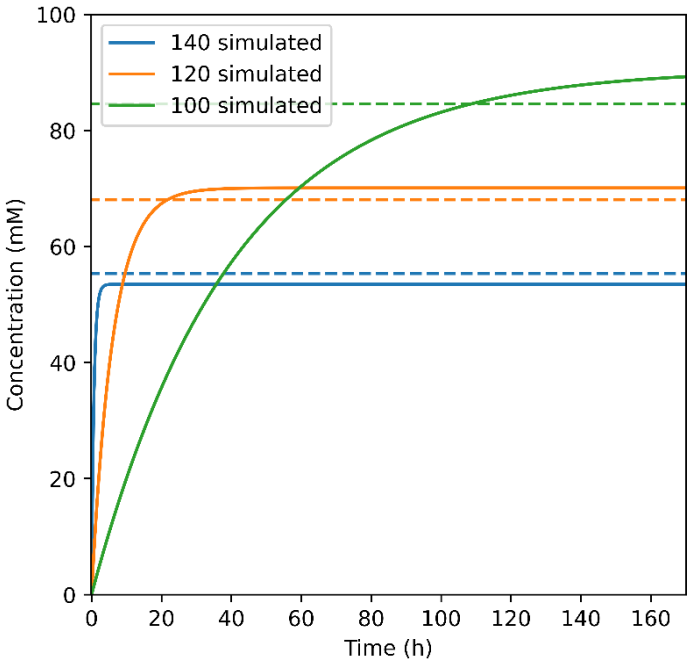

Figure 5.9: Simulated reaction profiles for 140, 120 and 100 °C (—) along with calculated equilibrium concentrations (---).

Constructing an Arrhenius plot (Figure 5.10) from the k_{obs} gave an activation energy of 120 kJ·mol^{-1} which is in agreement with the activation energy of 117 kJ·mol^{-1} reported by Santos *et al.*[8] for a cerium oxide with an Eley-Rideal mechanism. Constructing a similar plot using $Rate_0$ showed that this value was also temperature dependant in an Arrhenius-like fashion giving an activation energy of 104 kJ·mol^{-1} which is again in agreement with Santos *et al.* with a value of 106 kJ·mol^{-1} for a Langmuir-Hinshelwood mechanism. $Rate_0$ has been used in this section for the sake of simplicity, in reality this is likely to be the product of the forward rate constant and starting material concentrations.

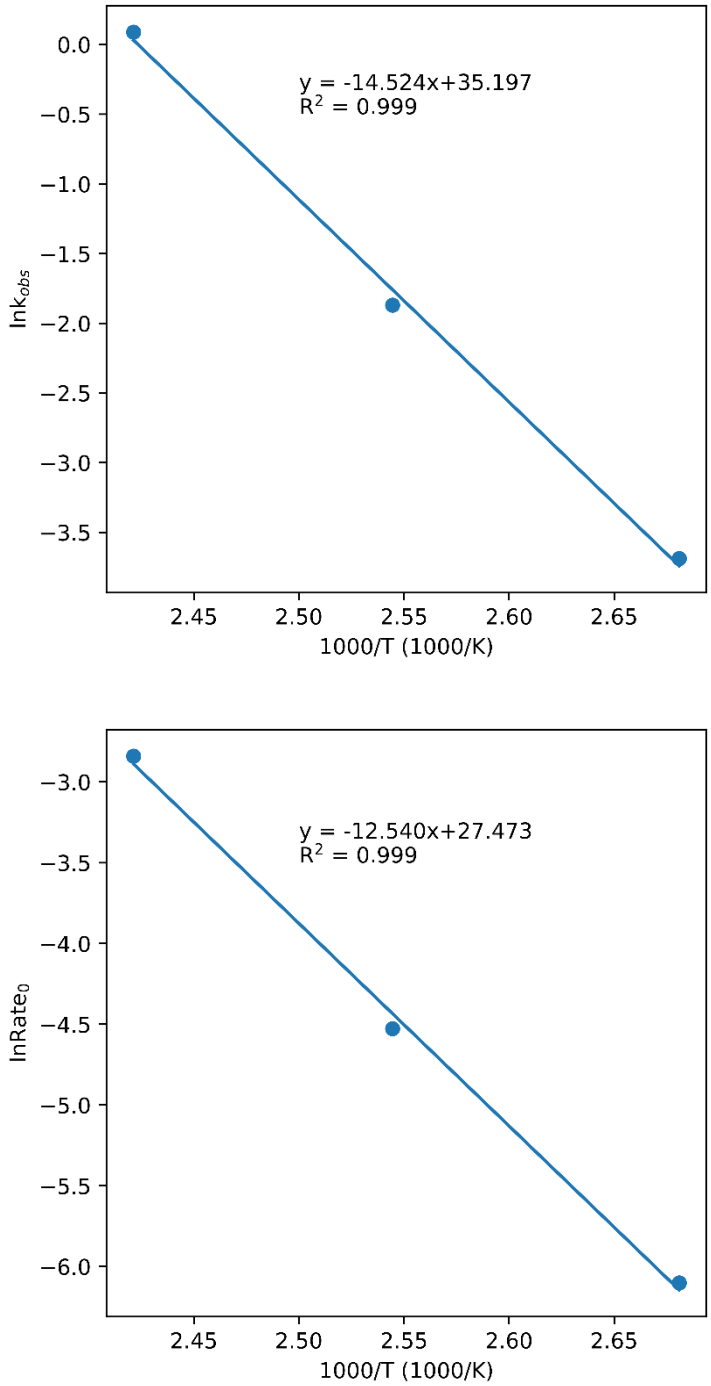

Figure 5.10: Arrhenius plot of approximated k_{obs} (top) and $Rate_0$ (bottom) for the formation of DMC from CO_2 and methanol over a commercial cerium oxide catalyst.

The kinetic analysis presented in this chapter and the thermodynamics presented in Chapter 4 together provide confidence that the plateaus were caused by the equilibrium. The kinetic and thermodynamic values for equilibrium concentrations show good agreement for both DMC and DEC forward reactions.

Further studies focussed on the continuous synthesis of DMC and DEC in order to improve the productivity of a dehydrating agent free system. The majority of experiments were conducted using the commercial CeO_2 due to its superior activity and availability, though some experiments were conducted using $Ce_{0.75}Zr_{0.25}O_2$ described in Chapters 2 and 3, in order to determine if the stability of the catalyst could be improved by doping of a pure oxide in dehydrating agent free flow reactions as well as batch reactions.[17]

5.3.3 Continuous synthesis of DMC and DEC

There are a number of advantages in moving a reaction from batch to flow. These include rapid screening of experimental conditions, continuous monitoring of catalyst stability,[7,23,26,32,33] as well as more consistent results. Whilst batch reactions enable screening of reaction conditions,[12] they typically have a lower productivity,[1] and due to the heat transfer into a large autoclave, heating and cooling times may influence the observed conversion.

5.3.4 Error in sample collection

One of the challenging aspects of a high-pressure flow reaction with compressible media was the sample collection. In the experimental setup used, the sample was collected from the outlet of a pneumatically actuated oscillating needle valve back-pressure regulator. As the sample was a liquid, and the reaction was rapidly depressurised from 200 to 0 bar, a fine mist was created which was difficult to collect. In order to be confident that the concentration of the final sample was equal to the concentration inside the reactor, three known concentrations of DMC were flowed through the reactor without a catalyst and at 40 °C. Figure 5.11 shows the percentage error in the measured concentration versus the expected concentration.

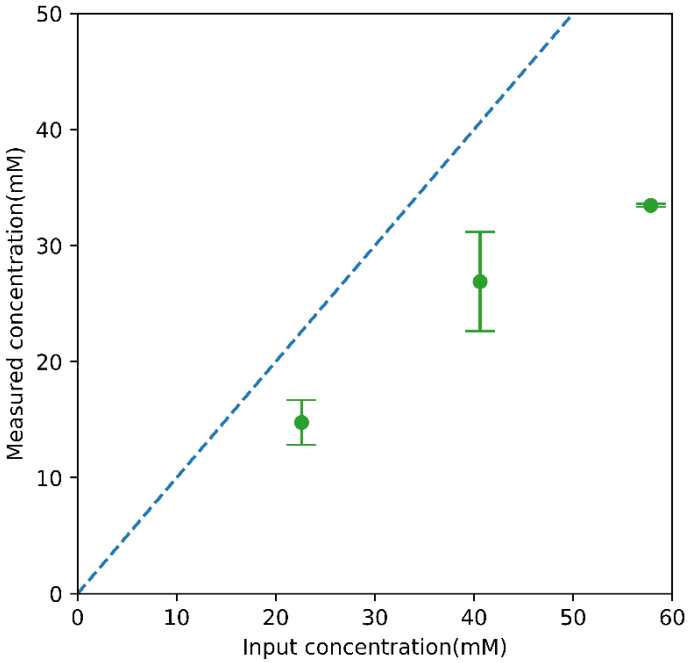

Figure 5.11: Difference in measured versus input concentration, in the measurement of concentration of a known stock solution of variable concentrations of DMC in methanol at 0.2 mL.min^{-1} stock and 1 mL.min^{-1} CO_2, error bars show standard deviation (n=4). Dashed line (--) shows ideal recovery.

At 0.2 mL.min^{-1} the concentration measured at the outlet of the back-pressure regulator was, on average, 41% lower than expected. This decreased linearly with increasing stock solution flow rate (Figure 5.12). The conversions and DMC concentrations presented in the following sections have thus been adjusted using the equation of the line in Figure 5.12 to account for the systemic sampling losses and to give a more accurate picture of the concentration inside the reactor.

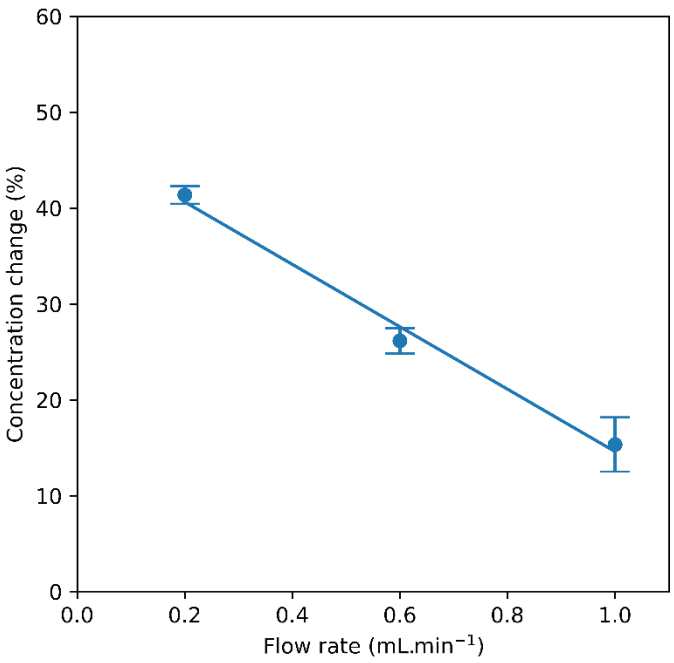

Figure 5.12: error in measurement of DMC concentration with increasing flow rate. point at 0.2 mL.min^{-1} is the mean error across 3 concentrations of DMC (n=12). points at 0.6 and 1 mL.min^{-1} used 58 mM stock solution (n=6). Error bars show standard deviation.

DEC stock solutions showed much lower errors at 0.2 mL.min^{-1}, with a slightly greater error at lower concentrations averaging a difference of 2 mM. The effect of flow rate on this error was not measured for ethanol. Due to the more accurate sample collection shown in Figure 5.13, the DEC values presented in the following sections have not been corrected. As a result, the concentrations within the reactor may be slightly higher than reported.

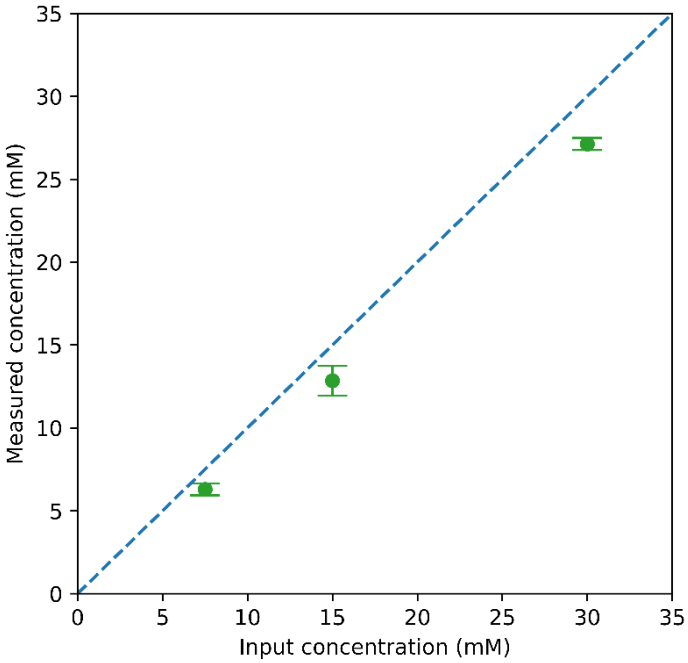

Figure 5.13: Difference in measured versus input concentration, in the measurement of concentration of a known stock solution of variable concentrations of DEC in ethanol at 0.2 mL.min^{-1} stock and 1 mL.min^{-1} CO_2, error bars show standard deviation (n=4). Dashed line (--) shows ideal recovery.

The difference between the DMC and DEC results may be due to a difference in volatilities of methanol, ethanol, DMC, and DEC; less DEC was lost due to aerosolization at the backpressure regulator than DMC.

5.3.5 Effect of pressure in flow

With these errors quantified an initial test reaction was carried out to determine the effect of pressure in flow. A temperature of 100 °C was selected as it gave a wide range of CO_2 densities, from 0.1 g.mL^{-1} (70 bar at 100 °C) to 0.48 g.mL^{-1} (200 bar at 100 °C) and thus a range of phase behaviour from vapour-liquid, near-critical to supercritical. Figure 5.14 shows that pressure had little effect under these conditions. However, increasing catalyst mass (and thus bed volume) increased methanol conversion.

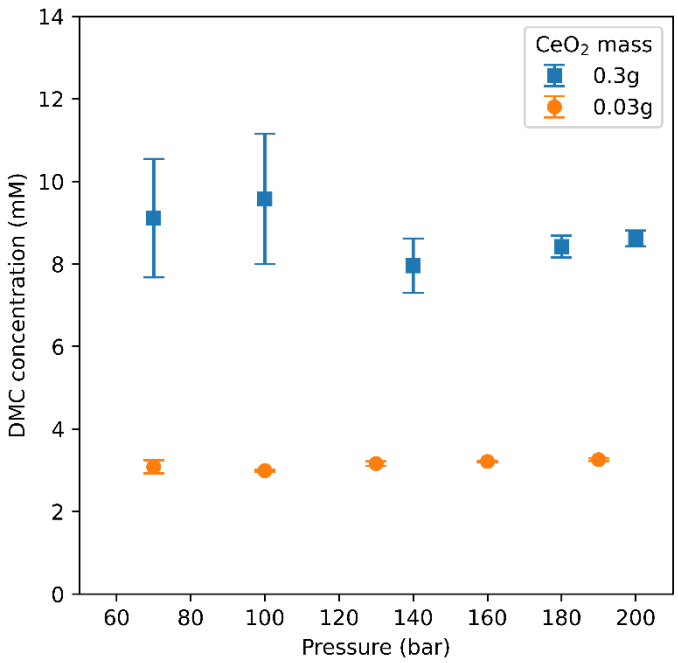

Figure 5.14: Effect of pressure on DMC concentration in flow. Conditions: 100 °C, 0.2 mL.min^{-1} methanol, 1 mL.min^{-1}CO$_2$, commercial CeO$_2$, Error bars show standard deviation (N = 3)

The little variation in DMC concentration with changing pressure may indicate that the mixture was well mixed at each of the densities investigated, as the same CO_2: MeOH ratio (4.6: 1), and as a result the concentration of starting materials, was maintained across each pressure. This indicated that the assumption in the product removal calculations in Chapter 4, that a single homogeneous phase existed may be correct for the range of temperatures and pressures discussed. At lower pressures it has been previously demonstrated that pressure has a greater influence on conversion, Zhang *et al.* report a 4-fold increase in conversion from 4 bar to 12 bar.[22] However at those pressures it was likely that a biphasic system existed within their reactor and thus the increased pressure led to greater dissolution of CO_2 into the liquid phase.

5.3.6 Effect of temperature in flow

Batch reactions showed that the rate of formation of DAC from CO_2 and alcohols increased with increasing temperature. Figure 5.15 shows the effect of temperature on the formation of DMC in flow. Similar to what was observed in batch, as the temperature increased, so too did the rate. However, in flow a greater rate was observed, achieving a 0.33% conversion in 4 minutes compared to 1 hour in batch. The reason for this 15-fold increase could be the improved mixing of the CO_2 and methanol in the supercritical conditions in the flow

reactor along with improved catalyst contact. While this expanded liquid phase and homogeneous mixing showed a decrease in activity in batch reactions (Chapter 3), due to a decrease in catalyst contact and lower methanol concentration, this was not observed in flow. The geometry of the reactor allowed the homogeneous mixture good contact with the catalyst throughout its residence time.

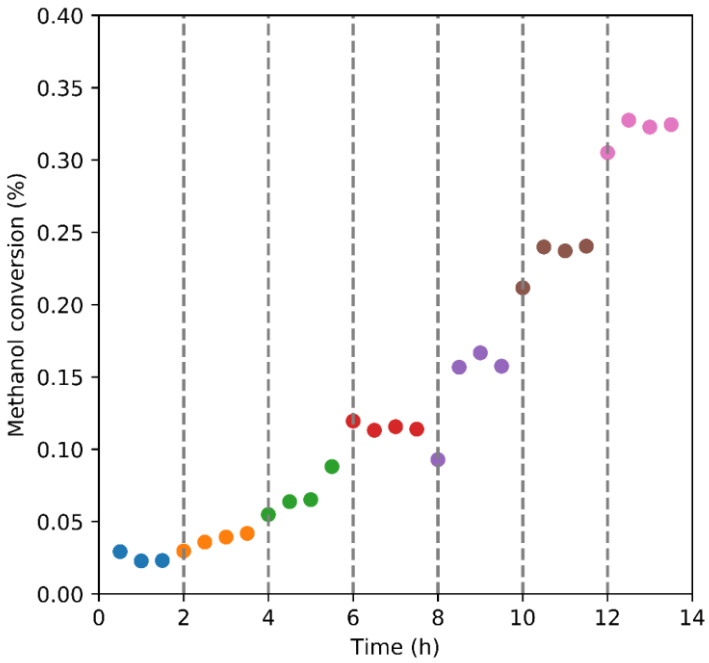

Figure 5.15: Effect of temperature on methanol conversion in continuous flow. Samples were collected at half-hour intervals, temperature was changed following the collection of 3 samples (vertical dashed lines). Conditions: 0.2 mL.min^{-1} methanol, 1 mL.min^{-1} CO_2, 200 bar, 0.3 g commercial CeO_2.

We saw that the samples collected in the 30 minutes where the reactor temperature had been changed vary from those collected for the following 1.5 h. For this reason, these samples were omitted from the mean conversions (Figure 5.16) for each temperature.

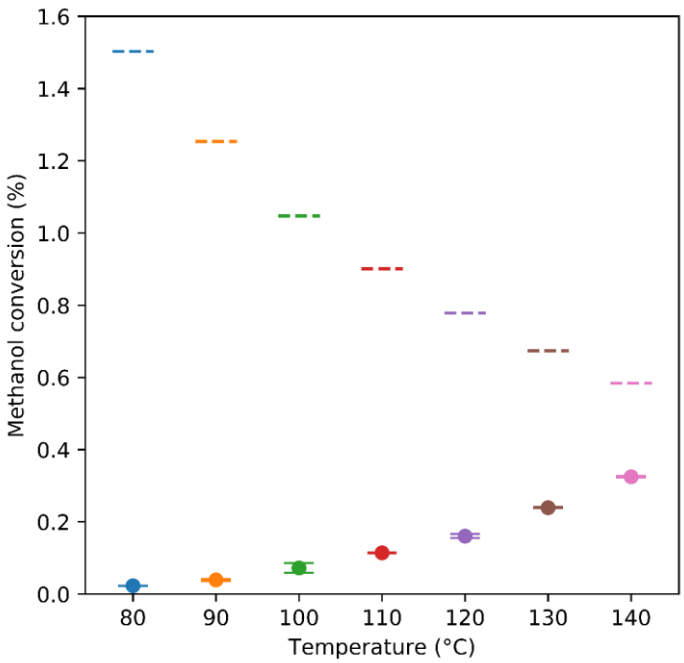

Figure 5.16: Mean conversion compared with equilibrium conversions (--). Conditions: 0.2 mL.min^{-1} methanol, 1 mL.min^{-1} CO_2, 200 bar, 0.3 g commercial CeO_2. Error bars show standard deviation (n=3).

With the residence time used none of the temperatures saw conversions near or above the calculated equilibrium. As temperature increases, the equilibrium decreases and rate increased, such that at 140 °C the reaction was much closer to its calculated equilibrium than the other temperatures investigated. We would expect that further increasing the temperature would eventually lead to a decrease in conversion which has been observed with other catalyst systems using $Ti_{0.1}Ce_{0.9}O_2$,[33] and Cu-Ni@VSiO.[22]

The formation of DEC in flow followed the same trend as DMC, although lower conversions were observed. Figure 5.17 shows the effect of temperature on ethanol conversion in flow. For DEC four temperatures were tested and, as with DMC, 30 minutes appeared to be sufficient time to allow for the system to reach steady state upon changing temperature.

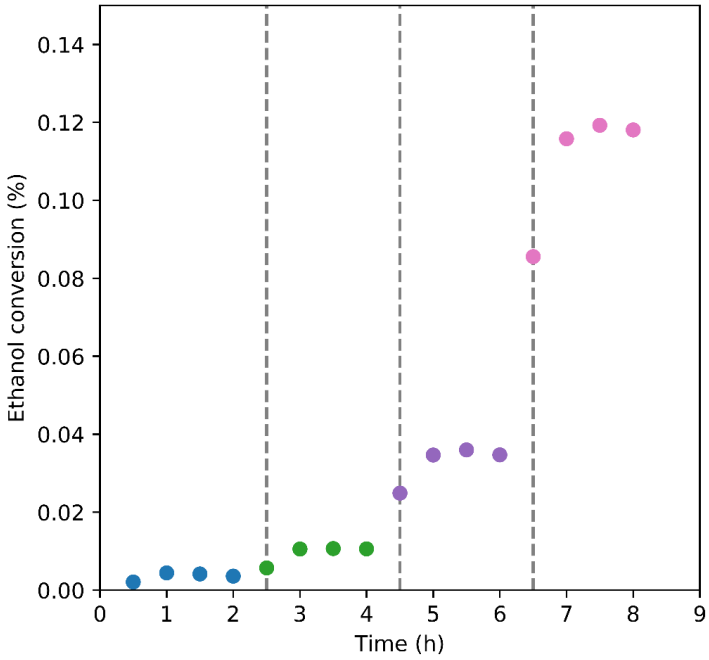

Figure 5.17: Effect of increasing temperature on conversion of ethanol. Temperature changes are marked with a vertical dashed line. Reaction conditions: 0.2 mL.min^{-1} ethanol, 1 mL.min^{-1} CO_2, 200 bar, 0.3 g catalyst, catalyst contact time 4.2 min.

Figure 5.18 shows the mean conversions at each temperature. Unlike the DMC reactions, DEC concentration remained further from equilibrium, achieving around 25% of the expected DEC concentration at 140 °C.

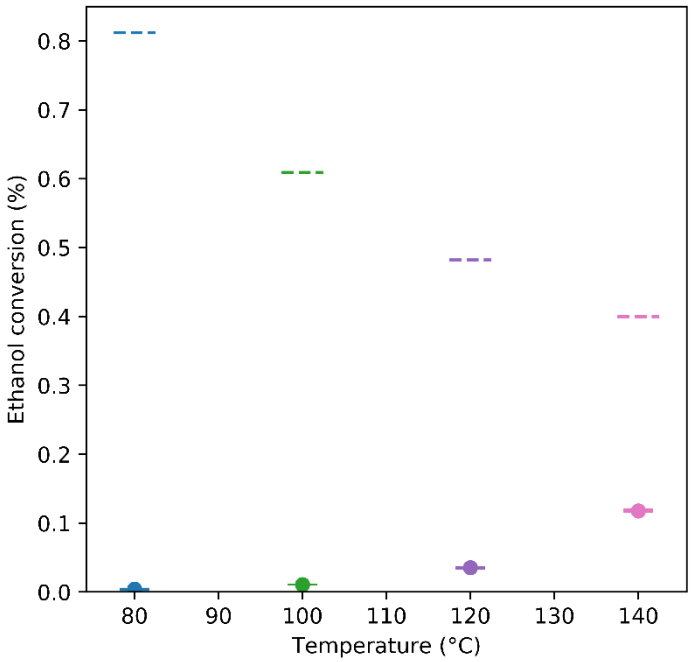

Figure 5.18: The effect of increasing temperature on conversion of ethanol, and calculated equilibrium (- -), Reaction conditions: 0.2 mL.min^{-1} ethanol, 1 mL.min^{-1} CO_2, 200 bar, 0.3 g catalyst, catalyst contact time 4.2 min. Error bars show standard deviation (n=3).

This section shows that in the transition from batch to flow, a much more productive system can be observed for both DEC and DMC. In both cases, increasing temperature led to an increase in conversion, with 140 °C approaching the calculated equilibrium more so than at lower temperatures, at the same feed rates. We saw the same compromise between kinetics and thermodynamics in flow as those in batch above (Section 5.3.1). A higher conversion is theoretically possible, but the timescales to achieve this are unlikely to be economical.

The flow set up also allowed for easier control of reaction conditions. The improved mixing and catalyst contact allowed for a 0.33% methanol conversion 15 times faster than observed in batch.

5.3.7 Effect of varying flow rates

Changing the alcohol flow rate has two effects, firstly the residence time and contact time with the catalyst decreases. Secondly, the methanol: CO_2 ratio changes. At 0.2 mL.min^{-1} methanol and 1 mL.min^{-1} CO_2 there was a 4.6:1 molar excess of CO_2 in the reactor. Increasing the methanol flow rate to 0.5 mL.min^{-1} decreased the molar excess of CO_2 to 2:1. For these experiments, the catalyst bed was scaled 10-fold up to 3 g to minimise the effect of any catalyst deactivation and ensure that any decrease in conversion observed was due to the change in flow rate, and not catalyst activity.

The effect of changing residence time and methanol ratio is shown in Figure 5.19. As the flowrate was increased from 0.2 to 0.4 mL.min^{-1}, methanol conversion remained between 0.33 and 0.35%. Further increasing the methanol flow rate decreased conversion down to a minimum of 0.13% at 1 mL.min^{-1}.

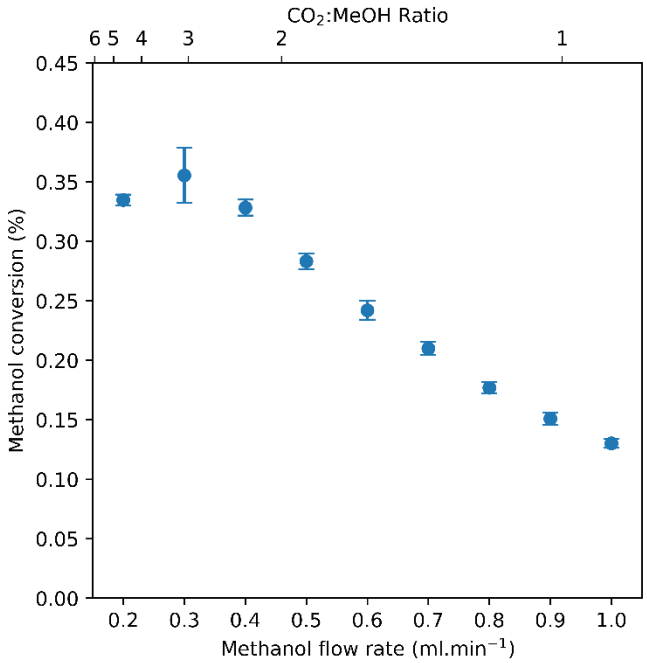

Figure 5.19: Change in methanol conversion with increasing methanol flowrate. Reaction conditions: 3 g CeO_2, 5 mL bed volume, 140 °C, 200 bar CO_2, at 1 mL.min^{-1}. Error bars show standard deviation (n=3).

Whilst the percentage of methanol converted decreased, consistent with a similar system reported Dibenedetto *et al.*[4] the overall number of moles converted increased due to the increased throughput. This led to a higher productivity in the system. Figure 5.20 shows how the productivity of the system changed with increasing methanol flow. A maximum productivity of 215 mmol.L_{cat}^{-1}.h^{-1} was observed at a flow rate of 0.6 mL.min^{-1}.

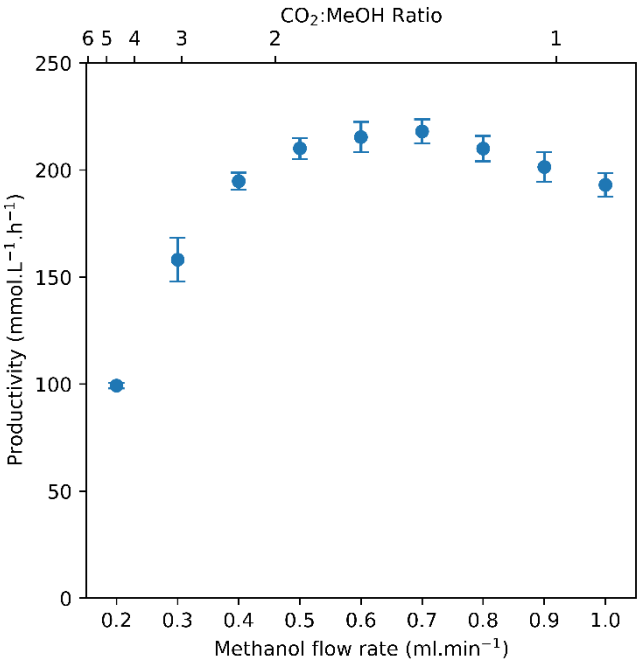

Figure 5.20: Effect of methanol flow rate on productivity. Reaction conditions: 3 g CeO_2, 5 mL bed volume, 140 °C, 200 bar CO_2, at 1 mL.min^{-1}. Error bars show standard deviation (n=3).

Increasing the CO_2 flow rate increased the CO_2: methanol ratio whilst also decreasing the catalyst contact time (Figure 5.21). This decreased catalyst contact seems to be more impactful on the productivity, as at 4 mL.min^{-1} of CO_2 the methanol was in contact with the catalyst for 1 minute, leading to lower methanol conversion and therefore lower productivity.

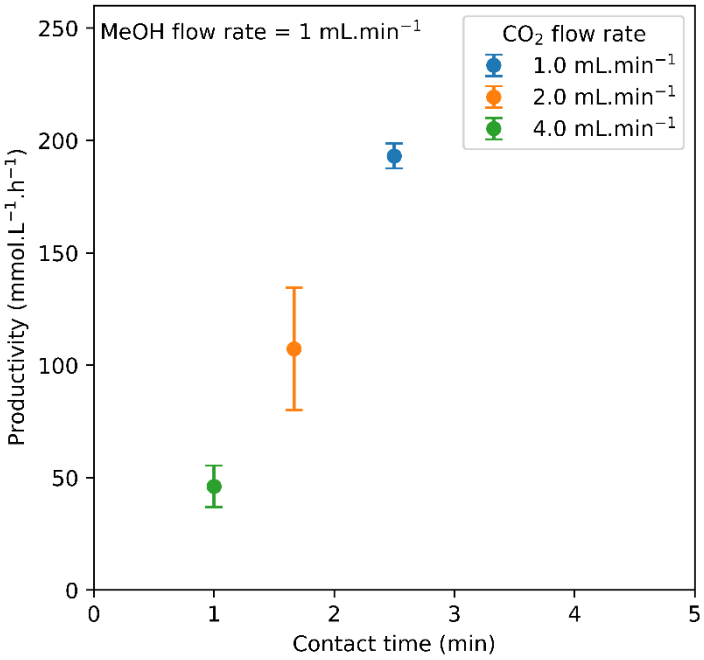

Figure 5.21: Relationship between contact time and productivity at different CO2 flow rates. Reaction conditions: 3 g CeO_2, 140 °C, 200 bar CO_2, 1 mL.min^{-1} MeOH. Error bars show standard deviation (n=3).

It would be expected that, if the catalyst is saturated at a given flow rate, it is unable to turn over all the starting material at any given time. As it has been shown in the batch reactions described in Section 5.2.2, the rate of reaction decreases as it approaches equilibrium. Thus, operating below the equilibrium allows the reaction to proceed at a rate that is advantageous for high productivity.

The peak DEC productivity achieved in Section 5.2.3 was 20.5 mmol.L_{cat}^{-1}.h^{-1} which, while unoptimized, was comparable to the productivity obtained by Wang *et al.*[1] which had a productivity 32 mmol.L_{cat}^{-1}.h^{-1} with no water removal or 47 mmol.L_{cat}^{-1}.h^{-1} with a non-reactive water removal system in place. Scaling up the catalyst bed, by increasing the mass of catalyst from 0.3 g to 3 g, increased both conversion and productivity. Figure 5.22 shows how ethanol conversion and productivity changes with increasing ethanol flow rate. Ethanol conversion was slightly lower than reported by Dibenedetto *et al.*[4] under comparable conditions. Similar to the methanol shown above, and Dibenedetto, peak conversion was observed at the lower flow rates, corresponding to a longer residence time, however productivity improved with increasing flow rate to a peak of 241 mmol.L_{cat}^{-1}.h^{-1} at 0.6 and 0.7 mL.min^{-1}.

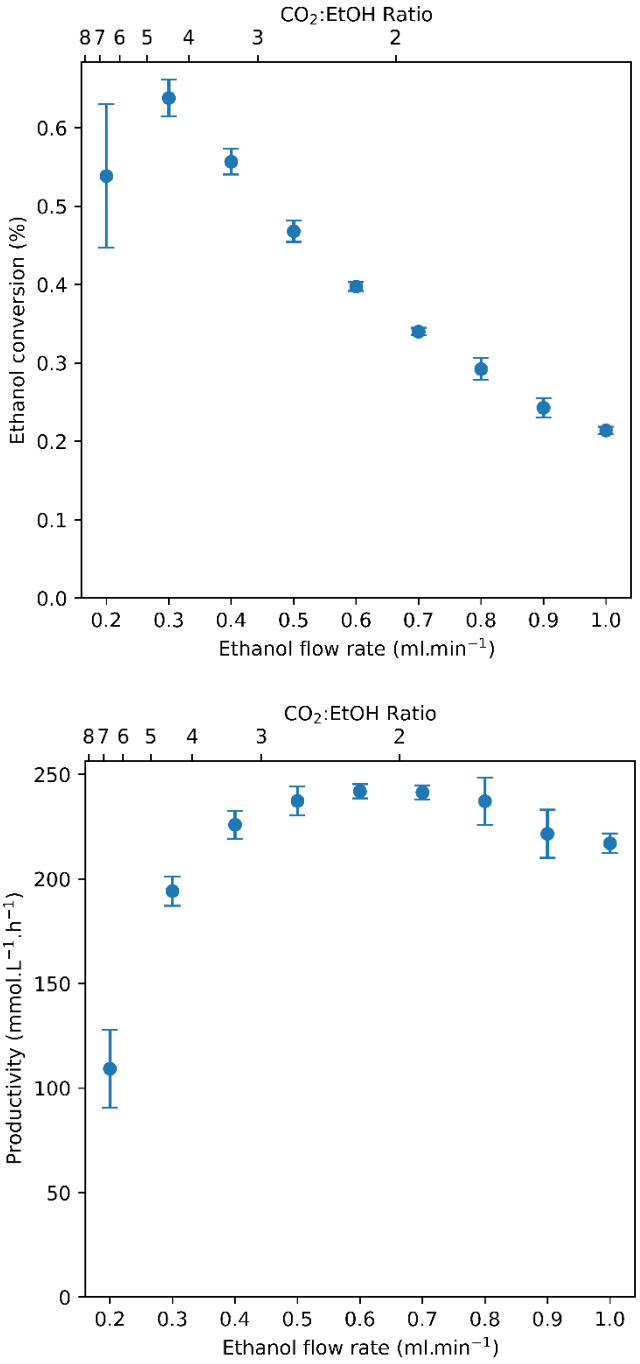

Figure 5.22: Effect of ethanol flow rate on conversion (top) and productivity (bottom). Reaction conditions: 2.9 g CeO_2, 5 mL bed volume, 140 °C, 200 bar CO_2, at 1 mL.min^{-1}. Error bars show standard deviation (n=3).

The 10-fold increase in catalyst led to a 6-fold improvement in conversion. The ethanol conversion exceeded methanol conversion under these conditions. However, the amount of DEC and DMC produced, in mmols, was similar as is demonstrated by the similar results for productivity. Due to its larger molecular

mass and similar density, fewer moles of ethanol were in the reactor compared to methanol, at the same flow rate. The same number of moles of methanol and ethanol were being converted, but fewer starting moles of ethanol led to a higher conversion. It is worth noting that both the methanol and ethanol conversions fall below the calculated equilibrium conversions at each flow rate.

5.3.8 Catalyst stability

A wide spectrum of catalyst materials has been developed for the synthesis of dialkyl carbonates, many of which are active. Measurement of catalyst stability is frequently performed using batch recycling,[34–36] as shown in Chapter 3. Using a flow system can give valuable insights into catalyst deactivation that may not be apparent after a small number of batch recycles.[37] Stability of a range of catalyst materials has been investigated in flow for the direct synthesis of DMC both with a dehydrating agent,[23,26,32] and in the absence of a dehydrating agent.[7,33] Catalyst stability is crucial for a productive flow system in the long-term and one of the advantages of using a flow system is that it negates the need for catalyst recovery between batch-wise recycling reactions. As good activity and no obvious signs of deactivation were observed in Chapter 3, the long-term stability of commercial, unmodified ceria was assessed for the formation of DMC and DEC in the absence of a dehydrating agent.

Figure 5.23 shows the methanol conversion and relative activity of the catalyst over the course of 96 h. The system lost 69% of its activity, corresponding to a deactivation constant ($k_{d(\mathrm{obs})}$) of 0.15 day^{-1} or a catalyst half-life of 3.1 days.

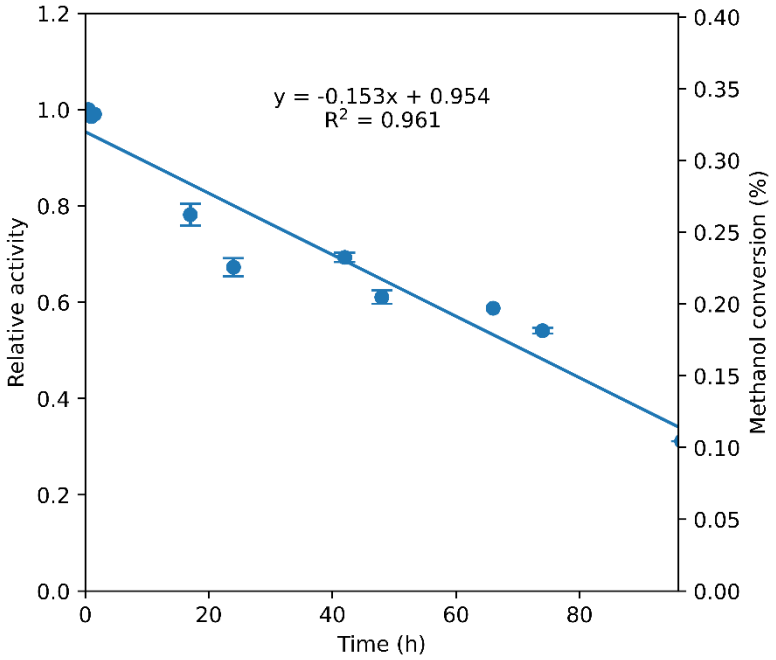

Figure 5.23: Deactivation of commercial cerium oxide in continuous flow. Reaction conditions: 0.2 mL.min^{-1} methanol, 1 mL.min^{-1} CO_2, 200 bar, 140 °C, 0.3 g CeO_2, contact time 4.2 minutes. Error bars show standard deviation (n=3).

Figure 5.24 shows the ethanol conversion over 15 h. We see deactivation of the catalyst for this reaction also, losing around 45% of its activity. This corresponds to a $k_{d(obs)}$ of 0.77 day^{-1} or a catalyst half-life of 16 h, five times faster than deactivation with methanol.

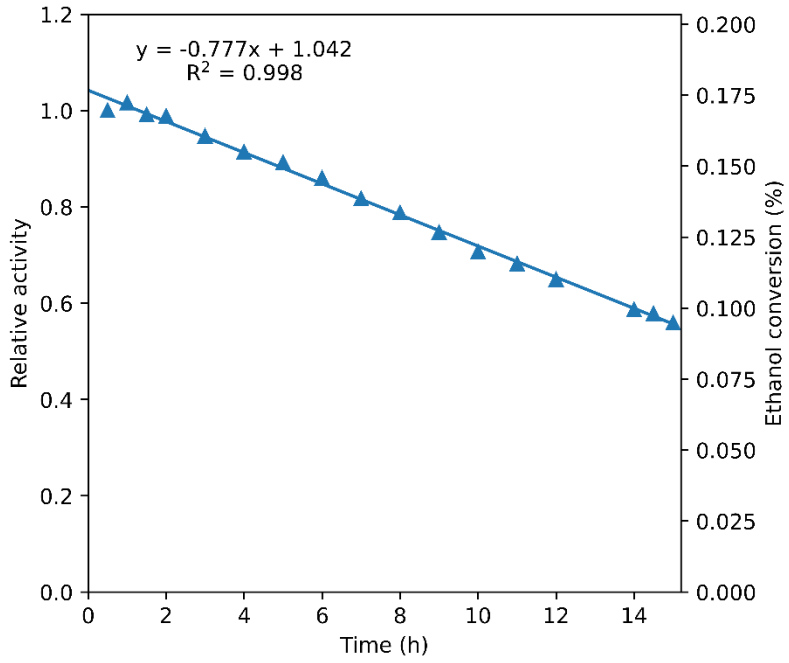

Figure 5.24: Deactivation of commercial cerium oxide in flow during the formation of DEC. Reaction conditions: 0.2 mL.min^{-1} alcohol, 1 mL.min^{-1} CO_2, 200 bar, 140 °C, 0.3 g CeO_2, contact time 4.2 min.

The more rapid deactivation of the commercial ceria catalyst in the reactions with ethanol suggests that the alcohol may be responsible for the deactivation. Though deactivation by water is a possibility, the results show that the greatest deactivation occured with ethanol at similar contact times, which had the lower rate of water production. Attempts to regenerate the activity of the catalyst by heating the bed to 120 °C under reduced pressure failed to improve activity, implying that this was a chemical change to the catalyst rather than product inhibition by adsorption.

It has been previously reported that deactivation correlates to the reduction of Ce^{IV} to Ce^{III} in the catalyst.[17] Figure 5.25A however, shows that little to no reduction from Ce^{IV} to Ce^{III} was observed after 6 h in flow with either ethanol or methanol.[38] Aresta *et al.*[17] also report a change in the oxygen region, which is observed in Figure 5.25B. This peak at 533 eV has been correlated to -OH on the surface, but is also attributed to defect sites and is not related to the oxidation state of the Ce.[39] This could imply that a greater degree of hydroxylation is occurring on the surface or that hydrolysis of Ce-O-Ce may be occurring to form Ce-OH.

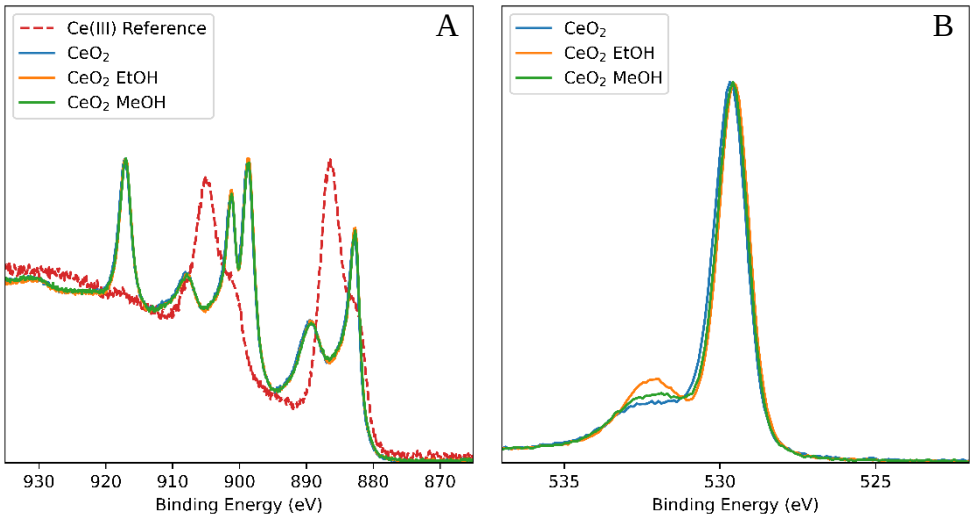

Figure 5.25: XPS of unused catalyst (CeO_2) and following a 6 h reaction with ethanol and methanol. A) Cerium atom region with a Ce(III) reference. B) Oxygen region.

This result is inconclusive however, the time between the reaction and analysis may allow for some reoxidation of the surface. Further analysis with catalyst used for different lengths of time, with a quicker turnaround for analysis, would be required to elucidate a mechanism for deactivation.

5.3.9 Accelerated aging

Accelerated aging experiments were conducted in order to determine how quickly the catalyst deactivates at lower temperatures. This was achieved by cycling the temperature of the catalyst bed in order to switch the operation of the catalyst bed between high and low conversion regimes. It was expected that the deactivation of the catalyst, much like the formation of product, would be temperature dependant. The catalyst deactivation experiments, described above, were conducted at 140 °C, and show a linear deactivation profile. However, when the catalyst bed was cycled between 140 and 100 °C, during the formation of DMC, a different profile was observed. Figure 5.26 shows the profile of the accelerated aging with the commercial CeO_2 material. As expected, the relative activity dropped between 140 and 100 °C, but we also saw a decrease in activity over the short timescale which was not recorded in Figure 5.23, due to the more frequent sampling.

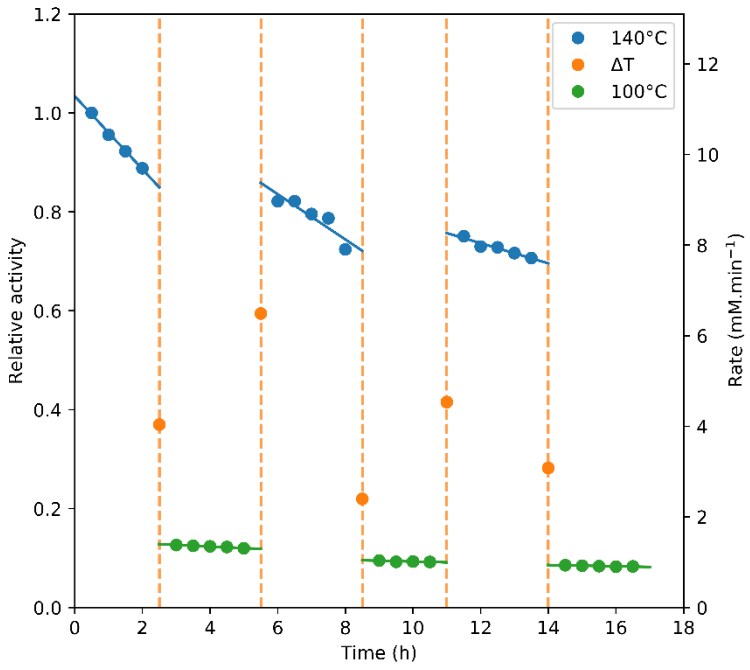

Figure 5.26: Accelerated aging experiment of commercial CeO_2 between 140 °C (●) and 100 °C (●). Reaction conditions: 0.3 g commercial CeO_2, 0.2 mL.min^{-1} MeOH, 1 mL.min^{-1} CO_2 bed volume 4.1 mL, catalyst contact 4.2 min.

The gradient of this deactivation became less steep with each cycle indicating that the rate of deactivation was decreasing with each cycle which could be due to deactivation of the catalysts most active sites. We also observed a decrease in deactivation constants for both 100 and 140 °C with each cycle (Table 5.4).

If a system with automated temperature cycling was available, this change in k_d could be observed further, perhaps converging on the value observed in Figure 5.23.

Whilst the commercial CeO_2 catalyst showed the highest conversions investigated, we can also see that deactivation occurs. Comparing the stability with $Ce_{0.75}Zr_{0.25}O_2$ synthesised in Chapter 2, shows that the mixed metal oxide was much more stable (Figure 5.27). The $Ce_{0.75}Zr_{0.25}O_2$ appeared to have a bedding in period, which was not observed with the commercial ceria, where the rate of reaction fluctuates over the first 2 h before stabilising. A larger difference in activity was observed between 140 and 100 °C with the commercial CeO_2 than with the mixed metal oxide. The commercial CeO_2 saw a 90% decrease in activity when going from 140 to 100 °C, whereas the mixed metal oxide saw only a 55% decrease. With suitable scale up, the mixed metal oxide may be able to operate at lower temperatures with less of a decrease in activity than is seen with the commercial catalyst; whilst also demonstrating lower rates of deactivation.

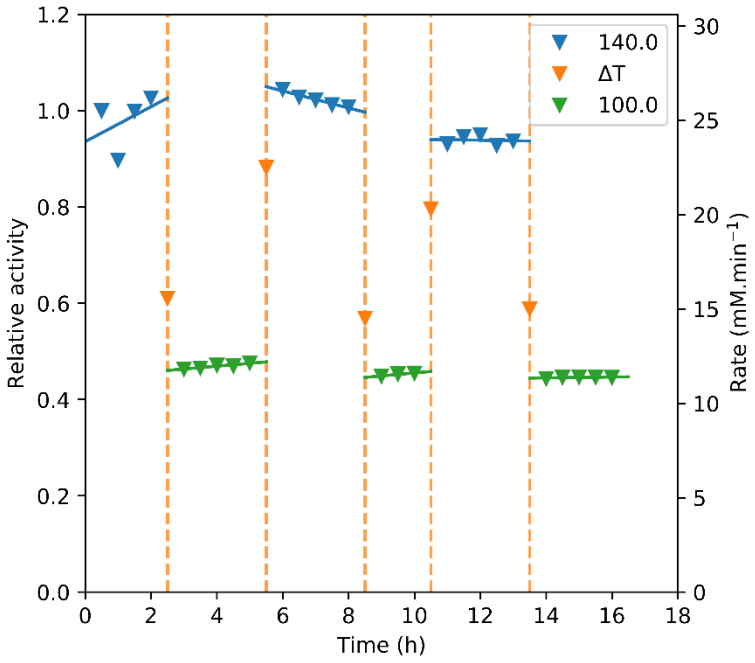

Figure 5.27: Accelerated aging of $Ce_{0.75}Zr_{0.25}O_2$ cycling between 140 °C (▼) and 100 °C (▼). Reaction conditions: 0.3 g $Ce_{0.75}Zr_{0.25}O_2$, 0.2 mL.min^{-1} MeOH, 1 mL.min^{-1} CO_2 bed volume 0.21 mL, catalyst contact time 0.17 min.

The first cycle at 140 °C, as well as each cycle at 100 °C, actually saw an increase in activity for the mixed metal oxide. By the third cycle at 140 °C, this

appeared to have stabilised and a k_d of -0.03 was observed (Table 5.5). Over the course of the experiment a 7% decrease in activity was observed at 140 °C and a 4% decrease at 100 °C which is an order of magnitude lower than 30% and 35% decrease observed in the commercial catalyst at 140 °C and 100 °C respectively.

Table 5.5: Comparison of the observed deactivation constants between the commercial cerium oxide catalyst and $Ce_{0.75}Zr_{0.25}O_2$.

Catalyst	Temperature cycle	140 °C $k_{d(obs)}$ (d^{-1})	100 °C $k_{d(obs)}$ (d^{-1})
Commercial	1	-1.77	-0.078
	2	-1.10	-0.040
	3	-0.49	-0.031
$Ce_{0.75}Zr_{0.25}O_2$	1	0.87	0.142
	2	-0.42	0.149
	3	-0.03	0.021

While the mixed metal oxide was more stable, with a higher rate of reaction, the catalyst material was also more dense with the mixed metal oxide bed occupying 0.2 mL in contrast with the commercial ceria bed occupying 4.1 mL, corresponding to a contact time of 0.17 and 4.2 minutes respectively. This in turn means that methanol and CO_2 spent more time in contact with the commercial bed allowing for more conversion to take place. Figure 5.28 shows a comparison of the cumulative product formation over the 16 h for each catalyst, with the commercial catalyst producing around a six times greater amount of DMC.

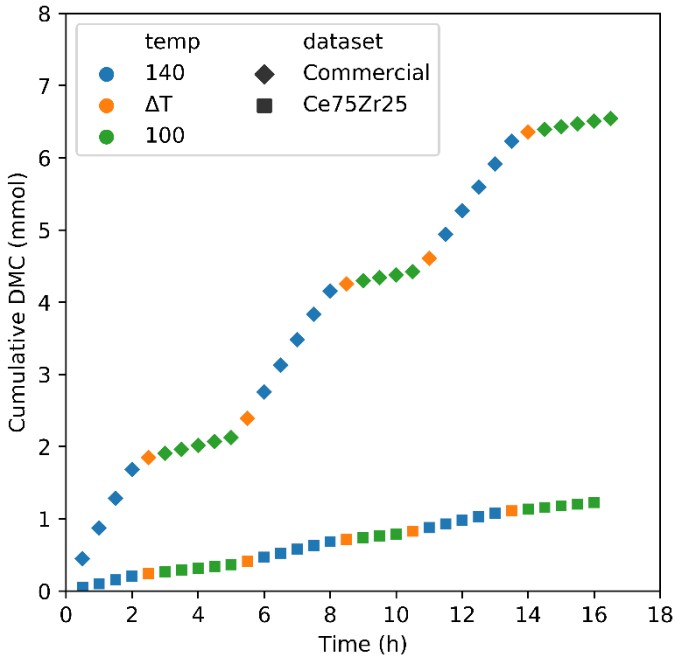

Figure 5.28: Comparison of the cumulative DMC formed during the 16 h of the accelerated aging experiments.

From a process perspective, a comparison of productivity shows that the mixed metal oxide out-performed the commercial CeO_2 in both productivity and stability (Table 5.6). Given the difference in density of the prepared mixed metal oxide compared to the commercial CeO_2, around 19 g of mixed metal oxide would be required to achieve a comparable residence time to 0.3 g of commercial CeO_2. This would be a compromise, potentially sacrificing productivity in exchange for a greater space-time yield.

Table 5.6 Comparison of mean productivity at 140 and 100 °C for commercial CeO_2 and $Ce_{0.75}Zr_{0.25}O_2$.

Catalyst	Temperature (°C)	Mean productivity ($mmol.L_{cat}^{-1}.h^{-1}$)	Mean rate of DMC formation ($mM.min^{-1}$)
Commercial	140	175	8.85
	100	21.9	1.10
$Ce_{0.75}Zr_{0.25}O_2$	140	500	25.0
	100	233	11.6

Because the rate of reaction decreased as it approached equilibrium, the comparison of rate between the two catalysts at 140 °C may not provide meaningful information. Due to the commercial CeO_2 being closer to

equilibrium conversion of 0.6%. At 100 °C, however, both catalysts were further away from equilibrium and the mixed metal oxide had a higher observed rate of 11.6 $mM.min^{-1}$ compared to the observed rate of the commercial CeO_2 at 1.10 $mM.min^{-1}$, 10 times lower. Comparison of the cumulative product at 100 °C alone (Figure 5.29) shows that the commercial CeO_2 had produced twice as much DMC as the mixed metal oxide but had 20 times greater catalyst contact time.

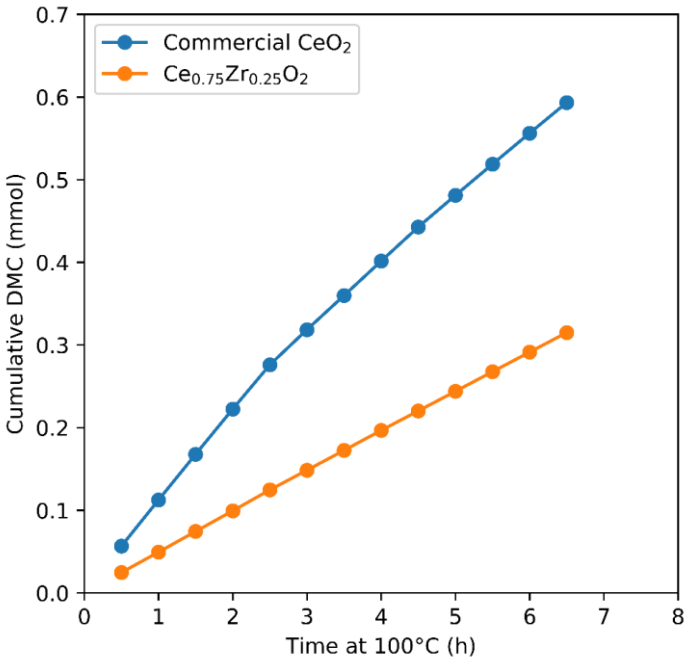

Figure 5.29: Comparison of cumulative product formed at 100 °C with commercial CeO_2 and $Ce_{0.75}Zr_{0.25}O_2$.

Utilising a larger mass of the more stable catalyst within the same volume, makes sense from a process perspective, as the bed is likely to last longer, and therefore the reactor would require less downtime to change out the spent bed. There likely exists a compromise where the higher operating costs due to a larger catalyst bed are offset by the savings related to reduced downtime and lower reaction temperature.

In ideal circumstances, both catalysts would be compared at similar conversions, however, achieving higher conversions with the mixed metal oxide would require changing the catalyst bed size or changing the reagent flow-rate. The synthesis of the required 19 g of mixed metal oxide was not attempted due to time constraints of the project. Lowering the flow rate for the mixed metal

oxide, to increase contact time, made sample collection impossible due to the increased aerosolization at the back-pressure regulator. Similarly, increasing the reagent flow rates for the commercial cerium oxide, lowering the contact time, will put the commercial catalyst into a lower conversion regime. However, in order to achieve a comparable contact time with the commercial catalyst would require a flow rate of 4 $mL.min^{-1}$ methanol and 20 $mL.min^{-1}$ CO_2 which, while allowing for rapid collection of samples, is beyond the capability of the pumps used.

5.3.10 Product removal

With a stable catalyst bed and a productive flow reactor system, removal of products from the reactor and the recycling of reactants becomes the limiting factor in scale-up. Thermodynamic limitations constrain the formation of dialkyl carbonates within the reactor but as shown in Chapter 4, disturbing the equilibrium by removal of products allows for a greater conversion.

The product removal strategy investigated in this work was supercritical separation. This depends on the ability of CO_2 to change its solvent strength depending on the density used.[40] As discussed in Chapter 1, with increasing density, the ability of CO_2 to solvate DMC and methanol increases and, in theory, an optimal density exists which would allow for the dissolution of methanol, but not DMC and water. In practice however, methanol may act as a cosolvent for water, which alone would not be soluble in CO_2.[41]

This section investigates two important factors for product separation: The stability of DMC, and the phase behaviour of the quaternary CO_2, methanol, DMC and water mixture.

5.3.10.1 DMC hydrolysis

It has been reported that DMC easily undergoes hydrolysis,[42] which we have demonstrated under catalytic conditions. After the catalyst bed however, we would expect the rate of uncatalyzed hydrolysis to be lower. We would also expect that the concentration of DMC should not drop below equilibrium, as the thermodynamics apply with and without the catalyst present. However, if sufficient enrichment of the products is achieved, the concentration may exceed the equilibrium and the stability to hydrolysis without a catalyst present

becomes an important consideration.

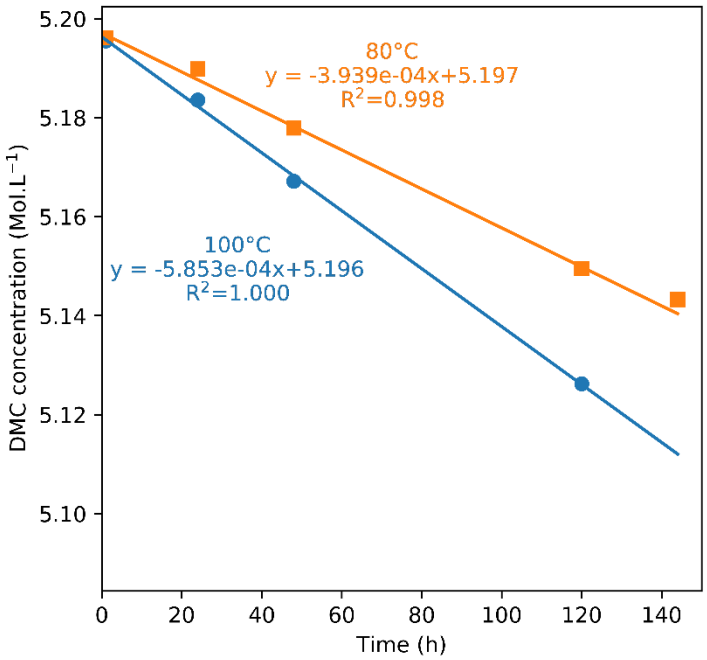

Figure 5.30 shows the hydrolysis of DMC followed by quantitative ^{1}H NMR spectroscopy over a week. In this experiment a stock solution consisting of 5.19 M DMC and 5.73 M H_2O was used. As DMC and H_2O are immiscible, DMSO was used to homogenise the solution, and the pH was adjusted to 3 with dilute HNO_3 in order to replicate the acidity of carbonic acid likely to form within the reactor. The change in DMC concentration followed a linear trend, suggesting that at these concentrations the reaction proceeded in a zero-order fashion.

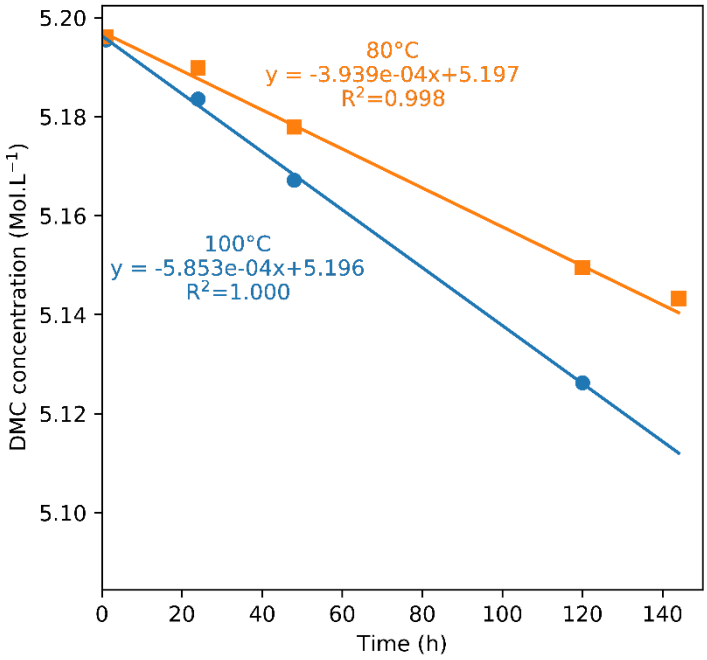

Figure 5.30: Hydrolysis of DMC at 80 (■) and 100 (●) °C in the absence of a catalyst. Conditions: 12 mmol DMC, 13 mmol H_2O in 1 mL of DMSO. 50 µL d6-DMSO was added for solvent lock adjusted to pH 3 using H_2NO_3. Final concentrations: 5.19 M DMC, 5.73 M H_2O.

The half-life of a zero-order reaction can be calculated using Equation 5.7

Equation 5.7: $$t_{1/2} = \frac{[DMC]_0}{2k}$$

Where:

k = rate

$[DMC]_0$ = initial DMC concentration

$t_{1/2}$ = half life

This gave a half-life of 185 days at 100 °C and a half-life of 275 days at 80 °C (Table 5.7) for the mixtures examined. Assuming the rate of hydrolysis remains constant, an equilibrium concentration of DMC under typical reaction conditions at 100 °C (87 mM) is expected to have a $t_{1/2}$ of 3 days. This should be sufficient time for a product removal strategy to be successful.

Table 5.7: Kinetic parameters for the hydrolysis of DMC in water at 80 and 100 °C with half-lives for the experimental values, as well as for the equilibrium conversion at 100 °C (87 mM).

Temperature (°C)	k x 10^{-4} ($mol.L^{-1}.h^{-1}$)	$[DMC]_0$ ($mol.L^{-1}$)	$t_{1/2}$ (days)
80	3.939	5.197	275
		0.087	4
100	5.853	5.196	185

		0.087	3

5.3.10.2 Phase Behaviour

One potential method of product separation is the use of supercritical CO_2 to create a product enriched phase which can then be separated from the reactor. For a CO_2 separation this entails the formation of a biphasic system in which the products are found in one phase at a concentration greater than in the reaction mixture.[43] Camy *et al.*[41] model the phase behaviour of a quaternary mixture of CO_2, MeOH, DMC and H_2O, showing that liquid-vapour phase can be achieved between the temperatures and pressures investigated in this chapter. Unfortunately, these were calculated for concentrations far exceeding equilibrium (60–100% MeOH conversion).

Initial phase behaviour experiments used a stock solution with the concentrations of 4% DMC and water in methanol. Figure 5.31 shows the change in liquid and vapour phase volume at 50 °C with increasing CO_2 pressure. At 0 bar (leftmost image), the stock solution occupied a volume of 1.5 mL, which remained unchanged up to 70 bar. Upon reaching 70 bar (centre image) there appeared to be a liquid-liquid (L-L) biphasic layer below the vapour phase, both liquid phases are similar in volume. Increasing the pressure caused the liquid phase to be further expanded by CO_2 and at 100 and 110 bar (rightmost image) the liquid phase had become homogeneous again and has expanded to around 4.5 times its original volume.

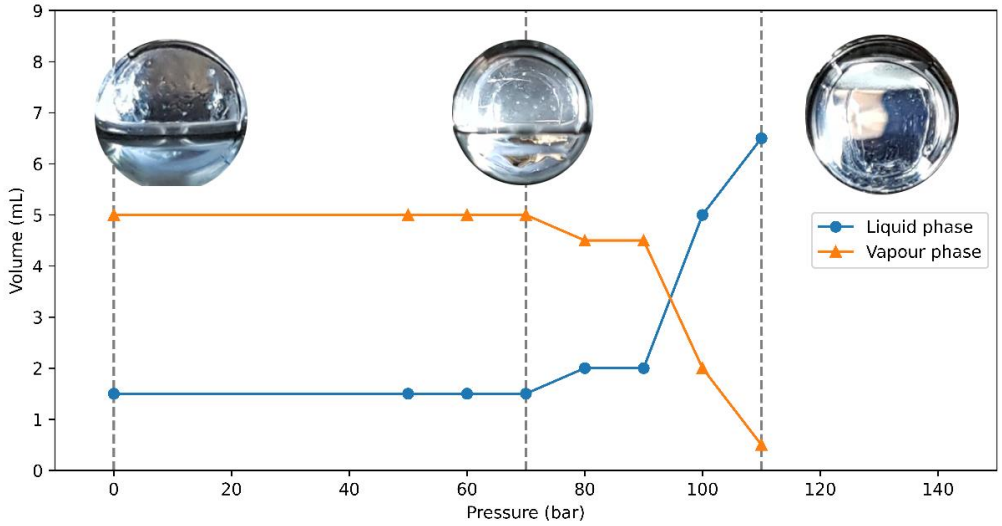

Figure 5.31: Volume of liquid and vapour phases of a 4% DMC mixture at 50 °C at varying pressures. Inset images taken at 0, 70, 110 bar CO_2 (vertical dashed lines).

Investigating the change from a L-L mixture, additional images were taken at 50 and 90 bar CO_2 (Figure 5.32 left and centre respectively). At 50 bar mixing between the vapour and liquid phase appeared to be occurring, but there was very little expansion of the liquid phase. Increasing the pressure to 90 bar, the L-L phase observed at 70 bar merged into a single expanded liquid phase occupying approximately 2 mL. A change in the refractive index was also visible at 90 bar indicating that the mixture was close to the critical point. Changing the stock solution to one of 7 mol% DMC and water showed a larger L-L phase (Figure 5.32 right), indicating that these phases may be enriched with product. However, any change to the pressure (such as by the back pressure regulator) perturbs the L-L phase. This sensitivity may impede efforts to use this method for product separation.

Figure 5.32: Images taken at 50 bar (left), 90 bar (centre) at 50 °C with a 4 mol% mixture of DMC and water in methanol. Right image at 70 bar CO_2, 50 °C with a 7 mol% mixture of DMC and water in methanol.

Figure 5.33 shows isochoric view cell experiments at 110 bar (at 50 °C). For these experiments a mixture closer to reaction concentrations, a 0.4% DMC and water mixture in methanol, was used. As the inset images show, lensing can be observed at 50 and 65 °C this made it difficult to distinguish between a phase boundary and the back of the view cell. What is clear in the images is that there was a large, expanded liquid phase within the autoclave. Upon reaching 80 °C and equilibrating for an hour a phase boundary was visible about halfway up the window. This disappeared at 90 °C where just a homogenous CO_2 expanded liquid phase was observed.

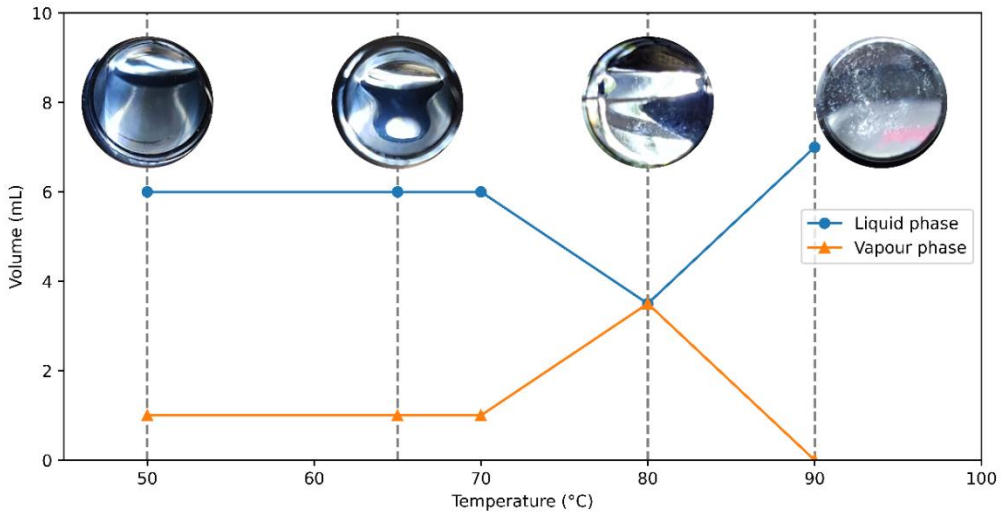

Figure 5.33 Volume of liquid and vapour phases with the view cell pressurised to 110 bar at 50 °C and heated to varying temperatures. Inset images taken at 50, 65, 80 and 90 °C (vertical dashed lines).

A preliminary attempt at supercritical separation used a high-pressure bottle with a length of tubing separated by two valves, in an attempt to isolate the lower liquid phase from the rest of the vessel. This should allow for separation without perturbing the phase behaviour in the vessel at large. Figure 5.34 shows a schematic of the separator used.

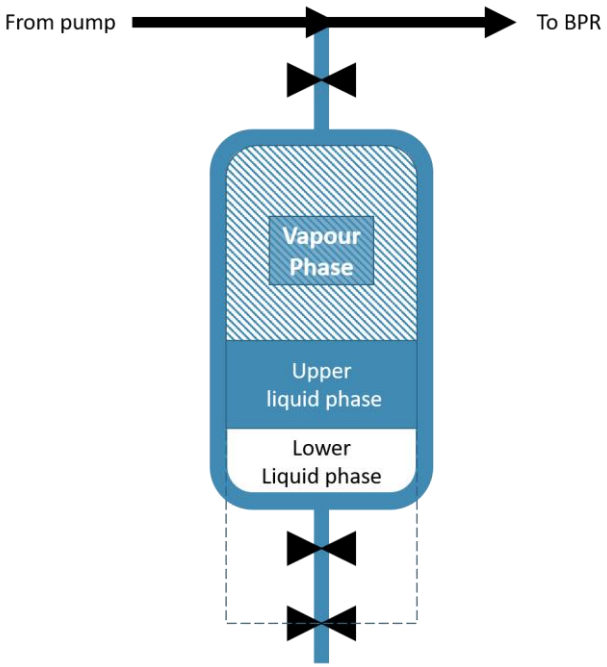

Figure 5.34: Schematic of the separator used in preliminary experiments. The lower liquid phase is allowed to collect at the bottom of the separator and between the two lower valves, in order to remove a sample the top valve is closed and the lower valve is connected to a length of tubing and slowly depressurised into a sample vial.

Preliminary experiments separated the lower phase, and it was analysed by GC-FID which did not show any enrichment of DMC, with a decrease in DMC concentration between the stock. This may indicate that the lower phase was methanol or water rich, or that losses of DMC are seen in sample collection similar to that described in section 5.3.3, due to aerosolization during depressurisation.

Due to the uncertainty in this method, high-pressure NMR was employed. A sapphire NMR tube with titanium fittings was loaded with a 0.4% DMC and water in a methanol mixture with sodium trimethylsilylpropanesulfonate (DSS) as an internal standard. DSS was selected as it was not expected to partition between phases but remain in the lower liquid phase due to its charge. Figure 5.35 shows the NMR spectrum under ambient conditions where methanol's CH_3 peak was observed at 3.34 ppm and the OH group was observed at 4.91 ppm. DMC and water are observed at 3.73 and 4.61 ppm, respectively. Upon pressurising to 70 bar with CO_2 the water peak was overwhelmed by the OH peak which shifted to 4.57 ppm. Pressurising to 110 bar shifts the OH peak further down to 3.32 ppm. DMC remained distinguishable from the other peaks across all pressures.

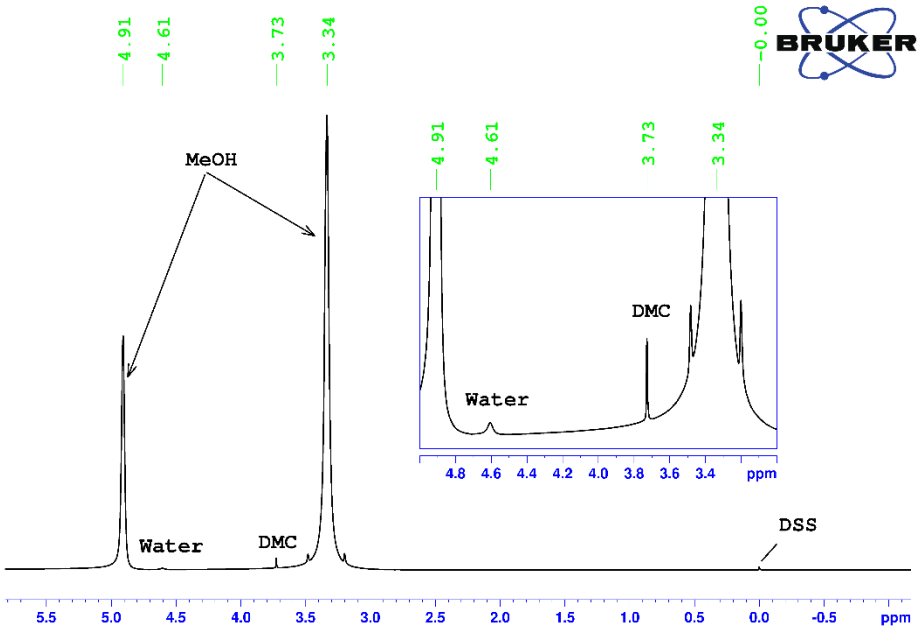

Figure 5.35: NMR of 0.4% DMC and water mixture in methanol with DSS standard. Conditions ambient temperature and pressure. Inset: zoomed in view of the region containing the characteristic DMC and water peaks.

To determine if any partitioning of DMC was occurring between the liquid and vapour phase, integral of the DMC peak was taken at each of the pressures investigated with the integral of DSS was normalised to 1. Table 5.8 shows the change in DMC and methanol. There was a small change in the DMC integral with increasing pressure, however the shifting methanol -OH peak overlapped with the CH_3 peak at 110 bar making the region difficult to integrate.

*Table 5.8: Comparison of DMC and CH_3 integrals relative to the DSS standard and change in OH shift with increasing CO_2 pressure at 50 °C. *at 110 bar the OH peak and CH_3 peaks overlap making determination of the CH_3 integral difficult.*

Pressure (bar)	DMC integral	CH_3 integral (MeOH)	OH shift (MeOH) (ppm)
0	2.8	859	4.91
70	2.2	821	4.58
110	2.4	—*	3.32

With mixtures with a concentration similar to that seen in our reactors, there was little to no quantifiable separation under the conditions investigated. Higher temperatures may give better separation, but this becomes more challenging experimentally. Further experiments would be needed to determine if separation by utilising the phase behaviour of near- and supercritical CO_2 is feasible at equilibrium concentrations and below. Other methods of separation, such as membranes, may be a more practical method.

5.4 Conclusion

In this chapter the dehydrating agent free synthesis of DMC and DEC has been investigated in batch and flow mode. The batch synthesis confirmed that commercial CeO_2 was the most active catalyst even in dehydrating agent free reactions. Additionally, the results obtained support the thermodynamic calculations performed in Chapter 4, with the observed plateaus approaching the calculated equilibrium conversions.

Kinetic modelling techniques were used to describe the ceria-catalysed synthesis of DMC giving activation energies (120 $kJ.mol^{-1}$ and 104 $kJ.mol^{-1}$)

consistent with previously reported literature examples. Values for equilibrium concentrations were calculated using the kinetic model and are within 6.5% of those calculated in Chapter 4. This was further confirmed using reverse reactions, which showed hydrolysis of DMC towards the calculated equilibrium, demonstrating that the plateau was not caused by other factors such as product inhibition of catalyst deactivation. DEC also showed a good agreement with calculated equilibrium conversions and was within 1.7% of the values calculated in Chapter 4.

Flow experiments have investigated the effect of temperature and reagent flow rate on DMC productivity with the commercial cerium oxide catalyst. As expected, the highest temperature investigated (140 °C) led to the greatest conversion of 0.3%, achieving 50% of the calculated equilibrium with 4 minutes of catalyst contact, which is 15 times faster than observed in batch. The rate of reaction of lower temperatures (100 and 120 °C) were also greater in flow than in batch. Changing the reagent flow rate had a significant impact on both conversion and productivity. The highest conversions were achieved at low flowrates (0.35% at 0.3 $mL.min^{-1}$ methanol), but optimal productivity was achieved at greater flow rates (225 $mmol.L^{-1}.h^{-1}$ at 0.6 $mL.min^{-1}$ methanol).

The effect of temperature on DEC conversion was also investigated, showing a 7 times improvement in rate in flow compared to batch, though DEC was further from its calculated equilibrium in flow than DMC. Flow rate experiments with a scaled up catalyst bed for DEC showed an improved conversion, exceeding 0.6% at 0.3 $mL.min^{-1}$ and achieving higher productivities than the methanol reactions (240 $mmol.L^{-1}.h^{-1}$ at 0.6 $mL.min^{-1}$ ethanol).

Studies on catalyst stability and accelerated aging have also been performed. The most active catalyst, commercial CeO_2, has been shown to lose 50% of its activity after 3 days online for DMC and 16 h for DEC. Interestingly, the mixed metal oxide which was less active in batch ($Ce_{0.75}Zr_{0.25}O_2$) showed greater stability and rate of reaction than the commercial catalyst for DMC synthesis, with a catalyst half-life of 16 days. This suggests the need for further investigations for optimisation of the mixed metal oxide to balance stability, productivity and conversion.

Preliminary experiments for product removal have focused on DMC stability and phase behaviour. We have shown that DMC remained stable under acidic conditions, in the absence of catalyst, for long enough to allow for product separation. Phase behaviour experiments have shown that a three-phase mixture occurred at 50 °C and 70 bar CO_2, indicating that separation of products using this method may be possible. High pressure NMR studies were inconclusive, showing no DMC enrichment at the temperatures and pressures investigated. Further studies are necessary to fully explore the supercritical separation of DMC and water from CO_2 and methanol, and modifications to experimental setup and analysis are needed to fully analyse each phase.

5.5 References

(1) Wang, J.; Hao, Z.; Wohlrab, S. Continuous CO2 Esterification to Diethyl Carbonate (DEC) at Atmospheric Pressure: Application of Porous Membranes for in-Situ H2O Removal. *Green Chem.* **2017**. https://doi.org/10.1039/C7GC00916J.

(2) Li, C. F.; Zhong, S. H. Study on Application of Membrane Reactor in Direct Synthesis DMC from CO2 and CH3OH over Cu-KF/MgSiO Catalyst. *Catal. Today* **2003**, *82* (1–4), 83–90. https://doi.org/10.1016/S0920-5861(03)00205-0.

(3) Li, C.; Zhong, S. Study on Application of Membrane Reactor in Direct Synthesis DMC from CO 2 and CH 3 OH over Cu – KF / MgSiO Catalyst. **2003**, *82*, 83–90. https://doi.org/10.1016/S0920-5861(03)00205-0.

(4) Dibenedetto, A.; Aresta, M.; Angelini, A.; Ethiraj, J.; Aresta, B. M. Synthesis, Characterization, and Use of Nb V/Ce IV-Mixed Oxides in the Direct Carboxylation of Ethanol by Using Pervaporation Membranes for Water Removal. *Chem. - A Eur. J.* **2012**, *18* (33), 10324–10334. https://doi.org/10.1002/chem.201201561.

(5) Leino, E.; Mäki-Arvela, P.; Eta, V.; Murzin, D. Y.; Salmi, T.; Mikkola, J. P. Conventional Synthesis Methods of Short-Chain Dialkylcarbonates and Novel Production Technology via Direct Route from Alcohol and Waste CO2. *Appl. Catal. A Gen.* **2010**, *383* (1–2), 1–13.

https://doi.org/10.1016/j.apcata.2010.05.046.

(6) Leino, E.; Mäki-Arvela, P.; Eränen, K.; Tenho, M.; Murzin, D. Y.; Salmi, T.; Mikkola, J. P. Enhanced Yields of Diethyl Carbonate via One-Pot Synthesis from Ethanol, Carbon Dioxide and Butylene Oxide over Cerium (IV) Oxide. *Chem. Eng. J.* **2011**, *176–177*, 124–133. https://doi.org/10.1016/j.cej.2011.07.054.

(7) Chiang, C. L.; Lin, K. S.; Yu, S. H. Improvement of Dimethyl Carbonate Formation via Methanol Carbonation over Vanadium-Doped Cu–Ni/AC Catalyst. *J. Taiwan Inst. Chem. Eng.* **2019**, *98*, 132–149. https://doi.org/10.1016/j.jtice.2018.08.001.

(8) Santos, B. A. V.; Pereira, C. S. M.; Silva, V. M. T. M.; Loureiro, J. M.; Rodrigues, A. E. Kinetic Study for the Direct Synthesis of Dimethyl Carbonate from Methanol and CO2 over CeO2 at High Pressure Conditions. *Appl. Catal. A Gen.* **2013**, *455*, 219–226. https://doi.org/10.1016/j.apcata.2013.02.003.

(9) Kabra, S. K.; Turpeinen, E.; Keiski, R. L.; Yadav, G. D. Direct Synthesis of Dimethyl Carbonate from Methanol and Carbon Dioxide: A Thermodynamic and Experimental Study. *J. Supercrit. Fluids* **2016**, *117*, 98–107. https://doi.org/10.1016/j.supflu.2016.05.039.

(10) Zhao, T.; Hu, X.; Wu, D.; Li, R.; Yang, G.; Wu, Y. Direct Synthesis of Dimethyl Carbonate from Carbon Dioxide and Methanol at Room Temperature Using Imidazolium Hydrogen Carbonate Ionic Liquid as a Recyclable Catalyst and Dehydrant. *ChemSusChem* **2017**, *10* (9), 2046–2052. https://doi.org/10.1002/cssc.201700128.

(11) Sun, J.; Lu, B.; Wang, X.; Li, X.; Zhao, J.; Cai, Q. A Functionalized Basic Ionic Liquid for Synthesis of Dimethyl Carbonate from Methanol and CO2. *Fuel Process. Technol.* **2013**, *115*, 233–237. https://doi.org/10.1016/j.fuproc.2013.06.009.

(12) Jiang, C.; Guo, Y.; Wang, C.; Hu, C.; Wu, Y.; Wang, E. Synthesis of Dimethyl Carbonate from Methanol and Carbon Dioxide in the Presence of Polyoxometalates under Mild Conditions. *Appl. Catal. A Gen.* **2003**,

256 (1–2), 203–212. https://doi.org/10.1016/S0926-860X(03)00400-9.

(13) Tomishige, K.; Kunimori, K. Catalytic and Direct Synthesis of Dimethyl Carbonate Starting from Carbon Dioxide Using CeO2-ZrO2 Solid Solution Heterogeneous Catalyst: Effect of H2O Removal from the Reaction System. *Appl. Catal. A Gen.* **2002**, *237* (1–2), 103–109. https://doi.org/10.1016/S0926-860X(02)00322-8.

(14) Li, A.; Pu, Y.; Li, F.; Luo, J.; Zhao, N.; Xiao, F. Synthesis of Dimethyl Carbonate from Methanol and CO2 over Fe-Zr Mixed Oxides. *J. CO2 Util.* **2017**, *19*, 33–39. https://doi.org/10.1016/j.jcou.2017.02.016.

(15) Lee, H. J.; Park, S.; Jung, J. C.; Song, I. K. Direct Synthesis of Dimethyl Carbonate from Methanol and Carbon Dioxide over H3PW12O40/CeXZr1-XO2 Catalysts: Effect of Acidity of the Catalysts. *Korean J. Chem. Eng.* **2011**, *28* (7), 1518–1522. https://doi.org/10.1007/s11814-011-0020-x.

(16) Ikeda, Y.; Sakaihori, T.; Tomishige, K.; Fujimoto, K. Promoting Effect of Phosphoric Acid on Zirconia Catalysts in Selective Synthesis of Dimethyl Carbonate from Methanol and Carbon Dioxide. *Catal. Letters* **2000**, *66* (1–2), 59–62. https://doi.org/10.1023/A:1019043422050.

(17) Aresta, M.; Dibenedetto, A.; Pastore, C.; Cuocci, C.; Aresta, B.; Cometa, S.; De Giglio, E.; Degiglio, E. Cerium(IV)Oxide Modification by Inclusion of a Hetero-Atom: A Strategy for Producing Efficient and Robust Nano-Catalysts for Methanol Carboxylation. *Catal. Today* **2008**, *137* (1), 125–131. https://doi.org/10.1016/j.cattod.2008.04.043.

(18) Lee, H. J.; Joe, W.; Song, I. K. Direct Synthesis of Dimethyl Carbonate from Methanol and Carbon Dioxide over Transition Metal Oxide/Ce0.6Zr0.4O2 Catalysts: Effect of Acidity and Basicity of the Catalysts. *Korean J. Chem. Eng.* **2012**, *29* (3), 317–322. https://doi.org/10.1007/s11814-011-0185-3.

(19) Wu, X. L.; Xiao, M.; Meng, Y. Z.; Lu, Y. X. Direct Synthesis of Dimethyl Carbonate on H3PO4 Modified V2O5. *J. Mol. Catal. A Chem.* **2005**, *238* (1–2), 158–162.

https://doi.org/10.1016/j.molcata.2005.05.018.

(20) Liu, B.; Li, C.; Zhang, G.; Yao, X.; Chuang, S. S. C.; Li, Z. Oxygen Vacancy Promoting Dimethyl Carbonate Synthesis from CO2 and Methanol over Zr-Doped CeO2 Nanorods. *ACS Catal.* **2018**, *8* (11), 10446–10456. https://doi.org/10.1021/acscatal.8b00415.

(21) Choi, J.-C. C.; He, L.-N. N.; Yasuda, H.; Sakakura, T.; Yasudaa, H.; Sakakura, T. Selective and High Yield Synthesis of Dimethyl Carbonate Directly from Carbon Dioxide and Methanol. *Green Chem.* **2002**, *4* (3), 230–234. https://doi.org/10.1039/b200623p.

(22) Zhang, M.; Alferov, K. A.; Xiao, M.; Han, D.; Wang, S.; Meng, Y. Continuous Dimethyl Carbonate Synthesis from CO2 and Methanol Using Cu-Ni@VSiO as Catalyst Synthesized by a Novel Sulfuration Method. *Catalysts* **2018**, *8* (4). https://doi.org/10.3390/catal8040142.

(23) Pimprom, S.; Sriboonkham, K.; Dittanet, P.; Föttinger, K.; Rupprechter, G.; Kongkachuichay, P. Synthesis of Copper-Nickel/SBA-15 from Rice Husk Ash Catalyst for Dimethyl Carbonate Production from Methanol and Carbon Dioxide. *J. Ind. Eng. Chem.* **2015**, *31*, 156–166. https://doi.org/10.1016/j.jiec.2015.06.019.

(24) Santos, B. a. V.; Pereira, C. S. M.; Silva, V. M. T. M.; Loureiro, J. M.; Rodrigues, a. E. Design of a True Moving Bed Reactor for the Direct Synthesis of Dimethyl Carbonate. *Chem. Eng. Sci.* **2015**, *123*, 406–419. https://doi.org/10.1016/j.ces.2014.11.017.

(25) Bansode, A.; Urakawa, A. Continuous DMC Synthesis from CO 2 and Methanol over a CeO 2 Catalyst in a Fixed Bed Reactor in the Presence of a Dehydrating Agent. *ACS Catal.* **2014**, *4*, 3877–3880. https://doi.org/dx.doi.org/10.1021/cs501221q.

(26) Stoian, D.; Bansode, A.; Medina, F.; Urakawa, A. Catalysis under Microscope: Unraveling the Mechanism of Catalyst de- and Re-Activation in the Continuous Dimethyl Carbonate Synthesis from CO2 and Methanol in the Presence of a Dehydrating Agent. *Catal. Today* **2016**, *283*, 2–10. https://doi.org/10.1016/j.cattod.2016.03.038.

(27) Hintermair, U.; Roosen, C.; Kaever, M.; Kronenberg, H.; Thelen, R.; Aey, S.; Leitner, W.; Greiner, L. A Versatile Lab to Pilot Scale Continuous Reaction System for Supercritical Fluid Processing. *Org. Process Res. Dev.* **2011**, *15* (6), 1275–1280. https://doi.org/10.1021/op200053w.

(28) Python Software Foundation. Python https://www.python.org/.

(29) Chris, L. pySerial https://github.com/pyserial/pyserial.

(30) Virtanen, P.; Gommers, R.; Oliphant, T. E.; Haberland, M.; Reddy, T.; Cournapeau, D.; Burovski, E.; Peterson, P.; Weckesser, W.; Bright, J.; et al. SciPy 1.0: Fundamental Algorithms for Scientific Computing in Python. *Nat. Methods* **2020**. https://doi.org/10.1038/s41592-019-0686-2.

(31) Nnaji, N. J.; Ani, J. U.; Ekwonu, A. M. The Solution of Reversible First Order Reaction Equation Revisited. *Acta Chim. Pharm. Indica* **2013**, *3* (3), 212–218.

(32) Stoian, D.; Medina, F.; Urakawa, A. Improving the Stability of CeO2 Catalyst by Rare Earth Metal Promotion and Molecular Insights in the Dimethyl Carbonate Synthesis from CO2 and Methanol with 2-Cyanopyridine. *ACS Catal.* **2018**, *8* (4), 3181–3193. https://doi.org/10.1021/acscatal.7b04198.

(33) Chen, Y.; Wang, H.; Qin, Z.; Tian, S.; Ye, Z.; Ye, L.; Abroshan, H.; Li, G. TiXCe1-XO2 Nanocomposites: A Monolithic Catalyst for the Direct Conversion of Carbon Dioxide and Methanol to Dimethyl Carbonate. *Green Chem.* **2019**, *21* (17), 4642–4649. https://doi.org/10.1039/c9gc00811j.

(34) Al-Darwish, J.; Senter, M.; Lawson, S.; Rezaei, F.; Rownaghi, A. A. Ceria Nanostructured Catalysts for Conversion of Methanol and Carbon Dioxide to Dimethyl Carbonate. *Catal. Today* **2020**, *350*, 120–126. https://doi.org/10.1016/j.cattod.2019.06.013.

(35) Kumar, P.; Srivastava, V. C.; Gläser, R.; With, P.; Mishra, I. M. Active Ceria-Calcium Oxide Catalysts for Dimethyl Carbonate Synthesis by

Conversion of CO2. *Powder Technol.* **2017**, *309*, 13–21. https://doi.org/10.1016/j.powtec.2016.12.016.

(36) Saada, R.; Kellici, S.; Heil, T.; Morgan, D.; Saha, B. Greener Synthesis of Dimethyl Carbonate Using a Novel Ceria-Zirconia Oxide/Graphene Nanocomposite Catalyst. *Appl. Catal. B Environ.* **2015**, *168–169*, 352–362. https://doi.org/10.1016/j.apcatb.2014.12.013.

(37) Yakabi, K.; Milne, K.; Buchard, A.; Hammond, C. Selectivity and Lifetime Effects in Zeolite-Catalysed Baeyer–Villiger Oxidation Investigated in Batch and Continuous Flow. *ChemCatChem* **2016**, *8* (22), 3490–3498. https://doi.org/10.1002/cctc.201600955.

(38) Mullins, D. R. The Surface Chemistry of Cerium Oxide. *Surf. Sci. Rep.* **2015**, *70* (1), 42–85. https://doi.org/10.1016/j.surfrep.2014.12.001.

(39) Mullins, D. R.; Overbury, S. H.; Huntley, D. R. Electron Spectroscopy of Single Crystal and Polycrystalline Cerium Oxide Surfaces. *Surf. Sci.* **1998**, *409* (2), 307–319. https://doi.org/10.1016/S0039-6028(98)00257-X.

(40) Theyssen, N.; Scovell, K.; Poliakoff, M.; Foster, N. R.; Lucien, F. P.; Mammucari, R.; Rayner, C. M.; Rose, P. M.; Barnes, D. C. *Green Solvents: Supercritical Solvents, Volume 4*; 2013.

(41) Camy, S.; Pic, J. S.; Badens, E.; Condoret, J. S. Fluid Phase Equilibria of the Reacting Mixture in the Dimethyl Carbonate Synthesis from Supercritical CO2. *J. Supercrit. Fluids* **2003**, *25* (1), 19–32. https://doi.org/10.1016/S0896-8446(02)00087-6.

(42) Tamboli, A. H.; Chaugule, A. A.; Kim, H. Catalytic Developments in the Direct Dimethyl Carbonate Synthesis from Carbon Dioxide and Methanol. *Chem. Eng. J.* **2017**, *323*, 530–544. https://doi.org/10.1016/j.cej.2017.04.112.

(43) Pollet, P.; Hart, R. J.; Eckert, C. A.; Liotta, C. L. Organic Aqueous Tunable Solvents (OATS): A Vehicle for Coupling Reactions and Separations. *Acc. Chem. Res.* **2010**, *43* (9), 1237–1245.

https://doi.org/10.1021/ar100036j.

Chapter 6 - Conclusions and Future work

6.1 Catalyst screening in flow

Investigation of catalyst materials in batch reactions with dehydrating agents in Chapter 3, and without dehydrating agents in Chapter 5, showed the commercial cerium oxide to have the greatest conversion. However, we also demonstrated that the mixed metal oxides showed a greater stability compared to the commercial cerium oxide, which lost activity after a single use-recovery cycle (Chapter 3). As most of the experiments conducted in Chapter 5 utilised the commercial cerium oxide, future work would look at screening more catalyst materials in flow, such as the pure and mixed metal oxides synthesised in Chapter 2, evaluating their stability and activity especially at lower temperatures. The lower temperature conversion is particularly important for recirculating reactor systems, as this reduces the amount that the reaction mixture needs to be cooled before the separation step, saving energy, and making the process greener.

Screening a wider variety of doped mixed metal oxides may also help to find a more active catalyst as Lee *et al.* demonstrate.[1–3] As discussed in Chapter 2, there is a positive correlation between the catalyst's acidity and basicity, and its activity in the synthesis of dialkyl carbonates. In this work we were unable to obtain quantitative measurements of the acid and base sites for the catalysts synthesised, future work in this area would involve performing quantitative TPD on the catalysts we have synthesised in order to correlate activity with acid/base concentrations. As the equilibrium conversions are below 1%, a focus on catalyst stability may be the more important factor keeping a recirculating reactor online for continuous product removal. The mixed metal oxides synthesised in this work proved to be stable in both batch (Chapter 3) and flow (Chapter 5), and thus are an ideal starting point for tests involving a recirculating reactor system.

6.2 Substrate scope

The work within this thesis focused on the synthesis of DMC and DEC as thermodynamic values were available for these compounds. We have demonstrated a productive system for the synthesis of DMC and DEC and have progressed the understanding of the thermodynamics of the reaction. We have also presented two additional techniques for determining the equilibrium concentration: The reaction

from twice the plateau, and kinetic analysis using curve fitting to determine the equilibrium concentration. As discussed in Chapter 1, the currently explored substrate scope for direct synthesis is much smaller than for other methods, such as phosgenation. Therefore, a screening of alcohol compounds with a range of catalysts for the synthesis of their corresponding carbonates would be another topic for further study. Initial candidates such as isopropanol and tert-butanol would give an idea how steric bulk impacts the formation of dialkyl carbonates. Similarly, phenol and benzyl alcohol can be investigated to determine the effect of acidity, some initial work on the synthesis of diphenyl carbonate was conducted, however, preliminary results with CeO_2 showed only diphenyl ether being produced. Therefore, development of catalysts with the correct balance of acidic and basic sites is required for activity towards other substrates.

6.3 Product separation

The thermodynamic model shown in this work uses first principle thermodynamic equations, coupled with numerical optimisation to determine the equilibrium conversions under a variety of conditions. The python class developed can be utilised by anybody with an understanding of the python programming language and used for calculating the equilibrium conversions of any system in which the ΔH and ΔS are known. Further work with this may be to integrate kinetics to determine how much time separation cycles are expected to take, or how long the reaction is allowed to progress before a separation is performed. In Chapter 4, we used this model to predict that the removal of both products is necessary for the reaction to achieve higher conversions with fewer product removal cycles.

The work in this thesis has shown that a productive flow system can be achieved for the synthesis of dialkyl carbonates (Chapter 5), in order to improve this further, product separation would need to be added to the reactor system. Separation by a change in phase behaviour may be possible, though we were unable to demonstrate enrichment in our initial experiments. If enrichment of products in one phase is achieved, this would provide a more elegant solution to the problem of product separation than the use of membranes or molecular sieves, as this removes the need for regeneration of molecular sieves and the decreasing performance due to saturation or fouling. As described in Chapter 4, even an inefficient removal of both products is expected to outperform an efficient removal of a single product,

therefore early optimisation of a single product removal may be a less effective use of resources.

Future work can focus on separation techniques with a recycling of the remaining reaction mixture. Choi *et al.*[4] have shown that water removal alone can be used to achieve high alcohol conversions. Practically, carbonate removal by pervaporation membranes has been demonstrated[5] and in principle, should allow for a 2-step removal process (Figure 6.1), where water is removed in one step, carbonate removed in a second step and the remaining mixture is passed back over a catalyst bed. Membranes have been utilised in other reports demonstrating that this approach is potentially viable.[6,7] The more selective this separation, the less downstream processing (such as by distillation) needs to be performed to achieve a pure product.

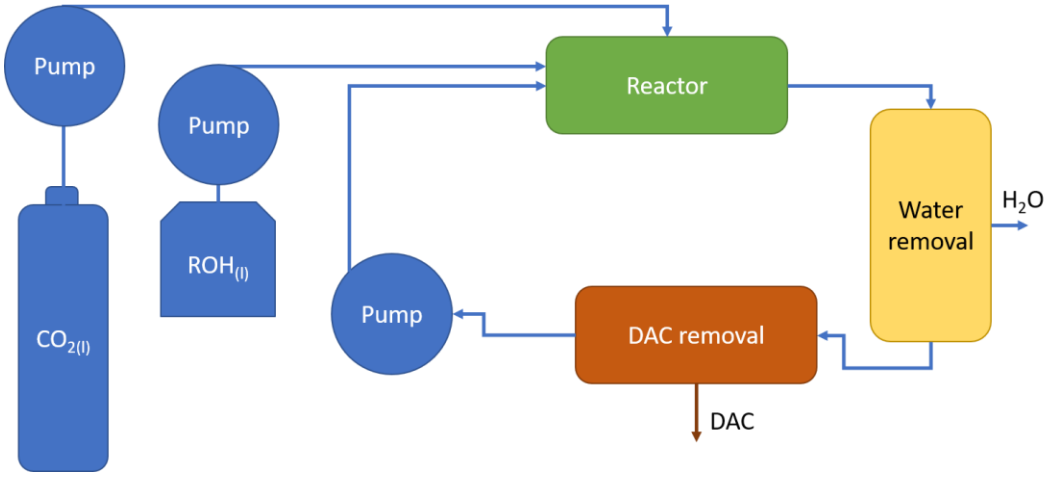

Figure 6.1: Concept for a recirculating reactor with 2-step separation of water and DAC.

Lower pressure systems may also be a target for further investigation, as this would reduce costs for pressuring the system. In Chapter 5 we demonstrated that pressure had a very small impact on the conversion of methanol between 50-200 bar. We chose to focus on high pressure systems due to the potential for product separation by tuning of phase behaviour. However, Li and Zhong[6] demonstrated that low pressure systems are capable of producing DMC with an alcohol conversion of 9% at 4 bar CO_2 when utilising a membrane reactor. Similarly Wang *et al.*[8] demonstrate a DEC system with a similar productivity to our unoptimized system at 1 bar CO_2 and 100 °C compared to our 200 bar CO_2 140 °C. The lowering of pressure to 1 bar may make separation of products by tuning phase behaviour inaccessible, due to the system being further from the near- and supercritical densities, but should allow

for a wider range of membrane materials to be tested, should that method of product removal be investigated.

6.4 Closing remarks

The direct synthesis of dialkyl carbonates without the use of a chemical dehydrating agent is challenging, due to the thermodynamics of the reaction. However chemical dehydrating agents simply shift the problem of product separation to one of dehydrating agent synthesis and regeneration. This increases the carbon footprint of the process and introduces chemicals with toxicities comparable to the phosgene that the direct synthesis seeks to replace. It has been demonstrated in this work, however, that the thermodynamic challenge is not insurmountable. The focus of the direct synthesis needs to be placed not on small gains in activity, but on product separation and catalyst stability, as this route gives the greatest potential gains in terms of process productivity. This takes the thermodynamic challenge and transforms it into an engineering and process design challenge. Solving this problem may allow for the production of DMC, DEC and other carbonates, in a way that is safer and more sustainable than current methods, allowing for the growing demand for these compounds to be met.

6.5 References

(1) Lee, H. J.; Park, S.; Jung, J. C.; Song, I. K. Direct Synthesis of Dimethyl Carbonate from Methanol and Carbon Dioxide over H3PW12O40/CeXZr1-XO2 Catalysts: Effect of Acidity of the Catalysts. *Korean J. Chem. Eng.* **2011**, *28* (7), 1518–1522. https://doi.org/10.1007/s11814-011-0020-x.

(2) Lee, H. J.; Joe, W.; Song, I. K. Direct Synthesis of Dimethyl Carbonate from Methanol and Carbon Dioxide over Transition Metal Oxide/Ce0.6Zr0.4O2 Catalysts: Effect of Acidity and Basicity of the Catalysts. *Korean J. Chem. Eng.* **2012**, *29* (3), 317–322. https://doi.org/10.1007/s11814-011-0185-3.

(3) Lee, H. J.; Park, S.; Song, I. K.; Jung, J. C. Direct Synthesis of Dimethyl Carbonate from Methanol and Carbon Dioxide over Ga2O3/Ce0.6Zr0.4O2 Catalysts: Effect of Acidity and Basicity of the Catalysts. *Catal. Letters* **2011**, *141* (4), 531–537. https://doi.org/10.1007/s10562-010-0544-4.

(4) Choi, J.-C. C.; He, L.-N. N.; Yasuda, H.; Sakakura, T.; Yasudaa, H.; Sakakura, T. Selective and High Yield Synthesis of Dimethyl Carbonate Directly from Carbon Dioxide and Methanol. *Green Chem.* **2002**, *4* (3), 230–234. https://doi.org/10.1039/b200623p.

(5) Wang, L.; Han, X.; Li, J.; Zhan, X.; Chen, J. Separation of Azeotropic Dimethylcarbonate/Methanol Mixtures by Pervaporation: Sorption and Diffusion Behaviors in the Pure and Nano Silica Filled Pdms Membranes.

Sep. Sci. Technol. **2011**, *46* (9), 1396–1405. https://doi.org/10.1080/01496395.2011.571227.

(6) Li, C. F.; Zhong, S. H. Study on Application of Membrane Reactor in Direct Synthesis DMC from CO2 and CH3OH over Cu-KF/MgSiO Catalyst. *Catal. Today* **2003**, *82* (1–4), 83–90. https://doi.org/10.1016/S0920-5861(03)00205-0.

(7) Dibenedetto, A.; Aresta, M.; Angelini, A.; Ethiraj, J.; Aresta, B. M. Synthesis, Characterization, and Use of Nb V/Ce IV-Mixed Oxides in the Direct Carboxylation of Ethanol by Using Pervaporation Membranes for Water Removal. *Chem. - A Eur. J.* **2012**, *18* (33), 10324–10334. https://doi.org/10.1002/chem.201201561.

(8) Wang, J.; Hao, Z.; Wohlrab, S. Continuous CO2 Esterification to Diethyl Carbonate (DEC) at Atmospheric Pressure: Application of Porous Membranes for in-Situ H2O Removal. *Green Chem.* **2017**. https://doi.org/10.1039/C7GC00916J.

Appendix 1 – Interplanar spacings

Interplanar spacing (d) was calculated using the equation below

$$d = \sqrt{\frac{a^2}{h^2 + k^2 + l^2}}$$

Decomposition samples

CeO_2 (1:0)

Angle (2θ)	d-spacing	hkl
28.842	3.093	111
33.415	2.679	200
47.593	1.909	220
56.705	1.622	311
69.676	1.348	400
76.714	1.241	331

CeO_2 (1:0.5)

Angle (2θ)	d-spacing	hkl
28.706	3.107	111
33.058	2.707	200
47.729	1.903	220
56.45	1.628	311
69.285	1.355	400
77.02	1.237	331

CeO_2 (1:0.75)

Angle (2θ)	d-spacing	hkl
28.825	3.094	111
33.109	2.703	200
47.729	1.903	220
56.398	1.630	311

Appendix

CeO_2 (1:1.15)

Angle (2θ)	d-spacing	hkl
28.638	3.114	111
33.381	2.682	200
47.576	1.909	220
56.483	1.627	311

CeO_2 (1:1.5)

Angle (2θ)	d-spacing	hkl
28.791	3.098	111
33.364	2.683	200
47.542	1.911	220
56.620	1.624	311
76.952	1.238	331

CeO_2 (1:2)

Angle (2θ)	d-spacing	hkl
28.74	3.103	111
33.551	2.668	200
47.933	1.896	220
56.620	1.624	311
70.186	1.339	400
76.986	1.237	331

CeO_2 (1:5)

Angle (2θ)	d-spacing	hkl
28.706	3.107	111
33.296	2.688	200
47.933	1.896	220
56.483	1.627	311
69.710	1.347	400
76.748	1.240	331

Appendix

Commercial CeO_2

Angle (2θ)	d-spacing	hkl
28.691	3.108	111
33.226	2.694	200
47.611	1.908	220
56.484	1.627	331
59.187	1.559	222
69.510	1.351	400
76.825	1.239	331
79.268	1.207	420

Precipitation samples

$CeO_{2(P)}$

Angle (2θ)	d-spacing	hkl
28.915	3.085	111
33.370	2.682	200
47.755	1.902	220
56.920	1.616	311
70.195	1.339	400

$Ce_{0.9}Zr_{0.1}O_2$

Angle (2θ)	d-spacing	hkl
28.675	3.110	111
33.115	2.703	200
47.605	1.908	220
56.440	1.629	311
69.700	1.348	400
76.825	1.239	331

$Ce_{0.9}Al_{0.1}O_2$

Angle (2θ)	d-spacing	hkl
28.405	3.139	111
33.100	2.704	200
47.470	1.913	220
56.260	1.633	311
77.065	1.236	331

Appendix

$Ce_{0.75}Zr_{0.25}O_2$

Angle (2θ)	d-spacing	hkl
28.510	3.128	111
33.100	2.704	200
47.560	1.910	220
56.395	1.630	311
76.825	1.239	331

$Ce_{0.5}Zr_{0.5}O_2$

Angle (2θ)	d-spacing	hkl
28.540	3.125	111
32.935	2.717	200
47.545	1.910	220
56.260	1.633	311
69.250	1.355	400
76.855	1.239	331

$Ce_{0.25}Zr_{0.75}O_2$

Angle (2θ)	d-spacing	hkl
29.620	3.013	111
34.045	2.631	200
49.135	1.852	220
58.645	1.572	331

$Ce_{0.1}Zr_{0.9}O_2$

Angle (2θ)	d-spacing	hkl
34.915	2.567	200
49.960	1.824	220
59.560	1.550	331

Appendix 2 – DRIFTS

Catalysts were diluted to 1% w/w with KBr and measurements were taken using a PerkinElmer Frontier FT-IR with DRIFT cell attachment for 32 scans, between 4000 and 600 cm^{-1} at a resolution of 2 cm^{-1}.

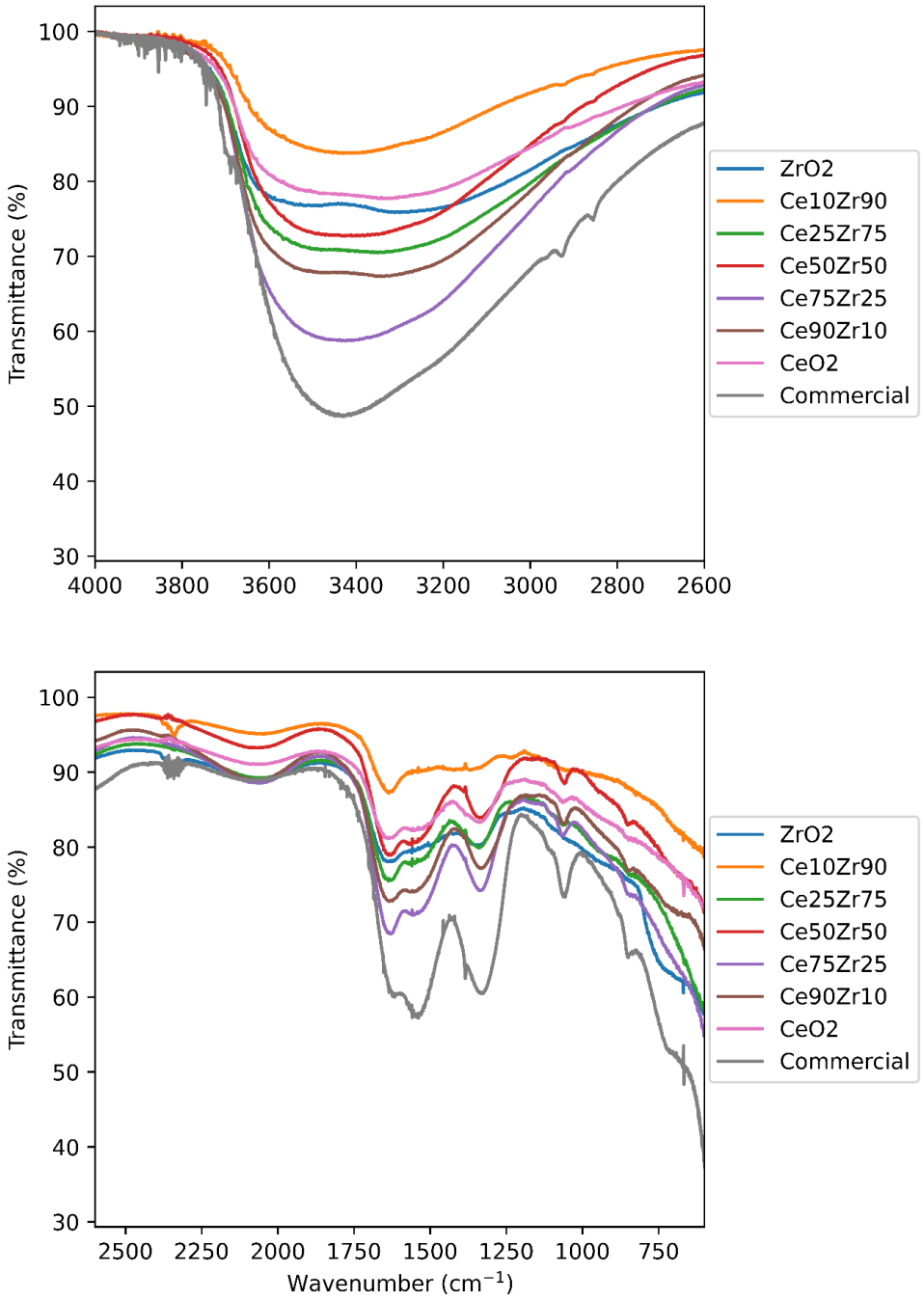

Figure A 1: DRIFTS of pure and mixed metal oxides synthesised in Chapter 2. Top: from 4000-2600 cm^{-1}. Bottom: from 2600-600 cm^{-1}.

Each of the spectra show a broad peak in the region of 3800-2800 cm^{-1} which is potentially residual water or surface hydroxyl species. The band at 1625 cm^{-1} could be attributed to H-O-H bending modes. There may also be some contribution in the 2300–3000 cm^{-1} region which can also be attributed to hydrocarbons C-H stretching which could be due to residual template impurity. The bands between 1000-1500 cm^{-1} could be attributed to carbonate species formed by the adsorption of atmospheric CO_2 to the metal oxide surface. The small band at 1060 cm^{-1} could be attributed to the stretching of Ce-O-C from residual template impurity.

Appendix 3 –Dehydrating agent reaction data

Analysis was performed on a Varian 3900 GC equipped with an FID detector at 300 °C with a H_2 flow rate of 40 $mL.min^{-1}$, air flow rate of 400 $mL.min^{-1}$, and Argon makeup flow rate of 30 $mL.min^{-1}$. Helium was used as a carrier gas at a constant linear velocity of 39.4 $cm.s^{-1}$ through a CP-Sil 5CB column from Agilent (50 m length, 0.32 mm ID, 5 µm film thickness). 0.5 µL of sample was injected with a split ratio of 100 and an injector temperature of 300 °C. The column was held at 50 °C for 5 min, then the temperature ramped up to 70 °C at 3 $°C.min^{-1}$, then to 180 °C at 7 $°C.min^{-1}$, and finally up to 300 °C at 23 $°C.min^{-1}$.

Calibration Curve:

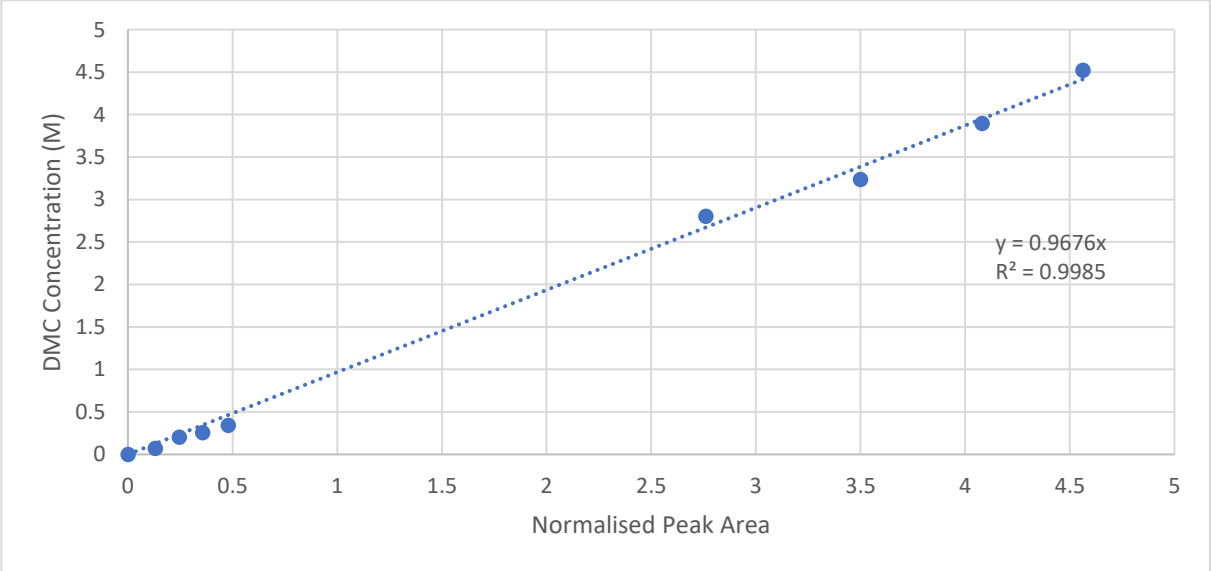

Figure A 2: DMC calibration curve for use in dehydrating agent reactions

Appendix

Table A 1: Compound retention time for dehydrating agent reactions.

Compound	Retention time (min)
Methanol	6.34
DMC	10.49
TMM	12.78
DIC	19.68
Mesitylene	22.61
2-Cyanopyridine	25.52
TMB	44.67

Table A 2: Conversion and concentration data for varying times for dehydrating agents reactions. Reaction conditions: 0.03 g Commercial CeO_2. 1 g methanol, 50 mol% dehydrating agent, 50 bar CO_2 (at 40 °C), 120 °C.

Dehydrating agent	Time (h)	DMC concentration (M)	Methanol Conversion (%)
TMM	1.00	0.012	0.28%
TMM	2.00	0.014	0.32%
TMM	3.00	0.027	0.62%
TMM	4.00	0.053	1.30%
TMM	5.00	0.061	1.40%
TMM	6.00	0.091	2.11%
TMM	20.00	0.259	6.03%
2-cyanopyridine	1.00	0.28	6.79%
2-cyanopyridine	2.00	0.56	13.49%
2-cyanopyridine	3.00	1.22	27.39%
2-cyanopyridine	4.33	1.33	31.29%
2-cyanopyridine	5.00	1.63	40.03%
2-cyanopyridine	6.00	1.53	37.13%
2-cyanopyridine	20.00	3.57	81.64%
DIC	1.00	0.96	19.35%
DIC	2.00	1.34	27.28%
DIC	3.00	1.55	32.08%
DIC	4.00	1.92	38.10%
DIC	5.00	1.84	38.98%
DIC	6.00	2.13	39.84%
DIC	20.00	1.93	46.88%

Curve fit equation:

$$y = a \cdot e^{b \cdot x} + c$$

Where

y = [DMC]

Appendix

a = $[DMC]_0 - [DMC]_{eq}$

b = k_{obs}

x = time

c = $[DMC]_{eq}$

To give the equation:

$$[DMC] = \left([DMC]_0 - [DMC]_{eq}\right) \cdot e^{k_{obs} \cdot t} + [DMC]_{eq}$$

$[DMC]_0$ = 0 for these experiments

The first order rate equation for DMC is:

$$Rate = k_{obs} \cdot [DMC] + Rate_0$$

$[DMC]_{eq}$ is the x-intercept of this equation is therefore:

$$Rate_0 = k_{obs} \cdot [DMC]_{eq}$$

Table A 3: Curve fit coefficients for the three dehydrating agents tested

Dehydrating agent	k_{obs}	$[DMC]_{eq}$	$Rate_0$
TMM	0.010	1.51	0.015
2-cyanopyridine	0.090	4.29	0.386
DIC	0.490	1.93	0.946

Variable Temperature:

Table A 4: Conversion and concentration data for varying temperature for DIC reactions. Reaction conditions: 0.03 g Commercial CeO_2. 1 g methanol, 1.668 g DIC, 50 bar CO_2 (at 40 °C).

Temperature (°C)	Time (h)	DMC concentration (M)	Methanol Conversion (%)
80	2.00	0.19	4.73
80	3.00	0.18	4.40
90	2.00	0.34	8.63
90	3.00	0.46	11.34
100	1.00	0.65	13.89
100	2.00	1.06	22.96
100	3.00	1.01	21.72
100	4.00	1.25	27.04
100	5.00	1.65	35.57
100	6.00	1.39	30.55

110	1.00	0.93	20.27
110	2.00	1.19	24.87
110	4.00	1.29	30.82
110	5.00	0.98	23.90
110	6.00	1.32	33.04
120	1.00	0.96	19.35
120	2.00	1.34	27.28
120	3.00	1.55	32.08
120	4.00	1.92	38.10
120	5.00	1.84	38.98
120	6.00	2.13	39.84

Variable density:

Table A 5: Conversion and concentration data for varying density for DIC reactions. Reactors were weighed before and after pressurisation, though several reactors were too heavy for the balance. Reaction conditions: 0.03 g Commercial CeO_2. 1 g methanol, 1.668 g DIC, 120 °C, 3 h.

Pressure (bar)	Density ($g.mL^{-1}$)	Mass CO_2 (g)	Methanol Conversion (%)	Concentration (M)
30	0.05	—	22.03	0.91
50	0.1	—	32.08	1.55
55	0.15 (0.139)	2.77	26.97	1.13
65	0.2 (0.224)	4.47	24.77	1.03
70	0.25 (0.225)	4.5	25.81	1.06
80	0.4 (0.417)	8.354	2.26	0.1
90	0.5	—	3.41	0.14

Single tests:

Table A 6: Conversion and concentration data for varying catalyst for DIC reactions. Reaction conditions: 0.03 g catalyst. 1 g methanol, 1.668 g DIC, 50 Bar CO_2 (at 40 °C), 100 °C, 2 h.

Catalyst	Conversion (%)	Concentration (M)
$Ce_{0.9}Al_{0.1}O_x$	8.02%	0.321
CeO_2 precipitation	7.81%	0.325
ZrO_2 precipitation	6.93%	0.279
$Ce_{0.1}Zr_{0.9}O_2$	10.32%	0.444
$Ce_{0.5}Zr_{0.5}O_2$	12.04%	0.519
$Ce_{0.25}Zr_{0.75}O_2$	10.90%	0.441
$Ce_{0.75}Zr_{0.25}O_2$	12.24%	0.497
CeO_2 0.75:1 Decomposition	10.40%	0.440
CeO_2 0.5:1 Decomposition	6.87%	0.297

Catalyst stability:

Table A 7: Conversion and concentration data for varying catalyst for DIC reactions. Reaction conditions: 0.03 g catalyst. 1 g methanol, 1.668 g DIC, 50 bar CO_2 (at 4 0°C), 100 °C, 2 h.

Catalyst	Cycle	Conversion (%)	Cumulative TON	Cumulative DMC (mmol)
Commercial CeO_2	1	22.97	41.51	3.01
Commercial CeO_2	2	10.29	56.99	4.37
Commercial CeO_2	3	11.67	74.54	5.90
Commercial CeO_2	4	14.32	96.08	7.78
Commercial CeO_2	5	13.55	116.46	9.56
Commercial CeO_2	6	14.30	137.97	11.43
CeO_2 Precipitation	1	13.72	21.23	1.80
CeO_2 Precipitation	1	13.71	21.21	1.80
CeO_2 Precipitation	2	11.10	38.41	3.26
CeO_2 Precipitation	2	11.18	38.50	3.27
CeO_2 Precipitation	3	12.15	57.21	4.85
CeO_2 Precipitation	3	12.41	57.70	4.89
CeO_2 Precipitation	4	11.79	75.45	6.40
CeO_2 Precipitation	4	11.86	76.05	6.45
CeO_2 Precipitation	5	11.24	92.83	7.88
CeO_2 Precipitation	5	11.53	93.88	7.96
CeO_2 Precipitation	6	15.66	117.06	9.93
CeO_2 Precipitation	6	16.10	118.78	10.08
$Ce_{0.75}Zr_{0.25}O_2$	1	11.79	16.95	1.55
$Ce_{0.75}Zr_{0.25}O_2$	2	11.73	33.80	3.09
$Ce_{0.75}Zr_{0.25}O_2$	3	11.22	49.93	4.56
$Ce_{0.75}Zr_{0.25}O_2$	4	9.92	64.19	5.86
$Ce_{0.75}Zr_{0.25}O_2$	5	11.68	83.90	7.39
$Ce_{0.75}Zr_{0.25}O_2$	6	13.72	103.62	9.19
$Ce_{0.25}Zr_{0.75}O_2$	1	12.88	15.69	1.69
$Ce_{0.25}Zr_{0.75}O_2$	2	12.35	30.72	3.31

$Ce_{0.25}Zr_{0.75}O_2$	3	7.45	39.79	4.29
$Ce_{0.25}Zr_{0.75}O_2$	4	15.36	58.50	6.31
$Ce_{0.25}Zr_{0.75}O_2$	5	15.38	77.21	8.32
$Ce_{0.25}Zr_{0.75}O_2$	6	14.54	94.92	10.23
ZrO_2 Precipitation	1	13.34	14.77	1.75
ZrO_2 Precipitation	1	13.10	14.51	1.72
ZrO_2 Precipitation	2	11.47	27.47	3.26
ZrO_2 Precipitation	2	11.33	27.07	3.21
ZrO_2 Precipitation	3	11.57	40.28	4.77
ZrO_2 Precipitation	3	11.71	40.03	4.74
ZrO_2 Precipitation	4	12.31	53.92	6.39
ZrO_2 Precipitation	4	12.52	53.90	6.39
ZrO_2 Precipitation	5	11.96	67.17	7.96
ZrO_2 Precipitation	5	11.78	66.95	7.93
ZrO_2 Precipitation	6	13.83	82.49	9.78

Appendix 4 – Thermodynamics code implementation

Below is the class as used for thermodynamics in Chapter 4. The purpose of this class is to calculate equilibrium concentrations at a given temperature. With additional functions for temperature correction and setting starting concentration. Using this class with some additional code allows the calculation of concentrations at multiple temperatures, and concentration. Some basic examples are given below and in the ReadMe on GitHub (https://github.com/DeemoONeill/Thermodynamics_class). This was written with no external dependencies; however performance can be improved using scipy and numpy for numerical optimisers and matrix operations.

```
# -*- coding: utf-8 -*-
```

```
"""
Created on Tue Feb  5 16:22:54 2019

@author: Matt O'Neill

Class for performing numerical optimisation to determine
equilibrium
concentrations of reactants and products in an equilibrium limited
reaction (DG > 0) where DH and DS are known.
"""

import math as ma
from collections import deque
from decimal import Decimal, Context, ROUND_FLOOR, MAX_EMAX
from decimal import setcontext
import logging

BAR_TO_PA = 100000
R = 8.314
logging.basicConfig(filename="thermolog.log", level=logging.WARNING)

PRECISIONCONTEXT = Context(Emax=MAX_EMAX, prec=28, rounding=ROUND_FL
OOR)
setcontext(PRECISIONCONTEXT)

class Thermo:

    """Takes values of DH and DS at a given temperature
    ------------------
    Keyword arguments:
    ------------------
    DH -- Enthalpy change of the reaction at Temperature T (float)

    DS -- Entropy change of the reaction at Temperature T (float)

    T -
- Temperature at which DH and DS were calculated (default 298)

    ------------
    Key Methods:
    ------------
    Reactants(names, starting_concentrations, stoichiometry)
    Products(names, starting_concentrations, stoichiometry)
    sets properties of the reactants and products - names,
    starting_concentrations and stoichiometrys should all be given a
s
    lists (even for single values)
```

```
    dictionary_flush()
    Sets all keys in the dictionary to empty lists

    return_dictionary()
    Returns the dictionary of calculated values includes T, DH, DS,
    product and reactant concentrations

    thermodynamics(temperature = 298, error=1e-09, p=20, K=True,
    return_dict = False)
    calculates reactant and product concentrations for the given
    temperature. Takes Temperature, error, P, K, and return_dict
    arguments. error gives the tolerance between Keq calculated from
 DG
    and Keq calculated by products/reactants
    p is used in the same way as in PID systems, it is multiplied by
 the
    difference between the setpoint and current measurement, and use
d to
    adjust the concentration values.
    K is whether the values for temperature are saved in Kelvin or C
elsius
    (no support for F)
    return_dict returns the dictionary at the end of the calculation
.
    mainly used for single calculations
    """
    def __init__(self, DH=None, DS=None, T=298):

        self.DSstd = Decimal(DS)
        self.DHstd = Decimal(DH)
        self._DS_T = Decimal(self.DSstd)
        self._DH_T = Decimal(self.DHstd)
        self._dictionary = {'DH': [], 'DS': [], 'T': []}
        self._T0 = Decimal(T)

    def _Calc_DG(self, T):

        self.DG = self._DH_T - T * self._DS_T
        return self.DG

    def Reactants(self, names, starting_concentrations, stoichiometr
y,
                  heat_capacities=None):

        """Sets the reactant properties for the reaction
        ------------------
        Keyword arguments:
        ------------------
```

```
        names -- a list of chemical names
        starting_concentrations -- a list of starting concentrations
        stoichiometry -- takes a list of the reaction stoichiometry
        --------
        example:
        --------
        for the reaction CO2 + 2MeOH --> DMC + H2O

        dmc = thermo(DH=-24, DS=-0.12, T=298)
        dmc.Reactants(['CO2', 'MeOH'], [8, 24.5], [1,2])
        """

        self._ReactantNames = names
        self._ReactantStartingConcentration = list(
            map(Decimal, starting_concentrations)
            )
        self._ReactantStoichiometry = stoichiometry
        self._ReactantHeatCapacities = list(
            map(Decimal, heat_capacities)
            ) if heat_capacities else heat_capacities
        for name in self._ReactantNames:
            try:
                self._dictionary[name]
            except KeyError:
                self._dictionary[name] = []

    def Products(self, names, starting_concentrations, stoichiometry
,
                 heat_capacities=None):
        """Sets the product properties for the reaction
        ------------------
        Keyword arguments:
        ------------------
        names -- a list of chemical names
        starting_concentrations -- a list of starting concentrations
        stoichiometry -- takes a list of the reaction stoichiometry
        --------
        example:
        --------
        for the reaction CO2 + 2MeOH --> DMC + H2O

        dmc = thermo(DH = -24, DS = -0.12, T = 298)
        dmc.Products(['DMC', 'H2O'], [0, 0], [1,1])

        """
        self._ProductNames = names
        self._ProductStartingConcentration = list(
            map(Decimal, starting_concentrations))
```

```
        self._ProductStoichiometry = list(map(Decimal, stoichiometry
))
        self._ProductHeatCapacities = list(
            map(Decimal, heat_capacities)
            ) if heat_capacities else heat_capacities
        for name in self._ProductNames:
            try:
                self._dictionary[name]
            except KeyError:
                self._dictionary[name] = []

    def _temperature_correction(self, T):
        products = sum([stoic*product for stoic, product in zip(self
._ProductStoichiometry, self._ProductHeatCapacities)])
        reactants = sum([stoic*reactant for stoic, reactant in zip(s
elf._ReactantStoichiometry, self._ReactantHeatCapacities)])
        self._DH_T = self.DHstd + (products - reactants) * Decimal(T
 - self._T0)
        self._DS_T = self.DSstd + (products - reactants) * Decimal(m
a.log(T/self._T0))
        return self._Calc_DG(T)

    def _appender(self, T, DG):
        self._dictionary['DS'].append(self._DS_T)
        self._dictionary['DH'].append(self._DH_T)
        if self._dictionary.get("DG"):
            self._dictionary['DG'].append(DG)
        else:
            self._dictionary['DG'] = [DG]
        self._dictionary['T'].append(T)
        return

    def flush_dictionary(self):
        """Flushes the dictionary, sets each key to an empty list
        """
        for key in self._dictionary:
            self._dictionary[key] = []

    def return_dictionary(self):
        """Returns the data containing dictionary"""
        return self._dictionary

    def thermodynamics(self, temperature=298, error=1e-
16, p=20, K=True,
                       Tcorrection=False, Pcorrection = False, P=Non
e, return_dict=False):
        """Calculates the equilibrium concentrations for each of the
```

```
        products and reactants in the reaction at a given temperatur
e.

        first DG is calculated using:
        DG = DH - TDS

        followed by the equilibrium constant Keq:
        Keq = exp(-DG/RT)

        The concentrations of each of the reactants and products are
 then
        adjusted until this valuse of Keq is reached using the equat
ion:
        Keq = [Products]**S/[Reactants]**S

        ------------------
        Keyword arguments:
        ------------------

        temperature -
- The temperature in Kelvin at which the equilibrium
        concentrations should be calculated (default 298)

        error -- tolerance for when Keq calculated from DG and from
        concentrations are considered equal (default 1e-9)

        p -
- The proportional correction applied to the result. if the
        calculation is slow, try adjusting the value for P (default
20)

        K -
- whether or not Tempertature is appended to the dictionary in
        Kelvin (True) or °C (False). (default True)

        return_dict -
- whether to return the dictionary after calculation
        (default False)


        p = Decimal(p)
        if Tcorrection:
            DG = self._temperature_correction(temperature)
        else:
            DG = self._Calc_DG(temperature)

        self.DGkeq = Decimal(ma.exp(-
(DG*1000)/(Decimal(8.314)*Decimal(temperature))))
```

```
        if "DGkeq" in self._dictionary.keys():
            self._dictionary["DGkeq"].append(self.DGkeq)
        else:
            self._dictionary["DGkeq"] = [self.DGkeq]
        pconc = deque(self._ProductStartingConcentration.copy())
        sconc = deque(self._ReactantStartingConcentration.copy())
        denominator = 1
        numerator = 1
        # Reactants
        for i, value in enumerate(sconc):
            denominator *= value ** self._ReactantStoichiometry[i]
        # initial product
        for i, value in enumerate(pconc):
            numerator *= value ** self._ProductStoichiometry[i]
        Conckeq = numerator / denominator
        cycles = 0
        logging.debug(f"Before adjustment: pconc = {pconc}, sconc =
{sconc}")
        adjustment = Decimal(p//5)
        while ma.isclose(self.DGkeq, Conckeq, rel_tol=error) is Fals
e:
            iterator = Decimal(p)*(Decimal(self.DGkeq)-
Decimal(Conckeq))
            numerator = 1
            denominator = 1
            if cycles % 20 == 0:
                logging.debug(f"iterator = {iterator}, conc keq = {C
onckeq}")
                logging.debug(f"error = {Decimal(self.DGkeq)-
Decimal(Conckeq)}")
                logging.debug(f"p = {p}")
            # Products
            for i, value in enumerate(sconc):
                working = value
                if working - (iterator * self._ReactantStoichiometry
[i]) < 0:
                    iterator = iterator/100000
                    p = p/10
                working -= iterator * self._ReactantStoichiometry[i]
                denominator *= working ** self._ReactantStoichiometr
y[i]
                sconc[i] = working

            for i, value in enumerate(pconc):
                working = value
                if working + (iterator * self._ProductStoichiometry[
i]) < 0:
                    iterator = iterator/100000
```

```
                    p = p/10
                working += iterator * self._ProductStoichiometry[i]
                numerator *= working ** self._ProductStoichiometry[i
]
                pconc[i] = working
            if cycles % 10000 == 0 and cycles > 0:
                p = Decimal(p) - Decimal(adjustment) if Decimal(p) -
 Decimal(adjustment) > 0 else 1
                logging.debug(f"p = {p}")
            Conckeq = numerator / denominator
            cycles += 1
        logging.debug(f"After adjustment: Numerator = {numerator}, p
conc = {pconc}, sconc = {sconc}")
        for i, svalue in enumerate(sconc):
            self._dictionary[self._ReactantNames[i]].append(svalue)
        for i, pvalue in enumerate(pconc):
            self._dictionary[self._ProductNames[i]].append(pvalue)
        if K:
            self._appender(temperature, DG)
        else:
            self._appender((temperature-273), DG)
        if return_dict:
            return self.return_dictionary()

    @staticmethod
    def temp_corrected_Cp(shomate_constants, T, kmol=False):
        t = Decimal(T)/Decimal(1000)
        A, B, C, D, E = shomate_constants
        if kmol:
            return (A + B*t + C*t**2 + D*t**3 + E/(t**2))/1000
        else:
            return A + B*t + C*t**2 + D*t**3 + E/(t**2)

    @staticmethod
    def calcKeqfromDG(DG, T):
        return ma.exp(-(DG*1000)/(8.314*T))

    @staticmethod
    def calcKeqfromDHDS(DH, DS, T):
        DHcomp = (DH*1000)/(8.314*T)
        DScomp = (DS*1000)/(8.314)
        return ma.exp(DHcomp-DScomp)

    def P_correction(self, DG, P, T, P0 = 1):
        DG = DG * 1000
        return (DG - ((Decimal(R) * Decimal(T)) * Decimal(ma.log((De
cimal(P)/P0))))))/1000
```

```
def srk_p(Tc, Pc, T, d, w, Mr):
    """SRK equation to calculate pressure
    from a given density for a compound

    Arguments:
        Tc {Float} -- Critical Temperature [K]
        Pc {Float} -- Critical Pressure [Pa]
        T {Numeric} -- Temperature [K]
        d {Float} -- Density [g/ml]
        w {Float} -- Acentric factor
        Mr {Float} -- Molecular mass [kg/mol]

    Returns:
        P {Float} -- Pressure [Pa]
    """
    v = Mr/(d*1000)
    #Setup logic for the equation
    aC = 0.42748 * (((R**2)*Tc**2)/(Pc))
    b = 0.08664*((R*Tc)/Pc)
    fT = (1 + (0.48+(1.574*w)-(0.176*w**2))*(1-(T/Tc)**0.5))**2
    aT = aC * fT
    #setting the value of P according the the equation.
    P=(((R*T)/(v-b)) - (aT)/(v*(v+b)))
    return P
```

Code snippets

Instantiating the class

```
# Instantiating the class
dmc = Thermo(DH=-27.19, DS=-0.1795)

# Starting concentrations and stoichiometries
dmc_start = {"names": ["MeOH", "CO2"],
             "starting_concentrations": [24.7, 1],
             "stoichiometry": [2, 1]}

dmc_prod = {"names": ["DMC", "H2O"],
             "starting_concentrations": [0, 0],
             "stoichiometry": [1, 1]}

# Using **kwargs to pass the dictionary of concentrations
# and stoichiometries to the Reactants and Products functions.
dmc.Reactants(**dmc_start)
dmc.Products(**dmc_prod)
```

dmc_prod and dmc_start starting concentrations can be changed to calculate the effects of ppm levels of water or DMC in the starting mixture or the effect of changing CO_2 density or MeOH:CO_2 Ratio

Calculation across a range of temperatures:

```
for T in range(start = 297, stop = 417, step = 4):
    dmc.Products(**dmc_prod)
    dmc.Reactants(**dmc_start)
    dmc.thermodynamics(T, p = 500)
```

Appendix 5 – Synthesis of surface modified CeO_2

Cerium oxide prepared as described in Chapter 2.2.2 was modified using 1H,1H,2H,2H-Perfluorooctyltriethoxysilane (FOTS).

First, 1 g of CeO_2 was washed at 80 °C in H_2NO_3 (pH 4), this was centrifuged, washed with deionised water, and dried under vacuum. 0.2 g was suspended in 30 mL dry THF (distilled from sodium). 0.1 mL FOTS was then added and stirred at room temperature for 72 h, before filtering with a Buchner funnel and washing with ethanol and deionised water. The catalyst was tested as described in Chapter 5.3.1. Due to the poor improvement in performance, this was not tested further.

Appendix 6 – Batch without dehydrating agent data

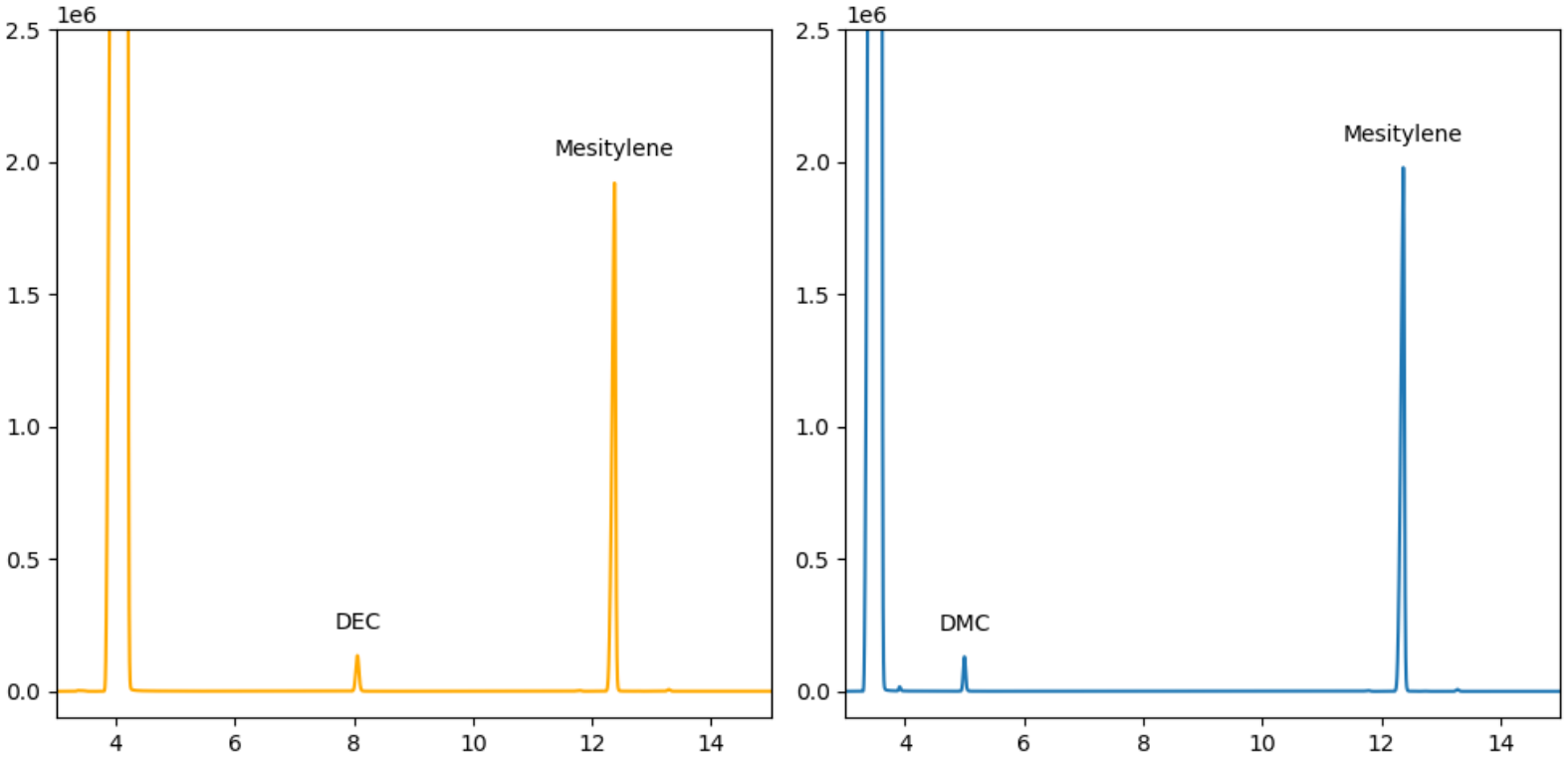

Figure A 3: Example GC for DEC (left) and DMC (right) with mesitylene as a standard. Small peak at 3.9 minutes is Mono-methyl carbonate but was not quantified. Peaks surrounding Mesitylene are small quantities of impurities.

Table A 8: Compound retention time for dehydrating agent free reactions.

Compound	Retention time (min)
Methanol	3.51
Ethanol	4.01
DMC	5.00
DEC	8.06
Mesitylene	12.38

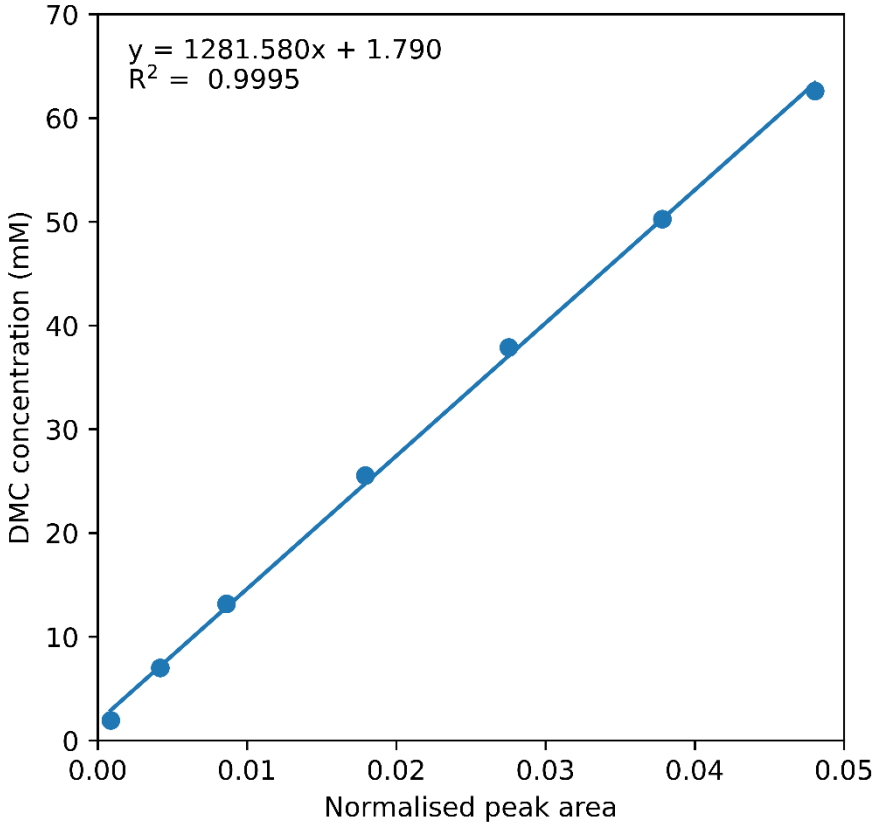

Figure A 4: Calibration curve for DMC, plotted as DMC concentration against DMC peak area, normalised with mesitylene peak area.

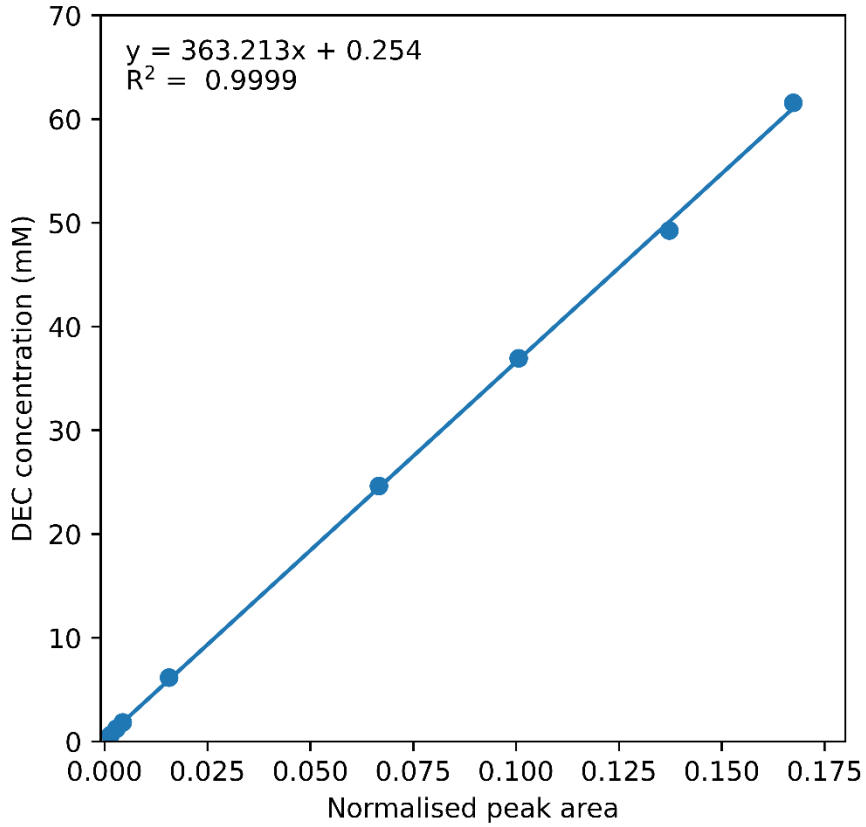

Figure A 5: Calibration curve for DEC, plotted as DEC concentration against DEC peak area, normalised with mesitylene peak area.

Forward reactions

Table A 9: Conversion and concentration data for varying times and temperatures for dehydrating agent free reactions. Reaction conditions: 0.3 g Commercial CeO_2. 5 mL methanol, 70 bar CO_2 (at 40 °C).

T (°C)	Time (h)	[DMC] (mM)	Methanol conversion (%)
140	0.5	23.95	0.194
140	0.5	16.25	0.131
140	1	37.62	0.304
140	1	33.34	0.270
140	1	33.83	0.274
140	2	45.22	0.366
140	2	52.44	0.424
140	2	52.91	0.428
140	3	36.24	0.293
140	3	60.33	0.488
140	3	59.86	0.484
140	6	52.38	0.424

140	6	40.02	0.324
140	6	59.65	0.483
140	20	55.66	0.450
120	0.5	3.48	0.028
120	0.5	4.86	0.039
120	1	12.95	0.105
120	1	11.26	0.091
120	1	8.88	0.072
120	2	16.58	0.134
120	2	21.49	0.174
120	3	31.80	0.257
120	3	25.27	0.204
120	3	29.94	0.242
120	6	53.06	0.429
120	6	32.34	0.262
120	6	35.42	0.287
120	20	57.42	0.465
120	30	78.21	0.633
100	0.5	0.84	0.007
100	0.5	2.28	0.018
100	0.5	2.20	0.018
100	1	1.58	0.013
100	1	3.43	0.028
100	1	3.22	0.026
100	2	4.24	0.034
100	2	4.49	0.036
100	3	6.40	0.052
100	3	8.01	0.065
100	6	12.94	0.105
100	6	12.49	0.101
100	6	10.76	0.087
100	30	47.59	0.385

Reverse reactions

Table A 10: Conversion and concentration data for varying times and temperatures for reverse dehydrating agent free reactions. Reaction conditions: 0.3 g Commercial CeO_2. 5 mL methanol, 70 bar CO_2 (at 40 °C).

T (°C)	Time (h)	[DMC] (mM)	Methanol conversion (%)
140	0	123.56	1.000
140	0.5	105.87	0.857
140	2	73.85	0.598
140	6	63.67	0.515
140	20	68.27	0.552
120	0	156.81	1.269
120	0.5	144.24	1.167
120	1	140.44	1.136
120	2	137.65	1.114
120	3	134.42	1.088
120	5	117.31	0.949
120	6	114.74	0.928
100	0	154.52	1.250
100	0.5	149.15	1.207
100	1	149.27	1.208
100	2	148.38	1.201
100	3	147.39	1.192
100	5	145.46	1.177
100	6	146.02	1.181

Ethanol 140°C

Table A 11: Conversion and concentration data for varying times for dehydrating agent free synthesis of DEC. Reaction conditions: 0.3 g Commercial CeO_2. 5 mL ethanol, 70 bar CO_2 (at 40 °C).

Time (h)	[DEC] (mM)	Ethanol conversion (%)
0.5	5.56	0.065
0.5	9.22	0.108
0.5	4.35	0.051
1	12.98	0.152
1	18.43	0.215
1	15.53	0.181
2	18.12	0.212
2	24.48	0.286
2	16.89	0.197
3	17.98	0.210
3	22.22	0.259

3	29.00	0.339
5	25.24	0.295
5	18.31	0.214
5	24.32	0.284
6	27.50	0.321
6	21.31	0.249
6	21.04	0.246

Appendix 7 – Flow Data

Methanol Variable temperature

Table A 12: Conversion and concentration data for varying times and temperatures for flow DMC dehydrating agent free reactions. Reaction conditions: 0.3 g Commercial CeO_2. 0.2 mL.min^{-1} methanol, 200 bar1mL.min^{-1} CO_2).

Time (h)	Temperature (°C)	[DMC] (mM)	Methanol Conversion (%)
0.5	80	3.70	0.030
1	80	2.89	0.023
1.5	80	2.93	0.024
2	90	3.76	0.030
2.5	90	4.54	0.037
3	90	4.99	0.040
3.5	90	5.30	0.043
4	100	6.95	0.056
4.5	100	8.07	0.065
5	100	8.25	0.067
5.5	100	11.15	0.090
6	110	15.14	0.123
6.5	110	14.33	0.116
7	110	14.63	0.119
7.5	110	14.42	0.117
8	120	11.75	0.095
8.5	120	19.84	0.161
9	120	21.10	0.171
9.5	120	19.94	0.162
10	130	26.78	0.217
10.5	130	30.37	0.246
11	130	30.02	0.243
11.5	130	30.44	0.247
12	140	38.61	0.313
12.5	140	41.46	0.336
13	140	40.86	0.331
13.5	140	41.07	0.333

Ethanol Variable temperature

Table A 13: Conversion and concentration data for varying times and temperatures for flow DEC dehydrating agent free reactions. Reaction conditions: 0.3 g Commercial CeO_2. 0.2 mL.min^{-1} ethanol, 200 bar1mL.min^{-1} CO_2.

Time (h)	Temperature (°C)	[DEC] (mM)	Ethanol conversion (%)
0.5	80	0.00	0.002
1	80	1.63	0.004
1.5	80	1.60	0.004
2	80	1.54	0.004
2.5	100	1.79	0.006
3	100	2.36	0.011
3.5	100	2.41	0.011
4	100	2.41	0.011
4.5	120	4.18	0.025
5	120	5.47	0.035
5.5	120	5.59	0.036
6	120	5.42	0.035
6.5	140	11.43	0.086
7	140	14.91	0.114
7.5	140	14.32	0.111
8	140	15.31	0.119

Methanol flowrate CO_2 flowrate = 1mL.min^{-1}

Table A 14 Conversion and concentration data for varying flow rates for flow DMC dehydrating agent free reactions. Reaction conditions: 3 g Commercial CeO_2.140 °C, 200 bar 1mL.min^{-1} CO_2.

Methanol flow rate (mL.min^{-1})	Time (h)	[DMC] (mM)	Methanol conversion (%)
0.2	0.50	42.12	0.341
0.3	0.83	46.76	0.378
0.3	1.17	41.07	0.332
0.3	1.50	43.95	0.356
0.4	1.75	41.79	0.338
0.4	2.00	40.47	0.327
0.4	2.25	40.06	0.324
0.4	2.50	40.02	0.324
0.5	2.70	36.21	0.293
0.5	2.90	34.87	0.282
0.5	3.10	34.46	0.279
0.5	3.30	34.51	0.279
0.6	3.47	31.34	0.254
0.6	3.63	29.77	0.241
0.6	3.80	29.20	0.236

0.6	3.97	29.36	0.238
0.7	4.11	26.92	0.218
0.7	4.25	25.90	0.210
0.7	4.40	25.46	0.206
0.7	4.54	25.53	0.207
0.8	4.66	22.71	0.184
0.8	4.79	21.85	0.177
0.8	4.91	21.72	0.176
0.8	5.04	21.22	0.172
0.9	5.15	19.57	0.158
0.9	5.26	18.54	0.150
0.9	5.37	18.38	0.149
0.9	5.48	18.12	0.147
1	5.58	16.74	0.135
1	5.68	16.08	0.130
1	5.78	15.83	0.128
1	5.88	15.70	0.127

Ethanol Flowrate. CO_2 flowrate = 1mL.min^{-1}

Table A 15: Conversion and concentration data for varying flow rates for flow DEC dehydrating agent free reactions. Reaction conditions: 3 g Commercial CeO_2.140 °C, 200 bar 1mL.min^{-1} CO_2.

Ethanol flow rate (mL.min^{-1})	Time (h)	[DEC] (mM)	Ethanol conversion (%)
0.2	0.50	37.02	0.587
0.2	1.00	50.25	0.432
0.3	1.33	54.42	0.635
0.3	1.67	51.49	0.601
0.3	2.00	49.45	0.577
0.4	2.25	49.37	0.577
0.4	2.50	44.51	0.520
0.4	2.75	42.63	0.498
0.5	2.95	39.08	0.456
0.5	3.15	37.47	0.438
0.5	3.35	36.43	0.425
0.6	3.52	31.10	0.363
0.6	3.68	30.18	0.352
0.6	3.85	29.99	0.350
0.7	3.99	27.71	0.324
0.7	4.14	26.46	0.309
0.7	4.28	26.32	0.307
0.8	4.40	25.90	0.302
0.8	4.53	24.38	0.285
0.8	4.65	24.08	0.281

0.9	4.76	20.78	0.243
0.9	4.88	18.70	0.218
0.9	4.99	18.69	0.218
1	5.09	17.51	0.204
1	5.19	16.79	0.196

Catalyst stability

Long term Commercial Cerium oxide stability for DMC synthesis

Table A 16: Conversion and concentration data catalyst stability for DMC synthesis in flow dehydrating agent free reactions. Reaction conditions: 0.3 g Commercial CeO_2.140 °C, 0.2 mL.min^{-1} MeOH 200 bar 1mL.min^{-1} CO_2.

Time (h)	[DMC] (mM)	Methanol conversion (%)	Activity
17	31.39	0.254	0.94
17	32.58	0.264	0.98
17	33.25	0.269	1.00
24	27.31	0.221	0.82
24	27.57	0.223	0.83
24	28.78	0.233	0.87
42	29.18	0.236	0.88
42	28.65	0.232	0.86
42	28.36	0.229	0.85
48	25.72	0.208	0.77
48	24.90	0.201	0.75
66	24.36	0.197	0.73
74	22.15	0.179	0.67
74	22.62	0.183	0.68
74	22.50	0.182	0.68
96.5	12.90	0.104	0.39
96.5	12.91	0.104	0.39

Long term Commercial Cerium oxide stability for DEC synthesis

Table A 17: Conversion and concentration data catalyst stability for DMC synthesis in flow dehydrating agent free reactions. Reaction conditions: 0.3 g Commercial CeO_2.140 °C, 0.2 mL.min^{-1} EtOH 200 bar 1 mL.min^{-1} CO_2.

Time (h)	[DEC] (mM)	Ethanol conversion (%)	activity
0.5	14.52	0.170	1.00
1	14.76	0.172	1.02
1.5	14.40	0.168	0.99
2	14.35	0.168	0.99
3	13.75	0.161	0.95
4	13.27	0.155	0.91

5	12.95	0.151	0.89
6	12.48	0.146	0.86
7	11.86	0.139	0.82
8	11.44	0.134	0.79
9	10.84	0.127	0.75
10	10.26	0.120	0.71
11	9.90	0.116	0.68
12	9.42	0.110	0.65
14	8.52	0.099	0.59
14.5	8.40	0.098	0.58
15	8.12	0.095	0.56

Commercial ceria accelerated aging

Table A 18 Conversion and concentration data for accelerated aging in flow dehydrating agent free reactions. Reaction conditions: 0.3 g Commercial CeO_2. 0.2 mL.min^{-1} MeOH, 200 bar 1mL.min^{-1} CO_2.

Time (h)	Temperature (°C)	[DMC] (mM)	Methanol conversion (%)
0.5	140	37.23	0.301
1	140	35.59	0.288
1.5	140	34.35	0.278
2	140	33.07	0.268
2.5	ΔT	13.77	0.111
3	100	4.71	0.038
3.5	100	4.65	0.038
4	100	4.61	0.037
4.5	100	4.56	0.037
5	100	4.46	0.036
5.5	ΔT	22.14	0.179
6	140	30.58	0.247
6.5	140	30.59	0.248
7	140	29.62	0.240
7.5	140	29.30	0.237
8	140	26.96	0.218
8.5	ΔT	8.18	0.066
9	100	3.55	0.029
9.5	100	3.44	0.028
10	100	3.47	0.028
10.5	100	3.44	0.028
11	ΔT	15.47	0.125
11.5	140	27.95	0.226
12	140	27.18	0.220
12.5	140	27.11	0.219
13	140	26.68	0.216
13.5	140	26.30	0.213

14	ΔT	10.51	0.085
14.5	100	3.19	0.026
15	100	3.15	0.025
15.5	100	3.12	0.025
16	100	3.08	0.025
16.5	100	3.10	0.025

$Ce_{0.75}Zr_{0.25}O_2$ accelerated aging

Table A 19: Conversion and concentration data for accelerated aging in flow dehydrating agent free reactions. Reaction conditions: 0.3 g $Ce_{0.75}Zr_{0.25}O_2$,. 0.2 mL.min^{-1} MeOH, 200 bar 1mL.min^{-1} CO_2.

Time (h)	Temperature (°C)	[DMC] (mM)	Methanol conversion (%)
0.5	140	4.424	0.0358
1	140	3.971	0.0321
1.5	140	4.419	0.0358
2	140	4.542	0.0368
2.5	ΔT	2.701	0.0219
3	100	2.050	0.0166
3.5	100	2.059	0.0167
4	100	2.085	0.0169
4.5	100	2.078	0.0168
5	100	2.106	0.0170
5.5	ΔT	3.901	0.0316
6	140	4.621	0.0374
6.5	140	4.550	0.0368
7	140	4.523	0.0366
7.5	140	4.479	0.0362
8	140	4.461	0.0361
8.5	ΔT	2.517	0.0204
9	100	1.984	0.0161
9.5	100	2.004	0.0162
10	100	2.011	0.0163
10.5	ΔT	3.523	0.0285
11	140	4.118	0.0333
11.5	140	4.186	0.0339
12	140	4.204	0.0340
12.5	140	4.106	0.0332
13	140	4.146	0.0336
13.5	ΔT	2.602	0.0211
14	100	1.962	0.0159
14.5	100	1.974	0.0160
15	100	1.976	0.0160
15.5	100	1.975	0.0160
16	100	1.972	0.0160

Appendix 8 – Product stability NMR

The chemical shift for DMC changes slightly depending on the pH. At pH 3 DMC has a chemical shift of 3.62 in DMSO. The splitting of the methanol is dependant on the water present. With dry methanol, DMSO and DMC a doublet and quartet is observed due to the coupling of the CH_3 group with the -OH group

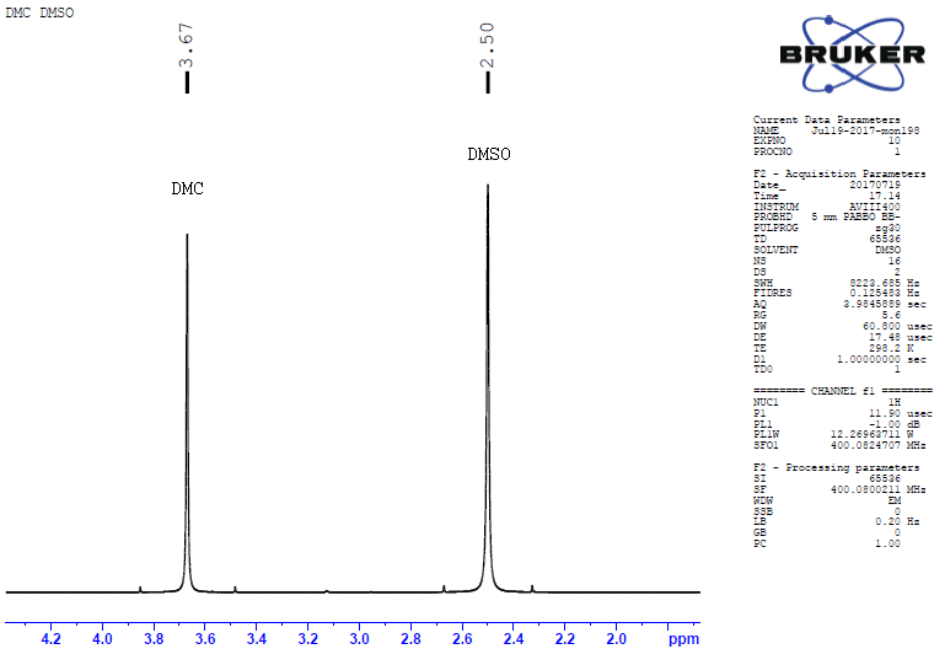


```
Current Data Parameters
NAME       Jul19-2017-mon198
EXPNO                     10
PROCNO                     1

F2 - Acquisition Parameters
Date_           20170719
Time                17.14
INSTRUM          AVIII400
PROBHD    5 mm PABBO BB-
PULPROG             zg30
TD                 65536
SOLVENT             DMSO
NS                    16
DS                     2
SWH              8223.685 Hz
FIDRES           0.125483 Hz
AQ               3.9845889 sec
RG                     5.6
DW                60.800 usec
DE                17.48 usec
TE                298.2 K
D1              1.00000000 sec
TD0                    1

======== CHANNEL f1 ========
NUC1                   1H
P1                 11.90 usec
PL1                -1.00 dB
PL1W         12.26968711 W
SFO1         400.0824707 MHz

F2 - Processing parameters
SI                 65536
SF           400.0800211 MHz
WDW                   EM
SSB                    0
LB                  0.20 Hz
GB                     0
PC                  1.00
```

Figure A 6: NMR spectrum of DMC in DMSO

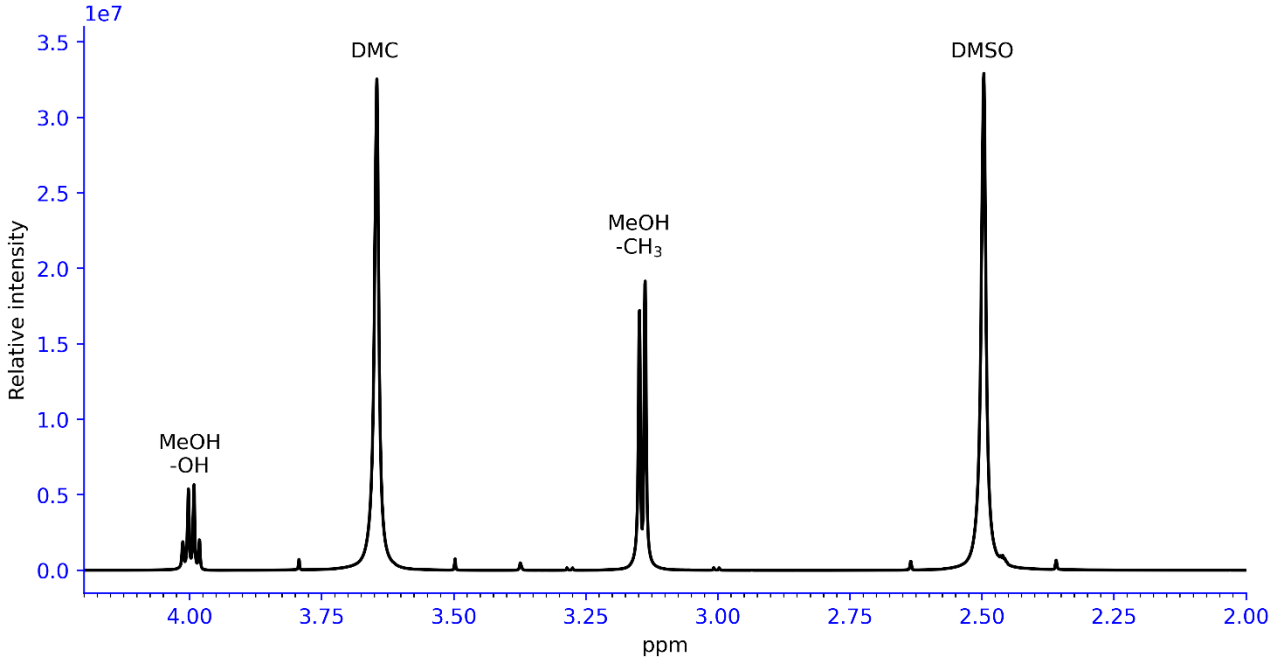

Figure A 7: NMR of DMC and MeOH in DMSO

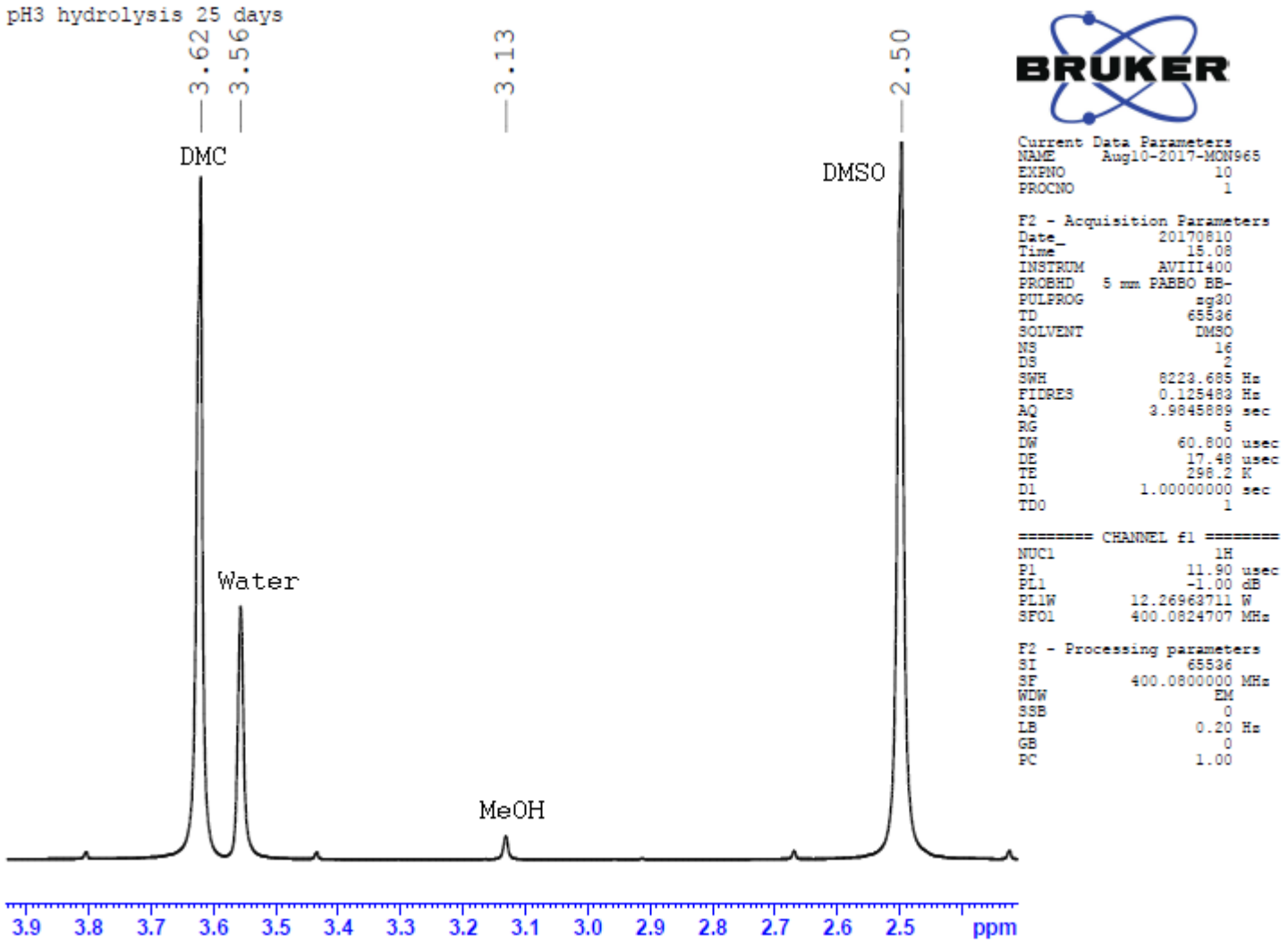

Figure A 8: Spectrum showing 25th day of DMC hydrolysis at 80°C

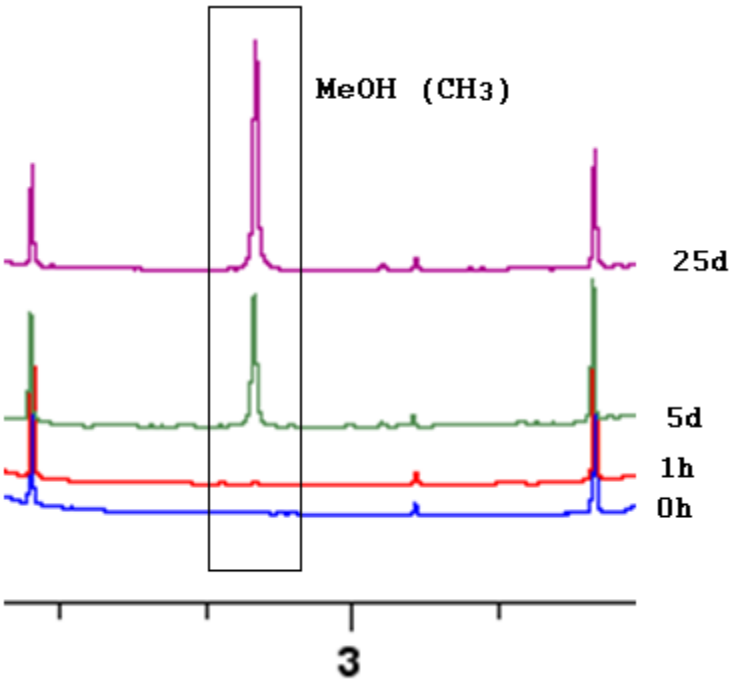

Figure A 9: Growth of methanol peak from 0h (blue), 1h (red), 5d (green), 25d (magenta)

Table A 20: Concentration of DMC over time in DMSO at pH 3 at 80 and 100 °C

T (°C)	Time (h)	[DMC] (M)
80	0	5.190
	1	5.188
	24	5.181
	48	5.171
	120	5.138
	144	5.131
	288	5.093
	312	5.088
	360	5.079
	384	5.072
100	0	5.190
	1	5.184
	24	5.172
	48	5.150
	120	5.127
	144	5.114
	168	5.099
	192	5.084

Appendix 9 – High Pressure NMR

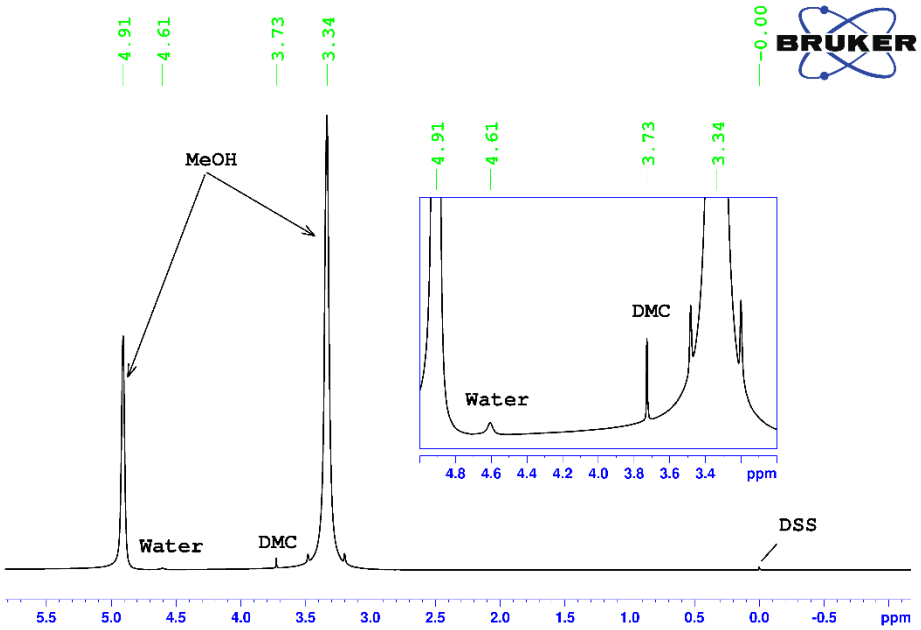

Figure A 10: NMR of 0.4% DMC and water mixture in methanol with DSS solvent. Conditions ambient temperature and pressure. Inset: zoomed in view of the region containing the characteristic DMC and water peaks.

In order to confirm the assignment of water at 4.61 ppm 3 NMR were measured with increasing water concentration shown in

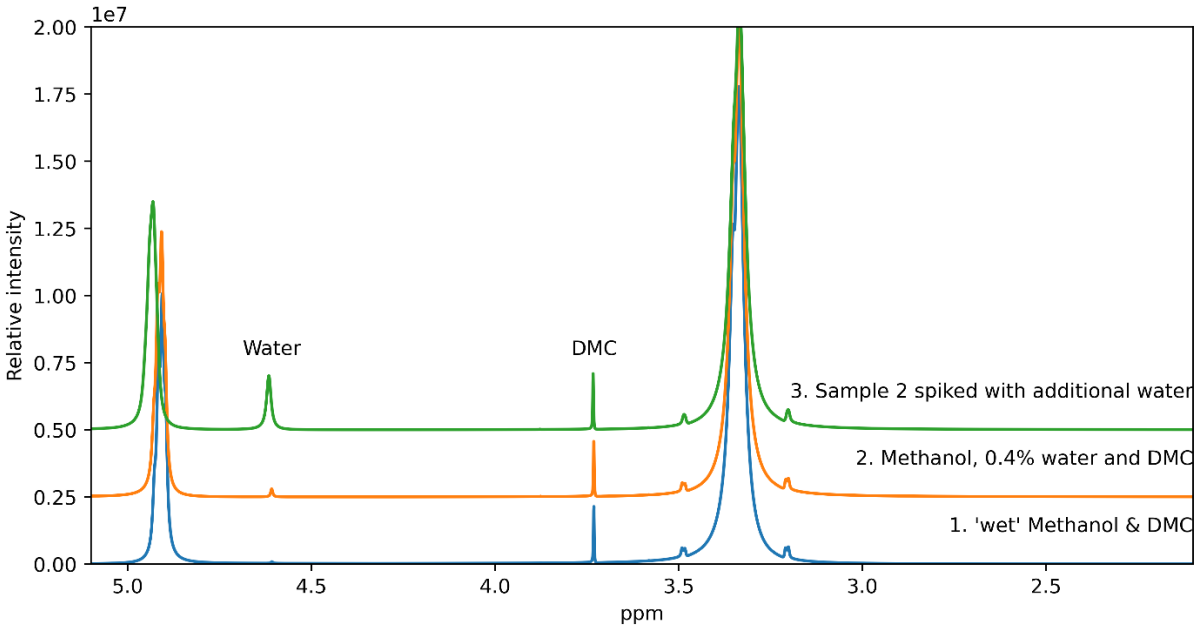

Figure A 11: Growth of water peak at 4.6 ppm with increasing water concentration. Conditions: 25°C 1) 0.4% DMC in methanol. 2) 0.4% DMC and water in methanol. 3) 0.4% DMC and water in methanol, spiked with an additional 10 µL

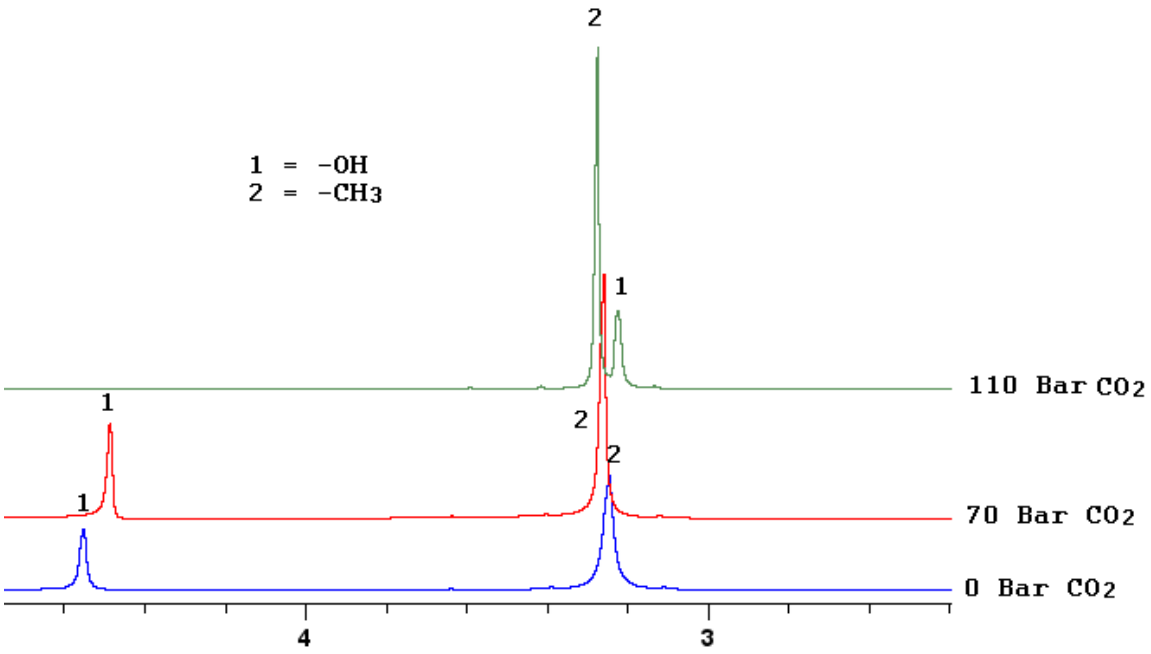

Figure A 12: Change in -OH position with increasing CO_2 pressure